

Electronic Thesis and Dissertation Repository

January 2013

Concrete Bridge Girders with Exposed Flexural Reinforcement

Trevor K. Scott
The University of Western Ontario

Supervisor
Prof. F. M. Bartlett
The University of Western Ontario

Graduate Program in Civil and Environmental Engineering
A thesis submitted in partial fulfillment of the requirements for the degree in Master of
Engineering Science
© Trevor K. Scott 2013

Follow this and additional works at: <https://ir.lib.uwo.ca/etd>



Part of the [Structural Engineering Commons](#)

Recommended Citation

Scott, Trevor K., "Concrete Bridge Girders with Exposed Flexural Reinforcement" (2013). *Electronic Thesis and Dissertation Repository*. 1090.
<https://ir.lib.uwo.ca/etd/1090>

This Dissertation/Thesis is brought to you for free and open access by Scholarship@Western. It has been accepted for inclusion in Electronic Thesis and Dissertation Repository by an authorized administrator of Scholarship@Western. For more information, please contact wlsadmin@uwo.ca.

**CONCRETE BRIDGE GIRDERS WITH EXPOSED FLEXURAL
REINFORCEMENT**

(Thesis format: Monograph)

by

Trevor K. Scott

Graduate Program in
Civil and Environmental Engineering

A thesis submitted in partial fulfillment
of the requirements for the degree of
Master of Engineering Science

The School of Graduate and Postdoctoral Studies
The University of Western Ontario
London, Ontario, Canada
January 2013

© Trevor K. Scott, 2013

THE UNIVERSITY OF WESTERN ONTARIO
SCHOOL OF GRADUATE AND POSTDOCTORAL STUDIES

CERTIFICATE OF EXAMINATION

Supervisor

Dr. F.M. Bartlett

Examiners

Dr. M. A. Youssef

Dr. W. Zhou

Dr. S. Salisbury

The thesis by

Trevor K. Scott

entitled:

Concrete Bridge Girders with Exposed Flexural Reinforcement

is accepted in partial fulfillment of the
requirements for the degree of
Master of Engineering Science

Date _____

Chair of the Thesis Examination Board

ABSTRACT

Reinforced concrete highway bridge girders are regularly repaired by replacing deteriorated concrete with new concrete, temporarily exposing the flexural reinforcement. The absence of bond between the concrete and steel at this stage makes it difficult to compute the flexural capacity and the current code criteria provide no guidance to assist practitioners.

The research reported in this thesis rectifies this knowledge gap. A thorough examination is presented of experimental and analytical investigations by others to determine the typical behaviour, including probable failure modes, of reinforced concrete specimens with exposed flexural reinforcement. Based on these findings, two analytical approaches are developed to predict the longest length of flexural reinforcement that could be exposed that ensures a girder will still exhibit a ductile failure with no reduction in yield capacity. The Strain Compatibility Analysis derived by Harris was enhanced to involve realistic concrete stress-strain relationships and was validated experimentally using five 4-metre T-section specimens subjected to simultaneous point and uniformly distributed loading. A Strut-and Tie Analysis was also derived for this generic loading condition that could only be indirectly validated experimentally. The ratios of the test failure load to the failure load predicted using the Strain Compatibility Analysis had a mean value of 1.00 and a standard deviation of 0.068.

Keywords: Bridges; Girder; Exposed Reinforcement; Assessment/Repair; Rehabilitation; Reinforced Concrete.

For my Grandma.

I wish you were still here to celebrate this great achievement with me.

ACKNOWLEDGEMENTS

First and foremost, I want to offer my deepest thanks to my supervisor, Dr. Mike Bartlett. His help, guidance, and invaluable knowledge have been instrumental in completing my thesis. Dr. Bartlett has been a remarkable mentor and it has been a privilege to have met and worked with him over the past three years.

Thank you to Mr. Wilbert Logan for all his insight and assistance throughout the experimental testing in the UWO Structures Laboratory.

Thank you to all my fellow colleagues who I have shared these past three years with. This journey has been an amazing experience and I am glad to have met and formed such great friendships.

I gratefully acknowledge financial support from the Natural Sciences and Engineering Research Council (NSERC), in the form of a CGS-M Grant and a Discovery Grant and from the Faculty of Engineering at the University of Western Ontario.

A special thank you to my mother, father, and brother, for always being there and supporting me throughout my whole life and helping me become the person I am today. And finally, to my grandma, for always being my biggest fan.

TABLE OF CONTENT

	PAGE
Certificate of Examination	ii
Abstract	iii
Acknowledgements	v
Table of Content	vi
List of Figures	viii
List of Tables	xi
List of Appendices	xii
Nomenclature	xiv
Chapter 1: Introduction	1
1.1 Background	1
1.1.1 Chloride Intrusion.....	2
1.1.2 Carbonation	2
1.2 Bridge Rehabilitation Techniques	3
1.3 Evaluation of Bridge Girders During Rehabilitation	5
1.4 Objectives	6
1.5 Outline of Thesis	6
Chapter 2: Review of Literature	8
2.1 Introduction	8
2.2 Scope of Experimental Investigations	8
2.3 Findings of Previous Experimental Investigations.....	14
2.3.1 Observed Failure Modes	14
2.3.2 Flexural Capacity	15
2.3.3 Cracking Patterns	17
2.3.4 Effective Depth of the Flexural Reinforcement	22
2.4 Analytical Model for Girders with Exposed Flexural Reinforcement	22
2.5 Influence of the Important Parameters	31
2.5.1 Configuration 2.....	32
2.5.2 Configurations 3 and 4	36
2.5.3 Configuration 5.....	37
2.5.4 Configurations 6 and 7	38
2.6 Summary and Conclusions	40
Chapter 3: Analysis of Girders with Exposed Flexural Reinforcement	43
3.1 Introduction	43
3.2 Typical T-section.....	44
3.3 Strain Compatibility Analysis	45
3.3.1 Methodology	46
3.4 Strut-and-Tie Analysis	57
3.4.1 Methodology	58

3.4.2 Case 1: Point Load ($\omega = 0$)	61
3.4.3 Case 2: Uniformly Distributed Load ($\omega \neq 0, P = 0$)	64
3.4.4 Case 3: Both Point and Uniformly Distributed Loads ($\omega \neq 0,$ $P \neq 0$)	66
3.4.5 Comparisons	71
3.5 Summary and Conclusions	72
Chapter 4: Experimental Investigation	74
4.1 Introduction	74
4.2 Objectives	74
4.3 Control Specimen	75
4.4 Testing Apparatus.....	78
4.5 Specimens with Exposed Flexural Reinforcement.....	85
4.6 Testing Procedure.....	90
4.7 Results	93
4.7.1 Control Specimen	93
4.7.2 Specimens with Exposed Flexural Reinforcement.....	97
4.7.3 Effectiveness of Testing Apparatus.....	99
4.7.4 Impact of Steel Spacers	99
4.7.5 Effect of Unsymmetrical Loading Configurations.....	102
4.8 Summary and Conclusions	105
Chapter 5: Comparison of Experimental and Predicted Results.....	108
5.1 Introduction	108
5.2 Comparison to Strain Compatibility Analysis Predictions.....	108
5.2.1 Ultimate Flexural Capacity	109
5.2.2 Neutral Axis Depth.....	111
5.2.3 Reinforcement Strain at Failure	111
5.3 Comparison to Strut-and-Tie Analysis Predictions.....	113
5.3.1 Orientation of Principal Compressive Strains	115
5.4 Summary and Conclusions	117
Chapter 6: Summary, Conclusions and Recommendations for Future Research	119
6.1 Summary	119
6.2 Conclusions	122
6.3 Recommendations for Future Research	124
References.....	126
Appendice	129
Curriculum Vitae.....	210

LIST OF FIGURES

	PAGE
Figure 1-1: Typical Deteriorated Reinforced Concrete Bridge Girders.	1
Figure 1-2: Patch Repair Process: (a) Removal of Contaminated Concrete (b) Concrete Replacement (MTO 2010).....	4
Figure 1-3: Compatible Strain Requirement: (a) Satisfied for Bonded Flexural Reinforcement, (b) Not Satisfied when Flexural Reinforcement is Exposed.....	5
Figure 2-1: Elevation of Specimen with Exposed Flexural Reinforcement with Important Parameter Identified.....	11
Figure 2-2: Failure Modes Observed in the Previous Experimental Investigations.	15
Figure 2-3: Change in Longitudinal Strains in Concrete Section on Exposure of Flexural Reinforcement (Redrawn from Cairns and Zhao 1993).	16
Figure 2-4: Contrast in Crack Patterns between: (a) Control Specimen and (b) Specimen with Exposed Flexural Reinforcement (Cairns and Zhao 1993).	18
Figure 2-5: Crack Patterns of Specimens Designed to Exhibit a Shear Failure: (a) Control, (b) and (c) Specimens with Exposed Flexural Reinforcement (Cairns 1995).	20
Figure 2-6: Loading and Cracking Patterns for (a) Specimen Configuration 3, and (b) Specimen Configuration 4 (Raouf and Lin 1997).....	21
Figure 2-7: Crack Patterns Observed with: (a) Loss of Cover Only, and (b) Loss of Cover and Flexural Bond (Minkarah and Ringo 1982).....	21
Figure 2-8: Location of the Neutral Axis Depth, c , for a Girder with no Flexural Reinforcement Exposed (Redrawn from Cairns and Zhao 1993).....	25
Figure 2-9: Location of the Neutral Axis Depth, c , for a Girder with Exposed Flexural Reinforcement (Redrawn from Cairns and Zhao 1993).	25
Figure 2-10: Location of the Neutral Axis Depth, c , for a Girder with Exposed Flexural Reinforcement to Maintain Compatibility, Eqn. [2.4] (Redrawn from Cairns and Zhao 1993).	26
Figure 2-11: Neutral Axis Depth, c , Variation Along Length of Test Specimen with Exposed Flexural Reinforcement (Bartlett 1998).	26
Figure 2-12: Loading and Variation of the Neutral Axis Depth for Specimens: (a) Configuration 3 and, (a) Configuration 4 (Redrawn from Raouf and Lin 1997).....	27
Figure 2-13: Beam Action with Constant Lever Arm if Flexural Reinforcement is Fully Bonded.....	28
Figure 2-14: Arching Action with Varying Lever Arm if Flexural Reinforcement is Exposed.....	29
Figure 2-15: Reduction in Ultimate Capacity in Specimens with Exposed Flexural Reinforcement: Test Results (Redrawn from Cairns and Zhao 1993)....	33

Figure 2-16:	Variation in Extreme Compressive Strain in Concrete with Length of Exposed Flexural Reinforcement at a Given Applied Moment for Different Load Spacings (Redrawn from Cairns and Zhao 1993).....	35
Figure 2-17:	Influence of Span/Depth Ratio on Behaviour using the Numerical Model (Redrawn from Cairns and Zhao 1993).....	36
Figure 2-18:	Variation of the Reduction in Capacity with Changes in the Distance from the Left Support to the Left Two Point Load (Raof and Lin 1997).....	37
Figure 2-19:	Variation of the Reduction in Capacity with Changes in the Position of the Single-point Load: Small-scale Specimens, $L = 1760$ mm (Redrawn from Raof and Lin 1997).....	39
Figure 3-1:	Typical T-section Cross-section.	45
Figure 3-2:	Flow Chart Depicting the Incremental Procedure of the Strain Compatibility Analysis (SCA).....	47
Figure 3-3:	Neutral Axis Depth, Strain Distribution, Stress Distribution and Internal Forces for both the Positive (+ve) and Negative (-ve) Curvatures.	50
Figure 3-4:	Todeschini's Compressive Stress-strain Relationship for a Concrete Strength, f_c' , of 40 MPa.....	53
Figure 3-5:	Revised Neutral Axis Depth, Strain Distribution, Stress Distribution and Internal Forces for Cases 1 and 6.....	54
Figure 3-6:	Basic Geometry of the Left Compressive Strut.	59
Figure 3-7:	Loading for Case 1 ($\alpha = 0.375$ shown).	62
Figure 3-8:	Effect of the Location of the Point Load on the Critical Distance to the End of the Exposed Length, ℓ_e , at Yield.....	63
Figure 3-9:	Loading for Case 2.....	64
Figure 3-10:	Load Case 2: (a) Shear Force Diagram, (b) Bending Moment Diagram.....	65
Figure 3-11:	Loading for Case 3 ($\alpha = 0.25$ Shown).....	67
Figure 3-12:	Effect of the Location of the Point Load on the Critical Distance to the End of the Exposed Length, ℓ_{eL} , for Different Values of K at Yield.	70
Figure 3-13:	Effect of the Location of the Point Load on the Critical Distance to the End of the Exposed Length, ℓ_{eL} , at Yield for Load Cases 1, 2 and 3....	71
Figure 4-1:	Control Specimen with Reinforcement Details: (a) Plan (Note: Web Reinforcement not Shown for Clarity), (b) Elevation, (c) Cross-section and (d) 180° Standard Hook Detail for Flexural Reinforcement (All Dimensions in mm).....	76
Figure 4-2:	Control Specimen: (a) Reinforcement and Formwork (b) Casting.....	78
Figure 4-3:	Testing Apparatus: (a) Plan, (b) Partial Elevations Showing Unloaded (Left) and Loaded (Right) Control Specimen and (c) End Elevation (All Dimensions in mm).	80

Figure 4-4:	End Joint to Accommodate Rotation: (a) Unassembled, and (b) Installed.	83
Figure 4-5:	Flange Void Forms (a) 75 mm PVC Piping, (b) Bolt and Wing Nut Underneath Formwork.	84
Figure 4-6:	Elevations of Test Specimens with Loading Configuration, Void Location and Steel Spacer Locations.	86
Figure 4-7:	Steel Spacer: (a) Illustration of the Load Transfer through the Steel Spacer and (b) Steel Spacer In-situ.	88
Figure 4-8:	Strain Gauges used in the Experimental Investigation: (a) Small 45 Degree Rosette Strain Gauges, (b) Constructed 45 Degree Rosette Strain Gauge, (c) Strain Gauge on Concrete Flange, and (d) Strain Gauges on Flexural Reinforcement and Stirrups.	89
Figure 4-9:	Foam Insulation Void Enclosing the Flexural Reinforcement.	90
Figure 4-10:	Designed Testing Procedure for Specimens.	91
Figure 4-11:	Elevations of Specimens with Crack Locations and Deflected Shapes.	94
Figure 4-12:	Moment-deflection Relationships: (a) Control Specimen and Specimen 1; (b) Specimen 2 and 3; and, (c) Specimens 4 and 5.	95
Figure 4-13:	Testing Apparatus: Partial Elevations Showing Unloaded (Left) and Loaded (Right) for Control Specimen, (a) Predicted and, (b) Observed.	100
Figure 4-14:	Impact of Steel Spacer under the Interior Load ω Near the Left Support: (a) Specimen 2 and, (b) Specimen 3.	102
Figure 4-15:	Orientation of the Principal Compressive Strains at the End of the Exposed Length for Specimen 1 (Symmetrical Loading Configuration).	103
Figure 4-16:	Orientation of the Principal Compressive Strains at the End of the Exposed Length for Specimen 2 (Unsymmetrical Loading Configuration).	104
Figure 4-17:	Orientation of the Principal Compressive Strains at the End of the Exposed Length for Specimen 3 (Unsymmetrical Loading Configuration).	104
Figure 5-1:	Variation of the SCA-predicted Neutral Axis Depth and Compressive Force Centroid at Failure and Observed Cracking Patterns.	112
Figure 5-2:	Orientation of the Predicted and Observed Principal Compressive Strains at the Supports of Specimen 3: (a) Left, (b) Right.	116

LIST OF TABLES

	PAGE
Table 2-1: Test Specimens and Loading Configurations Studied by Others.	9
Table 2-2: Parameters Investigated in Current Literature.	12
Table 2-3: Details of Specimens with Exposed Flexural Reinforcement.....	13
Table 3-1: Summary of the Magnitude and Location of the Concrete Compressive Force for each Case (Compression Zone Shaded).....	51
Table 3-2: Summary of Critical Values for Load Case 3.....	69
Table 4-1: Whiffle Tree System Components.....	82
Table 4-2: Properties of Specimens with Exposed Flexural Reinforcement.....	85
Table 4-3: Testing Loads for each Specimen.	92
Table 4-4: Predicted and Observed Test Results.....	96
Table 5-1: Predicted Strain Compatibility Analysis and Test Results.	110
Table 5-2: Predicted Strut-and-Tie Analysis and Test Results.	114

LIST OF APPENDICES

	PAGE
Appendix A: Literature Review Details.....	129
A.1: Introduction.....	130
A.2: Minkarah and Ringo (1982).....	130
A.3: Nokhasteh, Eyre and McLeish (1992)	131
A.4: Cairns and Zhao (1993)	132
A.5: Raooof and Lin (1993, 1995, 1997).....	136
A.6: Nemecc (1996).....	138
A.7: Xiong, Liu and Xie (2000).....	138
A.8: Sharaf and Soudki (2002)	140
Figure A-1: Details of: (a) Control Specimen (b) Test Specimen with Loss of Only Cover (c) Test Specimen with Loss of Cover and Flexural Bond (Minkarah and Ringo 1982).....	131
Figure A-2: Dimensions for a Typical Specimen with Exposed Flexural Reinforcement (Nokhasteh, Eyre and McLeish 1992).	132
Figure A-3: Details of Test Specimens, all Dimensions in mm (Cairns and Zhao 1993).	133
Figure A-4: Loading Configuration for the First Part of Study (Cairns and Zhao 1993).	134
Figure A-5: Details of Test Series Specimens A, B, and C (Cairns 1995).....	135
Figure A-6: Details of Small-scale Test Specimens with Width = 75 mm (Raooof and Lin 1997).....	137
Figure A-7: Details of Large-scale Test Specimens (Raooof and Lin 1997).	137
Figure A-8: Details of Test Specimens and Loading Configuration (Bartlett 1998).....	138
Figure A-9: Details of Short-term Test Specimens (Xiong, Liu and Xie 2000).....	139
Figure A-10: Details of Long-term Test Specimens (Xiong, Liu and Xie 2000).....	139
Figure A-11: Details of Test Specimens (Sharaf and Soudki 2002).	140
Appendix B: Analysis of Specimens with Exposed Flexural Reinforcement	141
B.1: Introduction.....	142
B.2: Strain Compatibility Analysis (SCA) Derivation	143
B.3: Strut-and-Tie Analysis (STA) Derivation.....	157
Appendix C: Experimental Investigation	166
C.1: Stress-strain Relationship for Reinforcement	167

C.2:	Dead-to-live Load Moment Ratio for a Typical Reinforced Concrete Bridge.....	173
C.3:	Design, Construction and Installation of Foam Void	177
C.4:	Testing Procedure	182
C.5:	Loading Histories of Specimens	187
C.6:	Cracking Moment, M_{cr}	190
Figure C-1:	Tensile Test for Bar Samples 1 and 2	169
Figure C-2:	Stress-strain Approximations for Test Bar Samples 1 and 2	172
Figure C-3:	Cedar Creek Road Underpass Bridge (MTO 2010).....	173
Figure C-4:	Elevation of Cedar Creek Road Underpass (Dillon Consulting 2001). ..	174
Figure C-5:	Typical Cross-section of Cedar Creek Road Underpass (Dillon Consulting 2001).....	174
Figure C-6:	The Ratio of Dead Load Moment, M_D , to Total Load Moment, M_T , over the Positive Moment Region of the Cedar Creek Road Underpass Bridge.....	176
Figure C-7:	Foam Insulation Void: (a) Plan of Individual Layers, (b) Section A-A at Stirrups, and (c) Section B-B between Stirrups (All Dimensions in mm).	178
Figure C-8:	Foam Insulation Void: (a) Layer 1, (b) Layer 2, (c) Layer 3 and (d) Layer 4.	179
Figure C-9:	Foam Insulation Void Placement: (a) Stirrups and Flexural Reinforcement Placement, (b) Layer 3 Placement, (c) Layer 4 Placement, (d) Beveled Edge of Layer 4.	181
Figure C-10:	Loading History for Control Specimen.....	188
Figure C-11:	Loading History for Specimen 1.....	188
Figure C-12:	Loading History for Specimen 2.....	188
Figure C-13:	Loading History for Specimen 3.....	189
Figure C-14:	Loading History for Specimen 4.....	189
Figure C-15:	Loading History for Specimen 5.....	189
Appendix D: Comparison of Experimental and Predicted Results.....		193
D.1:	Introduction.....	194
D.2:	Strain Compatibility Analysis Results for Specimen 1.....	194
D.3:	Orientation of Principal Compressive Strains.....	206
Figure D-1:	Loading Configuration for Specimen 1 (All Dimension in mm).....	195
Figure D-2:	Orientation of the Predicted and Observed Principal Compressive Strains at the Supports of Specimen 1: (a) Left, (b) Right.....	207
Figure D-3:	Orientation of the Predicted and Observed Principal Compressive Strains at the Supports of Specimen 2: (a) Left, (b) Right.....	208
Figure D-4:	Orientation of the Predicted and Observed Principal Compressive Strains at the Left Support of Specimen 5.	209

NOMENCLATURE

A_b	area of test bar sample in a reinforcement tensile test
A_s	area of tensile flexural reinforcement
A_s'	area of top (flexural compression) reinforcement
b	width of concrete compression zone
b_f	overall flange width
b_w	web width
C	resultant compressive force / force in compressive strut
$C(x)$	resultant compressive force in the concrete at centre of segment at x
C_L	force in the left compressive strut
c	neutral axis depth measured from the extreme compression fibre
$c(x)$	neutral axis depth at centre of segment
d	effective depth of flexural tensile reinforcement
d'	effective depth of top (flexural compression) reinforcement
d_c	depth of concrete removed
E_c	elastic modulus of concrete
E_s	elastic modulus of steel
f_c	concrete compressive stress at extreme fibre
f_c'	compressive strength of concrete
f_c''	maximum compressive stress in Todeschini's stress-strain relationship
$f_c(x)$	stress in the extreme compression fibre at centre of segment at x
f_{cr}	cracking strength of concrete
f_{cu}	limiting compressive stress in either the node or compressive strut
f_s	tensile stress in flexural reinforcement
f_y	yield strength of steel
f_u	ultimate strength of steel
H	horizontal force component of the compressive strut
h	overall height
h_a	height of node at support
h_{amax}	maximum height of node at support
h_f	flange thickness
h_s	depth of the top compressive strut or node at the location of the maximum moment
h_w	reduced web height where concrete is removed
i	iteration number
jd	lever arm between the internal tensile and compressive force resultants
$jd(x)$	lever arm at the centre of segment at x
jd_{max}	lever arm at the location of the maximum moment, M_{max}
K	ratio of point load to total distributed load ($K = P/\omega L$, $K \geq 0$)
$k_1(x)$	average stress of the resultant compressive force coefficient at centre of segment at x
$k_2(x)$	line of action of the resultant compressive force coefficient, measured from the extreme compression fibre, at centre of segment at x
L	span length

L_T	total length of specimen
L^*	gauge length of test bar samples
l_b	length of bearing at support
l_c	critical length of exposed flexural reinforcement
l_e	critical distance from support to end of exposed length
l_{eL}	critical distance from left support to end of exposed length
l_{end}	distance from support to end of exposed length
l_{eR}	critical distance from right support to end of exposed length
l_{exp}	length of exposed flexural reinforcement
M	applied bending moment
$M(x)$	bending moment at centre of segment at x
M_D	dead load moment
M_G	fraction of total live load moment applied to one girder
M_L	live load moment
M_P	moment due to the point load
M_{SCA}	predicted ultimate moment using the Strain Compatibility Analysis (SCA)
M_{STA}	predicted ultimate moment using the Strut-and-Tie Analysis (STA)
M_T	total moment
M_{cr}	cracking moment
M_{max}	maximum applied moment
M_y	yield moment
M_u	ultimate moment
M_ω	moment due to the simulated distributed load
N	number of specimens tested
n	number of segments / modular ratio (E_s/E_c)
P	point load
P_y	anticipated point load causing yield of flexural reinforcement
P_b	tensile load in test bar sample
P_{by}	yield tensile load in test bar sample
P_{bu}	ultimate tensile load in test bar sample
R_L	reaction at left support
R_R	reaction at right support
S	spacing between two-point loads
T	tensile force in flexural reinforcement
T_s	tensile force in exposed stirrups
V	applied shear
V_G	fraction of total live load shear applied to one girder
V_T	total live load shear
w	width of compressive strut
x	distance along the longitudinal axis of a girder from support to centre of segment
$y(x)$	depth of the centroid of the resultant compressive force from the neutral axis at centre of segment at x
Z	case number referring to the location of the neutral axis

Greek Symbols

α	normalized point load location from left support
α_1	ratio of the average stress in a rectangular compression block to the specified concrete compressive strength
γ_c	mass density of concrete (assumed 2300 kg/m ³)
Δ	displacement reading in a reinforcement tensile test
Δ_b	elongation of test bar sample
Δ_{by}	elongation of test bar sample at yield
Δ_{cs}	elongation of the concrete at the depth of the flexural reinforcement
Δ_m	displacement of Tinius-Olsen Machine
Δ_{mid}	midspan deflection of specimen
Δ_{my}	displacement attributed to the Tinius-Olsen Machine at yield of test bar sample
Δ_s	elongation of exposed flexural reinforcement
ΔT	change of tensile force in the flexural reinforcement
Δ_x	segment length
Δ_y	observed displacement reading at yield in a reinforcement tensile test
ϵ_c	compressive strain in concrete at extreme fibre
ϵ_{cs}	extrapolated strain in the concrete at the depth of the exposed flexural reinforcement
ϵ_{cu}	maximum compressive strain at extreme fibre
ϵ_c'	strain corresponding to the maximum compressive stress in Todeschini's concrete stress-strain relationship
$\epsilon_c(x)$	compressive strain in concrete at extreme fibre at centre of segment at x
ϵ_s	tensile strain in the exposed flexural reinforcement
ϵ_y	yield strain of steel
θ_L	orientation of the principal compressive strains in the concrete web at the left support
θ_R	orientation of the principal compressive strains in the concrete web at the right support
θ_{STA}	predicted orientation of the principal compressive strains / strut in the concrete web at the support using the Strut-and-tie Analysis (STA)
θ_s	inclination of compressive strut at support
θ_{sL}	inclination of the compressive strut at the left support
θ_{sR}	inclination of the compressive strut at the right support
ρ	flexural reinforcement ratio
ω	simulated uniformly distributed point load
ω_{DL}	specified uniformly distributed dead load
ω_{app}	simulated distributed point load due to the weight of the testing apparatus
ω_{ow}	simulated distributed point load due to the self- weight of the specimen
ω_s	mechanical flexural reinforcement ratio
ω_y	target simulated distributed point load causing yield of flexural reinforcement

CHAPTER 1: INTRODUCTION

1.1 BACKGROUND

Reinforced concrete highway bridge girders are susceptible to deterioration caused primarily by corrosion of the reinforcing steel, as shown in Figure 1-1. Concrete is alkaline in nature and, when placed, generally has a pH value between 12 and 13 (Bertolini et al. 2004, Nehdi 2011, Minkarah and Ringo 1982). If the concrete is uncracked, a passive oxide film forms around the reinforcement that prevents the intrusion of moisture and oxygen (Bertolini et al. 2004, Nehdi 2011, Minkarah and Ringo 1982). In this condition, the reinforcement is stable in a high pH solution that prevents the initiation of corrosion.



Figure 1-1: Typical Deteriorated Reinforced Concrete Bridge Girders.

The passive oxide film that forms around the reinforcement can begin to deteriorate either by intrusion of chloride ions into the concrete or by carbonation and is referred to

as the process of depassivation. Once the oxide film has completely deteriorated, the corrosion of the reinforcement is initiated. The volume of rust created can be six times that of the original steel (Nehdi 2011) and so can cause the concrete cover to crack, delaminate, and spall. The cracks are highlighted by brown rust stains, reflecting the pattern of the flexural reinforcement (Unterweger et al. 2009). When the delaminated section spalls, the concrete cover to the reinforcement is lost, further exposing the flexural reinforcement and initiating the next cycle of corrosion.

1.1.1 Chloride Intrusion

In Ontario, deicing salts are used on highways during the winter months to melt snow and ice (MTO 2008). These salts mix with snow and water to form a liquid brine that becomes an airborne spray due to traffic movement. When this spray comes into direct contact with the underside of the bridge, chloride ions penetrate the cracks, voids and surface pores of the concrete, lowering the pH (Bertolini et al. 2004). This dissolves the oxide film, exposing the flexural reinforcement to the moisture and oxygen necessary for corrosion to occur. This type of deterioration occurs at localized sections and causes cracking, visible rust stains, delamination, and spalling. The depth of contamination is typically greatest immediately above the travelled lanes (Bertolini et al. 2004, Nehdi 2011).

1.1.2 Carbonation

The flexural reinforcement can also be corroded by the carbonation process, where atmospheric carbon dioxide, CO₂, and moisture react with the concrete to gradually lower its pH (Nehdi 2011). Once the carbonation front reaches the depth of the flexural

reinforcement a process, similar to that for chloride intrusion, occurs. This type of deterioration is usually more uniform over the length of the girder causing flaking rust (Nehdi 2011).

1.2 BRIDGE REHABILITATION TECHNIQUES

Deteriorated reinforced concrete highway bridge girders are regularly repaired using the patch repair process, where the flexural reinforcement must be re-passivated by removing the existing contaminated concrete and replacing it with new concrete (Nedhi 2010, Bertolini et al. 2004), temporarily exposing the flexural reinforcement, as shown in Figure 1-2. The repair of a reinforced concrete girder is typically intended to ensure the structure achieves at least its original service life (Nehdi 2010). The three significant steps in the patch repair process are:

1. Removal of all contaminated concrete.
2. Preparation of the surface of the existing concrete including cleaning and application of a bonding agent.
3. Placement of the repair concrete.

The first step is most pertinent to the current study and so warrants further description. It involves removal of all, or a significant amount, of the existing contaminated concrete to expose a sound concrete substrate. This reduces the risk of further deterioration caused by contaminated concrete remaining after the repair (Guettala et al. 2006).

The perimeter of each deteriorated area is first outlined by saw-cutting through the cover to the first layer of flexural reinforcement without damaging it. The deteriorated concrete

in contact with and between the reinforcing bars is then removed using a light pneumatic hammer (OPSS 1994).

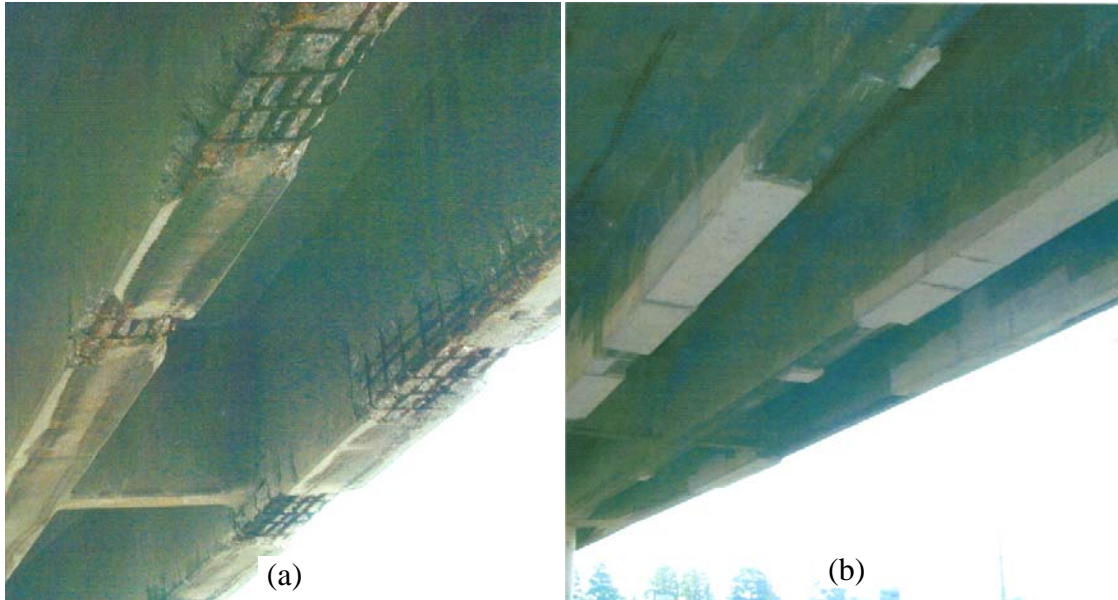


Figure 1-2: Patch Repair Process: (a) Removal of Contaminated Concrete (b) Concrete Replacement (MTO 2010).

The remaining contaminated concrete is removed using a smaller chipping hammer, which is easier to operate and reduces the possibility of damaging the uncontaminated concrete substrate or the flexural reinforcement. For each deteriorated area, the removal is performed to a minimum of 25 mm beyond the inner surface of the first layer of flexural reinforcement to ensure that there is sufficient space for the repair concrete to be consolidated around the flexural reinforcement and to create an adequate bond (Emmons et al. 2003). It has been independently established (Cairns and Zhao 1993) that a removal of concrete to a depth of at least 20 mm behind the flexural reinforcement will result in a durable repair with proper bond between the new material and the flexural reinforcement.

1.3 EVALUATION OF BRIDGE GIRDERS DURING REHABILITATION

While the cause of reinforcement corrosion has been exhaustively researched, the strength assessment of the girders with exposed flexural reinforcement has not been so thoroughly investigated (Eyre et al. 1992). Rehabilitation using the patch repair process causes the bond between the flexural reinforcement and concrete to be, at least temporarily, lost. Consequently the flexural capacity of the girder is uncertain because, while plane sections remain plane in the concrete at each cross section, the requirement for compatible strains in the flexural reinforcement and the adjacent concrete no longer holds, as shown in Figure 1-3 (Bartlett 1998, Cairns and Zhao 1993). The flexural capacity is not easily computed because the usual provisions for design, as specified in Section 8.8 of the Canadian Highway Bridge Design Code (CHBDC), CAN/CSA-S6-06 (CSA 2006) are not applicable. Sections 14 and 15 of the CHBDC outline the procedures for the evaluation, rehabilitation and repair of existing bridges, but provide no guidance to assist practitioners evaluating the capacity of reinforced concrete girders with exposed flexural reinforcement.

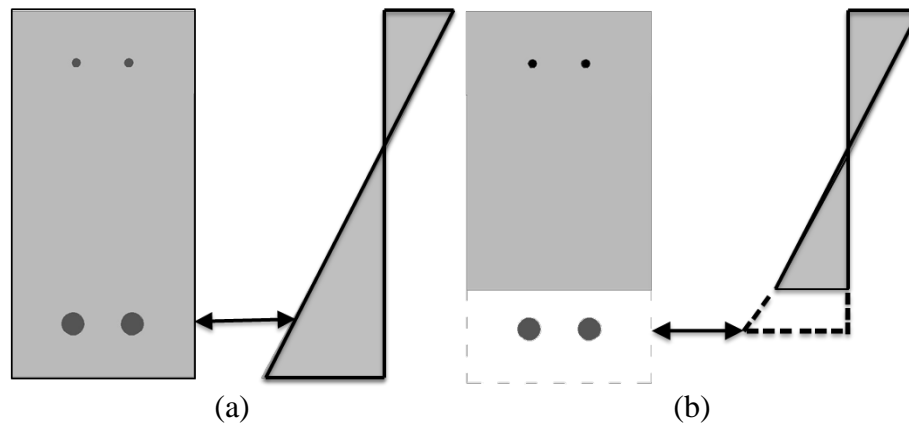


Figure 1-3: Compatible Strain Requirement: (a) Satisfied for Bonded Flexural Reinforcement, (b) Not Satisfied when Flexural Reinforcement is Exposed.

1.4 OBJECTIVES

The objective of the research reported in this thesis is to rectify the knowledge gap in the current code criteria for evaluating reinforced concrete highway girders with exposed flexural reinforcement. The research will provide an important tool to assist practicing engineers in evaluating these girders safety during rehabilitation.

The specific objectives of this research are as follows:

1. Examine thoroughly previous experimental and analytical investigations to determine the observed behaviour and possible failure modes of reinforced concrete beams with exposed flexural reinforcement.
2. Develop analytical methods that can accurately predict the maximum capacity of reinforced concrete highway girders with a given length of exposed flexural reinforcement or determine the maximum length that can be exposed that does not cause a reduction of the flexural capacity.
3. Conduct an experimental investigation of reinforced concrete T-section specimens with exposed flexural reinforcement to validate the analytical methods developed.

1.5 OUTLINE OF THESIS

Chapter 2 presents a literature review of previous experimental and analytical investigations concerning reinforced concrete specimens with exposed flexural reinforcement. Chapter 3 presents two analytical approaches developed to analyze reinforced concrete bridge T-section girders with exposed flexural reinforcement: (1) Strain Compatibility Analysis (SCA), and (2) Strut-and-Tie Analysis (STA). Both

approaches can be used to predict the longest length of flexural reinforcement that can be exposed that ensures a girder will still exhibit a ductile failure with no reduction in yield capacity. Chapter 4 presents a description and the results of a new experimental investigation of five 4-metre reinforced concrete T-section specimens with exposed flexural reinforcement, that was undertaken to evaluate the accuracy of the analytical approaches developed in Chapter 3. Chapter 5 presents a comparison of these experimental results with the analytical predictions to assess their validity. Finally, Chapter 6 presents the summary, conclusions and recommendations for future research.

CHAPTER 2: REVIEW OF LITERATURE

2.1 INTRODUCTION

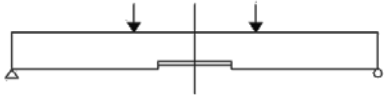


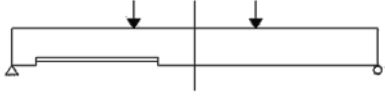
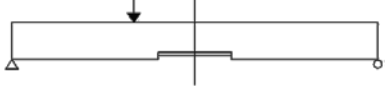


A literature review is necessary before developing analytical approaches and conducting an experimental study. This chapter will therefore examine previous experimental investigations to extract: a summary of the test specimen geometries and loading configurations; the findings of the studies; and, a general description of the behaviour of specimens with exposed flexural reinforcement.

2.2 SCOPE OF EXPERIMENTAL INVESTIGATIONS

Since 1980, eight experimental investigations on the effect of exposed flexural reinforcement have been conducted. A total of 219 specimens of moderate scale have been tested, comprising either single- or two-point loading with spans ranging from 1500 to 4000 mm. Table 2-1 summarizes the seven distinct specimen configurations tested. Configurations 1 - 4 all involve specimens with two-point loading. For Configuration 1, the exposed flexural reinforcement is located within the constant moment region between the applied loads and so has negligible effect. The girder behaves essentially as an intact girder: there would be no “tension stiffening” between flexural cracks so it would be less stiff and exhibit slightly larger deflections at serviceability-level loads. For Configuration 2, the exposed flexural reinforcement will impact the response because it extends beyond the central constant moment region. For Configuration 3, the exposed flexural reinforcement is located entirely in one of the constant shear regions. Tests using Configuration 3 have also been conducted with the flexural reinforcement exposed in both shear spans. Configuration 4 is similar to Configuration 3, but the flexural

reinforcement is exposed in only one half of the specimen in both the constant moment and constant shear regions.

Table 2-1: Test Specimens and Loading Configurations Studied by Others.

No.	Specimen Configuration	Dominant Failure Mode	Authors
1		Flexure	Cairns and Zhao (1993)
2		Flexure, Flexure/Shear	Nokasteh et al. (1992), Cairns and Zhao (1993), Bartlett (1998), Cairns (1995), Xiong et al. (2000), Sharaf and Soudki (2002)
3		Shear	Raof and Lin (1993, 1995, 1997), Cairns (1995)
4		Flexure, Flexure/Shear	Raof and Lin (1993, 1995, 1997)
5		Flexure, Shear	Minkarah and Ringo (1982)
6		Shear, Flexure	Raof and Lin (1993, 1995, 1997)
7		Shear/Flexure, Flexure	Raof and Lin (1993, 1995, 1997)

Configurations 5 - 7 involve specimens subjected to single-point loading. For Configuration 5, the exposed flexural reinforcement is located symmetrically about the

centreline of the specimen and the point load is located outside of the exposed length. For Configuration 6, the exposed flexural reinforcement is located in the high shear region near the left support with the load applied beyond the exposed length, near midspan. Configuration 7 is similar, but with the point load applied within the exposed length. A full description of all the previous investigations is presented in Appendix A.

Table 2-2 outlines the important parameters, shown in Figure 2-1, identified by past researchers as potentially influencing the behaviour of specimens with exposed flexural reinforcement. It also identifies the studies where the experimental findings were supplemented by structural analysis. The following parameters are deemed to be important:

1. Length of exposed flexural reinforcement, ℓ_{exp}
2. Area of tensile flexural reinforcement, A_s
3. Depth of concrete removed, d_c
4. Compressive strength of concrete, f_c'
5. Yield strength of flexural reinforcement, f_y
6. Presence of nominal top reinforcement, A_s'
7. Position of loading: location of load from left support, αL , for a single load or spacing, S , for symmetric two-point loads
8. Distance from the support to the end of the exposed length, ℓ_{end}

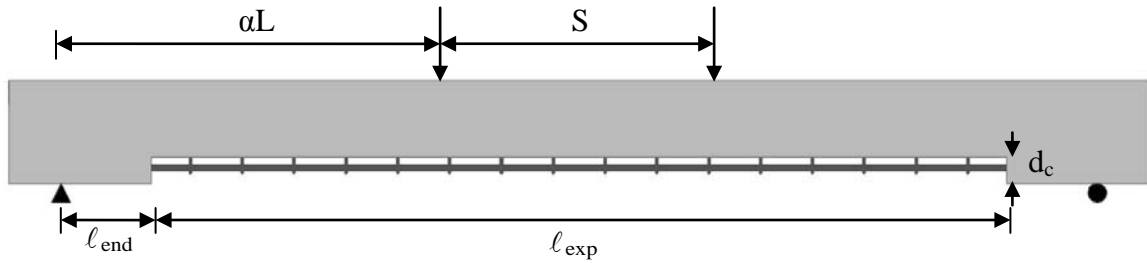


Figure 2-1: Elevation of Specimen with Exposed Flexural Reinforcement with Important Parameter Identified.

Table 2-3 summarizes the specimen dimensions, material properties, and loading configurations investigated. In addition to the variables previously defined, it indicates: the number of specimens tested, N ; span length, L ; overall height, h , and flange thickness, h_f ; overall flange width, b_f ; web width, b_w ; effective depth of flexural reinforcement, d ; stirrup arrangement, size and centre-to-centre spacing; and, specimen configuration.

These summaries indicate that most previous experimental investigations involved rectangular reinforced concrete specimens and all used either single- or two-point loading. Concrete bridge girders typically feature a substantial top slab and resist substantial uniformly distributed dead loads, so the scope of these investigations are not realistic. Therefore an experimental investigation of T-section specimens loaded with some combination of a uniformly distributed dead load and a live load is necessary to more accurately represent the type of girder and applied loading seen in the field.

Table 2-2: Parameters Investigated in Current Literature.

Authors	Length of Exposed Flexural Reinforcement	Area of Tensile Flexural Reinforcement	Depth of Concrete Removed	Strength of Concrete and Reinforcement	Presence of Top Nominal Steel	Loading Position	Location of Exposed Length	Analysis
Minkarah and Ringo (1982)	X	-	X	-	-	-	-	
Nokhasteh, Eyre, and McLeish (1992)	X	X	-	-	-	-	-	
Cairns and Zhao (1993)	X	X	-	X	-	X	-	X
Raoof and Lin (1993, 1995, 1997)								
Small - Scale Tests	X	-	-	-	-	X	-	
Large - Scale Tests	X	X	X	-	X	X	X	
Zhang and Raoof (1995)	X	-	X	X	X	-	-	X
Nemec, Harris (1996) and Bartlett (1998)	X	-	-	-	-	-	-	X
Cairns (1995)	X	-	-	-	-	X	X	X
Xiong, Liu, and Xie (2000)								
Short Term Tests	X	-	-	-	-	-	-	-
Long Term Tests	-	-	-	-	-	-	-	-
Sharaf and Soudki (2002)	X	-	-	-	-	-	-	-

Table 2-3: Details of Specimens with Exposed Flexural Reinforcement.

Authors	N	L (mm)	b (mm) (b _w /b)	h (mm) (h _f /h)	f _c ' (MPa)	Bottom RFT	d (mm)	A _s (mm ²)	f _y (MPa)	Stirrups	a (mm)	Config. #	Note
Minkarah and Ringo (1982)	40	2900	127	254	43.8	2-12.7mm	210	258	438	9.5mm @ 102 c/c	Varies	5	
Nokhasteh et al. (1992)	3	2000	130	200	Varies	Varies	167	Varies	365	Present	0.424	2	
Cairns and Zhao (1993)	19	Varies	Varies	Varies	Varies	Varies	Varies	Varies	Varies	Varies	Varies	1,2	
Raof, and Lin, (1993, 1995, 1997)													
Small - Scale Tests	44	1760	75	130	29	2-10mm	110	157.1	363	N/A	Varies	6,7	
Large - Scale Tests	88	3000	150	300	Varies	Varies	279	Varies	363	Varies	Varies	3(a),4(a),6,7	
Nemec, Harris (1996) and Bartlett (1998)	2	4000	200/800	90/400	40	2-25mm	342	1000	457	10 mm @ 200 c/c	0.4	2	T-Section
Cairns (1995)													
Series A	3	3000	150/230	300	37	2-25mm	257	1000	524/509	6 mm @ 200 c/c	0.265	2,4(b)	
Series B	3	3000	160/200	400	33	2-25mm	357	1000	509	6 mm @ 275 c/c	0.365	2,4(b)	
Series C	4	3000	180/500	95/305	29.4	2-25mm	263	1000	543	8 mm @ 185 c/c	0.265	2,4(b)	T-Section
Xiong, Liu, and Xie (2000)													
Short Term Tests	4	1800	120	200	-	2-12mm	175	226.2	548.5	6 mm @ 150 c/c	0.25	2	
Long Term Tests	4	1800	100	150	-	2-12mm	125	226.2	548.5	6 mm @ 150 c/c	0.25	2	
Sharaf and Soudki (2002)	5	1500	100	150	38	1-15mm	-	176.7	400	4 mm @ 50 c/c	0.333	2	

2.3 FINDINGS OF PREVIOUS EXPERIMENTAL INVESTIGATIONS

Marked differences in failure mode, flexural capacity, and crack patterns were observed between specimens with and without exposed flexural reinforcement that were otherwise identical. This section will synthesize the behaviour of specimens with exposed flexural reinforcement. Some previous researchers (e.g., Cairns and Zhao 1993, Harris 1996) developed analytical models to predict these behavioural changes. The influence of the important parameters previously identified is also summarized.

2.3.1 Observed Failure Modes

For the seven unique configurations shown in Table 2-1, the five failure modes shown in Figure 2-2 were observed. Ranked by frequency of occurrence, they are as follows:

1. Yielding of the exposed flexural reinforcement followed by crushing of the concrete on the compression face of the specimen
2. Crushing of the concrete on the compression face of the specimen before yielding of the exposed flexural reinforcement
3. Compression failure in the concrete at the ends of the exposed flexural reinforcement length
4. Anchorage failure at one end of the exposed flexural reinforcement
5. Shear failure

The first two modes are the most predominant for flexural failures, while the remaining three are most predominant for shear-flexural failures.

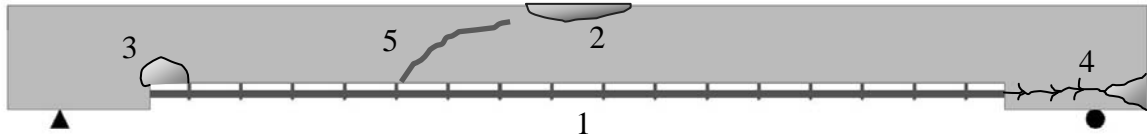


Figure 2-2: Failure Modes Observed in the Previous Experimental Investigations.

The specimens with exposed flexural reinforcement that would exhibit a ductile flexural failure if no reinforcement was exposed generally failed by one of failure modes 1 - 4 (e.g., Minkarah and Ringo 1982, Cairns and Zhao 1993). Failure modes 3 and 4 occurred only when the end of the exposed length was close to the support. The specimens that would have failed in shear, a brittle mode, if no reinforcement was exposed generally failed by failure modes 1, 2, 4, or 5 (Cairns 1995).

2.3.2 Flexural Capacity

Cairns and Zhao (1993) studied the change in flexural capacity of specimens that would exhibit a ductile failure if no reinforcement was exposed. Figure 2-3, redrawn from their paper, shows measured midspan concrete strain distributions, with tensile strains positive, at different depths from the extreme compression fibre for a specimen with a flexural reinforcement ratio, ρ , of 1.64% and ℓ_{exp} increasing from 0 to 63% of the 3000 mm span length. Exposure of the flexural reinforcement from zero to 1900 mm increased the extreme fibre compressive strain from -0.0008 to -0.0012, and reduced the neutral axis depth, c , from 120 mm to 80 mm. The associated curvatures increased by a factor of 2.25. They also tested 17 rectangular specimens with ℓ_{exp} ranging from 60 to 95% of the span length that exhibited a reduction in flexural capacity ranging from 1 to 48%.

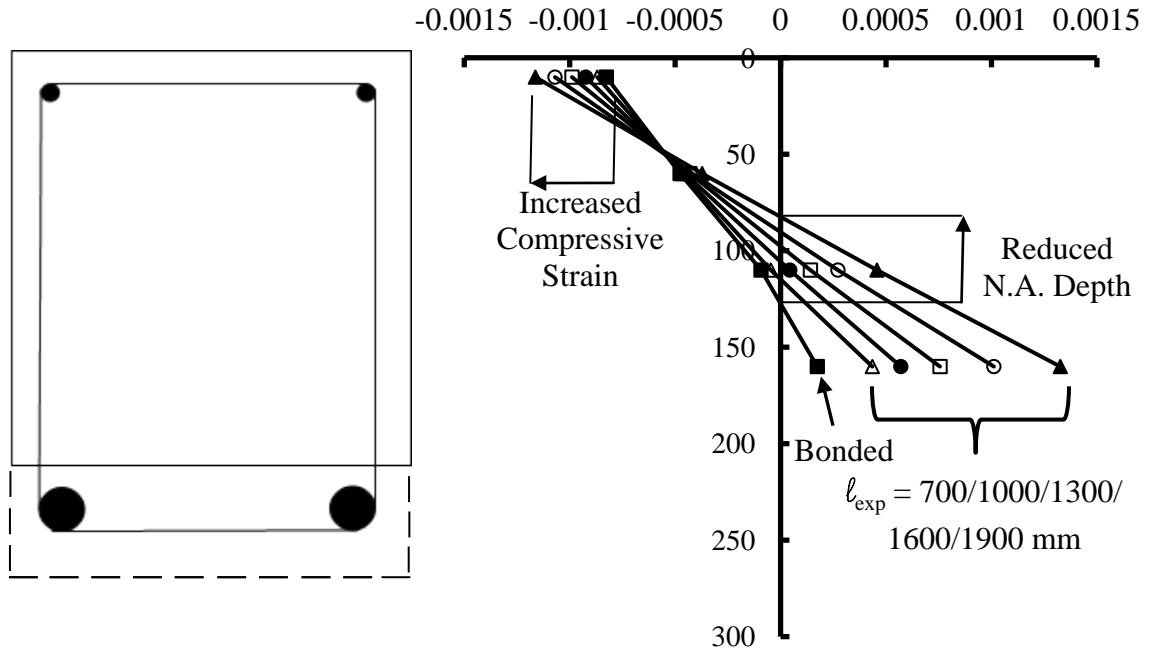


Figure 2-3: Change in Longitudinal Strains in Concrete Section on Exposure of Flexural Reinforcement (Redrawn from Cairns and Zhao 1993).

Bartlett (1998), Harris (1996) and Nemeč (1996) tested two 4000 mm long T-section specimens, one a control and the second a test specimen with 2000 mm of flexural reinforcement exposed symmetrically about the midspan. They observed that both the control and test specimens behaved in a linear elastic manner until the flexural reinforcement yielded, but the second specimen had only 81% of the stiffness of the control specimen. After the flexural reinforcement yielded, the load resisted by the control specimen continued to increase while that resisted by the other specimen gradually reduced before failure.

The capacity of specimens with exposed flexural reinforcement that would have failed in shear if no reinforcement was exposed differed markedly. Cairns and Zhao (1993) observed that exposure of the flexural reinforcement does not always reduce the shear capacity. Four specimens with exposed flexural reinforcement that would have failed in

shear if the flexural reinforcement was fully bonded exhibited an increased shear capacity and failed in flexure.

Cairns (1995) performed ten additional shear tests that confirmed that exposing the flexural reinforcement increased the shear capacity of specimens, in some cases by a substantial margin, for all but lightly-reinforced specimens. The failure loads of the test specimens were higher, typically between the calculated shear and flexural failure loads of the control specimens.

All remaining researchers (e.g., Minkarah and Ringo 1982, Nokasteh et al. 1992, Raof and Lin 1993, 1995, 1997, Xiong et al. 2000, and Sharaf and Soudki 2002) observed similar findings concerning the reduction of the flexural capacity of specimens with exposed flexural reinforcement.

2.3.3 Cracking Patterns

There is a wide consensus that exposing the flexural reinforcement substantially changes the crack patterns (Nokhasteh et al. 1992, Cairns and Zhao 1993, Xiong et al. 2000, Sharaf and Soudki 2002). As shown in Figure 2-4, the specimens with exposed flexural reinforcement typically had:

1. Fewer, wider and larger spaced flexural cracks in the high moment region
2. Greater flexural crack heights
3. Bifurcation at the flexural crack tips
4. No flexural cracks at the bottom face near the supports

5. Flexural cracks near the ends of the exposed length at the top (i.e., 'compression') face of the specimen.
6. Bond-splitting cracks at the ends of the exposed flexural reinforcement.

The cracks in specimens with exposed flexural reinforcement within the constant moment region were abrupt, appeared at very low loads, and as shown in Figure 2-4(b), had widths 25 times greater than those in control specimens. The large crack widths were attributed to the lack of bonded flexural reinforcement across the crack and the increased midspan curvature caused by exposing the flexural reinforcement (Cairns and Zhao 1993). These cracks, once initiated, propagated immediately to the neutral axis, where they typically bifurcated, often propagating horizontally in opposite directions (Minkarah and Ringo 1982, Cairns and Zhao 1993).

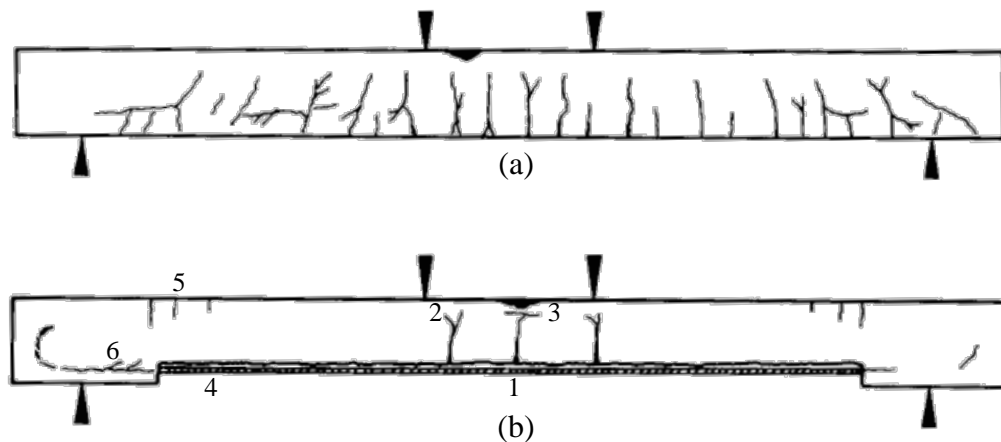


Figure 2-4: Contrast in Crack Patterns between: (a) Control Specimen and (b) Specimen with Exposed Flexural Reinforcement (Cairns and Zhao 1993).

Specimens loaded to service load levels before exposing the flexural reinforcement displayed only minor changes of crack patterns. The cracks were not as wide at midspan because numerous narrow flexural cracks already existed before the flexural

reinforcement was exposed. The crack height at service load levels increased, due again to the reduced neutral axis depth, c , caused by exposing the flexural reinforcement. Crack widths in the shear span at service load levels reduced when the flexural reinforcement was exposed. These crack patterns suggest that exposing the flexural reinforcement may cause a strain reversal to occur towards the support, with compression on the bottom face of the specimen.

In Cairns' (1995) ten additional shear tests, the crack patterns changed considerably if the flexural reinforcement was exposed. Figure 2-5 shows the crack patterns for the control specimen and the two specimens with exposed flexural reinforcement. The control specimen exhibited typical shear cracks near the left support. The specimens with exposed flexural reinforcement displayed critical diagonal cracks that were steeper and located closer to the applied point loads. The specimen in Figure 2-5(b) experienced an anchorage failure, while the specimen in Figure 2-5(c) experienced a shear failure at a cross section closer to the applied load. These crack patterns suggest that exposing the flexural reinforcement causes the number of diagonal cracks to reduce, and their location to move towards the higher moment regions (Cairns 1995).

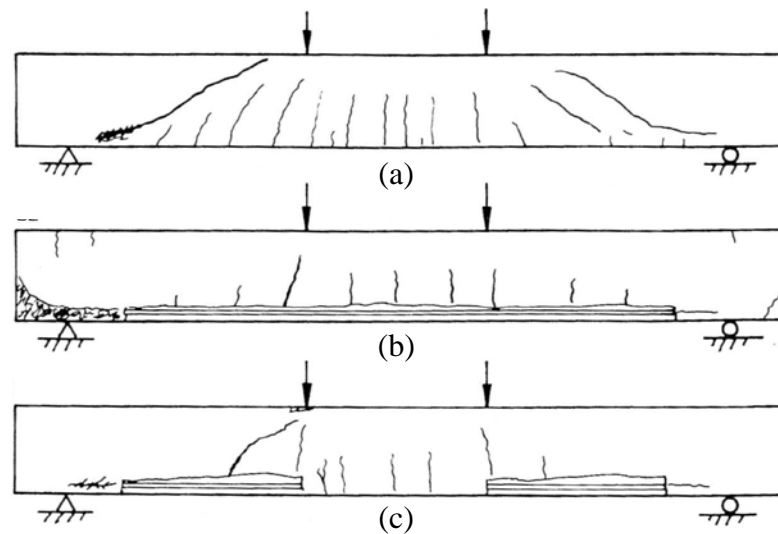


Figure 2-5: Crack Patterns of Specimens Designed to Exhibit a Shear Failure: (a) Control, (b) and (c) Specimens with Exposed Flexural Reinforcement (Cairns 1995).

Raouf and Lin (1993, 1995, 1997) tested specimens with Configurations 3 and 4 and typically observed crack patterns shown in Figure 2-6. For either configuration, the crack patterns from midspan to the right support, where no flexural reinforcement was exposed, were similar to those that would be observed if no reinforcement was exposed: vertical flexural cracks at the midspan that gradually change to inclined shear cracks towards the right support. There were two subtle differences between the crack patterns for the two configurations. First, Configuration 4 (Figure 2-6(b)) exhibited more shear cracks near the right support, likely due to the higher applied shear in this region. Second, the large crack within the exposed length for Configuration 4 is located directly under the left applied point load, while no crack occurs at the end of the exposed length. For Configuration 3 (Figure 2-6(a)), where the left point load is located beyond the exposed length, the large crack is located directly at the right end of the exposed length and no cracks were observed within the exposed length.

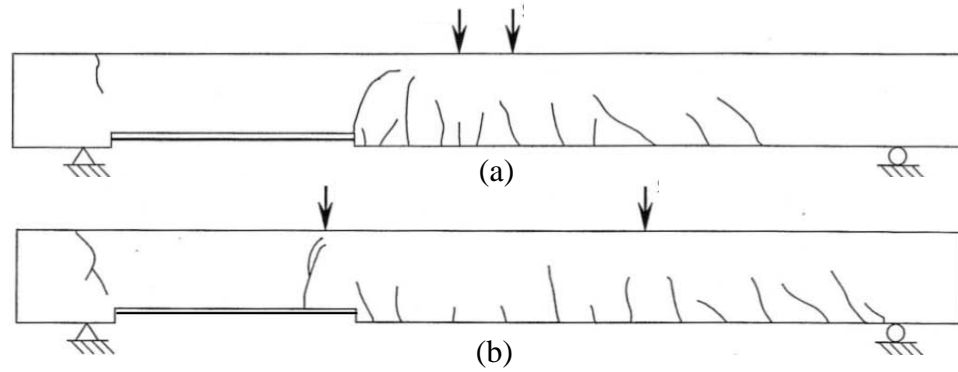


Figure 2-6: Loading and Cracking Patterns for (a) Specimen Configuration 3, and (b) Specimen Configuration 4 (Raof and Lin 1997).

Minkarah and Ringo (1982) observed different crack patterns for specimens with only the reinforcement cover removed and specimens with both the cover removed and the flexural bond lost, as shown in Figure 2-7. Removal of only the cover caused behaviour similar to that of the fully bonded control specimen, likely because bond is partially maintained to help control cracking. If both the cover and the flexural bond were lost, the height of the cracks under the point load increased, highlighting the local decrease in the neutral axis depth. A flexural crack was observed at the end of the exposed length and no flexural cracks were observed within the exposed length likely because the exposed flexural reinforcement could not transfer any of the stress at this crack to the concrete in the exposed length. Flexural cracks reappeared to the right of the exposed length likely because the flexural bond was present again.

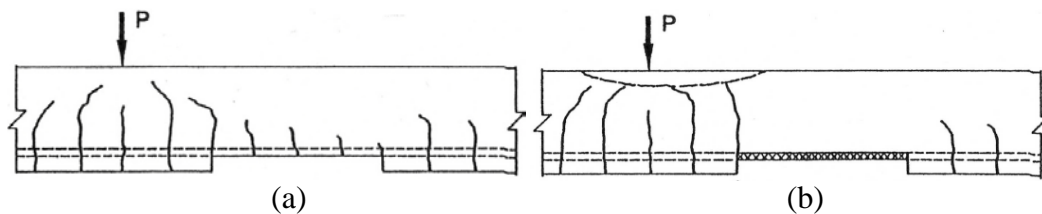


Figure 2-7: Crack Patterns Observed with: (a) Loss of Cover Only, and (b) Loss of Cover and Flexural Bond (Minkarah and Ringo 1982).

2.3.4 Effective Depth of the Flexural Reinforcement

Previous researchers (e.g., Nemec 1996, Cairns and Zhao 1993) observed that as the specimens deflected during testing, the gap between the bottom of the concrete web and the exposed flexural reinforcement reduced until the two came into contact. This reduces the effective depth of the flexural reinforcement, d , and so reduces the flexural capacity.

2.4 ANALYTICAL MODEL FOR GIRDERS WITH EXPOSED FLEXURAL REINFORCEMENT

Reinforced concrete girders are normally designed to exhibit ductile flexural failures initiated by yielding of the flexural reinforcement followed by crushing of the concrete (e.g., MacGregor and Bartlett 2000). This “under-reinforced” condition is preferable to ensure warning of the imminent failure. If the girder is “over-reinforced”, the concrete crushes before the flexural reinforcement yields and the failure occurs suddenly, without visible warning. When the flexural reinforcement yields and the concrete crushes simultaneously, failure is referred to as “balanced”. The response of deteriorated reinforced concrete girders during the repair process must be analyzed because, during the interval when the flexural reinforcement is exposed, the flexural failure mode can transition from under- to over-reinforced (Cairns and Zhao 1993).

The loss of the steel-concrete bond over portions of a girder causes plane sections to still remain plane in the concrete but invalidates the requirement of compatible strains in the flexural reinforcement and the adjacent concrete (Bartlett 1998, Cairns and Zhao 1993, Harris 1996, Zhang and Raof 1995, Cairns 1995). The girder will act more like a tied arch if the ends of the flexural reinforcement remain anchored in the concrete (Bartlett

1998) resulting in a redistribution of stresses and strains that is unlikely to have been considered in the original design.

Cairns and Zhao (1993) present a qualitative description of the structural behaviour of girders that exhibit a ductile failure if no reinforcement is exposed when concrete is removed. After flexural cracking, if the concrete compressive response is linear-elastic, horizontal force equilibrium requires that:

$$[2.1] \quad A_s f_s + f_c b \frac{c}{2} = 0$$

where f_s is the tensile stress in flexural reinforcement (negative if tension), and f_c is the concrete compressive stress in extreme fibre.

Moment equilibrium requires that:

$$[2.2] \quad M = A_s f_s j d$$

where M is the applied bending moment, and $j d$ is the lever arm between the internal tensile and compressive force resultants, equal to $d - (c/3)$.

The new compatibility requirement is that the longitudinal deformations of concrete and the flexural reinforcement must be compatible at the ends of the exposed flexural reinforcement length, ℓ_{exp} :

$$[2.3] \quad \int_0^{\ell_{\text{exp}}} \epsilon_s d\ell - \int_0^{\ell_{\text{exp}}} \epsilon_{cs} d\ell = 0$$

where ε_s is the tensile strain in exposed flexural reinforcement (negative if tension) and ε_{cs} is the extrapolated strain in the concrete at the depth of the exposed flexural reinforcement, computed assuming plane sections remain plane.

Before concrete is removed, the girder acts as a simple beam, as shown in Figure 2-8. The neutral axis depth, c , and the lever arm, jd , between the tensile force in the flexural reinforcement and the compressive force in the concrete are both approximately constant over the length of the girder. The necessary assumption is that perfect bond exists between the flexural reinforcement and the concrete so the strains in the flexural reinforcement and in the concrete at the depth of the flexural reinforcement are equal, Eqn. [2.3].

If ℓ_{exp} extends beyond the constant moment region of a girder subjected to symmetric four-point loading, Eqn. [2.3] is not automatically satisfied because the applied bending moment reduces in the constant-shear region between each loading point and the adjacent support, but ε_s must remain constant where the flexural reinforcement is exposed. The compatibility requirement can be written as:

$$[2.4] \quad \varepsilon_s \ell_{exp} - \int \varepsilon_{cs} dl = 0$$

To satisfy Eqn. [2.2], the lever arm, jd , must reduce at cross sections close to the supports, requiring an increase in the neutral axis depth, c , as shown in Figure 2-9, and so reducing the concrete compressive strain at the extreme compression fibre, ε_c . In this region, the neutral axis moves below the soffit of the girder and the concrete cross section

becomes fully stressed in compression. If ℓ_{exp} is long, the neutral axis then reappears above the cross section and moves downwards as the distance to the support reduces. The stresses in the concrete in this region have the opposite sense of those at midspan, with tension above the neutral axis and compression below it.

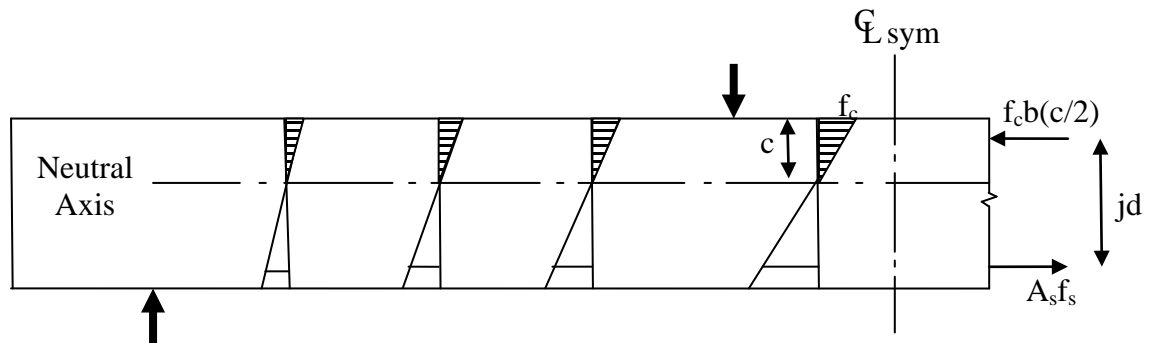


Figure 2-8: Location of the Neutral Axis Depth, c , for a Girder with no Flexural Reinforcement Exposed (Redrawn from Cairns and Zhao 1993).

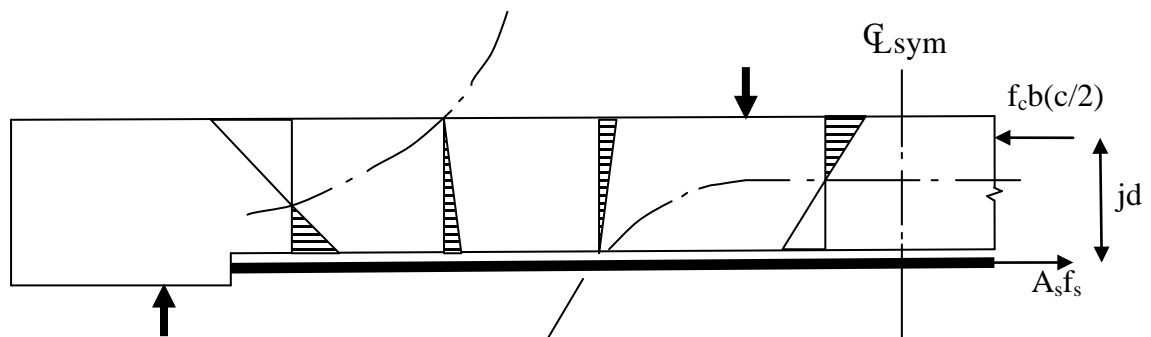


Figure 2-9: Location of the Neutral Axis Depth, c , for a Girder with Exposed Flexural Reinforcement (Redrawn from Cairns and Zhao 1993).

To satisfy the compatibility condition, Eqn. [2.4], the neutral axis depth at midspan must be reduced (Cairns 1995), as shown in Figure 2-10, to create large tensile strains in the concrete at the depth of the exposed flexural reinforcement. The associated increased curvature and extreme fibre concrete compressive strain can cause crushing of the concrete before the exposed flexural reinforcement yields.

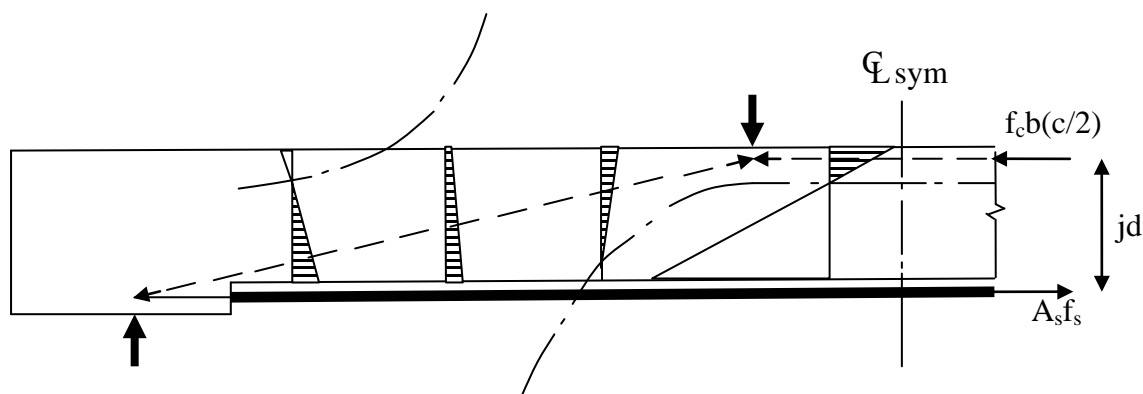


Figure 2-10: Location of the Neutral Axis Depth, c , for a Girder with Exposed Flexural Reinforcement to Maintain Compatibility, Eqn. [2.4] (Redrawn from Cairns and Zhao 1993).

Tests of a reinforced concrete T-section specimen with exposed flexural reinforcement (Bartlett 1998, Harris 1996) displayed a similar response to that described by Cairns and Zhao (1993). The neutral axis location varied along the length of the specimen as shown in Figure 2-11, resulting in high curvatures and large extreme fibre compressive strains in the concrete at midspan. Failure was initiated by the tensile steel yielding, but the ductility at failure was limited by a local crushing failure across the width of the compression flange.

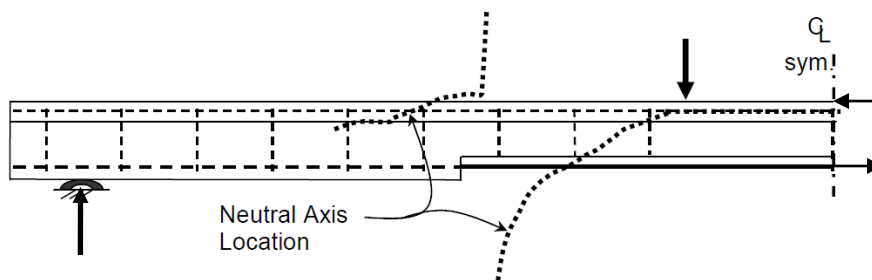


Figure 2-11: Neutral Axis Depth, c , Variation Along Length of Test Specimen with Exposed Flexural Reinforcement (Bartlett 1998).

Raouf and Lin (1993, 1995, 1997) tested specimens with Configurations 3 and 4. They observed similar responses as reported by Cairns and Zhao (1993) and Bartlett (1998).

Using the profiles of concrete strain distribution measured along the top and bottom surfaces of the specimen for applied loads of 20, 40, and 60 kN (Raouf and Lin 1997), the neutral axis depth, c , was determined. Figure 2-12 show the neutral axis location for Configurations 3 and 4. Near the right support of the test specimens, where no reinforcement was exposed, the neutral axis depth is fairly constant. Near the left support, at the end of the exposed flexural reinforcement, the neutral axis depth, c , increases and moves below the soffit of the test specimen. Within the exposed length, the neutral axis reappears above the test specimen and increases with a strain reversal with tensile strain (positive) at the top and compressive (negative) at the bottom.

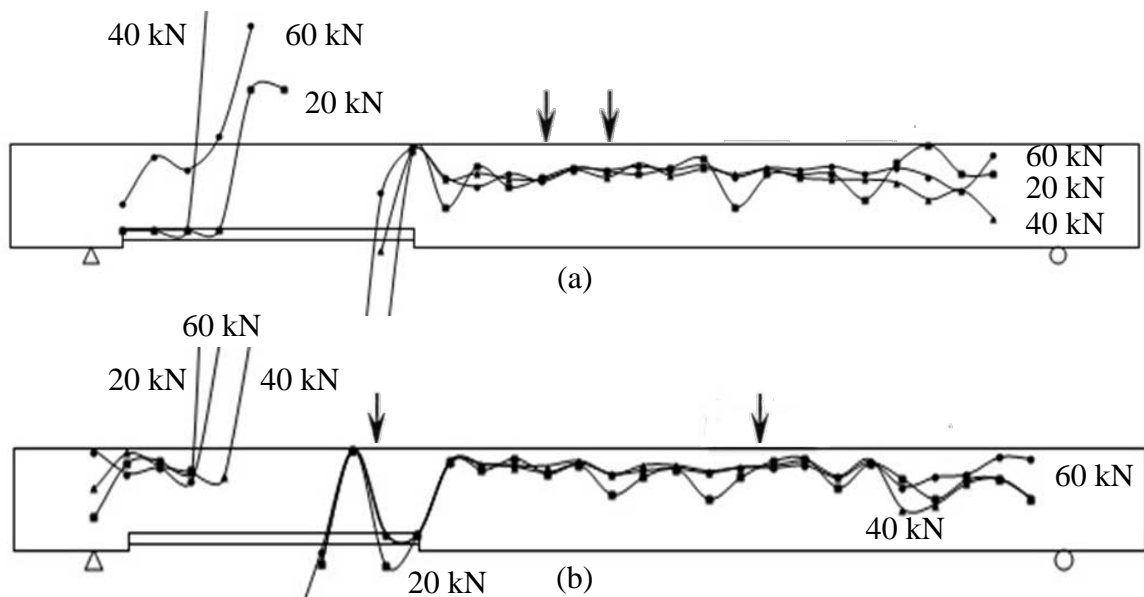


Figure 2-12: Loading and Variation of the Neutral Axis Depth for Specimens: (a) Configuration 3 and, (a) Configuration 4 (Redrawn from Raouf and Lin 1997).

This qualitative description can also be described as a transition of the behaviour from beam action to arching action (e.g., MacGregor and Bartlett 2000). In a reinforced concrete girder, shear can be carried by a combination of beam and arching action:

$$[2.5] \quad V = \frac{dM}{dx} = \frac{d(Tjd)}{dx} = T \frac{d(jd)}{dx} + jd \frac{d(T)}{dx}$$

where V is the applied shear force, T is the tensile force in the flexural reinforcement, and x is the distance along the longitudinal axis of the girder.

When the flexural reinforcement is fully bonded to the concrete, the applied shear is resisted entirely by beam action. The resultant compressive, C , and tensile forces are therefore separated by a constant lever arm, jd , and so reduce as the moment reduces, as shown in Figure 2-13:

$$[2.6] \quad \frac{d(jd)}{dx} = 0 \text{ and } V = \frac{d(T)}{dx} jd$$



Figure 2-13: Beam Action with Constant Lever Arm if Flexural Reinforcement is Fully Bonded.

If the flexural reinforcement is exposed, eliminating bond, the applied shear must be resisted entirely by arching action where the tensile force is constant and the lever arm, jd , must vary to satisfy the moment equilibrium over the exposed length, l_{exp} :

$$[2.7] \quad \frac{d(T)}{dx} = 0 \text{ and } V = T \frac{d(jd)}{dx}$$

The lever arm, jd , reduces and an inclined concrete thrust line, or compressive strut, forms between the support reaction and the load point, as shown in Figure 2-14. The flexural stress reversal near the support, i.e., with the top fibre in tension, is consistent with the formation of this strut. The ends of long exposed lengths can encroach on the inclined compressive strut near the support, significantly limiting its area and so reducing its capacity.

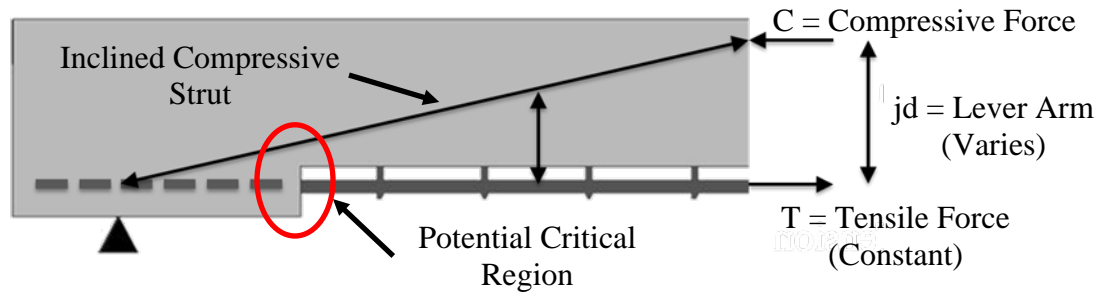


Figure 2-14: Arching Action with Varying Lever Arm if Flexural Reinforcement is Exposed.

For specimens that exhibit a shear failure if no reinforcement is exposed, the increased shear capacity observed when the flexural reinforcement is exposed cannot be currently explained. Girders are normally designed to ensure that the shear capacity is greater than the flexural capacity so the girder will fail in a ductile flexural mode instead of a brittle shear mode (MacGregor and Bartlett 2000). The shear capacity of girders with exposed

flexural reinforcement is therefore also important. Conventionally (e.g., Cairns 1995), the shear capacity is attributed to:

1. Concrete in the compression zone resisting shear
2. Aggregate interlock
3. Dowel action of flexural reinforcement
4. Transverse reinforcement, typically stirrups

If flexural reinforcement is exposed in a region subjected to shear, any dowel action is lost and the contribution of the stirrups is reduced if their bottom corner anchorages are exposed (Cairns 1995).

In light of the findings by Cairns (1995) and the consideration that bridge girders are normally designed to fail in a ductile flexural mode, the shear capacity of specimens with exposed flexural reinforcement will not be investigated in the current study.

In general, for a girder with given geometric and material properties, there exists a critical length of exposed flexural reinforcement, ℓ_c , where the failure transitions from ductile to brittle. At this transition point, the flexural reinforcement will yield and the concrete will simultaneously crush, with little reduction in flexural capacity attributable to exposing the flexural reinforcement. As ℓ_{exp} approaches ℓ_c , the flexural reinforcement strain at failure gradually reduces, but the girder will achieve its flexural yield capacity. Once ℓ_{exp} exceeds ℓ_c , the flexural reinforcement will not yield, the girder will exhibit a brittle failure, and the flexural capacity will reduce, sometimes substantially (Minkarah and

Ringo 1982, Nokhasteh et al. 1992, Cairns and Zhao 1993, Raoof and Lin 1997, Xiong et al. 2000, Sharaf and Soudki 2002).

Based on these considerations, there are currently three different analytical models for predicting the flexural capacity of reinforced concrete specimens with exposed flexural reinforcement, based on Eqns. [2.1] to [2.4]. Cairns and Zhao (1993) and Zhang and Raoof (1995) independently developed two unique models for rectangular reinforced concrete sections that accurately predicted the reduction in flexural capacity for the 17 specimens investigated by Cairns and Zhao (1993). Both models are only applicable to rectangular sections, and Cairns and Zhao (1993) do not present their model in detail. Harris (1996) developed an analysis for T-section beams with exposed flexural reinforcement that displayed a similar response to that observed by Cairns and Zhao (1993) and accurately predicted the flexural capacity of the one specimen investigated. The limitation of this model is that a linear compressive stress-strain relationship for the concrete is assumed, even in the high stress regions.

2.5 INFLUENCE OF THE IMPORTANT PARAMETERS

The influence of the various important parameters on the behaviour of specimens with exposed flexural reinforcement has been extensively investigated in the previous studies. This section summarizes the influence of the various parameters for each configuration investigated. Three of the parameters have been deemed to be particularly important: the length of exposed flexural reinforcement, ℓ_{exp} , the position and type of loading, αL , and the distance from the support to the end of the exposed length, ℓ_{end} . These are the only

parameters that can be controlled during the rehabilitation of an existing reinforced concrete bridge girder.

2.5.1 Configuration 2

The flexural capacity and behaviour of Configuration 2 specimens with exposed flexural reinforcement are significantly influenced by ℓ_{exp} . In the small-scale tests by Nokhasteh, Eyre and McLeish (1992), two otherwise identical specimens, with flexural reinforcement exposed over 25% and 85% of the 2000 mm span, were tested to failure. The specimen with the lesser ℓ_{exp} behaved as though no reinforcement had been exposed, showed no reduction in flexural capacity, and exhibited a ductile failure. The specimen with the longer ℓ_{exp} experienced a less ductile failure with a reduction in capacity of 6%. Therefore, the critical exposed length of flexural reinforcement, ℓ_c , for this flexural reinforcement ratio, 0.93%, lies between 25 and 85% of the span length.

Nokhasteh, Eyre and McLeish (1992) and Cairns and Zhao (1993) investigated the combined effects of the flexural reinforcement ratio, ρ , the concrete compressive strength, f'_c , and the flexural reinforcement yield strength, f_y , on the behaviour of test specimens with exposed flexural reinforcement. The mechanical reinforcement ratio, ω_s , is a dimensionless parameter that depends on these three variables:

$$[2.8] \quad \omega_s = \frac{A_s f_y}{f'_c b d}$$

A girder with no exposed reinforcement will exhibit a ductile, balanced, or brittle flexural failure if $\omega_s \lesssim 0.3$, ≈ 0.3 or $\gtrsim 0.3$, respectively (e.g. Bartlett 1982). Nokhasteh, Eyre and

McLeish (1992) tested two specimens with flexural reinforcement exposed over 85% of the span. Both exhibited brittle failures and the capacity reduced 26% as ω_s increased from 0.092 to 0.226. Cairns and Zhao (1993) reported that residual capacity reduces as ω_s increases, particularly for specimens with relatively long ℓ_{exp} as shown in Figure 2-15, redrawn from their paper. In particular, three specimens with flexural reinforcement exposed over approximately 95% of the span, corresponding to ℓ_{exp}/d ranging from 12.75 to 14.3, displayed a 14% capacity reduction for $\omega_s = 0.037$ and a 45% reduction for $\omega_s = 0.088$. They concluded that ℓ_c will be longer for lightly reinforced specimens and that the flexural capacity is more likely to be reduced in a heavily reinforced section.

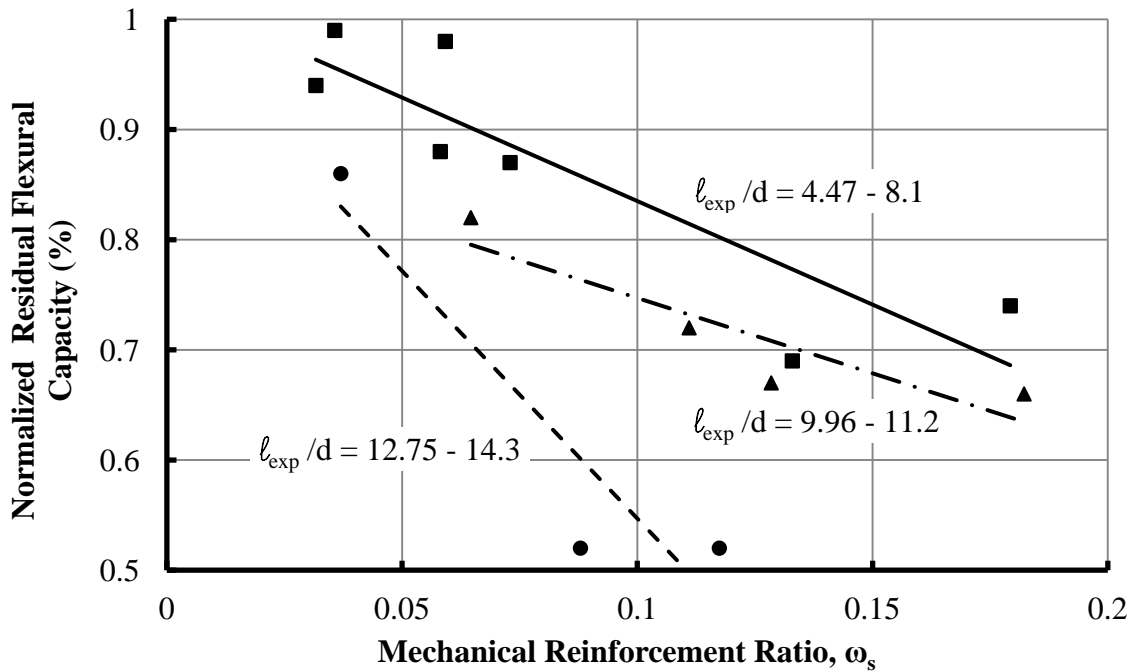


Figure 2-15: Reduction in Ultimate Capacity in Specimens with Exposed Flexural Reinforcement: Test Results (Redrawn from Cairns and Zhao 1993).

Thus the effects of the concrete compressive strength and flexural reinforcement yield strength, f_c' and f_y , respectively, on girders with exposed flexural reinforcement are

readily visualized. Eqn. [2.1] indicates that, for a given flexural reinforcement ratio A_s/bd , a reduction of f_c' must cause a reduction in the flexural reinforcement stress, f_s , and corresponding strain, ϵ_s , to satisfy equilibrium. Similarly, increasing f_y , or flexural reinforcement yield strain, ϵ_y , requires an increase in the concrete strain, ϵ_c to satisfy equilibrium. In either case, once l_{exp} reaches l_c causing ϵ_s to reduce below ϵ_y , there must be a reduction in the flexural capacity to satisfy Eqn. [2.2]. This implies that a reduction in f_c' , or an increase in f_y , will result in l_c decreasing and vice versa.

Cairns and Zhao (1993) also highlighted the importance of the applied load spacing, S , on the extreme compressive strains of the test specimen, as shown in Figure 2-16. They concluded that as S increased, the extreme compressive strains and corresponding midspan curvatures, for the same midspan moment decreased while still remaining in the linear elastic range of concrete response in compression. By increasing S , the length of the constant shear regions where reinforcement is exposed is reduced, so the effect of the exposed flexural reinforcement on the concrete compressive strains is reduced and the associated l_c increases. Conversely, when S is decreased, reducing the length of the constant moment zone, l_c decreases.

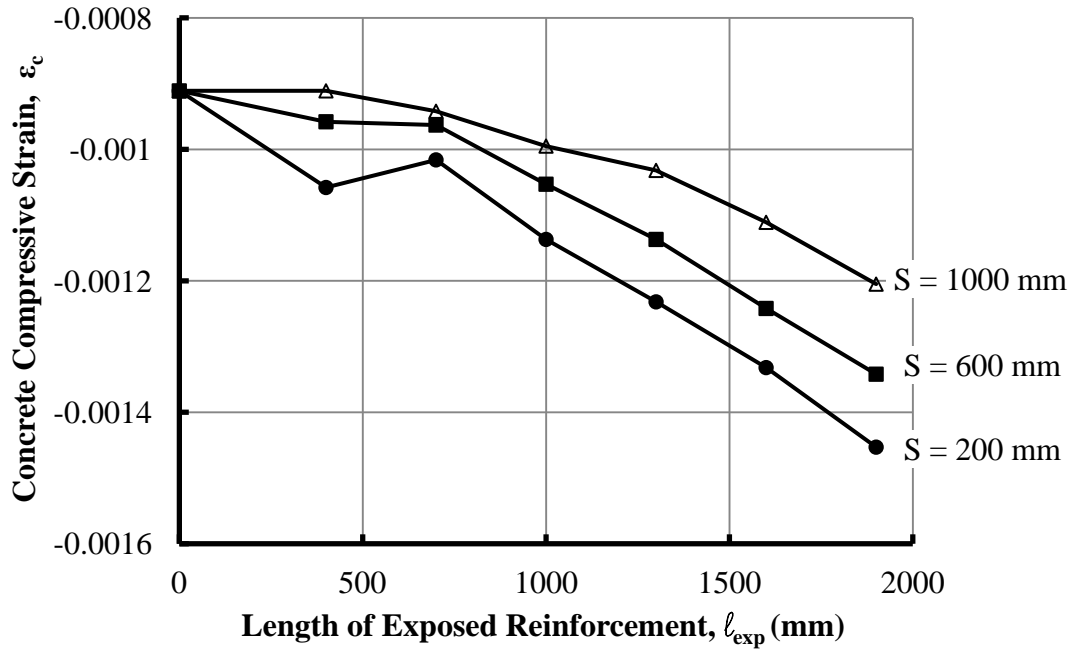


Figure 2-16: Variation in Extreme Compressive Strain in Concrete with Length of Exposed Flexural Reinforcement at a Given Applied Moment for Different Load Spacings (Redrawn from Cairns and Zhao 1993).

Cairns and Zhao (1993) developed a numerical model, based on Eqns. [2.1] to [2.3], that accurately predicted their test results. As shown in Figure 2-17, it predicts no reduction in capacity or flexural reinforcement strain when l_{exp} is contained within the constant moment zone, 20% of the span length for the case shown. However, when l_{exp} extends past the constant moment region, ϵ_s at failure gradually reduces to ϵ_y , approximately 0.0023 when $l_{exp}/L \approx 0.40$. This corresponds to the behavioural change from under-reinforced to balanced responses and so is the critical exposed length, l_c .

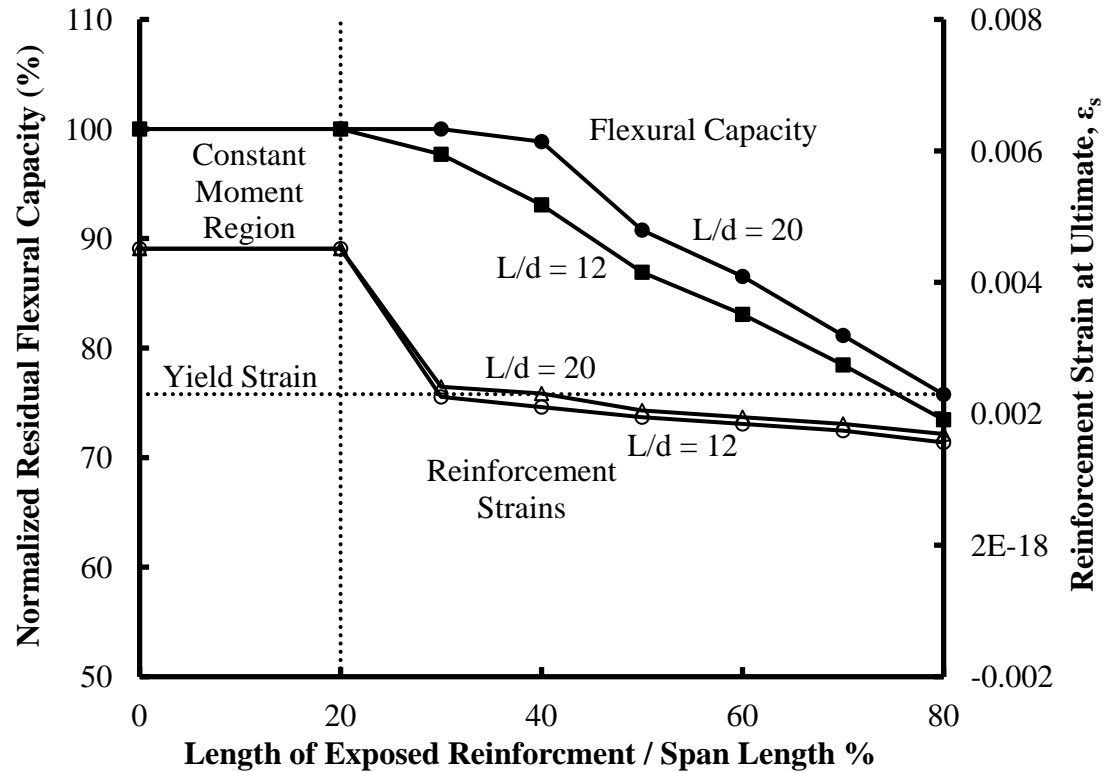


Figure 2-17: Influence of Span/Depth Ratio on Behaviour using the Numerical Model (Redrawn from Cairns and Zhao 1993).

2.5.2 Configurations 3 and 4

Raouf and Lin (1993, 1995, 1997) tested specimens with Configurations 3 and 4 examining the importance of the distance between point loads, S , and the presence of nominal top reinforcement, A_s' , and stirrups. The specimens without nominal top reinforcement or stirrups, designed to fail in shear, had a reduction in the normalized residual capacity as S reduced, as shown in Figure 2-18. Cairns (1995) and Cairns and Zhao (1993) noted a similar observation for Configuration 2. The failure mode changed from a shear to a flexural failure when the flexural reinforcement was exposed. The presence of nominal top reinforcement and stirrups changed the failure mode of the control specimen to a ductile flexural failure and there was no reduction in capacity of the

specimens with exposed flexural reinforcement, as shown in Figure 2-18. The observed capacity was insensitive to the area of the top nominal reinforcement (Raof and Lin 1997). Effects due to the absence of nominal top reinforcement and stirrups will not be considered in the current study because these features are typically present in reinforced concrete bridge girders.

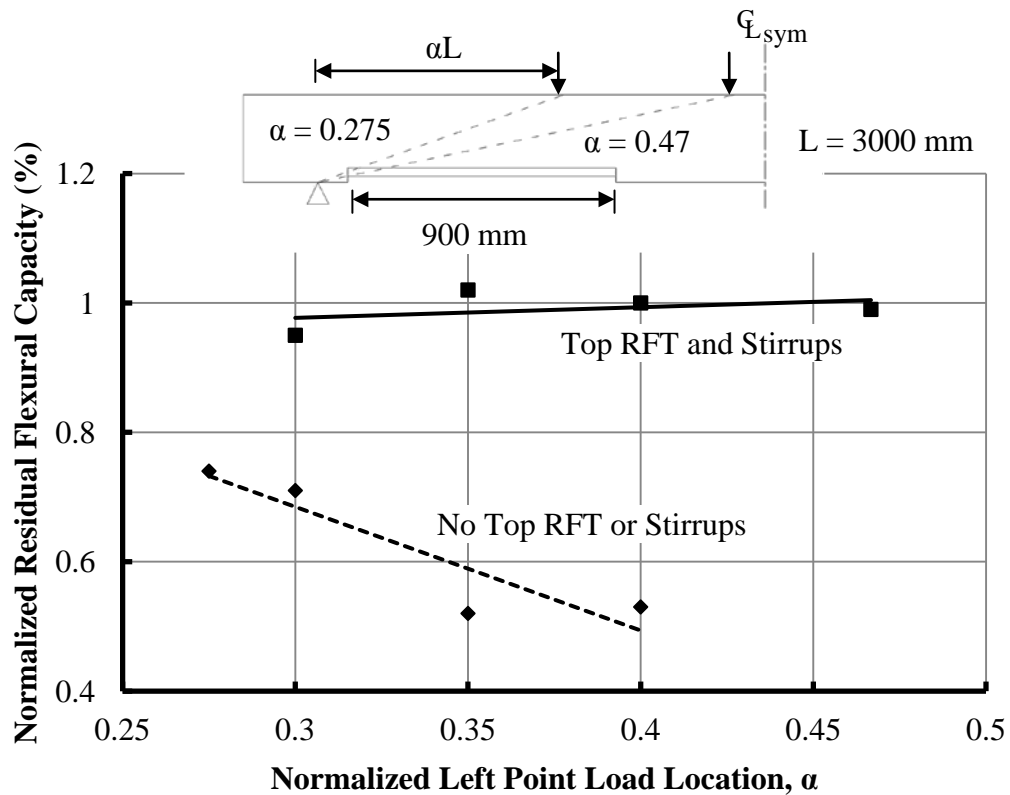


Figure 2-18: Variation of the Reduction in Capacity with Changes in the Distance from the Left Support to the Left Two Point Load (Raof and Lin 1997).

2.5.3 Configuration 5

Minkarah and Ringo (1982) investigated the loss of cover and flexural bond on rectangular specimens with flexural reinforcement ratios of 0.47%. If the flexural reinforcement was exposed and the bond was lost for up to 31% of the span, there was a

negligible reduction of flexural capacity. This confirms the concept of a critical exposed length of flexural reinforcement, l_c . For specimens with longer exposed flexural reinforcement lengths, l_{exp} , a reduction in flexural capacity with a brittle shear-compression failure of the concrete occurring directly below the point load was observed. The greater l_{exp} the greater the observed reduction in capacity with the greatest reduction being 21% when $l_{exp}/L = 63\%$.

2.5.4 Configurations 6 and 7

Raof and Lin (1993, 1995, 1997) also investigated the behaviour of a simply supported specimens with Configurations 6 and 7 using both small- and large-scale test specimens. They examined the influence of l_{exp} and A_s on the behaviour and capacity of the test specimens, obtaining similar findings as others had observed for other loading configurations (i.e., Cairns and Zhao 1993, Nokhasteh et al. 1992). Increasing either l_{exp} or A_s caused a greater reduction in capacity.

In the same tests, Raof and Lin (1993, 1995, 1997) investigated the influence of the normalized loading position from the left support, α , the distance from the support to the end of the exposed flexural reinforcement length, l_{end} , and the depth of concrete removed, d_c , on the behaviour of specimens with flexural reinforcement ratios of 1.6% for the small-scale tests and 0.75% for the large scale-tests. Their results are consistent with the behaviour of the inclined compressive strut previously described in the discussion of Figure 2-14. As α increases, the inclination of the compressive strut decreases, its location above the end of the exposed length reduces and its failure in

compression is possible. If the applied load is located closer to the end support, the inclined compressive strut will be more vertical and so less likely to intersect the end of the exposed length. If the point load is not located over the exposed length because α is small, the length of specimen between the support and the load behaves as a bonded flexural member. For Raouf and Lin's small-scale test specimens, the capacity reduced as α increased from approximately 0.12 to 0.4, with a maximum reduction in capacity of 50% and 20% when $\alpha = 0.4$, as shown in Figure 2-19. For greater values of α , the capacities increased as shown. A similar result was observed in their large-scale test specimens with the maximum capacity reduction of 25% when $\alpha = 0.4$.

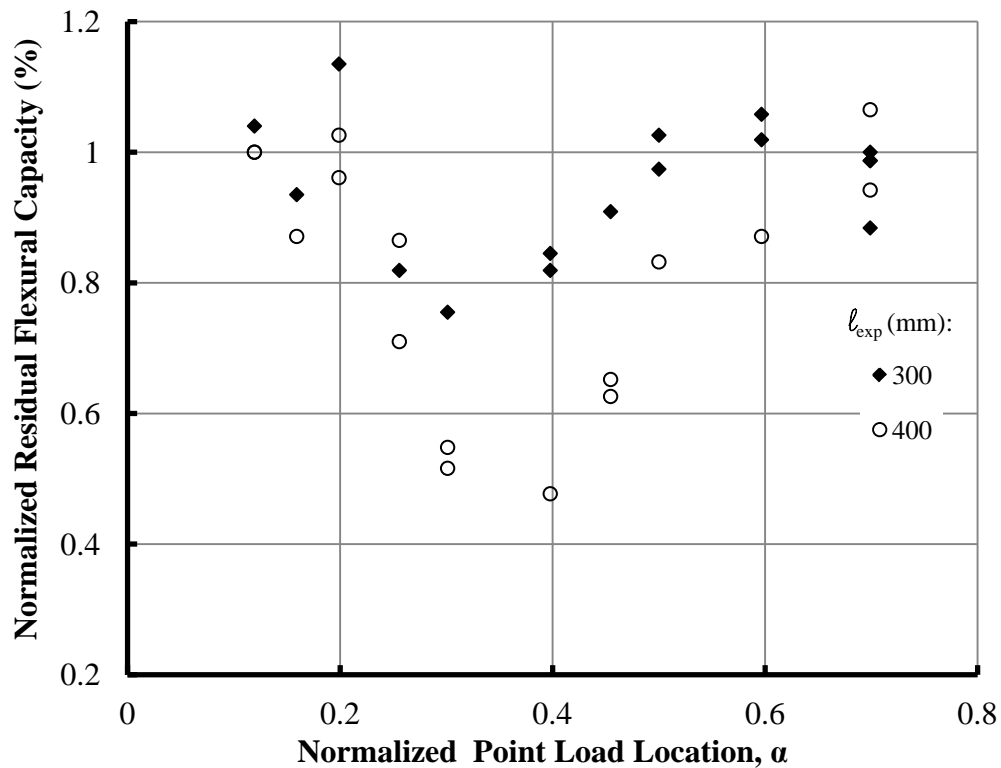


Figure 2-19: Variation of the Reduction in Capacity with Changes in the Position of the Single-point Load: Small-scale Specimens, $L = 1760$ mm (Redrawn from Raouf and Lin 1997).

Similarly, for a given inclination and location of the compressive strut, increasing ℓ_{exp} and so reducing the distance from the support to the exposed end, ℓ_{end} , causes the end of the exposed length to encroach on the inclined compressive strut and could cause failure. Raouf and Lin (1993, 1995, 1997) examined the importance of ℓ_{end} on the capacity of the test specimens in their large-scale tests. For an exposed length, ℓ_{exp} , of 900 mm (i.e., 0.3L) and a normalized point load location, α , of 0.3 there was a 10 % decrease in capacity when ℓ_{end} was reduced from 1200 mm to 100 mm.

Similarly, when the depth of concrete removed, d_c , increases, the distance between the end of the exposed length and the inclined compressive strut decreases until the two intersect and a compression failure of the strut occurs. Raouf and Lin (1993, 1995, 1997) investigated this effect while keeping all other parameters constant. There is no significant reduction in capacity when the concrete is removed slightly beyond the flexural reinforcement. Greater reductions in capacity were observed when the depth of concrete removed was greater than approximately 13% of the full depth of the specimen, depending on ℓ_{exp} (Raouf and Lin 1997). Current Canadian practices require the concrete to be removed to a clear depth of 25 mm behind the flexural reinforcement and therefore large d_c values will not be considered in this current study.

2.6 SUMMARY AND CONCLUSIONS

Previous researchers tested, and developed models for, reinforced concrete specimens with exposed flexural reinforcement subjected to only single- and two-point loading. Seven unique combinations of specimen geometry and load location were investigated. Observed differences in the failure mode, flexural capacity, and crack patterns were

attributed to exposing the flexural reinforcement. The following five distinct failure modes were observed:

1. Yielding of the exposed flexural reinforcement followed by crushing of the concrete on the compression face of the specimen
2. Crushing of the concrete on the compression face of the specimen before yielding of the exposed tensile flexural reinforcement
3. Compression failure in the concrete at the ends of the exposed flexural reinforcement length
4. Anchorage failure between one end of the exposed flexural reinforcement and the adjacent support
5. Shear failure

It can be concluded from this literature review that:

1. A reinforced concrete girder with exposed flexural reinforcement and given dimensional and material properties can exhibit a ductile failure with no reduction in yield capacity if failure modes 2 - 4 are avoided. The longest exposed length that satisfies this requirement has been defined as the critical length of exposed flexural reinforcement, l_c .
2. A reinforced concrete girder with exposed flexural reinforcement, that would exhibit a brittle shear failure if the reinforcement was not exposed, can have increased shear capacity. Further investigation of shear-critical members will not be carried out in the current study because bridge girders are normally designed to

fail in a ductile flexural mode and the limited experimental work shows exposing the flexural reinforcement increases the shear capacity.

3. All specimens investigated were subjected to only single- and two-point loading and few specimens were a T-section. Therefore an experimental investigation involving T-section specimens loaded with a combined uniformly distributed dead load and live load is necessary to more accurately represent the type of girder and applied loading seen in the field.
4. Closure of the gap between the bottom of the concrete web and the exposed flexural reinforcement causes reduction of the effective flexural reinforcement depth and so reduction of the flexural capacity.
5. Of the various parameters previously identified to be important and extensively studied, the following three are deemed worthy of further investigation because they can be controlled during the rehabilitation process: the length of exposed flexural reinforcement, ℓ_{exp} ; the position and type of loading, αL ; and, the distance from the support to the end of the exposed length, ℓ_{end} .

CHAPTER 3: ANALYSIS OF GIRDERS WITH EXPOSED FLEXURAL REINFORCEMENT

3.1 INTRODUCTION

It was concluded from the literature review presented in Chapter 2 that a girder can exhibit a ductile failure with no reduction in yield capacity (e.g., Cairns and Zhao 1993) if the following three conditions are satisfied:

1. The flexural reinforcement yields in tension before the concrete crushes in compression;
2. A concrete compression failure does not occur at the ends of the length of exposed flexural reinforcement; and,
3. The bond between each end of the exposed region and the adjacent support is sufficient.

The longest exposed length that satisfies all three conditions has been defined as the critical length of exposed flexural reinforcement, ℓ_c .

Two analytical approaches will be presented in this chapter: (1) Strain Compatibility Analysis (SCA), and (2) Strut-and-Tie Analysis (STA). Both satisfy horizontal force and moment equilibrium, Eqns. [2.1] and [2.2], respectively. The Strain Compatibility Analysis also satisfies strain compatibility, Eqn. [2.4] and has the capability to predict the stress and strain distributions at all cross sections for all applied load levels. The Strut-and-Tie Analysis is based on the lower bound theorem of plasticity: it has less stringent

compatibility requirements and therefore is only appropriate to predict the behaviour at the ultimate limit state (ULS).

The information presented in this chapter assists practitioners by developing these analyses for the cases where steel yield in tension precedes concrete crushing and no concrete failure occurs at the ends of the exposed flexural reinforcement, i.e., Conditions 1 and 2. Chapter 4 will present an experimental investigation to validate the use of these analyses for determining ℓ_c .

3.2 TYPICAL T-SECTION

The literature review presented in Chapter 2 indicated that most previous experimental investigations involved specimens with rectangular cross sections and all used either single- or two-point loading. Concrete bridge girders typically feature a substantial top slab and resist substantial uniformly distributed dead loads, so these experimental results are not representative. An experimental investigation of T-section specimens loaded with a combination of a uniformly distributed dead load and a point load would more accurately represent the type of girder and applied loading seen in the field. The cross-section of a typical T-section that will be used for developing the two analyses, and the symbols used to define its geometry, is shown in Figure 3-1. These dimensional variables are: overall height, h ; flange width, b_f ; flange thickness, h_f ; web width, b_w ; reduced web height where concrete is removed, h_w ; effective depth of flexural reinforcement, d ; area of flexural reinforcement, A_s ; and, depth of concrete removed, d_c .

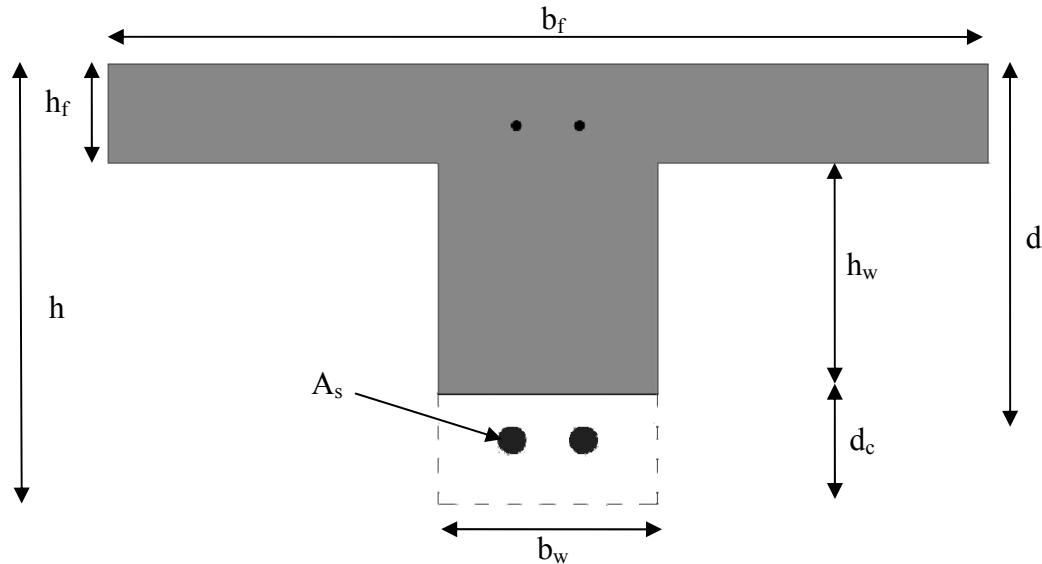


Figure 3-1: Typical T-section Cross-section.

3.3 STRAIN COMPATIBILITY ANALYSIS

Condition 1 addresses the most predominant failure mode observed in previous experimental investigations (e.g., Cairns and Zhao 1993): crushing of the concrete on the compression face of the specimen before the exposed flexural reinforcement yields in tension. It has been previously observed (Harris 1996) that a strut-and-tie model, though simple to develop and analyze, does not accurately describe the general behaviour of a specimen with exposed flexural reinforcement for this particular failure mode when the steel yields before the concrete crushes. Cairns and Zhao (1993) and Harris (1996) developed strain compatibility analyses using Eqns. [2.1], [2.2] and [2.4] representing horizontal force equilibrium, moment equilibrium and compatibility of the elongation of flexural reinforcement and concrete between the ends of the exposed region to determine the flexural capacity of beams with a given length of exposed flexural reinforcement,

l_{exp} .

Cairns and Zhao (1993) do not present their numerical model or the equations for the neutral axis depth in detail. Also, their analysis only considered rectangular sections, whereas a typical reinforced concrete bridge girder is a T-section. Therefore Harris (1996) developed a detailed analysis from first principles for T-sections. His analysis assumed that the concrete had a linear stress-strain relationship in compression, zero tensile strength, and, plane sections remained plane in the concrete section.

3.3.1 Methodology

Eqns. [2.1], [2.2] and [2.4] were used as the basis for the Strain Compatibility Analysis (SCA) to predict the critical length of exposed flexural reinforcement, ℓ_c . The analysis is an incremental procedure, as shown in Figure 3-2, consisting of incrementally increasing the length of exposed flexural reinforcement, ℓ_{exp} , for a girder subjected to a given loading configuration until the horizontal force equilibrium, moment equilibrium and strain compatibility requirements are exactly satisfied. Harris (1996) started his analysis from the same fundamental principles but his resulting equations cannot be derived analytically.

The cross-section, material properties (i.e., concrete strength, f_c' and steel yield strength, f_y), spans, and loadings of the girder must first be defined. The bending moment distribution along the length of the girder, $M(x)$, is then computed, including the magnitude and location of the maximum applied moment, M_{max} . In this Strain Compatibility Analysis, the exposed flexural reinforcement is assumed to yield at the location of M_{max} .

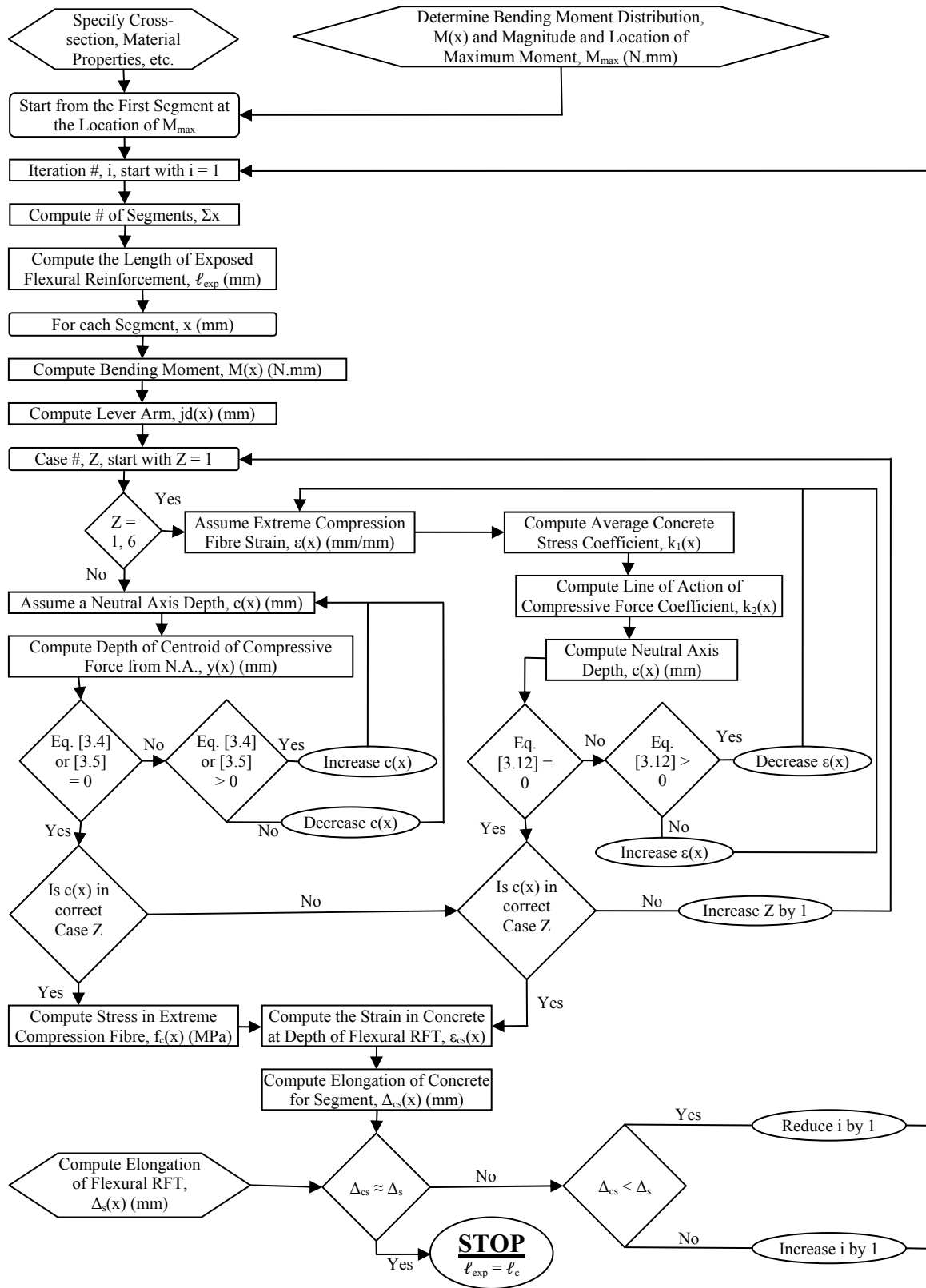


Figure 3-2: Flow Chart Depicting the Incremental Procedure of the Strain Compatibility Analysis (SCA).

The girder is then divided into small segments, of length, Δ_x , located at varying distances x from the left support. Starting from the segments located adjacent to the location of M_{\max} , the first iteration, $i = 1$, is performed. Based on the iteration number, i , the number of segments, n , is computed using the equation:

$$[3.1] \quad n = (2i - 1)$$

The length of exposed flexural reinforcement, ℓ_{exp} , is computed by multiplying the number of segments, n , by the segment length, Δ_x :

$$[3.2] \quad \ell_{\text{exp}} = n\Delta_x$$

At each segment location, x , the bending moment at the centre of the segment, $M(x)$, is determined. Rearranging Eqn. [2.2], to satisfy moment equilibrium, the corresponding lever arm at each segment, $jd(x)$, is computed as:

$$[3.3] \quad jd(x) = \frac{M(x)}{A_s f_y} = \frac{M(x)}{T}$$

The neutral axis depth from the extreme concrete compression fibre, $c(x)$, must be computed for each segment. For the specific T-section shown in Figure 3-1, six unique cases are possible that need to be considered when performing this analysis: either positive or negative curvature with the neutral axis in the flange, Cases 1 and 5, the web, Cases 2 and 6, or off the section, Cases 3 and 4, as shown in Figure 3-3. For positive curvature, Cases 1 to 3, the zone above the neutral axis is in compression and vice versa for Cases 4 to 6. The computation of $c(x)$ requires equations for the depth of the centroid of the resultant compressive force from the neutral axis, $y(x)$, the resultant compressive

force in the concrete, $C(x)$, and the stress in the extreme compression fibre, $f_c(x)$, for these six cases. These are presented in Table 3-1. Setting $C(x)$ equal to the tensile force in the flexural reinforcement, T , yields a rapid solution for $f_c(x)$. The complete derivation of these equations is presented in Appendix B.

Using these equations, an iterative procedure was developed to compute $c(x)$. Starting with the first case, $Z = 1$, a value of $c(x)$ is assumed and the respective $y(x)$ is computed. The geometric requirement of the internal forces shown in Figure 3-3 is, for the positive curvature cases:

$$[3.4] \quad c(x) = d - jd(x) + y(x)$$

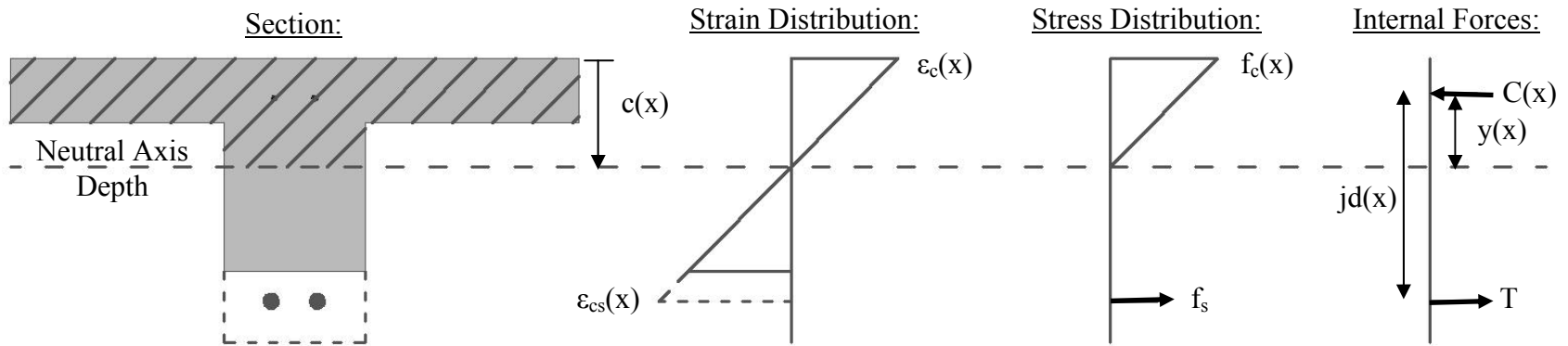
and for the negative curvature cases:

$$[3.5] \quad c(x) = h_w + h_f - d + jd(x) + y(x)$$

The value of $c(x)$ is repeatedly adjusted until the equalities given by Eqns. [3.4] or [3.5] are satisfied.

Once $c(x)$ is determined, its location is checked for consistency with the case assumed. If the assumed case is correct, the respective $f_c(x)$ is computed, otherwise $c(x)$ is recomputed for the next case. For example, the equations for Case 1 are used until $c(x)$ is located at the flange-to-web interface, when the equations for Case 2 become relevant. This procedure is repeated for all remaining cases at the transition zones specified in the “range” column of Table 3-1.

Positive (+ve) Curvature:



Negative (-ve) Curvature:

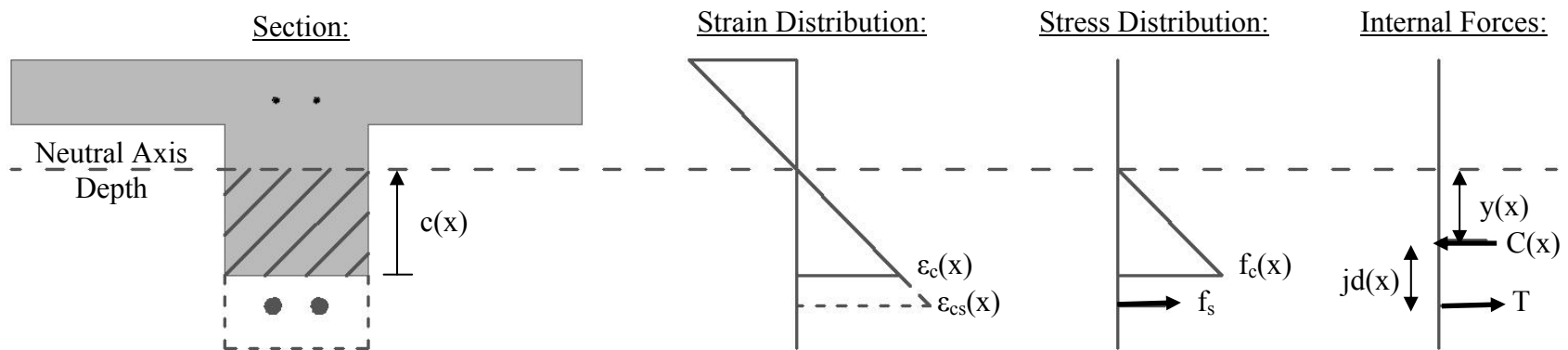
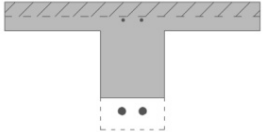
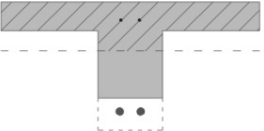
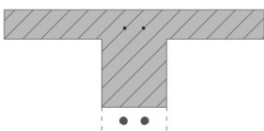
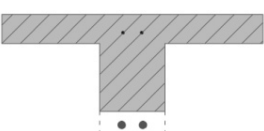
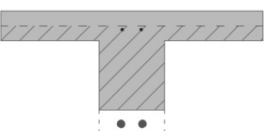
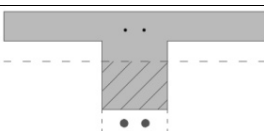


Figure 3-3: Neutral Axis Depth, Strain Distribution, Stress Distribution and Internal Forces for both the Positive (+ve) and Negative (-ve) Curvatures.

Table 3-1: Summary of the Magnitude and Location of the Concrete Compressive Force for each Case (Compression Zone Shaded).

Case	Range	Internal Compressive Force, C(x)	Centroid of Compressive Force, y(x)
	$0 \leq c(x) \leq h_f$	$\frac{f_c}{2} b_f c$	$\frac{2}{3} c$
	$h_f \leq c(x) \leq h_w$	$\frac{f_c b_f c}{2} \left[1 - \left(1 - \frac{b_w}{b_f} \right) \left(1 - \frac{h_f}{c} \right)^2 \right]$	$\frac{2c \left[1 - \left(1 - \frac{b_w}{b_f} \right) \left(1 - \frac{h_f}{c} \right)^3 \right]}{3 \left[1 - \left(1 - \frac{b_w}{b_f} \right) \left(1 - \frac{h_f}{c} \right)^2 \right]}$
	$h_w \leq c(x) \leq \infty$	$\frac{f_c b_f c}{2} \left[1 - \left(1 - \frac{b_w}{b_f} \right) \left(1 - \frac{h_f}{c} \right)^2 - \left(\frac{b_w}{b_f} \right) \left(1 - \frac{h_f}{c} - \frac{h_w}{c} \right)^2 \right]$	$\frac{2c \left[1 - \left(1 - \frac{b_w}{b_f} \right) \left(1 - \frac{h_f}{c} \right)^3 - \left(\frac{b_w}{b_f} \right) \left(1 - \frac{h_f}{c} - \frac{h_w}{c} \right)^3 \right]}{3 \left[1 - \left(1 - \frac{b_w}{b_f} \right) \left(1 - \frac{h_f}{c} \right)^2 - \left(\frac{b_w}{b_f} \right) \left(1 - \frac{h_f}{c} - \frac{h_w}{c} \right)^2 \right]}$
	$(h_f + h_w) \leq c(x) \leq \infty$	$\frac{f_c b_f c}{2} \left[\left(\frac{b_w}{b_f} \right) + \left(1 - \frac{b_w}{b_f} \right) \left(1 - \frac{h_w}{c} \right)^2 - \left(1 - \frac{h_f}{c} - \frac{h_w}{c} \right)^2 \right]$	$\frac{2c \left[\frac{b_w}{b_f} + \left(1 - \frac{b_w}{b_f} \right) \left(1 - \frac{h_w}{c} \right)^3 - \left(1 - \frac{h_f}{c} - \frac{h_w}{c} \right)^3 \right]}{3 \left[\frac{b_w}{b_f} + \left(1 - \frac{b_w}{b_f} \right) \left(1 - \frac{h_w}{c} \right)^2 - \left(1 - \frac{h_f}{c} - \frac{h_w}{c} \right)^2 \right]}$
	$h_w \leq c(x) \leq (h_f + h_w)$	$\frac{f_c b_f c}{2} \left[\frac{b_w}{b_f} + \left(1 - \frac{b_w}{b_f} \right) \left(1 - \frac{h_w}{c} \right)^2 \right]$	$\frac{2c \left[\left(\frac{b_w}{b_f} \right) + \left(1 - \frac{b_w}{b_f} \right) \left(1 - \frac{h_w}{c} \right)^3 \right]}{3 \left[\left(\frac{b_w}{b_f} \right) + \left(1 - \frac{b_w}{b_f} \right) \left(1 - \frac{h_w}{c} \right)^2 \right]}$
	$0 \leq c(x) \leq h_w$	$\frac{f_c}{2} b_w c$	$\frac{2}{3} c$

The linear stress-strain compressive relationship for the concrete, as used by Harris (1996), is unrealistic for Cases 1 and 6 due to the high stresses and strains present at the extreme compression fibre. Therefore the compressive stress-strain relationship for concrete developed by Todeschini (1964) outlined in MacGregor and Bartlett (2000) was used for these cases. Todeschini postulated that the concrete stress, f_c , at a given strain, ϵ_c , may be computed as:

$$[3.6] \quad f_c = \frac{2f_c''(\epsilon_c/\epsilon_c')}{1 + (\epsilon_c/\epsilon_c')^2}$$

In Eqn. [3.6], f_c'' is the maximum compressive stress, occurring at a strain ϵ_c' , and is usually taken to be $0.9f_c'$ (MacGregor and Bartlett 2000) to give results similar to those obtained using the rectangular stress block when the maximum extreme compression fibre strain, ϵ_{cu} , equals 0.0035 (CSA 2006).

The strain corresponding to the maximum compressive stress in the stress-strain relationship, ϵ_c' , is computed (MacGregor and Bartlett 2000) as:

$$[3.7] \quad \epsilon_c' = \frac{1.71f_c'}{E_c}$$

where E_c is the modulus of elasticity of concrete, MPa, given by (CSA 2006):

$$[3.8] \quad E_c = (3000\sqrt{f_c'} + 6900) \left(\frac{\gamma_c}{2300} \right)^{1.5}$$

and γ_c is the mass density of concrete, kg/m^3 , assumed to equal 2300 kg/m^3 for normal concrete.

Figure 3-4 shows Todeschini's stress-strain relationship for a concrete strength of 40 MPa. In this case $E_c = 25870$ MPa and, from Eq. [3.7], $\epsilon_c' = 0.0026$.

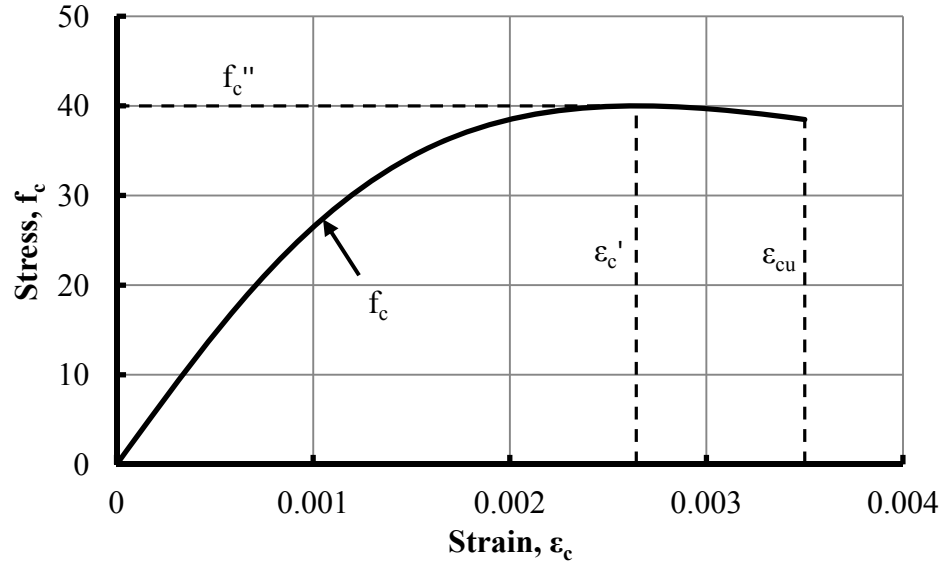
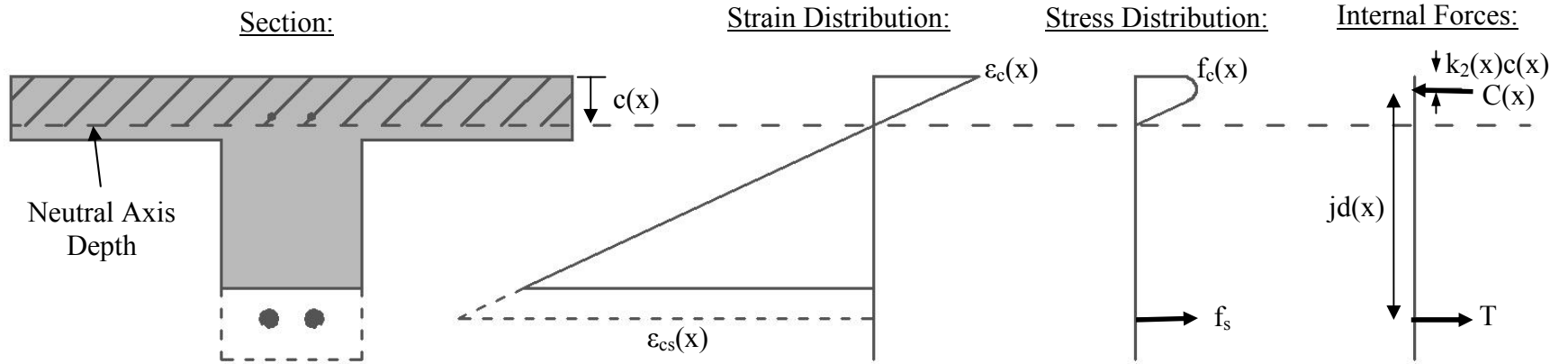


Figure 3-4: Todeschini's Compressive Stress-strain Relationship for a Concrete Strength, f'_c , of 40 MPa.

The iterative procedure to compute $c(x)$ changes for Cases 1 and 6 to accommodate the use of Todeschini's stress-strain relationship, but remains the same for Cases 2 to 5. The revised section, stress and strain distributions and internal force diagram for Cases 1 and 6 are shown in Figure 3-5. For each segment, an extreme compression fibre strain, $\epsilon_c(x)$, is assumed: at M_{\max} , the maximum value, ϵ_{cu} , of 0.0035 (CSA 2006) is adopted.

Case 1:



Case 6:

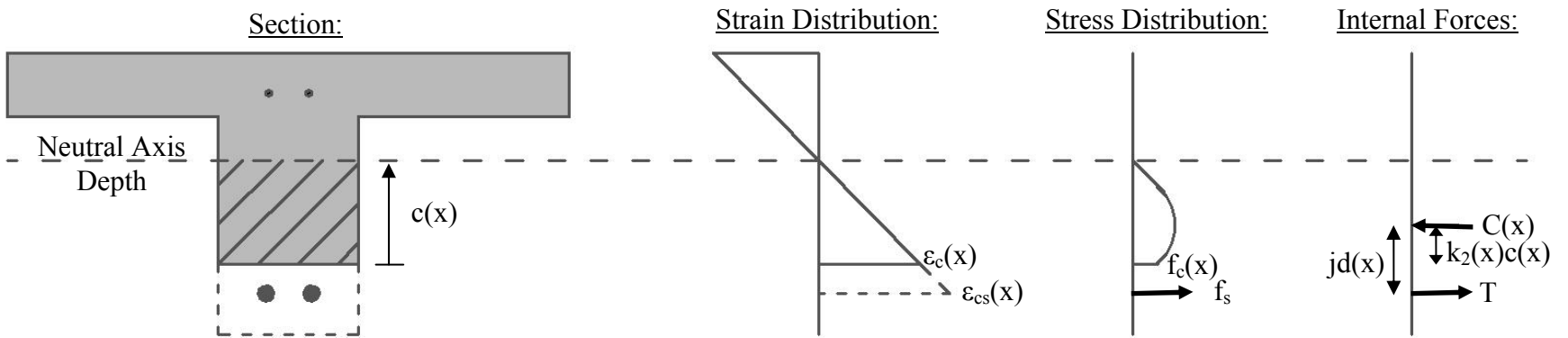


Figure 3-5: Revised Neutral Axis Depth, Strain Distribution, Stress Distribution and Internal Forces for Cases 1 and 6.

The coefficients that define the average stress and the line of action of the resultant compressive force, $k_1(x)$ and $k_2(x)$, respectively, are computed using the equations (MacGregor and Bartlett 2000):

$$[3.9] \quad k_1(x) = \frac{\ln\left(1 + \left(\frac{\epsilon_c(x)}{\epsilon_c'}\right)^2\right)}{\left(\frac{\epsilon_c(x)}{\epsilon_c'}\right)}$$

$$[3.10] \quad k_2(x) = 1 - \frac{2\left(\left(\frac{\epsilon_c(x)}{\epsilon_c'}\right) - \tan^{-1}\left(\frac{\epsilon_c(x)}{\epsilon_c'}\right)\right)}{\left(\frac{\epsilon_c(x)}{\epsilon_c'}\right)^2 k_1(x)}$$

Using $jd(x)$ and $k_2(x)$, $c(x)$ is computed to satisfy the following geometric requirement of the internal forces in Figure 3-5:

$$[3.11] \quad c(x) = \frac{(d - jd(x))}{k_2(x)}$$

To satisfy horizontal force equilibrium, the summation of the resultant compressive force in the concrete, $C(x)$, and the tensile force in the exposed flexural reinforcement, T , must equal to zero:

$$[3.12] \quad k_1(x)f_cbc(x) - A_s f_y = 0$$

where b is the width of the compression zone (i.e., b_f for Case 1 and b_w for Case 6).

For the segment located at M_{\max} , the horizontal force equilibrium requirement is satisfied for $\epsilon_{cu} = 0.0035$, but for the remaining segments, $\epsilon_c(x)$ must be repeatedly changed until Eqn. [3.12] is satisfied. If the left hand side of Eqn. [3.12] exceeds zero, $\epsilon_c(x)$ is decreased, and vice versa.

Once $\varepsilon_c(x)$, $f_c(x)$ and the correct $c(x)$ are computed, the extrapolated strain in the concrete at the depth of the flexural reinforcement is next determined for each segment, $\varepsilon_{cs}(x)$, using the strain distribution shown in Figure 3-5. For the positive curvature cases:

$$[3.13] \quad \varepsilon_{cs}(x) = \varepsilon_c(x) \left(1 - \frac{d}{c(x)} \right)$$

and for the negative curvature cases:

$$[3.14] \quad \varepsilon_{cs}(x) = \varepsilon_c(x) \left(1 + \frac{d - (h_w + h_f)}{c(x)} \right)$$

where, for Cases 2 to 5:

$$[3.15] \quad \varepsilon_c(x) = \frac{f_c(x)}{E_c}$$

To satisfy the strain compatibility requirement, Eqn. [2.4], the summation of the concrete elongation at the depth of the flexural reinforcement, Δ_{cs} , over the length of the exposed flexural reinforcement, computed as:

$$[3.16] \quad \Delta_{cs} = \int^{\ell_{exp}} \varepsilon_{cs} d\ell \approx \sum_{i=1}^n \varepsilon_{cs}(x) \Delta_x$$

must equal the elongation of the exposed flexural reinforcement, Δ_s , computed as:

$$[3.17] \quad \Delta_s = \frac{T \ell_{exp}}{A_s E_s}$$

where E_s is the modulus of elasticity of the flexural reinforcement, taken as 200000 MPa.

If Δ_{cs} and Δ_s are not equal, the length of exposed flexural reinforcement, ℓ_{exp} , is incorrect. If Δ_{cs} is greater than Δ_s , ℓ_{exp} is increased by increasing the iteration number, i , by one, and vice versa. Increasing i by one, increases ℓ_{exp} by one segment length towards each support as shown in Eqns. [3.1] and [3.2]. This iterative procedure is repeated until the values of Δ_{cs} and Δ_s are within 1% of one another, i.e.:

$$[3.18] \quad \frac{|\Delta_s - \Delta_{cs}|}{\Delta_s} \leq 0.01$$

The length that satisfies this requirement is defined as the critical length of exposed flexural reinforcement, ℓ_c , and represents the longest length that can be exposed while ensuring that the girder will reach its yield capacity.

3.4 STRUT-AND-TIE ANALYSIS

Condition 2 addresses another important failure mode that was observed by others (Cairns and Zhao 1993): crushing of the concrete at the end of the exposed length due to the compressive strut intersecting the exposed end. For a given loading configuration, the critical distance from the support to the end of the exposed length, ℓ_e , can be determined to ensure this failure will not occur. Harris (1996) previously developed a strut-and-tie model to predict the flexural capacity of a T-section specimen with exposed flexural reinforcement for Condition 1 but did not analyze the possibility of the ends of the exposed length encroaching on the inclined compressive strut, significantly reducing its area and possibly its capacity.

3.4.1 Methodology

A strut-and-tie model was developed for the current Strut-and-Tie Analysis (STA) to predict the critical length of exposed flexural reinforcement, ℓ_e . The analysis is a procedure to determine the length from the support to the point where the inclined compressive strut intersects the ends of the exposed length for a girder subjected to a given loading configuration. This distance has been defined as the critical distance from the support to the end of the exposed length, ℓ_e . The solution requires the following assumptions:

1. The depth of the top compressive strut or node at the location of the maximum moment, M_{\max} , must be assumed. The maximum thickness, h_s , is assumed to equal the stress block depth at yield of the identical beam with no reinforcement exposed.
2. The height of the node at both supports, h_a , is assumed to be symmetric about the resultant of the flexural reinforcement tension. For a girder with one layer of flexural reinforcement, the maximum height, h_{\max} , is $2(h - d)$.
3. The deteriorated concrete is assumed to be removed to a clear depth of 25 mm above the exposed flexural reinforcement.

For the basic geometry of the left compressive strut, as shown in Figure 3-6, the critical distance from the support to the end of the exposed length, ℓ_e , is determined:

$$[3.19] \quad \frac{w}{2\cos\theta_s} + d_c = (h - d) + \ell_e \tan\theta_s$$

where w and θ_s are the width and inclination from the horizontal, respectively, of the compressive strut.

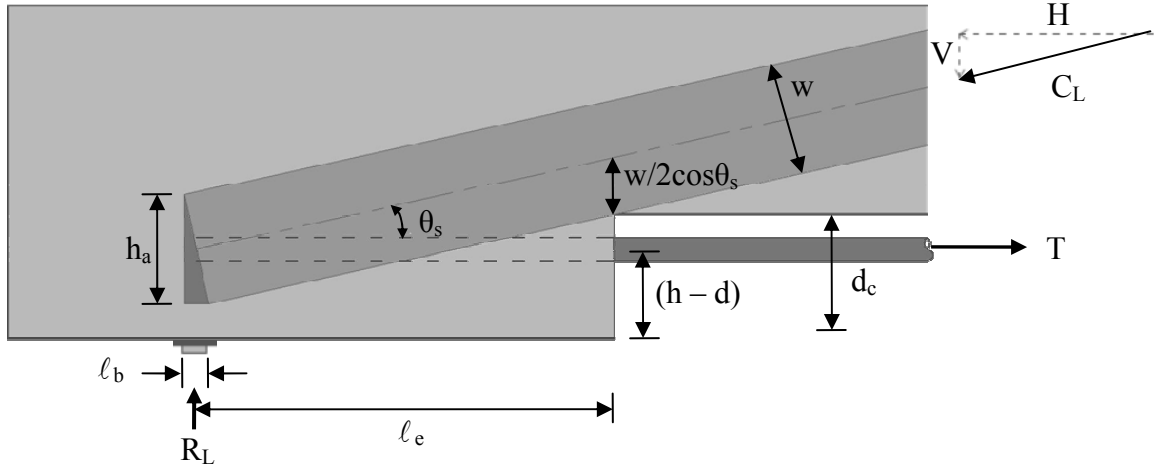


Figure 3-6: Basic Geometry of the Left Compressive Strut.

Recognizing that $w/\cos\theta_s = h_a + l_b \tan\theta_s$:

$$[3.20] \quad \frac{h_a}{2} + \frac{l_b}{2} \tan\theta_s + d_c = (h - d) + l_e \tan\theta_s$$

Rearranging:

$$[3.21] \quad l_e = \frac{(d + d_c - h + h_a/2)}{\tan\theta_s} + \frac{l_b}{2}$$

where:

$$[3.22] \quad \tan\theta_s = \frac{V}{H} = \frac{V}{T} = \frac{R_L j d_{\max}}{M_{\max}}$$

and, l_b is the length of the bearing at the left support, H is the horizontal component of the compressive strut force equal to the tensile force in the flexural reinforcement, V is

the vertical component of the compressive strut force equal to the reaction at the left support, R_L , and jd_{\max} is the lever arm at the location of the maximum moment, M_{\max} .

The length of the bearing at the left support, l_b , is:

$$[3.23] \quad l_b = w \sin \theta_s$$

The required constant width of the compressive strut at the support, w , is:

$$[3.24] \quad w = \frac{C_L}{b_w f_{cu}} = \frac{R_L}{b_w f_{cu} \sin \theta_s}$$

where C_L is the force in the compressive strut, and f_{cu} is the limiting compressive stress in the node or the strut.

Since the shear reinforcement is exposed and so does not create transverse tensile strains in the strut, the compressive strut stress limit will be assumed to be adequate and the stress in the node will govern. The most critical node in this strut-and-tie model is the compression-compression-tension node (CCT) located at the support, with a stress limit of (CHBDC 8.10.5.1):

$$[3.25] \quad f_{cu} = 0.88 \alpha_1 f_c'$$

where α_1 is the ratio of the average stress in a rectangular compression block to the specific concrete strength, defined in Clause 8.8.3(f) of the CHBDC (CSA 2006) as $\alpha_1 = 0.85 - 0.015 f_c'$.

By eliminating w using Eqn. [3.24], Eqn. [3.23] simplifies to:

$$[3.26] \quad \ell_b = \frac{V \sin \theta_s}{b_w f_{cu} \sin \theta_s} = \frac{R_L}{b_w f_{cu}}$$

The height of the node at the left support, h_a , is:

$$[3.27] \quad h_a = w \cos \theta = \frac{V \cos \theta_s}{b_w f_{cu} \sin \theta_s} = \frac{V}{b_w f_{cu} \tan \theta_s} = \frac{VM_{\max}}{Vj d_{\max} b_w f_{cu}} = \frac{M_{\max}}{j d_{\max} b_w f_{cu}} \leq h_{\max}$$

Eliminating $\tan \theta_s$, ℓ_b and h_a from Eqn. [3.21]:

$$[3.28] \quad \ell_e = \frac{M_{\max} (d + d_c - h + (M_{\max} / 2j d_{\max} b_w f_{cu}))}{R_L j d_{\max}} + \frac{R_L}{2b_w f_{cu}}$$

This ℓ_e value represents the minimum distance from the exposed end to the support for the inclined compressive strut not to intersect the exposed end.

To quantify the effect of different loading configurations on the critical distance from the support to the end of the exposed length, ℓ_e , three load combinations are analyzed. They comprise of: (1) a point load P , located at a distance of αL from one support, where $0.1 \leq \alpha \leq 0.9$; (2) a uniformly distributed load, simulated by four equally spaced point loads, ω ; and, (3) combined point and simulated uniformly distributed loads. For each combination considered, M_{\max} , $j d_{\max}$, and R_L are known and h_a and ℓ_b are computed to determine ℓ_e .

3.4.2 Case 1: Point Load ($\omega = 0$)

The single point-load magnitude, P , causing a moment that equals the flexural capacity of the beam was determined for given α values, as shown in Figure 3-7. The strut is narrow

in the wide flange region and increases its depth in the narrower web region to maintain a constant cross-sectional area, as shown.

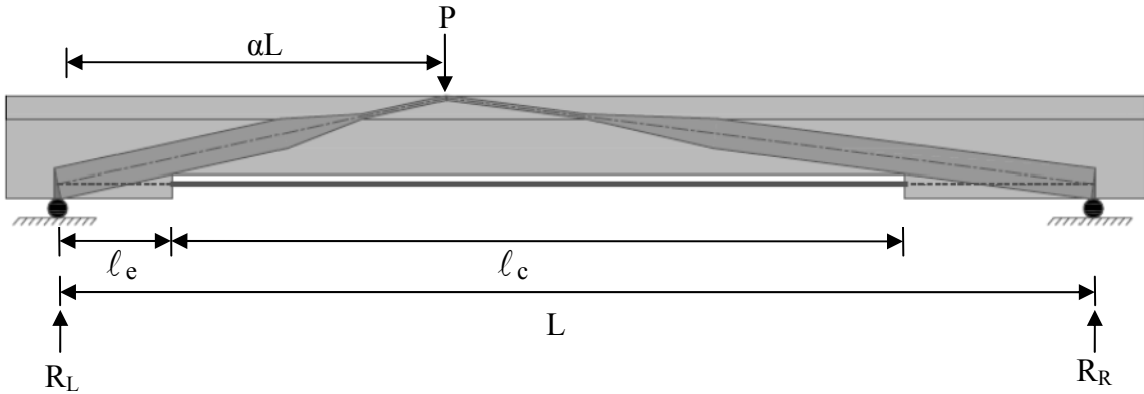


Figure 3-7: Loading for Case 1 ($\alpha = 0.375$ shown).

For a known value of α , simple moment equilibrium requires that the applied load, P , satisfy:

$$[3.29] \quad P = \frac{M}{L(\alpha - \alpha^2)}$$

where M is the moment capacity of the cross section.

The reaction at the left support is:

$$[3.30] \quad R_L = P(1 - \alpha)$$

Using Eqn. [3.22]:

$$[3.31] \quad \tan\theta_s = \frac{R_L j d_{\max}}{M_{\max}} = \frac{j d_{\max}}{L} \left(\frac{1 - \alpha}{\alpha(1 - \alpha)} \right) = \frac{j d_{\max}}{\alpha L}$$

The width of the compressive strut can be assumed to be constant and therefore l_e is:

$$[3.32] \quad l_e = \frac{\alpha L \left(d + d_c - h + \left(\frac{PL(\alpha - \alpha^2)}{2j d_{\max} b_w f_{cu}} \right) \right)}{j d_{\max}} + \frac{R_L}{2b_w f_{cu}}$$

Rearranging:

$$[3.33] \quad \ell_e = \frac{\alpha L}{jd_{\max}} \left(d + d_c - h + \left(\frac{PL(\alpha - \alpha^2)}{2jd_{\max} b_w f_{cu}} \right) \right) + \frac{P(1 - \alpha)}{2b_w f_{cu}}$$

The critical exposed length, ℓ_c , is:

$$[3.34] \quad \ell_c = L - [\ell_e(@\alpha) + \ell_e(@1 - \alpha)]$$

Where $\ell_e (@\alpha)$ is the value of ℓ_e computed using Eqn. [3.33] for the given α value.

Eqn. [3.33] defines the critical distance ℓ_e in terms of the normalized point load location, α . As shown in Figure 3-8 for the beam tested by Harris (1996), as α increases, moving the load away from the left support, ℓ_e increases linearly, demonstrating that the flatter struts carrying shear to the lesser reaction are the most critical.

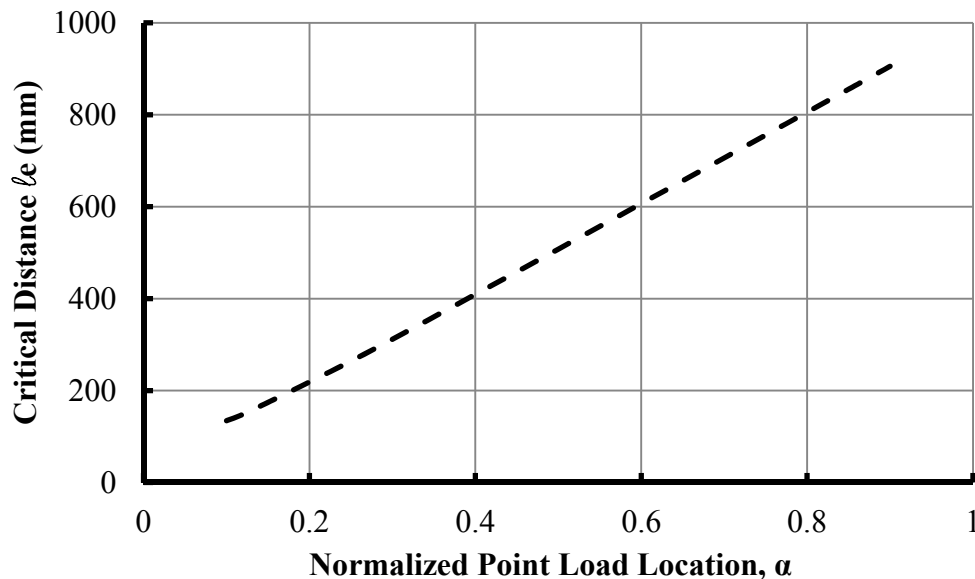


Figure 3-8: Effect of the Location of the Point Load on the Critical Distance to the End of the Exposed Length, ℓ_c , at Yield.

3.4.3 Case 2: Uniformly Distributed Load ($\omega \neq 0, P = 0$)

For this case, $P = 0$ and the four equal point loads, each ω , causing a moment due to a simulated uniformly distributed load that equals the flexural capacity of the beam were determined, as shown in Figure 3-9. Since the locations of the point loads are constant as shown, the profile of the strut centerline is constant at all load levels. Again, the width of the strut varies to maintain a constant strut cross-sectional area.

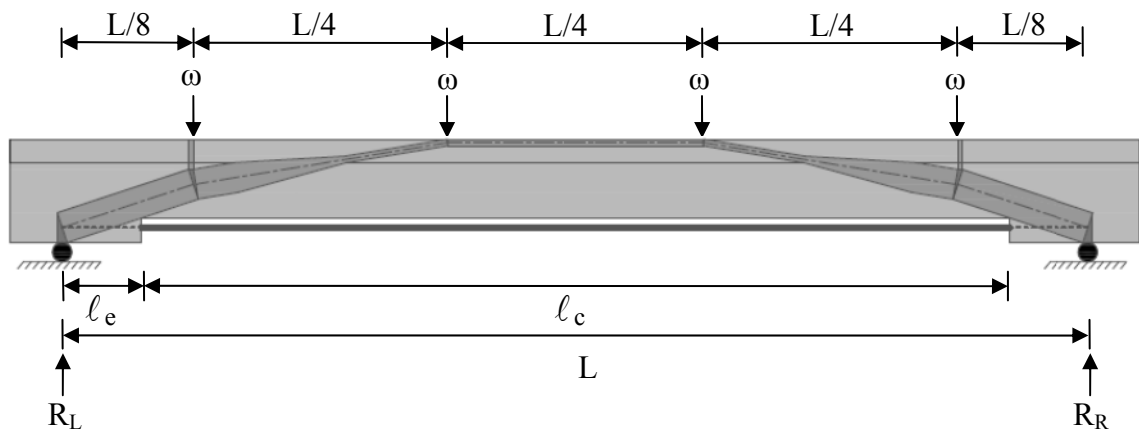


Figure 3-9: Loading for Case 2.

The shear force, V , and bending moment, M , diagrams, as shown in Figure 3-10 are first determined.

The moment at the midspan is set equal to M :

$$[3.35] \quad M = \frac{\omega L^2}{8} \Rightarrow \frac{\omega L}{4} = \frac{2M}{L}$$

The reaction at the left support at yield is:

$$[3.36] \quad R_L = \frac{\omega L}{2}$$

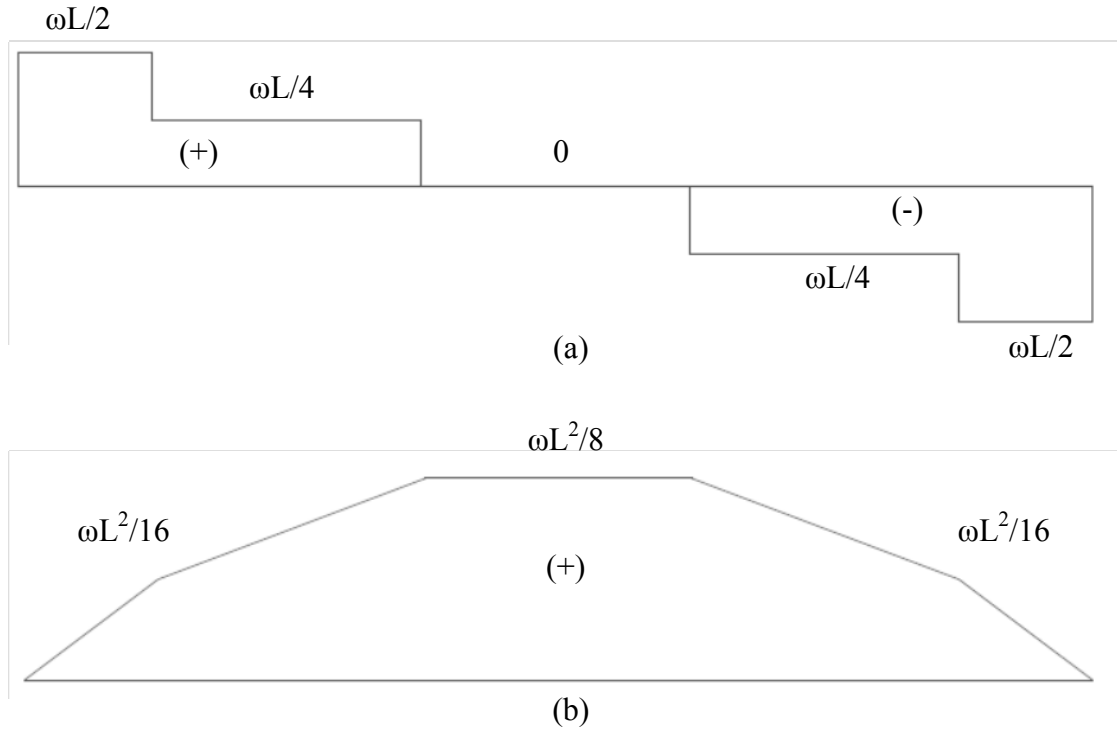


Figure 3-10: Load Case 2: (a) Shear Force Diagram, (b) Bending Moment Diagram.

Using Eqn. [3.22]:

$$[3.37] \quad \tan\theta_s = \frac{R_L j d_{\max}}{M_{\max}} = j d_{\max} \left(\frac{\omega L}{2} \frac{8}{\omega L^2} \right) = \frac{4j d_{\max}}{L}$$

The width of the compression strut can be assumed to be constant and therefore ℓ_e is:

$$[3.38] \quad \ell_e = \frac{L \left(d + d_c - h + (\omega L^2 / 16 j d_{\max} b_w f_{cu}) \right)}{4j d_{\max}} + \frac{\omega L}{4b_w f_{cu}}$$

Rearranging:

$$[3.39] \quad \ell_e = \frac{L}{4j d_{\max}} \left(d + d_c - h + \frac{\omega L^2}{16 j d_{\max} b_w f_{cu}} \right) + \frac{\omega L}{4b_w f_{cu}}$$

For this single loading configuration, the critical distance from the support to the end of the exposed length, ℓ_e , to equilibrate the yield flexural capacity of the beam tested by Harris (1996) is 264.2 mm. The critical exposed length, ℓ_c , is:

$$[3.40] \quad \ell_c = L - 2\ell_e$$

giving values at yield of 3472 mm. In Load Case 1, the least severe case occurs with the point load at midspan, $\alpha = 0.5$, for which the critical exposed length, ℓ_c , is 2985 mm at yield. The critical exposed length, ℓ_c , for Load Case 2 exceeds this value but the critical distance ℓ_e is shorter for Load Case 1 if $0.25 \gtrsim \alpha \gtrsim 0.75$.

3.4.4 Case 3: Both Point and Uniformly Distributed Loads ($\omega \neq 0$, $P \neq 0$)

Different combinations of a simulated uniformly distributed load, ω , and a point load P located at $0.1 \leq \alpha \leq 0.9$, as shown in Figure 3-11, were determined that would cause the maximum applied moment to be equal to the flexural capacity of the beam. The ratio of the point load to the total distributed load is denoted as K , i.e., $K = P/\omega L$. Because a uniformly distributed dead load is assumed always present, $K \geq 0$.

A typical reinforced concrete bridge, consisting of reinforced concrete girders and slab, was analyzed to determine that the ratio of the live load moment to the total moment was approximately $0.5 \leq M_L/M_T \leq 0.8$. The analysis is presented in Appendix C. Therefore the moment due to the point load would be 1 to 4 times that due to the simulated uniformly distributed load, M_ω :

$$[3.41] \quad M_P = (1.0 \text{ to } 4.0)M_\omega$$

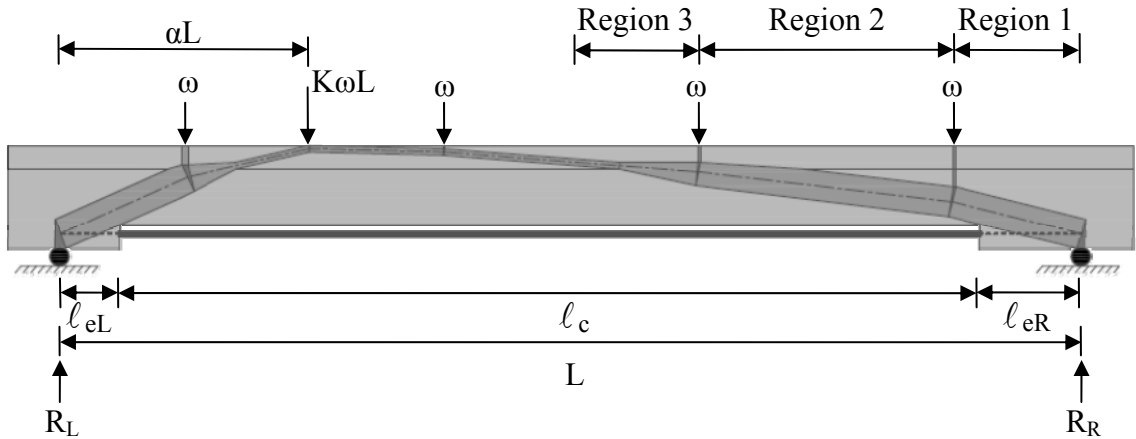


Figure 3-11: Loading for Case 3 ($\alpha = 0.25$ Shown).

Substituting in the maximum moment equations for M_L and M_D :

$$[3.42] \quad \frac{PL}{4} = (1.0 \text{ to } 4.0) \frac{\omega L^2}{8}$$

From Eqn. [3.42], for $P = K\omega L$:

$$[3.43] \quad \omega L^2 K = 4(1.0 \text{ to } 4.0) \frac{\omega L^2}{8}$$

which simplifies to, $K = 0.5$ to 2.0 .

The maximum moment (i.e., $V = 0$) can occur in one of the following three regions (for $\alpha \leq 0.5$):

Region 1: 0 to $L/8$ (from the left support)

Region 2: $L/8$ to $3L/8$ (from the left support)

Region 3: $3L/8$ to $L/2$ (from the left support)

The procedure to determine the maximum moment, M_{\max} , and its location in each region is as follows:

1. The normalized location, α , of the point load $K\omega L$ is known.
2. Limits for K are determined for each possible location of M_{\max} by assuming that the shear force, V , is 0.
3. The reaction at the left support, R_L , is calculated:

$$[3.44] \quad R_L = \frac{\omega L}{2} + K\omega L(1 - \alpha) = \omega L[0.5 + K(1 - \alpha)]$$

4. The method of sections is used to calculate the moment at $L/8$, $3L/8$ and αL and M_{\max} is defined as the greatest of these values.
5. The inclination of the compressive strut at the left support, θ_{sL} , is calculated using Eqn. [3.22].
6. The width of the compressive strut is assumed to be constant and the critical distance from the support to the left end of the exposed length, ℓ_{eL} , is:

$$[3.45] \quad \ell_{eL} = \frac{(d + d_c - h + (M_{\max}/2jd_{\max}b_w f_{cu}))}{\tan\theta_{sL}} + \frac{R_L}{2b_w f_{cu}}$$

7. A similar procedure is used to calculate θ_{sR} and ℓ_{eR} for the compressive strut at the right support.
8. The critical exposed length, ℓ_c , is:

$$[3.46] \quad \ell_c = L - \ell_{eL} - \ell_{eR}$$

The procedure outlined in Steps 1 - 5 was performed for the three regions, yielding the results shown in Table 3-2. The procedures for determining $\tan\theta_{sL}$ and $\tan\theta_{sR}$ and the location of the maximum moment, M_{max} , both depend on the normalized location of the point load, α , and the ratio of the point load to the total distributed load, K , as shown Table 3-2. The detailed calculations for this procedure are presented in Appendix B.

Table 3-2: Summary of Critical Values for Load Case 3.

α	K	$\tan\theta_{sL}$	$\tan\theta_{sR}$	M_{max} at
	$\geq \frac{0.5}{\alpha}$	$\left(\frac{jd}{\alpha L}\right)$	$\left(\frac{[0.5+K\alpha] \quad jd}{\alpha[0.5+K(1-\alpha)] \quad L}\right)$	αL
≤ 0.125	$\frac{0.25}{\alpha} \leq K \leq \frac{0.5}{\alpha}$	$\left(\frac{8[0.5+K(1-\alpha)] \quad jd}{[0.5+7K\alpha] \quad L}\right)$	$\left(\frac{8[0.5+K\alpha] \quad jd}{[0.5+7K\alpha] \quad L}\right)$	$\frac{L}{8}$
	$\leq \frac{0.25}{\alpha}$	$\left(\frac{8[0.5+K(1-\alpha)] \quad jd}{[1.0+5K\alpha] \quad L}\right)$	$\left(\frac{8[0.5+K\alpha] \quad jd}{[1.0+5K\alpha] \quad L}\right)$	$\frac{3L}{8}$
$0.125 \leq \alpha \leq 0.375$	$\geq \frac{0.25}{\alpha}$	$\left(\frac{8[0.5+K(1-\alpha)] \quad jd}{[2\alpha+8\alpha K(1-\alpha)+0.25] \quad L}\right)$	$\left(\frac{8[0.5+K\alpha] \quad jd}{[2\alpha+8\alpha K(1-\alpha)+0.25] \quad L}\right)$	αL
	$\leq \frac{0.25}{\alpha}$	$\left(\frac{8[0.5+K(1-\alpha)] \quad jd}{[1.0+5K\alpha] \quad L}\right)$	$\left(\frac{8[0.5+K\alpha] \quad jd}{[1.0+5K\alpha] \quad L}\right)$	$\frac{3L}{8}$
≥ 0.375	-	$\left(\frac{8[0.5+K(1-\alpha)] \quad jd}{[1.0+8K\alpha(1-\alpha)] \quad L}\right)$	$\left(\frac{8[0.5+K\alpha] \quad jd}{[1.0+8K\alpha(1-\alpha)] \quad L}\right)$	αL

The equations shown in Table 3-2 were used to determine ℓ_{eL} for all three regions. Figure 3-12 show the resulting relation between the normalized location of the point load, α , and the critical distance ℓ_{eL} , for specific values of K ranging from 0.5 to 2.0, at yield for the beam tested by Harris (1996). As α increases, ℓ_{eL} also increases, reaching a maximum value at yield at approximately $\alpha \approx 0.625$, indicating the critical case occurs at

the left support when the point load is slightly to the right of midspan. For $\alpha \gtrsim 0.625$, ℓ_{eL} begins to decrease, demonstrating the affect of the distributed load on the critical distance ℓ_{eL} .

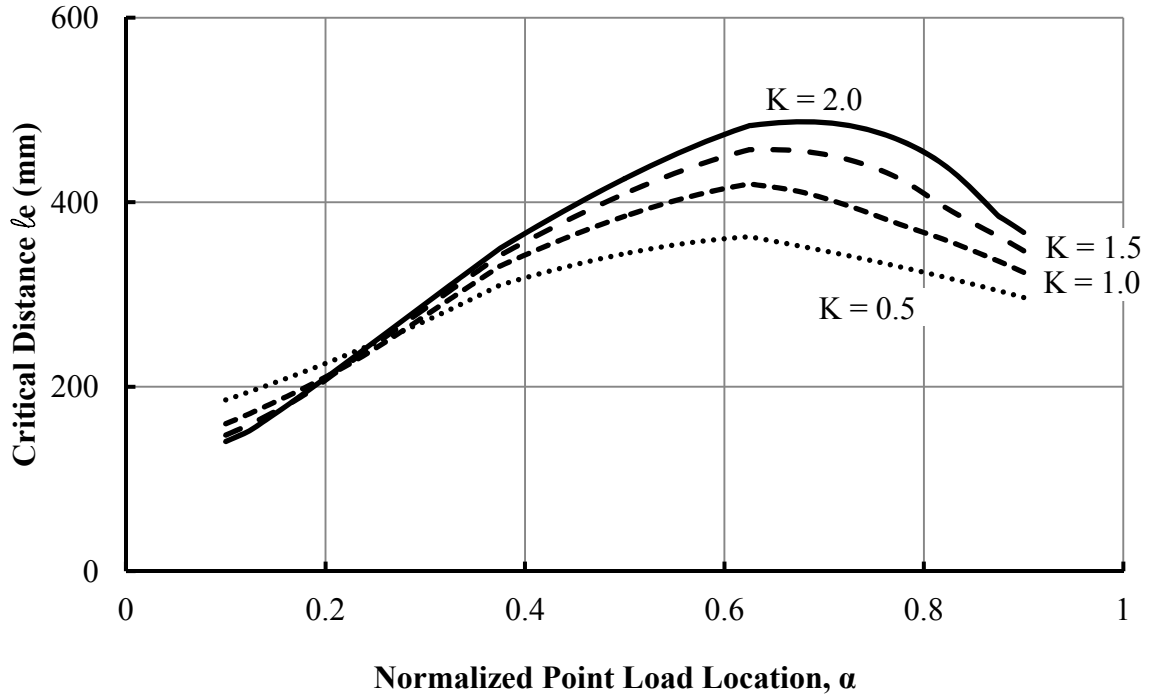


Figure 3-12: Effect of the Location of the Point Load on the Critical Distance to the End of the Exposed Length, ℓ_{eL} , for Different Values of K at Yield.

The results also show that as the relative contribution of the point load to the total load, K , increases, ℓ_{eL} decreases for $\alpha \lesssim 0.25$, and increases for $\alpha \gtrsim 0.25$ because, as shown in Table 3-2, for $\alpha \lesssim 0.25$, an increase in K will increase the moment at αL , increasing the inclination of the compressive strut at the left support, and subsequently decreasing ℓ_{eL} . Similarly, for $\alpha \gtrsim 0.25$, an increase in K will increase the moment at αL , but will also decrease the moment at $L/8$. This reduces the inclination of the compressive strut at the left support, θ_{sL} , and therefore increases ℓ_{eL} . The maximum ℓ_{eL} observed at yield was 465 mm when $K = 2$.

3.4.5 Comparisons

Figure 3-13 show the relationship between α and ℓ_{eL} at yield for all three load cases. The simulated uniformly distributed load, ω , significantly affects the critical distance ℓ_{eL} . If a distributed load is present, as is typical, ℓ_{eL} is reduced. As α reduces below approximately 0.25, Case 3 approaches Case 1 with ℓ_{eL} reducing linearly with α . As α approaches 0.1, ℓ_{eL} for Case 3 begins to level out and approach Case 2. For $\alpha > 0.625$, a similar result is seen where Case 3 approaches Case 2 with ℓ_{eL} decreasing towards $\alpha = 1$.

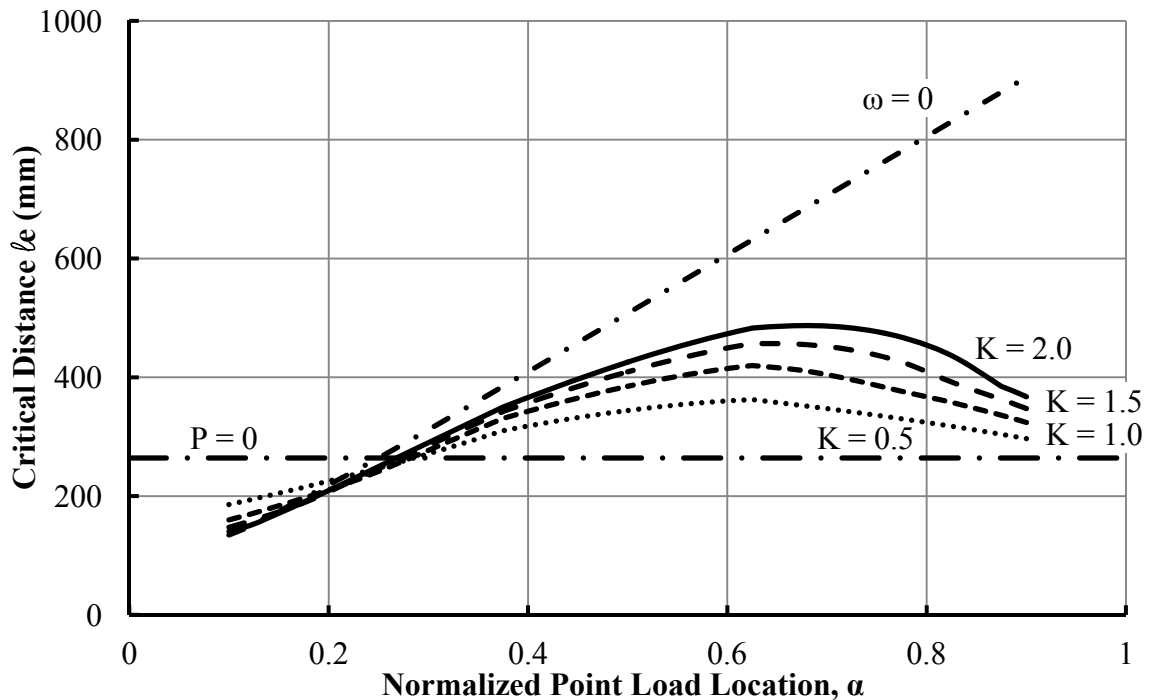


Figure 3-13: Effect of the Location of the Point Load on the Critical Distance to the End of the Exposed Length, ℓ_{eL} , at Yield for Load Cases 1, 2 and 3.

3.5 SUMMARY AND CONCLUSIONS

In this chapter, two analytical approaches have been developed to assist practitioners evaluating typical reinforced concrete bridge girders with exposed flexural reinforcement: (1) Strain Compatibility Analysis (SCA), and (2) Strut-and-Tie Analysis (STA). Both were based on the horizontal force and moment equilibrium, and the Strain Compatibility Analysis also satisfies strain compatibility requirements, Eqns. [2.1], [2.2] and [2.4], respectively. The analyses can be used for any length and location of exposed flexural reinforcement, moment distribution or cross section. The longest exposed length that satisfies both analyses has been defined as the critical length of exposed flexural reinforcement, ℓ_c .

The Strain Compatibility Analysis (SCA), using an accurate stress-strain concrete relationship, addressed the most predominant failure mode observed in previous experimental investigations (e.g., Cairns and Zhao 1993): crushing of the concrete on the compression face of the specimen before the exposed flexural reinforcement yields in tension.

The Strut-and-Tie Analysis (STA) addressed another important failure mode that was observed by others (Cairns and Zhao 1993): crushing of the concrete at the end of the exposed length due to the compressive strut intersecting the exposed end. The Strut-and-Tie Analysis was also used to analyze the critical distance from the support to the end of the exposed length, ℓ_e , where the compressive strut would intersect the exposed length for three cases: 1) point load only, 2) uniformly distributed load only, and 3) both point and uniformly distributed loads.

It can be concluded from the research presented in this chapter that:

1. A T-section specimen loaded with a combination of a uniformly distributed dead load and a point load would more accurately represent the type of girder and applied loading seen in the field because reinforced concrete bridge girders typically feature a substantial top slab and resist substantial uniformly distributed dead loads.
2. Both the Strain Compatibility Analysis (SCA) and Strut-and-Tie Analysis (STA) are important tools to assist practitioners evaluating reinforced concrete bridge girders with exposed flexural reinforcement.
3. The Strut-and-Tie Analysis results show that as the distance of the point load to the support increases the critical distance, ℓ_e , from the support to the end of the exposed length also increases.
4. The simulated uniformly distributed load significantly affects the critical distance from the support to the end of the exposed length, ℓ_e , computed using the Strut-and-Tie Analysis. Thus loading specimens using Case 3, with a combination of a point load and a simulated uniformly distributed load, will result in more realistic findings.

CHAPTER 4: EXPERIMENTAL INVESTIGATION

4.1 INTRODUCTION

To evaluate the accuracy of the analytical approaches developed in Chapter 3, T-section specimens with exposed flexural reinforcement were tested at the UWO Structures Laboratory. This chapter will describe the experimental test procedures and the design and construction of: the Control Specimen; the five specimens with exposed flexural reinforcement; and, the testing apparatus. The chapter will also describe how the effective depth of the exposed flexural reinforcement can be preserved by the insertion of steel spacers between it and the soffit of the concrete web and the effect of unsymmetrical loading configurations. The chapter will conclude with the results of the experimental investigation. Related detailed calculations are presented in Appendix C.

4.2 OBJECTIVES

The objectives of the experimental investigation reported in this chapter are:

1. To design a testing apparatus capable of the simultaneous application of a simulated uniformly distributed load and a point load.
2. To test a Control Specimen to assess the performance of the testing apparatus and to provide a baseline for comparison with specimens with exposed flexural reinforcement.
3. To determine the flexural behaviour of the specimens with exposed flexural reinforcement including quantification of the yield and ultimate moment

capacities, deflections and cracking patterns and to collect the data (e.g. strains, displacements, etc.) to help validate the two analytical approaches developed.

4. To study the effect of unsymmetrical loading configurations on the behaviour of specimens with exposed flexural reinforcement.
5. To study the impact of including steel spacers between the exposed flexural reinforcement and the underside of the concrete specimen web.

4.3 CONTROL SPECIMEN

The Control Specimen was designed as an under-reinforced T-section in accordance with the Canadian Highway Bridge Design Code (CHBDC), CAN/CSA-S6-06 (CSA 2006), with a flexural reinforcement ratio, ρ , of 0.37%, as shown in Figure 4-1. The Control Specimen has a total length, L_T , of 4400 mm, a simply supported span length, L , of 4000 mm, an overall height, h , of 400 mm, overall flange width, b_f , of 800 mm, a flange thickness, h_f , of 90 mm, and a web width, b_w , of 200 mm. The specified concrete strength, f'_c , is 40 MPa and the actual strength, based on eight cylinders tested immediately before and after the test, is 43.6 MPa (ASTM 2012).

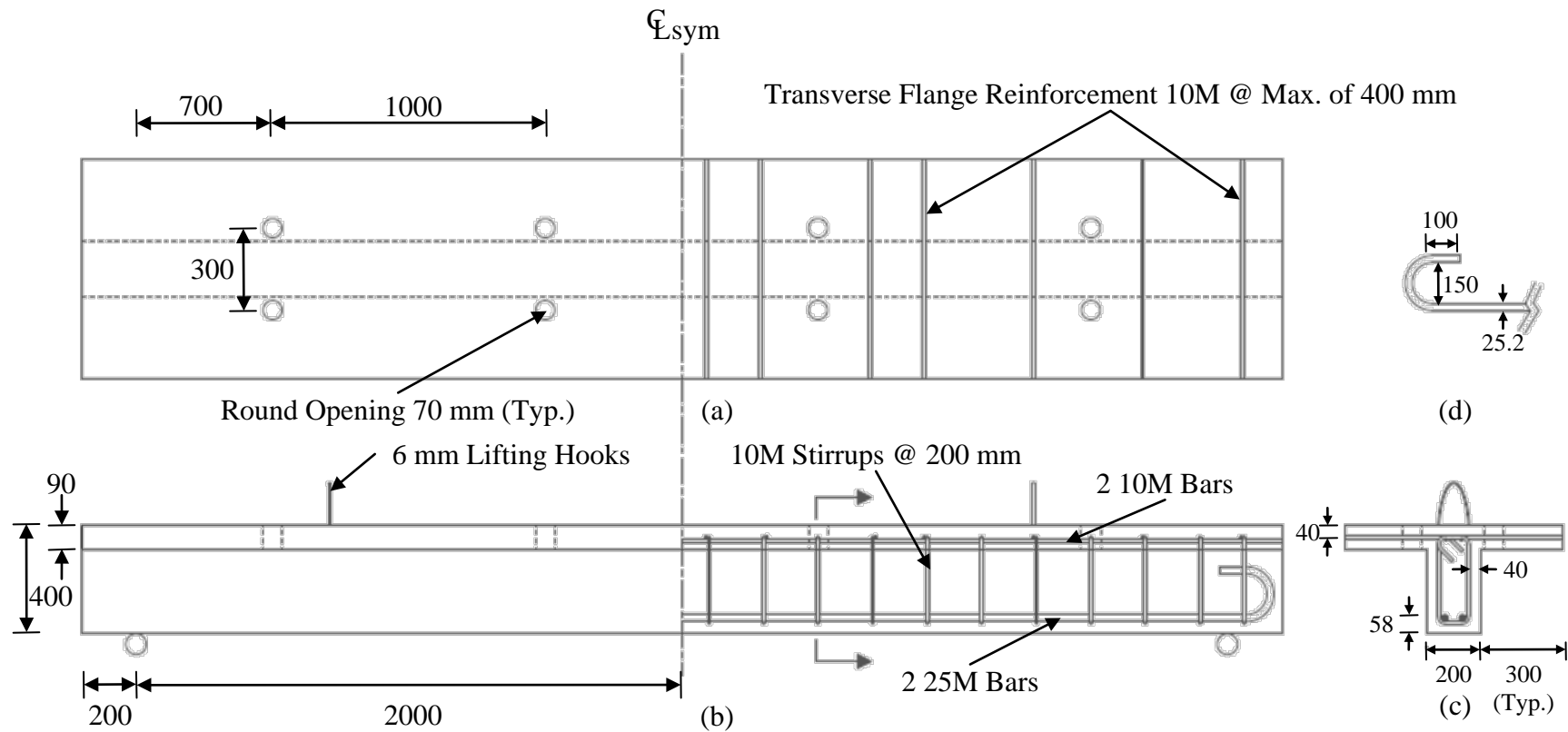


Figure 4-1: Control Specimen with Reinforcement Details: (a) Plan (Note: Web Reinforcement not Shown for Clarity), (b) Elevation, (c) Cross-section and (d) 180° Standard Hook Detail for Flexural Reinforcement (All Dimensions in mm).

The main flexural reinforcement consists of two 25M bars ($A_s = 500 \text{ mm}^2/\text{bar}$) at an effective flexural reinforcement depth, d , of 342 mm. The yield and ultimate strengths of the Grade 400 flexural reinforcement, f_y and f_u , are 456 MPa and 669 MPa, respectively, based on tests of samples obtained from the bars. The stress-strain relationship for the flexural reinforcement is presented in Appendix C. Anchorage of the flexural reinforcement at the support was ensured using a 180° standard hook (CSA 2006), as shown in Figure 4-1(d), which is capable of developing the yield strength of the bar at 365 mm from the end of the hook, or 210 mm from the support. The nominal top reinforcement, two 10M bars, at an effective depth, d' , of 56 mm, was provided primarily to anchor the stirrups. Lifting hooks consisting of 6 mm diameter undeformed steel hangers were embedded in the middle of the top flange at 910 mm from each end of the specimen.

The yield and ultimate moment capacities of the Control Specimen were computed to be 152.3 and 200.9 kN.m, respectively, using the actual material strengths. The associated shear forces were then computed and used to determine the required shear reinforcement. To avoid a premature shear failure, factored material strengths were used to determine the shear reinforcement spacing of 200 mm and so provide sufficient factored shear resistance of 220 kN that corresponds to a maximum midspan moment of 220 kN.m.

Nemec's (1996) Control Specimen failed due to a longitudinal crack in the compression flange adjacent to the flange/web junction at midspan. This failure mode is unlikely to occur in the field because transverse reinforcement is typically present in the concrete flange. A simple strut-and tie analysis (MacGregor and Bartlett 2000), indicated that this

failure could be prevented by adding 10M transverse reinforcement placed at a depth of 45 mm and spaced at a maximum distance of 400 mm throughout the compression flange. To accommodate for the flange block outs necessary to achieve the desired loading configuration, some bars were spaced at 200 mm.

The fabrication of the flexural reinforcement and formwork and casting of the Control Specimen, shown in Figure 4-2, took place the week of 30 January 2012 and on 15 February 2012, respectively.

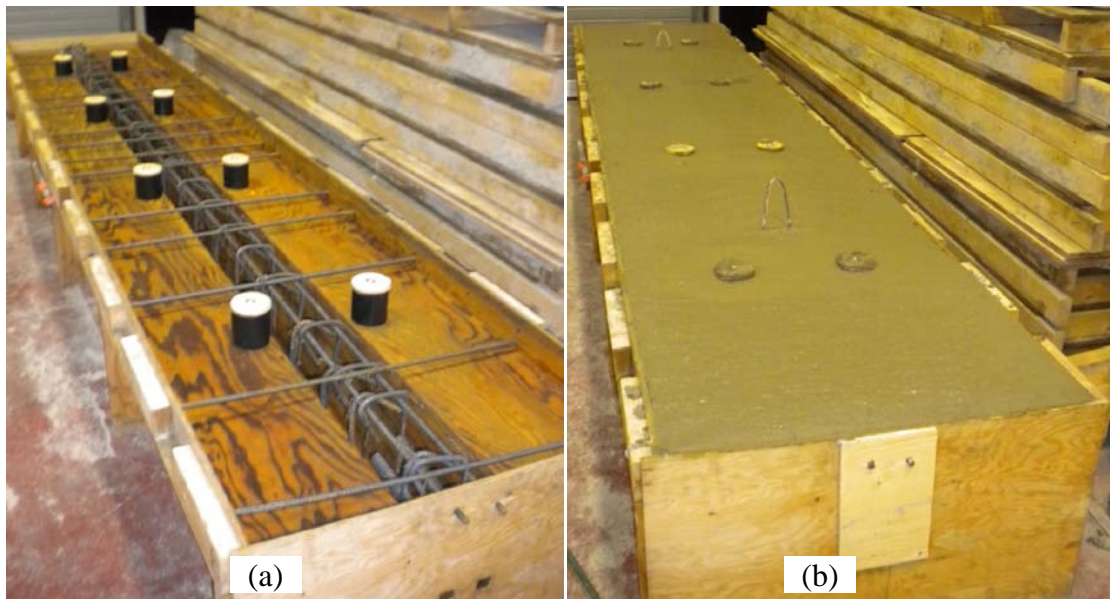


Figure 4-2: Control Specimen: (a) Reinforcement and Formwork (b) Casting.

4.4 TESTING APPARATUS

Reinforced concrete bridge girders resist substantial uniformly distributed dead loads, and therefore an experimental investigation involving a combination of a uniformly distributed dead load and a live load more accurately represents the applied loading observed in the field. A representative reinforced concrete bridge was analyzed to

determine the typical ratios of dead-to-total-load bending moments. It was concluded that the maximum dead load moment was 40% of the total moment at a critical section near the midspan, so the applied uniformly distributed load was computed to achieve this fraction. The live load was represented by a single-point load, P , and the uniformly distributed dead load was simulated using four equal point loads, ω , applied at the quarter points of the specimens. A slight error exists between the bending moment diagrams of the actual uniformly distributed load and the 4-point simulated uniformly distributed load. The 4-point simulated distributed load overestimates the bending moments at the exterior and interior point loads by 12 and 6%, respectively. Details of the loading analysis are presented in Appendix C.

An innovative testing apparatus was designed to apply the combination of the applied point load and simulated uniformly distributed load simultaneously, as shown in Figure 4-3. The point load was applied by the 1500 kN-MTS actuator to the top of the specimen along its centre axis. Four equal point loads were simultaneously applied by a system of whiffle trees to simulate the distributed load. To allow the point load to be applied at different locations along the length of the specimen, the whiffle tree system was designed to be mounted beneath the top flange.

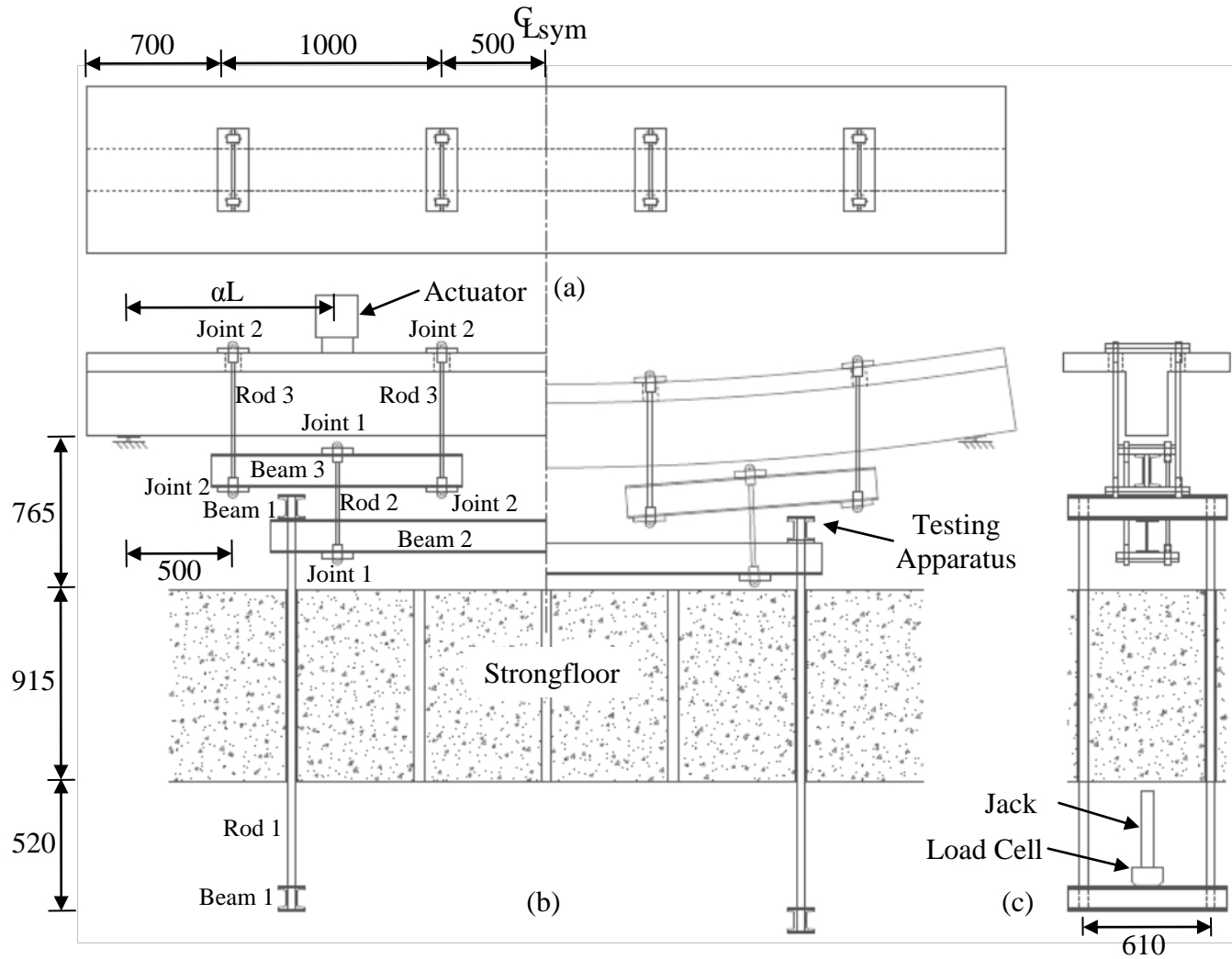


Figure 4-3: Testing Apparatus: (a) Plan, (b) Partial Elevations Showing Unloaded (Left) and Loaded (Right) Control Specimen and (c) End Elevation (All Dimensions in mm).

The whiffle tree system consisted of hydraulic jacks, spreader beams, steel rods and fabricated end joints, described in Table 4-1, designed in accordance with CSA-S16-09 “Design of Steel Structures” (CSA 2009). The system was designed to transfer the load from the hydraulic jacks bearing against the underside of the strongfloor to the bearing plates on top of the specimen to a maximum load of 50 kN at each quarter point. The two hydraulic jacks beneath the strongfloor were attached to the manual pump by a common hydraulic line. This ensured that the loads applied by each hydraulic jack were approximately equal.

A geometric analysis was performed to ensure that the testing apparatus did not interfere with the deformed specimen during the experiment, as shown in Figure 4-3(b). Nemec (1996) observed that a similar T-section control specimen had a maximum deflection of approximately 116 mm. Therefore, the testing apparatus was designed to accommodate a parabolic deflected shape with a maximum deflection of 150 mm at the centerline of the specimen.

Table 4-1: Whiffle Tree System Components.

Component	Classification	Length (mm)	Qty.	Weight (kN)	Notes
Beam 1	C100x11 @ 22 mm b/b	760	4	1.025	
Beam 2	W150x18	2743	1	0.483	Bearing stiffeners at the load location
Beam 3	C150x12	1372	2	0.648	
Rod 1	38 mm threaded rod	≈ 2100	4	0.926	Normal Steel/Accompanied by 2 appropriate nuts and washers
Rod 2	19.05 mm threaded rod	≈ 500	4	0.059	Medium-Strength Alloy Steel, ASTM A193 Grade B7, $F_v = 860$ MPa
Rod 3	19.05 mm threaded rod	≈ 600	8	0.144	Medium-Strength Alloy Steel, ASTM A193 Grade B7, $F_v = 860$ MPa
Joint 1			4		
Steel Bars	19.05 mm	300	4	0.026	
Steel Ball					
Joint Rod End	19.05 mm	-	8	-	
Plate	25 mm	300x150	4	0.326	
Joint 2			8		
Steel Bars	19.05 mm	400	8	0.070	
Steel Ball					
Joint Rod End	19.05 mm	-	16	-	
Plate	25 mm	400x150	8	0.879	
Hydraulic Jack	89 kN Capacity	≈ 500	2	0.497	Secured together by thread adapter
Load Cells	222.2 kN Capacity		2		
MTS Actuator	1500 kN Capacity	-	1		
Strongfloor	-	915	1		
Rubber Pads	19.05 mm	400x150	4	0.039	
Total				5.12 kN	
Equivalent Quarter Point Load, ω_{ow}				1.28 kN	

Joints 1 and 2 had to accommodate rotation, as shown Figure 4-3(b), and so were designed using 400 mm x 150 mm steel plates, 19.05 mm diameter rods and steel ball joints, as shown in Figure 4-4. Each steel plate had two 30 x 60 mm slots to allow clearance for the vertical tie rod to rotate. A circular groove was cut in the top of the plate to seat the transverse rod. This assembly created a pin joint that allowed the ball joints and the vertical tie rods to remain vertical while the steel plate and transverse bar could rotate up to 9° to accommodate the anticipated deflection of the specimens.

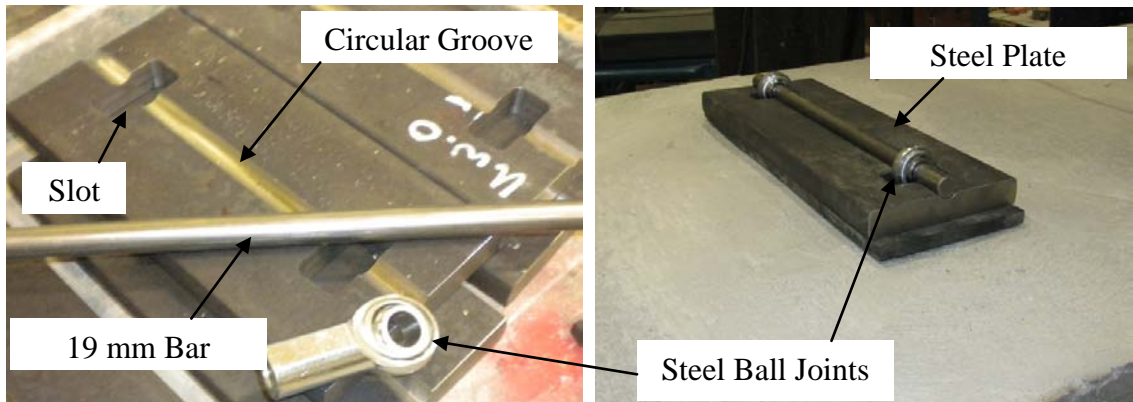


Figure 4-4: End Joint to Accommodate Rotation: (a) Unassembled, and (b) Installed.

Holes were necessary in the concrete specimen flange on either side of the web at its quarter points to accommodate the eight uppermost vertical tie rods. The required hole diameters and associated spreader beam clearances were determined by analysis of the deformed specimen, as shown in Figure 4-3(b). Holes with 70 mm diameters ensured sufficient clearance for the 6.5° rotation anticipated at the joint nearest the support. The minimum necessary initial vertical clearances of 10 and 105 mm were provided between the top of the ball joint of Joint 1 on Beam 3 and the soffit of the specimen and between the bottom of the ball joint of Joint 1 beneath Beam 2 and the top of the strongfloor, respectively.

The holes were formed using 75 mm PVC piping held in place by a circular wood cap that was secured beneath the flange formwork by a bolt and a wing nut, as shown in Figure 4-5. The circular wood cap prevented concrete from filling in the hole during casting and was removed after curing.

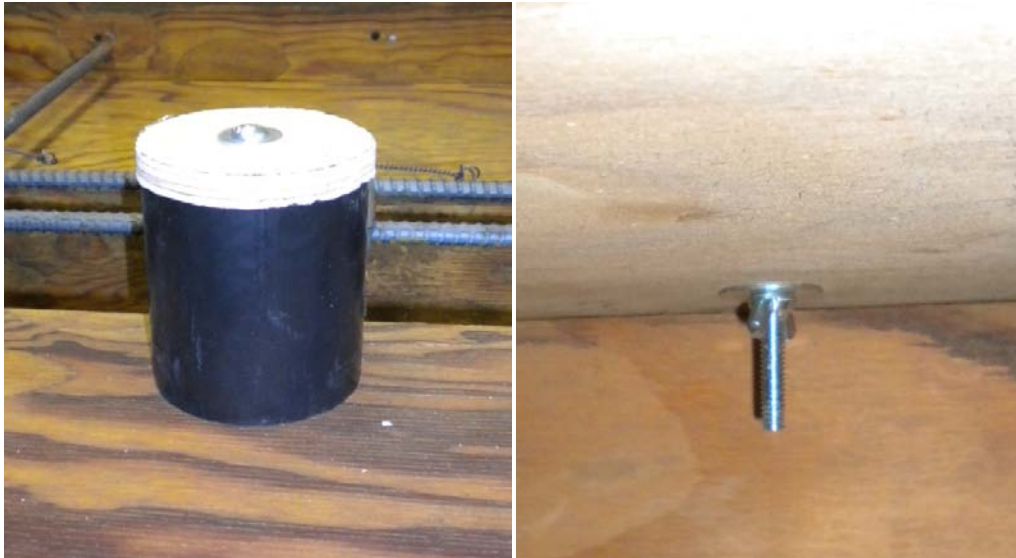


Figure 4-5: Flange Void Forms (a) 75 mm PVC Piping, (b) Bolt and Wing Nut Underneath Formwork.

Analysis of the deformed specimen was also used to determine the anticipated horizontal end movements at the supports during testing. Steel rollers with 19.05 mm diameters were provided at both supports to facilitate the expected horizontal end movement of approximately 25 mm and so ensure that the specimen would remain symmetric about its midspan during the test. The end movements also ensured that the vertical loading rods stayed vertical and so the flange hole clearances were not impacted. A 325 mm x 100 mm x 6.5 mm steel plate was placed above each steel roller to prevent local crushing of the concrete web at the support.

4.5 SPECIMENS WITH EXPOSED FLEXURAL REINFORCEMENT

Rehabilitation standards for deteriorated reinforced concrete bridge girders require concrete removal to a depth of 25 mm behind the first layer of flexural reinforcement (OPSS 1994). Five specimens were therefore designed and constructed in the same manner as the Control Specimen, but with various lengths of the bottom of the concrete web blocked out to expose the flexural reinforcement. The elevations of the five specimens, showing the loading configuration, point load location from the left support, αL , length of exposed flexural reinforcement, ℓ_{exp} , distance from the supports to the end of the exposed length, ℓ_{end} , and the steel spacer locations are shown in Figure 4-6. Table 4-2 summarizes, for each specimen, the measured flange and web widths, b_f and b_w , respectively, the concrete and steel material strengths, and the dates of casting and testing.

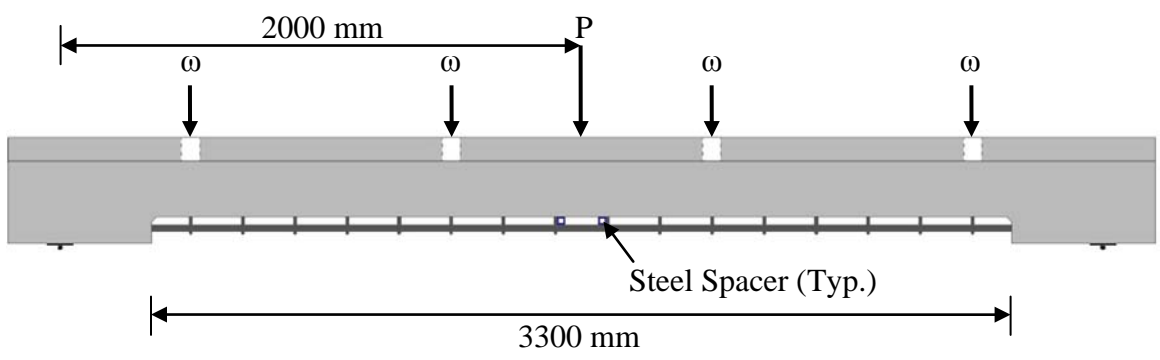
Table 4-2: Properties of Specimens with Exposed Flexural Reinforcement

Specimen	b_f (mm)	b_w (mm)	f_c' (MPa)	f_y (MPa)	f_u (MPa)	Cast	Test
1	810	202	43.6	456	669	15 Feb	26 Apr
2	812	205	44.0	402	612	31 June	31 July
3	820	203	44.0	402	612	31 June	2 Aug
4	814	206	33.9	402	612	10 July	7 Aug
5	812	202	33.9	402	612	10 July	8 Aug

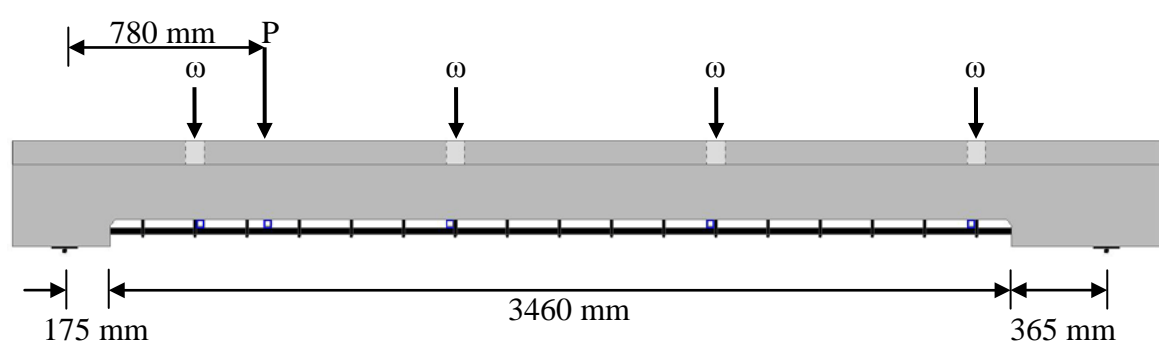
Specimens 1, 4 and 5 had the same loading configuration as the Control Specimen with lengths of exposed flexural reinforcement of 3300 mm, 3600 mm and 3600 mm, respectively, symmetrical about the midspan. Specimen 1 was used as a pilot test to observe the behavioural characteristics of a specimen with exposed flexural reinforcement compared to the Control Specimen and to confirm the effectiveness of the

testing apparatus. Specimens 2 and 3 had the same loading configurations, with the point load located at approximately 780 mm from the left support, to observe the effect of an unsymmetrical loading configuration on the behaviour of the specimens.

(a) Specimen 1:



(b) Specimens 2 and 3:



(c) Specimens 4 and 5:

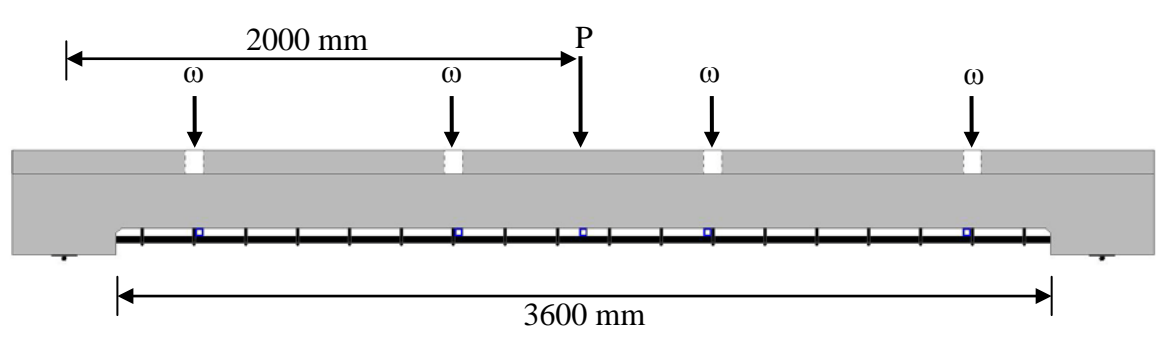


Figure 4-6: Elevations of Test Specimens with Loading Configuration, Void Location and Steel Spacer Locations.

As outlined in Chapter 2, previous researchers (e.g., Nemeč 1996) observed that during testing the gap between the bottom of the concrete web and the exposed flexural reinforcement reduced until the two came into contact. This reduces the lever arm between the flexural reinforcement and the resultant concrete compressive force and so reduces the flexural capacity. To try to prevent this occurrence, each specimen had steel spacers placed in the gap between the concrete and exposed flexural reinforcement at the location of the maximum moment to preserve the lever arm, as shown in Figure 4-6.

Additional steel spacers were placed at the ω point load locations for Specimens 3, 4 and 5 to determine if they would facilitate load transfer to the stirrups, which are otherwise ineffective while the flexural reinforcement is exposed. Installation of these spacers could create a plastic truss with several interior panels that could enhance the shear strength while the flexural reinforcement is exposed, as shown in Figure 4-7. The spacer can potentially facilitate the transfer of the compressive strut force, C , in the concrete web to be resolved as tension in the stirrup, T_s , and a change of tension in the flexural reinforcement, ΔT . If this occurs, there will be a reduction in tensile force in the flexural reinforcement to the left of the stirrup, and the behaviour will be similar to that of the Control Specimen. Specimens 2, 3 and 4 were reinforced with 25 mm x 25 mm steel spacers, while Specimen 5 had 50 mm x 25 mm steel spacers to observe if the wider spacer increased the load transferred.

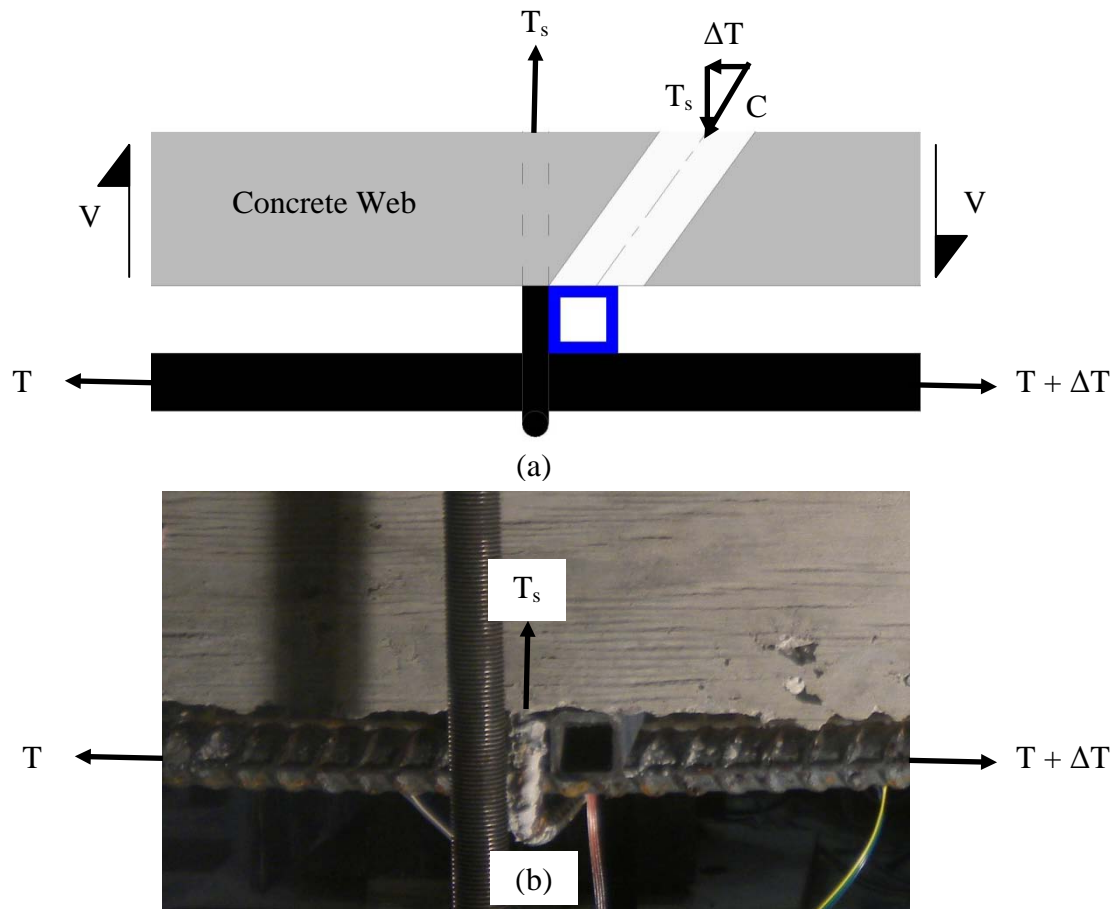


Figure 4-7: Steel Spacer: (a) Illustration of the Load Transfer through the Steel Spacer and (b) Steel Spacer In-situ.

Strain gauges were strategically placed on the specimens to facilitate validation of the two analytical approaches developed. Rosette strain gauges were placed on the side of the concrete web directly above the end of the exposed length where the anticipated inclined compressive strut would be located. For Specimen 1, 45 degree rosette strain gauges with a gauge length of 2 mm, type N31-FA-2-120-11, were used, as shown in Figure 4-8(a). The subsequent test indicated that these gauges were too small to record accurate strain readings in the concrete web. A rosette strain gauge was therefore constructed using gauges with lengths of 30 mm, type N11-FA-30-120-11, as shown in Figure 4-8(b). The

same strain gauges were placed on the top surface of the concrete flange for Specimens 2 through 5, as shown in Figure 4-8(c), to record the compressive strain at the extreme fibre of the top flange. Steel strain gauges, type CEA-06-250UW-120, were placed on the exposed flexural reinforcement to identify yield and to record any change of stress at each side of the stirrups, as shown in Figure 4-8(d). The same strain gauges were placed on the exposed portion of stirrups to determine any load transfer that may have occurred through the steel spacers, as shown in Figure 4-8(d).

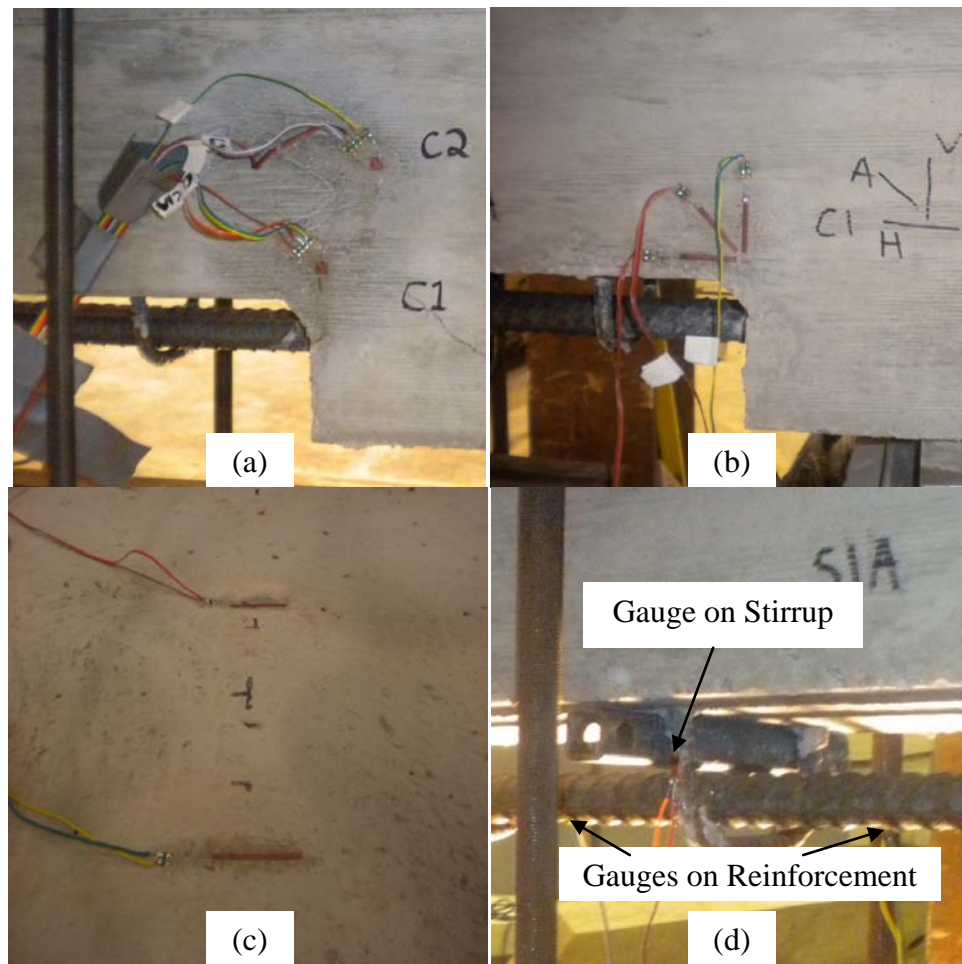


Figure 4-8: Strain Gauges used in the Experimental Investigation: (a) Small 45 Degree Rosette Strain Gauges, (b) Constructed 45 Degree Rosette Strain Gauge, (c) Strain Gauge on Concrete Flange, and (d) Strain Gauges on Flexural Reinforcement and Stirrups.

To simulate concrete removal to a depth of approximately 100 mm, i.e., removal to a depth of 25 mm behind the first layer of flexural reinforcement, a void comprised of four 25 mm layers of foam insulation glued together was designed and constructed to enclose the flexural reinforcement, as shown in Figure 4-9. A full description of the void design, construction and installation is presented in Appendix C.



Figure 4-9: Foam Insulation Void Enclosing the Flexural Reinforcement.

4.6 TESTING PROCEDURE

Identical testing procedures used for each specimen consisted of three stages, as shown in Figure 4-10. In the first stage, the specimens were loaded using the hydraulic jacks underneath the strongfloor to the target simulated distributed yield load, ω_y , at the quarter points. Before testing, the equivalent quarter point load of the self-weights of the

specimen and testing apparatus, ω_{ow} and ω_{app} , respectively, were calculated and deducted from the target distributed load value to determine the applied loads ω .

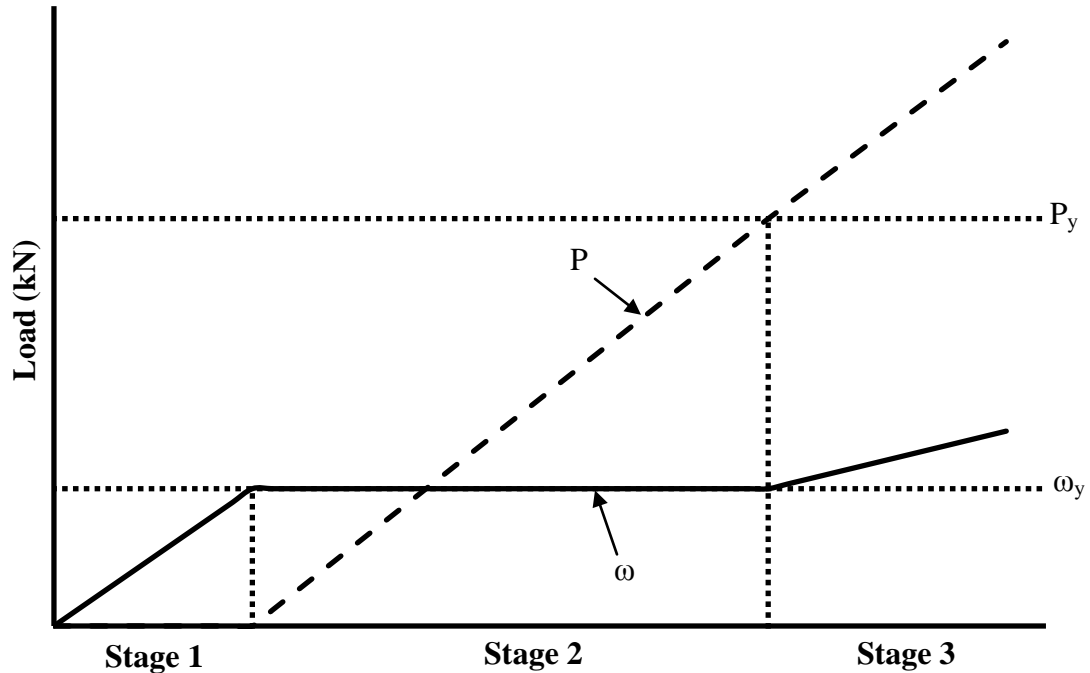


Figure 4-10: Designed Testing Procedure for Specimens.

In the second stage, the specimens were then loaded by the MTS actuator at a rate of 4 mm/min to the anticipated point yield load, P_y . The actuator was set to stroke control rather than load control to avoid a brittle failure. Deflection of the specimen due to the actuator load decreased the jack pressure, which was therefore manually increased to maintain the target simulated distributed yield load, ω_y .

In the third, and final stage, once the load in the actuator reached P_y , the simulated distributed load, ω , was manually increased to ensure that the actuator and hydraulic jack loads increased proportionally, at a ratio of $P_y/4\omega_y$, until failure. Failure was defined as

the maximum load the specimen was able to resist, as determined using the moment-deflection relationship.

The specific loads applied to each specimen, predicted for the yielding states, are shown in Table 4-3. The procedures for determining these values for the Control Specimen and Specimen 1 are presented in Appendix C.

Instrumentation readings were recorded and archived using the UWO data acquisition system at one second intervals. The load cell, actuator and strain gauge readings were also continually recorded. Cracks were monitored visually and the loads, location, width and length were recorded.

A Linear Voltage Displacement Transducer (LVDT) was positioned at the midspan of the specimens to continually measure the centerline vertical deflection, Δ_{mid} . LVDTs were also positioned at the supports of the Control Specimen and Specimen 1 to measure the horizontal end movements and so verify that the specimen was translating symmetrically about the midspan.

Table 4-3: Testing Loads for each Specimen.

Specimen	ω_{ow} (kN)	ω_{app} (kN)	ω_y (kN)	P_y (kN)
Control	3.26	1.28	26.0	91.3
1	2.85	1.28	26.3	91.3
2	2.85	1.28	22.8	80.7
3	2.85	1.28	22.8	80.7
4	2.85	1.28	22.7	80.3
5	2.81	1.28	22.7	80.3

4.7 RESULTS

All specimens were tested using the three-stage testing procedure outlined in Section 4.6. Detailed loading histories for each specimen are presented in Appendix C. The crack locations and deflected shapes of all specimens are shown in Figure 4-11. The moment-deflection relationships for the Control Specimen and Specimens 1 to 5 and the predicted cracking, M_{cr} , yield, M_y , and ultimate, M_u , moments for an identical beam with no exposed reinforcement, calculated in accordance with the CHBDC (CSA 2006) are shown in Figure 4-12. The key results are shown in Table 4-4.

4.7.1 Control Specimen

The observed and predicted behaviour of the Control Specimen agree very closely. Cracking initiated when the deflection reached 2 mm and the moment was approximately 27 kN.m, close to the predicted value of 22.5 kN.m. The flexural reinforcement yielded at a moment of 153.5 kN.m when the centreline deflection was 16.2 mm, and strain hardening commenced immediately thereafter. The failure moment, corresponding to crushing of the concrete compression flange, was 201.5 kN.m at a centreline deflection of 108.4 mm. Upon unloading, the elastic recovery of the Control Specimen was approximately 20 mm.

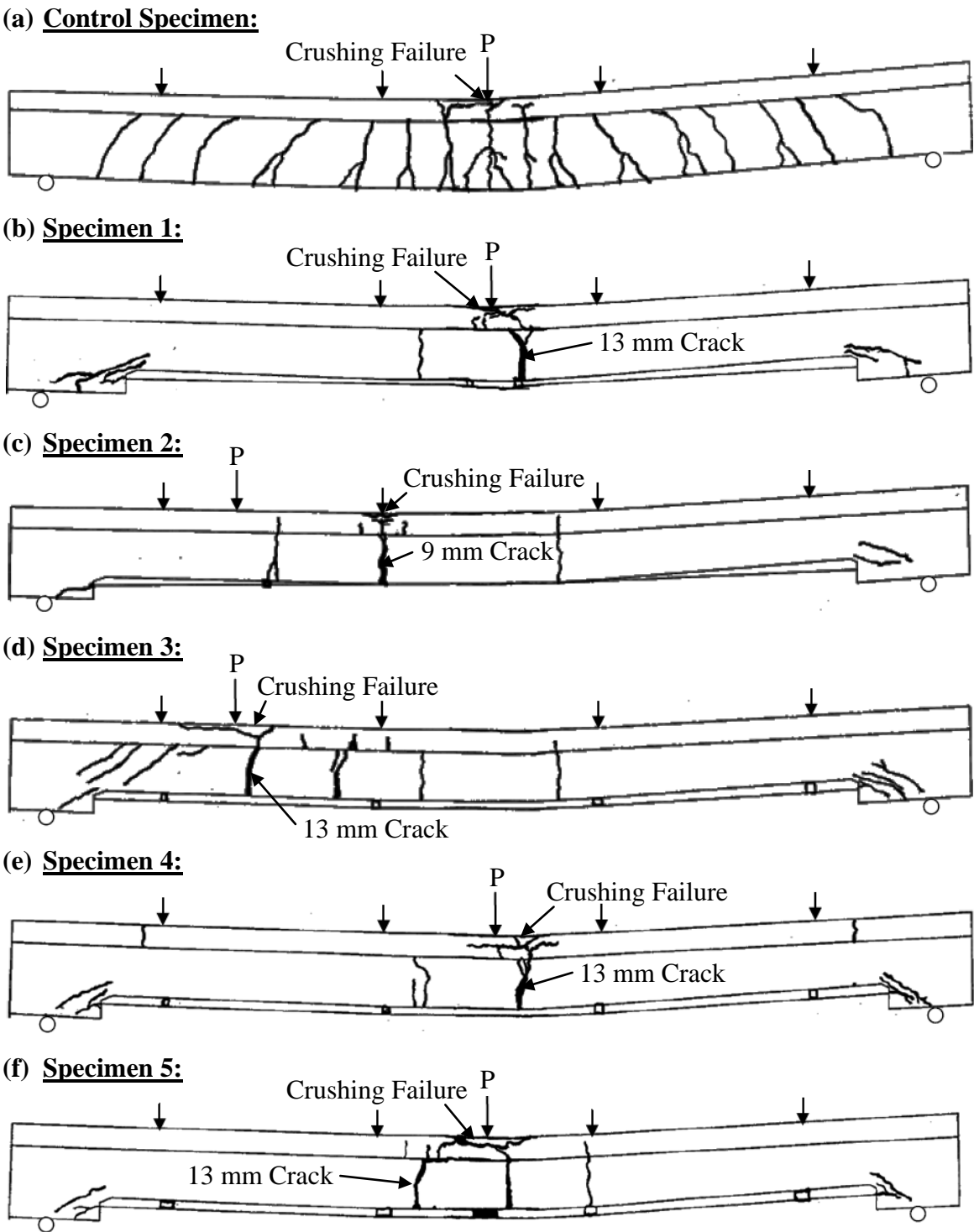


Figure 4-11: Elevations of Specimens with Crack Locations and Deflected Shapes ($\downarrow = \omega$ and $\downarrow = P$).

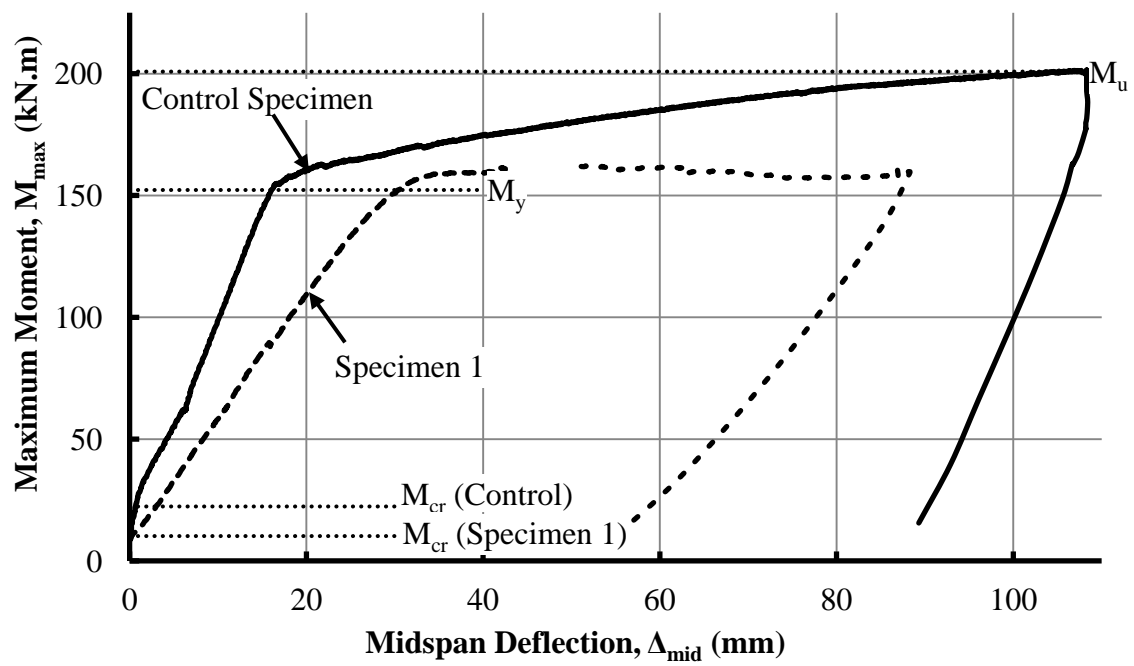


Figure 4-12(a): Moment-deflection Relationships: Control Specimen and Specimen 1;

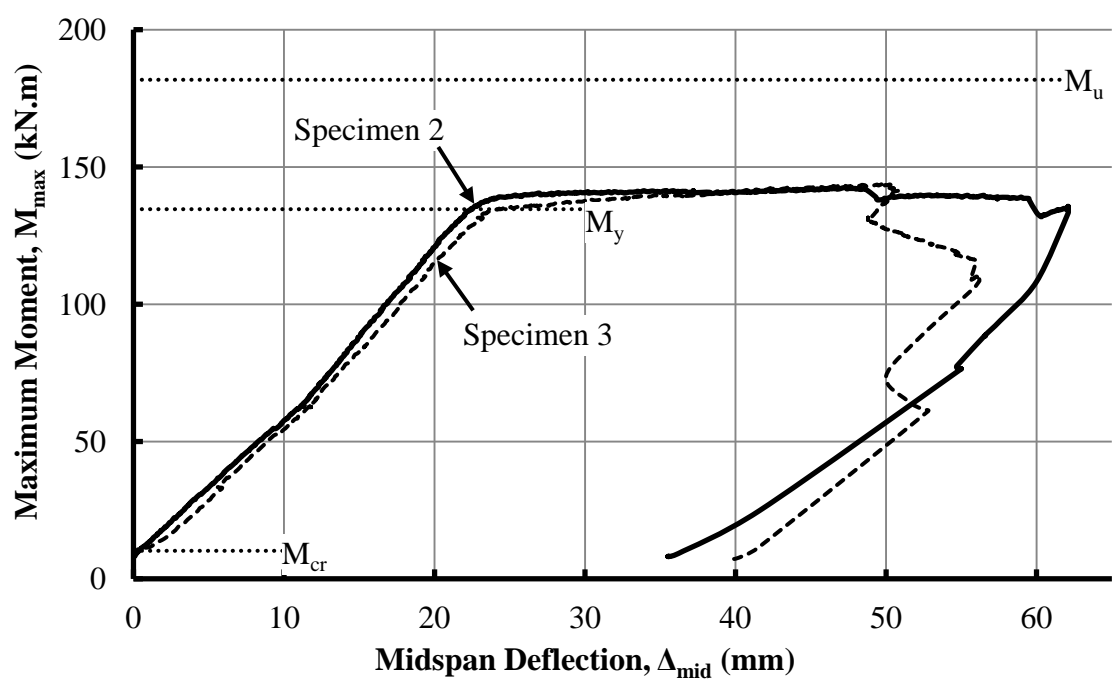


Figure 4-12(b): Moment-deflection Relationships: Specimens 2 and 3;

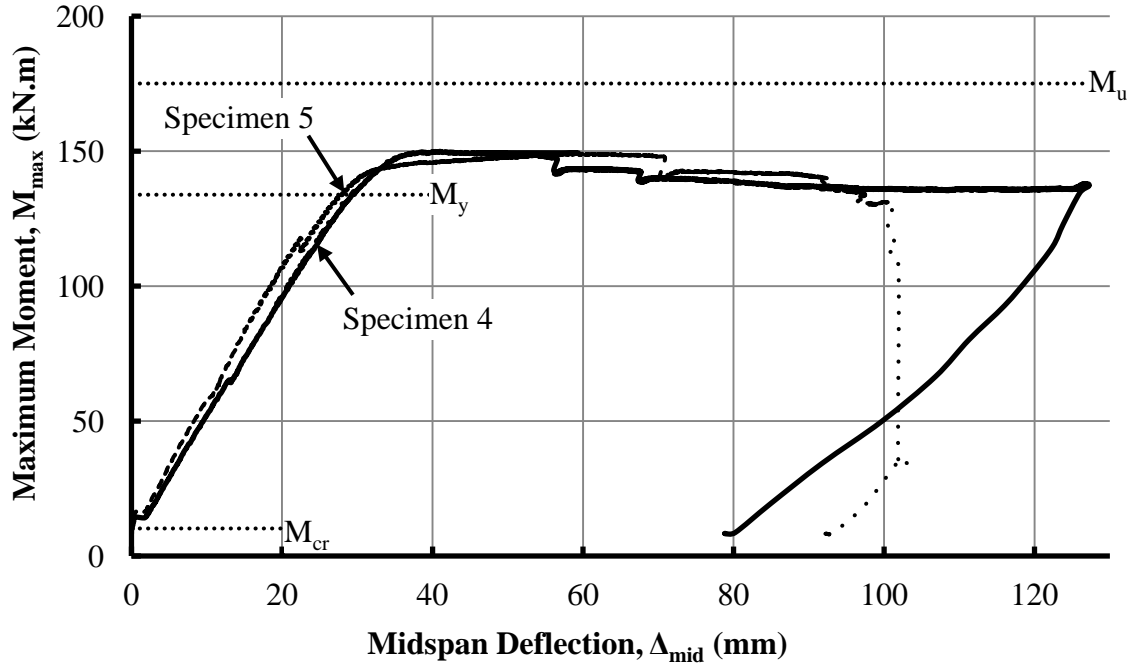


Figure 4-12(c): Moment-deflection Relationships: Specimens 4 and 5.

Table 4-4: Predicted and Observed Test Results.

Specimen	Predicted-No Exposed Flexural Reinforcement			Observed	
	M_{cr} (kN.m)	M_y (kN.m)	M_u (kN.m)	M_y (kN.m)	M_u (kN.m)
Control	22.5	152.3	200.9	153.5	201.5
1	10.2	152.2	203.3	152.9	158.4
2	10.2	134.6	190.5	135.2	142.5
3	10.2	134.6	192.5	133.6	143.7
4	9.4	133.9	184.2	142.8	149.9
5	9.4	133.8	184.2	137.8	149.0

Figure 4-11(a) shows the crack location and deflected shape of the Control Specimen near failure. Vertical flexural cracks initially formed near midspan and spread over the full length of the tension side of the specimen with increased loading. The crack spacing,

approximately 200 mm, was the same as the stirrup spacing. The cracks propagated up the web and into the concrete flange and bifurcated at the neutral axis at a depth of approximately 20 mm. The vertical cracks gradually became more inclined closer towards the supports, turning into shear cracks.

Longitudinal cracks due to transverse tensile stresses were observed along the centerline on top of the flange of the Control Specimen. The transverse flange reinforcement was sufficient to prevent the splitting failure mode observed in Nemeč's (1996) Control Specimen, which had no transverse reinforcement in the compression flange.

The Control Specimen accurately demonstrated the behaviour of a T-section beam with no reinforcement exposed and provided a baseline for comparison with the five specimens with exposed flexural reinforcement.

4.7.2 Specimens with Exposed Flexural Reinforcement

All the specimens with exposed flexural reinforcement exhibited very similar behaviour. As shown in Figure 4-11, cracking initiated with one or two cracks near the midspan when the moments due to simulated uniformly distributed load, ω , and the self-weights of the specimen and testing apparatus reached approximately 10 kN.m. As summarized in Table 4-4, these observed values agree closely with that predicted for an identical beam with reduced web depth, h_w , as shown in Appendix C. The observed yield moments were between 0.8% less and 6.6% greater than the yield moment computed for an identical beam without exposed reinforcement. After yielding, the flexural resistance increased only slightly and ductile behaviour with no strain hardening was observed as shown in Figure 4-12. All specimens failed by the crushing of the concrete compression region at

moments of 75% to 81% of that predicted for an otherwise identical beam with no exposed reinforcement.

The observed crack patterns and deflected shapes were, in general, similar to those observed by previous researchers (e.g., Cairns and Zhao 1993), as shown in Figure 4-11. Unlike the Control Specimen, only one or two vertical flexural cracks formed near the midspan before or soon after the simulated uniformly distributed load, ω , was applied, propagating up the web into the concrete flange and bifurcating at the neutral axis. The widths of these vertical cracks were significant because the exposed flexural reinforcement was ineffective in providing crack control. Inclined cracks appeared above the ends of the exposed length that are consistent with the inclination of the compressive strut in this region. Bond-splitting cracks also appeared at the re-entry point of the flexural reinforcement, particularly in Specimens 2, 3 and 5.

There were slight differences in the crack patterns observed. For Specimens 2 and 3, two large cracks appeared near midspan after the simulated uniformly distributed load, ω , was applied. After the unsymmetrical point load, P , was applied, the crack at the lesser-loaded side of the midspan closed, the crack at the greater-loaded side opened and more cracks appeared under the point load. The concrete in the flange crushed above the largest crack observed: under the interior load ω for Specimen 2 and under P for Specimen 3. For Specimen 3, long parallel inclined shear cracks also appeared at the high-shear region in the concrete web between P and the left support. For Specimen 4, flexural tensile cracks appeared in the top concrete flange near the supports, likely due to the stress reversal that

occurs in this region, as described by Cairns and Zhao (1993), with concrete in flexural tension above the neutral axis.

4.7.3 Effectiveness of Testing Apparatus

The testing apparatus essentially behaved as anticipated, as shown in Figure 4-13 for the Control Specimen. The spreader beams deflected as the specimens were loaded and the steel rods remained vertical, showing the effectiveness of their fabricated end joints. The spreader beam clearances and concrete flange void diameters were sufficient to prevent interference between the testing apparatus and the specimens during testing. The testing apparatus also effectively simulated the uniformly distributed load on the specimens: in particular, the hydraulic jacks beneath the strongfloor successfully applied equal loads at the specimen quarter points. The steel rollers at both supports effectively facilitated the horizontal movement of each end of the specimen, allowing symmetric translations about the midspan during testing.

4.7.4 Impact of Steel Spacers

As described in Section 4.5, steel spacers were placed in the gap between the concrete and exposed flexural reinforcement to: (1) maintain the effective depth of the flexural reinforcement, d , by preventing the gap above the reinforcement from closing, as had been observed by Nemec (1996); and, (2) facilitate load transfer through bearing to develop a plastic truss to resist shear in the exposed reinforcement region.

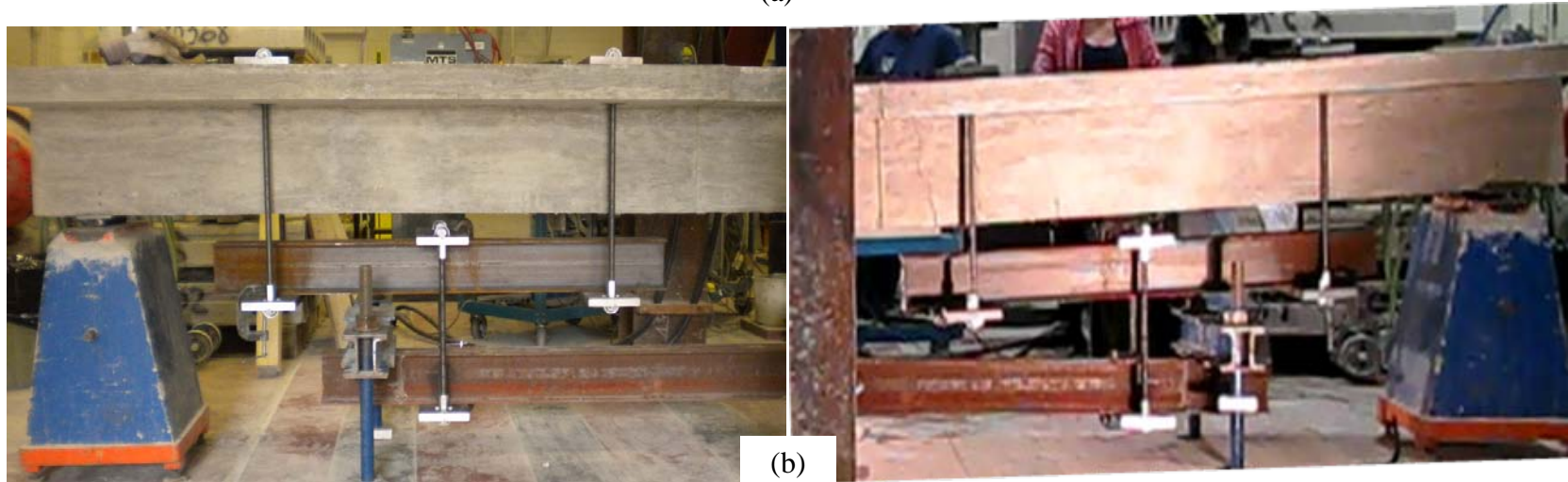
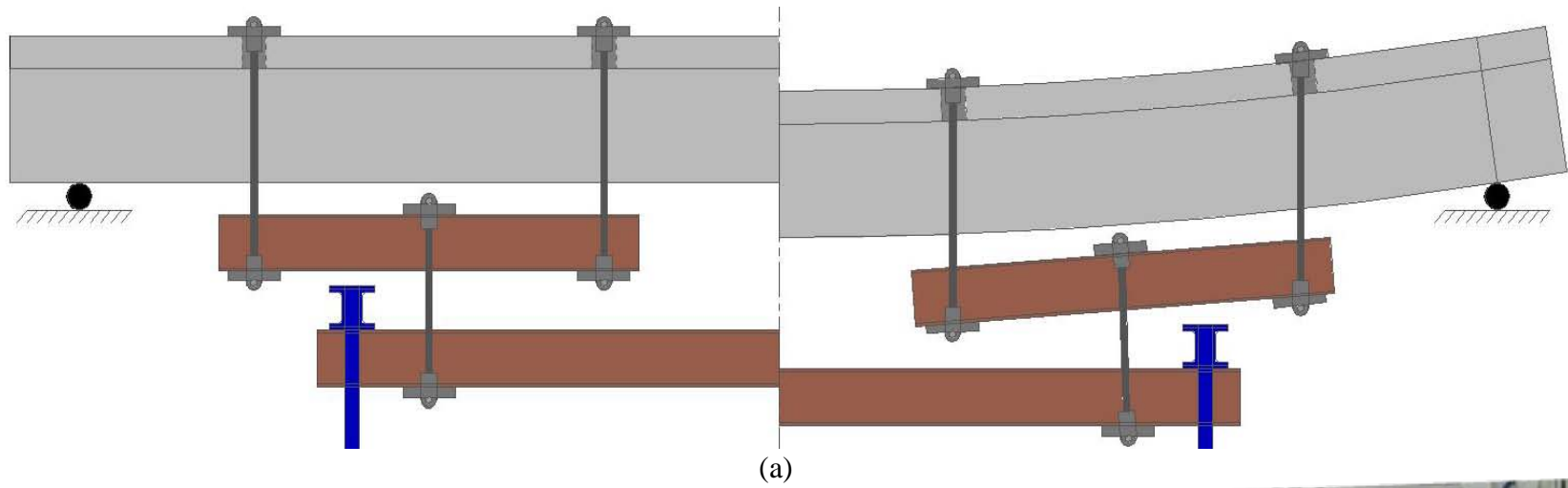


Figure 4-13: Testing Apparatus: Partial Elevations Showing Unloaded (Left) and Loaded (Right) for Control Specimen, (a) Predicted and, (b) Observed.

The steel spacers were successful in maintaining the depth of the flexural reinforcement, d , and subsequently the lever arm, jd , where they were placed. They allowed the specimens to reach and surpass their yield capacities, exhibiting a ductile behaviour until failure. The significance of the spacer location is demonstrated by the response of Specimens 2 and 3, which were otherwise identical. As shown in Figure 4-11, Specimen 2 had a steel spacer placed at the location of the maximum moment, M_{max} , while Specimen 3 had four steel spacers spaced equally along the exposed length. Specimen 2 exhibited a slightly higher yield moment than Specimen 3, Figure 4-12(b), but its ultimate moment was slightly lower because the gap between the concrete and the flexural reinforcement reduced, as shown in Figure 4-14, reducing jd . As shown in Figure 4-11, Specimen 3 failed at the location of the maximum moment, under the applied point load, whereas Specimen 2 failed closer to midspan where the gap had reduced. Therefore, steel spacers can be effective in maintaining the depth of the flexural reinforcement, particularly if they are spaced uniformly along the exposed length of the flexural reinforcement and so are located at, or near, the locations of the maximum applied moment and the maximum deflection.

The steel spacers did not facilitate load transfer from the concrete web to the exposed stirrups, as theorized in the discussion concerning Figure 4-7. Tensile strains in the stirrups along the length of exposed flexural reinforcement were negligible. Also, the measured strains in the exposed flexural reinforcement on either side of the stirrups revealed little or no change. Therefore, even with steel spacers inserted, the stirrups were ineffective in the region where the flexural reinforcement is exposed.



Figure 4-14: Impact of Steel Spacer under the Interior Load ω Near the Left Support: (a) Specimen 2 and, (b) Specimen 3.

4.7.5 Effect of Unsymmetrical Loading Configurations

Unsymmetrical loading configurations were studied to assess the typical reinforced concrete bridge conditions, i.e., uniformly distributed dead load and a live load moving along the length of the bridge. The unsymmetrical loading applied to Specimens 2 and 3 were compared to the symmetrical loading applied to Specimens 1, 4, and 5 to examine its effect on the inclination of the compressive strut near the ends of the exposed length. Strain rosettes were placed directly above the ends of the exposed lengths, to investigate the orientation and, for Specimen 2 and 3, change in orientation of the principal compressive strains at this location, as shown in Figure 4-8. Using these data, the orientation of the principal strains in the concrete web at the left and right supports, θ_L and θ_R from the horizontal, respectively, are shown for Specimen 1 in Figure 4-15, for Specimen 2 in Figure 4-16, and for Specimen 3 in Figure 4-17.

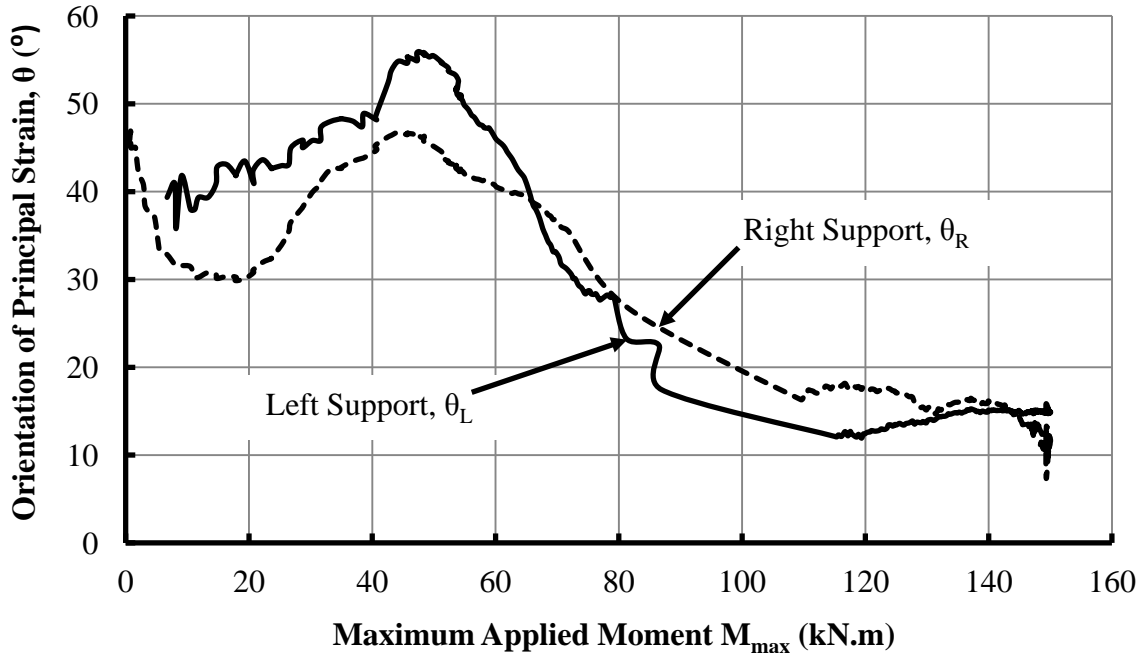


Figure 4-15: Orientation of the Principal Compressive Strains at the End of the Exposed Length for Specimen 1 (Symmetrical Loading Configuration).

Specimen 1 was subjected to symmetrical loading so the variation of θ_L and θ_R with the maximum applied moment should be similar. The simulated uniformly distributed load, ω , caused the principal compressive strains near both supports to be steep, between 40 to 50 degrees initially but the application of the point load, P , at midspan at a moment of approximately 62 kN.m, caused both θ_L and θ_R to decrease.

Specimens 2 and 3 were subjected to unsymmetrical loading so the variations of θ_L and θ_R with the maximum applied moment are different. Application of the point load, P , near the left support caused the principal compressive strains near the left support to become steeper and those near the right support to become more horizontal. In the interval when only ω was applied, to a moment of 63 kN.m, θ_L and θ_R were fairly constant but once P was applied, the values of θ_L and θ_R changed significantly.

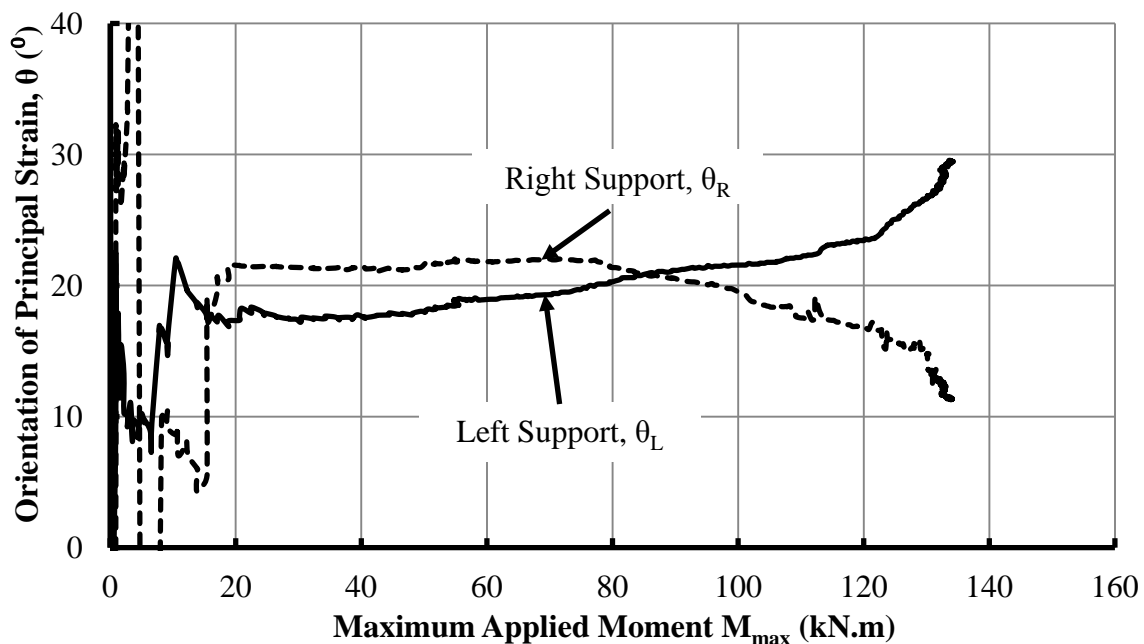


Figure 4-16: Orientation of the Principal Compressive Strains at the End of the Exposed Length for Specimen 2 (Unsymmetrical Loading Configuration).

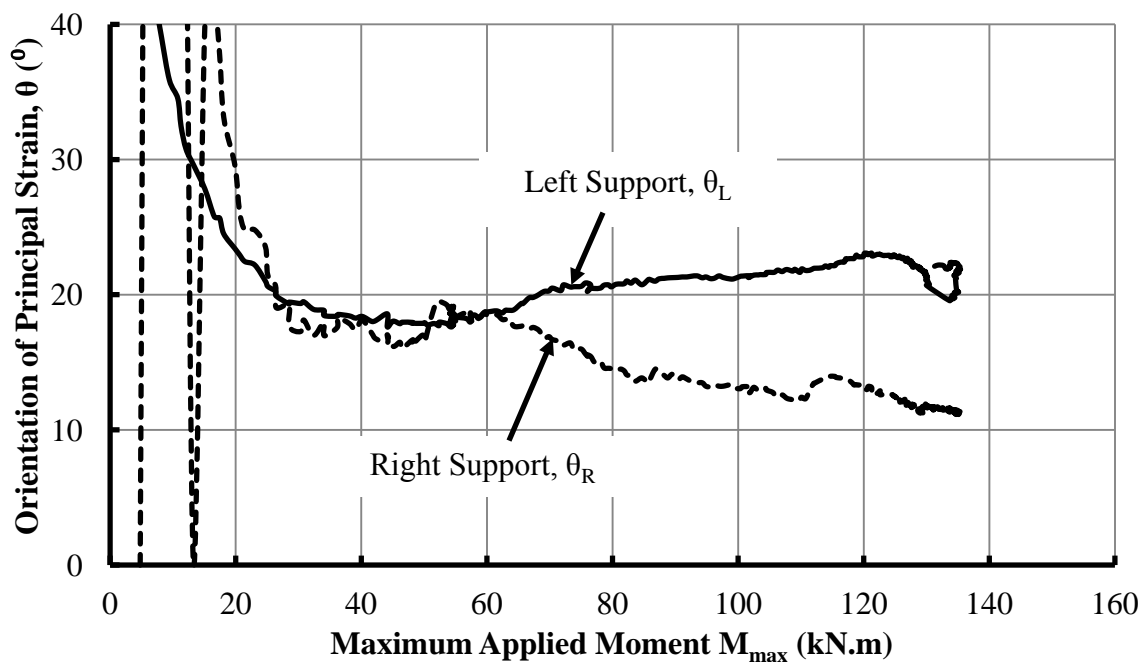


Figure 4-17: Orientation of the Principal Compressive Strains at the End of the Exposed Length for Specimen 3 (Unsymmetrical Loading Configuration).

4.8 SUMMARY AND CONCLUSIONS

This chapter has presented the experimental investigation of reinforced concrete T-section specimens with exposed flexural reinforcement including descriptions of: the design, construction and test procedure of the Control Specimen, the five specimens with exposed flexural reinforcement and testing apparatus; the impact of preserving the effective depth of the exposed flexural reinforcement by the insertion of steel spacers between the it and the soffit of the concrete web. This chapter also presented the results of the experimental investigation.

The Control Specimen accurately demonstrated the behaviour of a T-section beam with no reinforcement exposed and provided a baseline for comparison with the five specimens with exposed flexural reinforcement. The behaviour of the specimens with exposed flexural reinforcement was drastically different. All failed by crushing of the concrete flange at a moment greater than the yield moment, M_y , and less than the ultimate moment, M_u , of the same beam with no exposed reinforcement. With the flexural reinforcement exposed, strain hardening did not occur and so the capacity did not increase significantly beyond the yield moment.

An innovative testing apparatus was designed using an actuator and a system of whiffle trees to represent the concurrent point and uniformly distributed loads that more accurately represents typical loadings in the field. The testing apparatus effectively simulated a uniformly distributed load applied to the specimens, applying equal loads at the specimen quarter points without interfering with the specimens during testing. The

steel rollers at both supports effectively facilitated the horizontal movement of each end of the specimen, allowing symmetric translations about the midspan during testing.

Steel spacers were inserted in the gap between the exposed flexural reinforcement and the soffit of the concrete web to preserve the effective depth of the flexural reinforcement, d , and to observe the possibility of the steel spacers facilitating load transfer to the stirrups and create a plastic truss. Unsymmetrical loading configurations were also studied to examine their effect on the inclination of the compressive strut near the ends of the exposed length.

The results of the experimental investigation have yielded the following conclusions:

1. Reinforced concrete T-section specimens, having a flexural reinforcement ratio, ρ , of 0.37%, with their flexural reinforcement exposed over 82.5 to 90% of the span length can reach the flexural capacity of the original beam and exhibit a ductile failure.
2. Steel spacers placed in the gap between the concrete and exposed flexural reinforcement can be effective in maintaining the depth of the flexural reinforcement, particularly if they are spaced uniformly along the exposed length of the flexural reinforcement and so are located at, or near, the locations of the maximum applied moment and the maximum deflection. Even with steel spacers inserted, however, the stirrups are ineffective in the region where the flexural reinforcement is exposed.
3. The loading configuration can significantly impact the inclination of the compressive strut near the ends of the exposed length. When a specimen is

subjected to symmetrical loading the variation of the orientation of the compressive strut at the left and right supports are similar. The application of unsymmetrical loading can cause the compressive strut near the support with the greater reaction to become steeper and the compressive strut near the support with the lesser reaction to become more horizontal.

CHAPTER 5: COMPARISON OF EXPERIMENTAL AND PREDICTED RESULTS

5.1 INTRODUCTION

Experimental testing of the reinforced concrete T-section specimens with exposed flexural reinforcement was carried out in the UWO Structures Laboratory. This chapter includes a comparison of these experimental test results with those predicted to investigate the validity of the two analytical approaches developed in Chapter 3. Related detailed calculations are presented in Appendix D.

5.2 COMPARISON TO STRAIN COMPATIBILITY ANALYSIS PREDICTIONS

The Strain Compatibility Analysis (SCA) described in Section 3.3 was used to analyze the five specimens with exposed flexural reinforcement. The incremental procedure could not be used directly because the exposed length of flexural reinforcement, ℓ_{exp} , for each specimen was predetermined and therefore the number of segments, n , was constant. The procedure was therefore altered slightly by incrementally changing the lever arm, $jd(x)$, at the location of the maximum moment, M_{max} , until the horizontal force and moment equilibrium and the strain compatibility requirements outlined in Eqns. [2.1] to [2.4] were exactly satisfied. The initial lever arm at this location was taken equal to that at yield of the identical beam with no exposed reinforcement according to the CHBDC (CSA 2006). If Eqn. [2.4] was not satisfied, $jd(x)$ at the location of M_{max} was incorrect and so was increased by 0.1 mm. This iterative procedure was repeated until Eqn. [3.18] was satisfied. The resulting M_{max} was the predicted ultimate moment using the Strain

Compatibility Analysis, M_{SCA} , corresponding to a crushing failure of the concrete compression flange. The following assumptions were adopted:

- The maximum compressive stress, f_c'' in Eqn. [3.6], was assumed equal to f_c' ;
- The stresses in the exposed flexural reinforcement, f_s , were calculated using the stress-strain approximations obtained from tensile tests;
- The maximum compressive strain, ϵ_{cu} , was taken as the greater of the compressive strain recorded at failure by the strain gauges on the top surface of the concrete compression flange or 0.0035 (CSA 2006);
- The moment was assumed to be constant under the actuator head due to its rigidity; and,
- A segment length of $\Delta_x = 10$ mm was used.

5.2.1 Ultimate Flexural Capacity

As shown in Table 5-1, the predicted ultimate moments for each specimen correlate well with the observed values. The test-to-predicted ratios average 1.00 and have a standard deviation of 0.068. The failure modes for all five specimens were also consistent with those predicted: crushing of the concrete compression flange after yielding of the exposed flexural reinforcement. The higher predicted ultimate moments for Specimens 2 and 3 are attributed to the observed reduction of the gap between the exposed flexural reinforcement and the bottom of the concrete web, which was not accounted for in the analysis. The predicted ultimate moments were computed for ϵ_{cu} equal to the compressive strain recorded at failure and 0.0035: the observed difference was negligible. Details of

the prediction of the ultimate moment using the Strain Compatibility Analysis for Specimen 1 are presented in Appendix D.

Table 5-1: Predicted Strain Compatibility Analysis and Test Results.

Specimen	Observed	Predicted	Observed / Predicted	Reinforcement Strain at Failure		
	M_u (kN.m)	M_{SCA} (kN.m)		Obs.	Bonded Pred.	SCA Pred.
Control	201.5	-	-	-	0.044	-
1	158.4	157.2	1.01	0.0048	0.0446	0.0037
2	142.5	152.7	0.93	0.0146	0.0502	0.0136
3	143.7	157.1	0.92	0.0117	0.0531	0.0151
4	146.6	134.4	1.09	0.0030	0.0446	0.0032
5	145.8	134.3	1.08	0.0058	0.0446	0.0038
		Mean	1.00			
		Std Dev.	0.068			

The Strain Compatibility Analysis was also used to analyze Specimen 4 at a concrete compressive strain at midspan below the strain at failure. For an assumed concrete compressive strain value at midspan of 0.00179 the predicted and observed maximum moments were comparable, with values of 112.5 kN.m and 109.0 kN.m, respectively. The predicted and observed strain in the exposed flexural reinforcement were also similar with values of 0.00172 and 0.00168, respectively. This demonstrates that the current analysis can be used to accurately predict the maximum moment for any given concrete compressive strain.

5.2.2 Neutral Axis Depth

The variation of the neutral axis depth, $c(x)$, and location of the centroid of the compressive force, $y(x)$, at failure predicted using the Strain Compatibility Analysis correlates well with the observed cracking patterns, as shown in Figure 5-1. Flexural cracks were only observed in the tension zone near the location of M_{\max} . The neutral axis depth variation along the specimen length is similar to that observed by Cairns and Zhao (1993) and Harris (1996), described in Section 2.4. The neutral axis depth increases away from the location of M_{\max} moving below the soffit of the specimen and subsequently reemerging above the specimen causing concrete stresses of the opposite sense of those at M_{\max} (i.e., tensile above the neutral axis and compressive below it).

5.2.3 Reinforcement Strain at Failure

Marked differences in the flexural reinforcement strain at failure were observed, as also shown in Table 5-1. The predicted strain values shown are for an otherwise identical beam without exposed reinforcement, and for the specimen with exposed flexural reinforcement as computed using SCA. The observed strains are consistently significantly lower than those predicted assuming no exposed reinforcement. This phenomenon was cited by Cairns and Zhao (1993) as a cause of the reduced ductility of the observed response. The SCA-predicted strains are, in contrast, similar to those observed. The larger differences for Specimens 1, 2 and 3 are attributed to the assumption of ϵ_{cu} of 0.0035, necessary because the actual extreme compression fibre strains were not measured for these specimens.

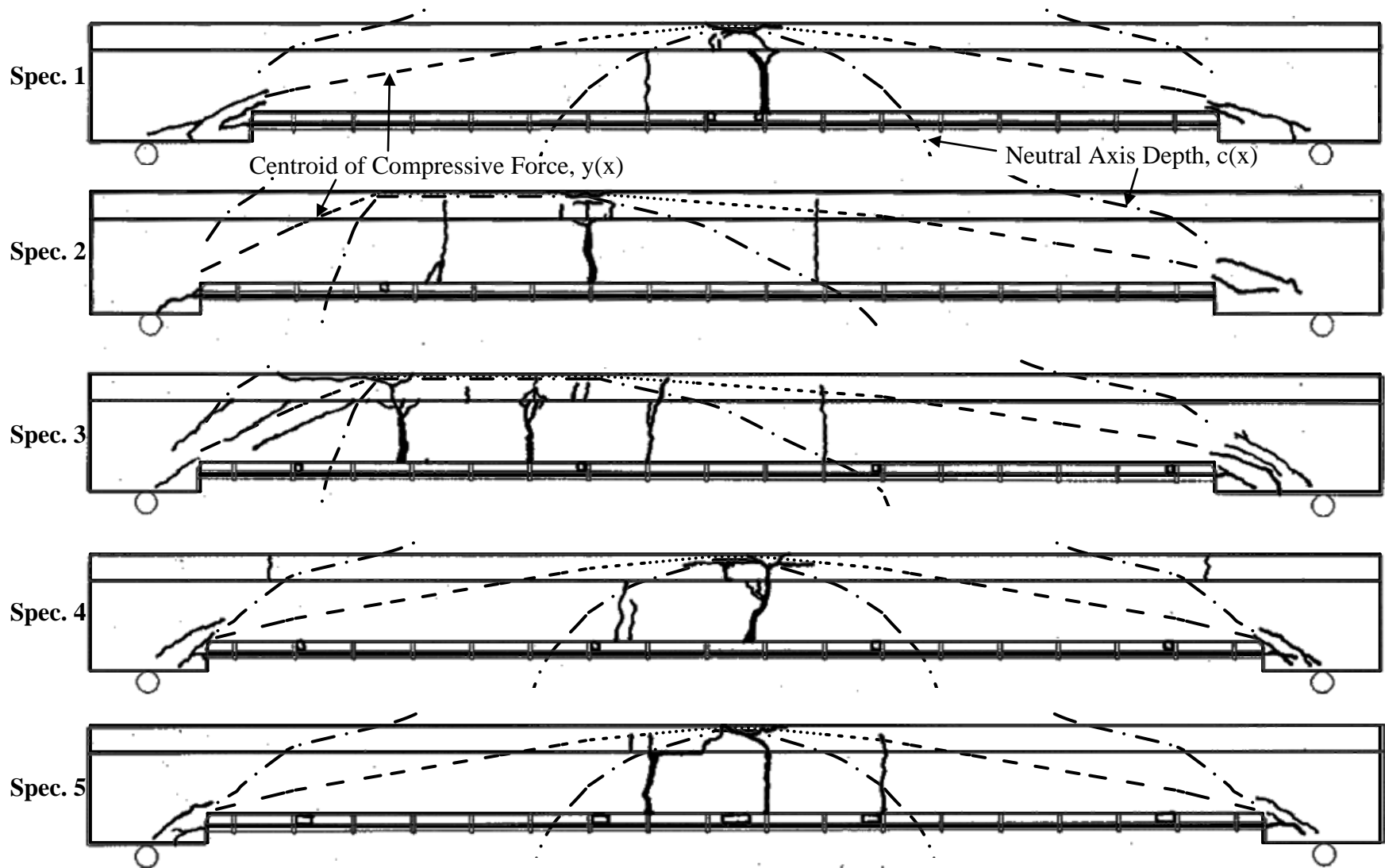


Figure 5-1: Variation of the SCA-predicted Neutral Axis Depth and Compressive Force Centroid at Failure and Observed Cracking Patterns.

5.3 COMPARISON TO STRUT-AND-TIE ANALYSIS PREDICTIONS

The Strut-and-Tie Analysis (STA) was also used to predict the capacity of the five specimens with exposed flexural reinforcement. The procedure described in Section 3.4 again could not be used directly because the length and position of the exposed flexural reinforcement, ℓ_{exp} , for each specimen was predetermined and so was altered slightly by rearranging Eqn. [3.45] to solve for the maximum moment. This predicted value, M_{STA} , corresponds to a crushing failure of the concrete web at the ends of the exposed length. Also, because α_1 is included in Eqn. [3.25] it is appropriate for comparison with experimental observed values to divide the concrete compressive strength value used in this equation by 0.90 in accordance with the note to Clause 10.1.6 in A23.3-04 (CSA 2004).

The STA-predicted ultimate moments are shown in Table 5-2, and can be only compared indirectly with the observed capacities because the associated predicted failure mode was not the failure mode observed. For Specimens 1, 2 and 3, the predicted M_{STA} exceed both the predicted M_{SCA} and observed M_u . For these specimens, the crushing failure of the web is not expected before the crushing in the compression flange predicted using the Strain Compatibility Analysis. This is consistent with what was observed. For Specimens 4 and 5, with greater lengths of exposed flexural reinforcement, web crushing failure at the ends of the exposed flexural reinforcement was predicted at loads that are a fraction of the observed ultimate loads. The crushing failure of the web was expected and not consistent with the failure observed. There is currently no proven explanation of this discrepancy, but possible explanations include: the simplification of the applied loading

(i.e., representing the load applied through the 150 mm diameter actuator head as a single point); small variations in the assumed and actual depths of the flexural reinforcement, depths of concrete removed and location of the exposed length; differences in the assumed and actual concrete strengths; and, strut confinement provided by the first fully enclosed stirrup between the support and the end of the exposed length.

Table 5-2: Predicted Strut-and-Tie Analysis and Test Results.

Specimen	Observed M_u (kN.m)	Predicted - (STA) M_{STA} (kN.m)	Observed / Predicted -	Orientation of Principal Compressive Strains at Failure			
				Obs. θ ($^\circ$)		θ_{STA} ($^\circ$)	
	θ_L	θ_R	θ_L	θ_R			
Control	201.5	-	-	-	-	-	-
1	158.4	179.6	0.88	14.9	13.5	12.7	
2	142.5	173.5	0.82	27.9	12.6	24.9	12.1
3	143.7	169.2	0.85	22.2	11.5	24.6	12.4
4	146.6	37.0	3.96	-*		13.4	
5	145.8	35.8	4.07	14.4		13.4	

* Bond issue with strain gauge.

5.3.1 Orientation of Principal Compressive Strains

Table 5-2 also indicates the predicted orientation of the principal compressive strains computed from the equations in Table 3-2. The STA-predicted orientations computed, θ_{STA} , are similar to those observed. The predicted and observed orientations at the left and right supports during testing of Specimen 3 are shown in Figure 5-2. The predicted θ_{STA} closely agree with those observed, the orientation remained fairly constant while the simulated uniformly distributed load, ω , was applied and began to increase at the left support and decrease at the right support as the point load, P , increased. The differences between the predicted and observed orientations may be due to the inherent difficulty of accurately measuring strains on the surface of the concrete web rather than the centre of the compressive strut within the web. The predicted and observed orientations of the principal compressive strains for the other specimens are presented in Appendix D.

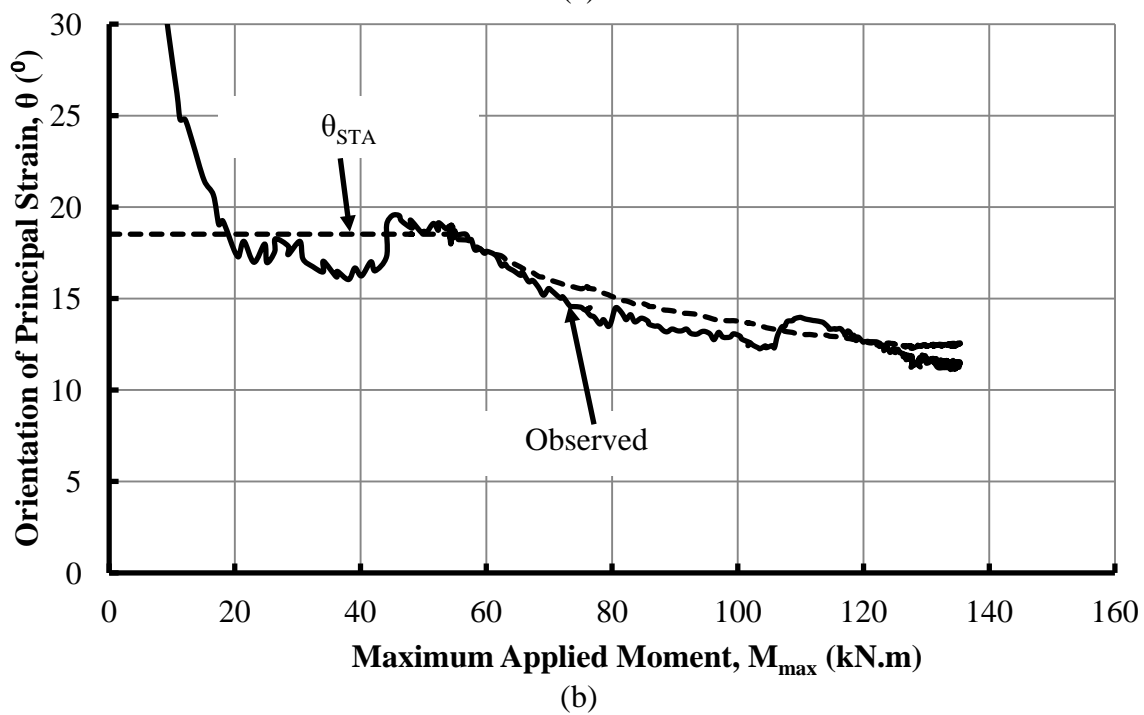
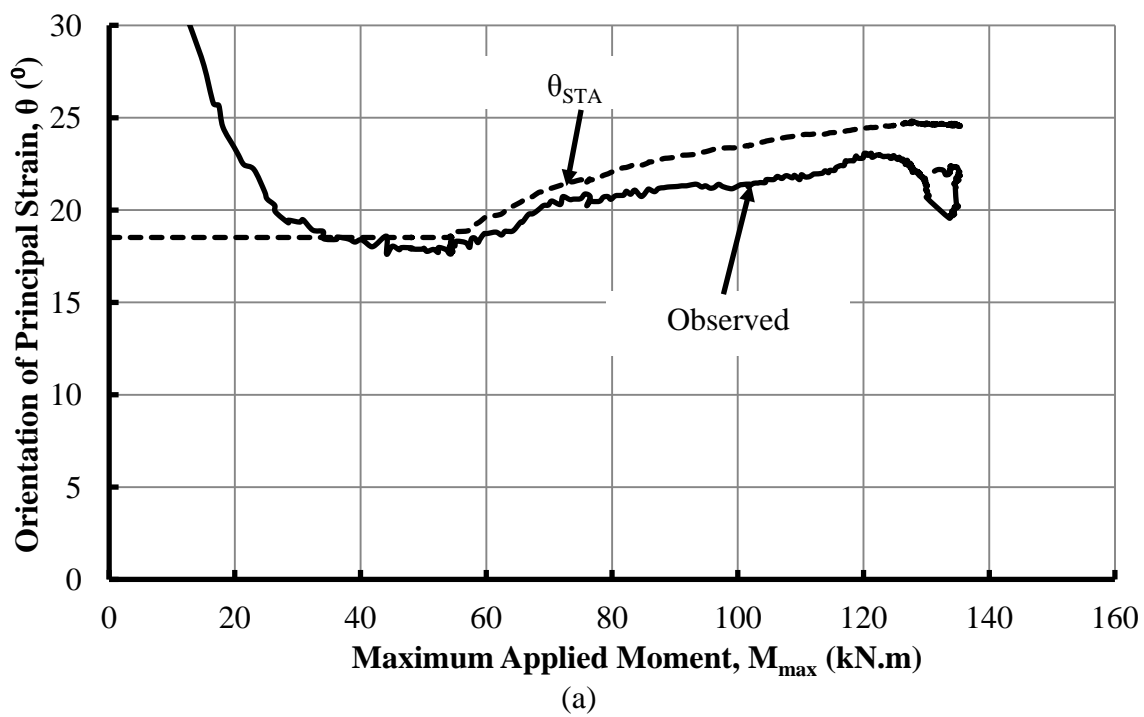


Figure 5-2: Orientation of the Predicted and Observed Principal Compressive Strains at the Supports of Specimen 3: (a) Left, (b) Right.

5.4 SUMMARY AND CONCLUSIONS

This chapter has presented a comparison of the experimental test results of the T-section specimens with exposed flexural reinforcement to predictions made using the two analytical approaches developed in Chapter 3.

The Strain Compatibility Analysis was validated by the experimental test results. The predicted ultimate moments computed using the Strain Compatibility Analysis for each specimen correlated well with the observed values with test-to-predicted ratios that averaged 1.00 and had a standard deviation of 0.068. The failure modes for all five specimens were also consistent with those predicted: crushing of the concrete compression flange after yielding of the exposed flexural reinforcement. The variation of the neutral axis depth and location of the centroid of the compressive force at failure predicted using the Strain Compatibility Analysis correlate well with the observed cracking patterns. Marked differences in the flexural reinforcement strain at failure were observed. The observed strains were consistently significantly lower than those predicted assuming no exposed reinforcement and were similar the SCA-predicted strains.

The Strut-and-Tie Analysis could only be indirectly validated by the experimental test results because the associated failure modes were not the failure modes observed. For specimens with shorter lengths of exposed flexural reinforcement, the predicted ultimate moments exceeded both the predicted ultimate moment from the Strain Compatibility Analysis and observed ultimate moment. For specimens with greater lengths of exposed flexural reinforcement, the predicted ultimate moments were significantly lower than those observed. There is currently no explanation for this discrepancy. The orientation of

the principal compressive strains predicted using the Strut-and-Tie Analysis were similar to those observed.

The results of the experimental investigation have yielded the following conclusions:

1. The Strain Compatibility Analysis accurately predicts the ultimate moment of a T-section beam with exposed flexural reinforcement for the failure modes corresponding to a crushing of the concrete compression flange either before or after yielding of the exposed flexural reinforcement.
2. The Strut-and-Tie Analysis gives a conservative predicted ultimate moment for a T-sections beam with exposed flexural reinforcement for the failure mode corresponding to a web crushing failure at the ends of the exposed flexural reinforcement. The Strut-and-Tie Analysis did, however, accurately predict the orientation of the principal compressive strains at the supports.

CHAPTER 6: SUMMARY, CONCLUSIONS AND RECOMMENDATIONS FOR FUTURE RESEARCH

6.1 SUMMARY

Reinforced concrete highway bridge girders are susceptible to deterioration caused primarily by corrosion of the reinforcing steel from the use of deicing salts. These bridge girders are repaired using the patch repair process, where the contaminated concrete is removed and replaced with new concrete, temporarily exposing the flexural reinforcement (e.g., Bertolini et al. 2004, Nehdi 2010). In this state, the flexural capacity is not easily computed because the usual provisions for design, as specified in Section 8.8 of the CHBDC (CSA 2006), are not applicable and no guidance is provided to assist practitioners. Thus, the focus of this research was to rectify this knowledge gap in the current code criteria by developing and validating new tools to assist practicing engineers wishing to quantify the safety of such girders during rehabilitation.

Chapter 2 presented a literature review of previous experimental and analytical investigations concerning reinforced concrete specimens with exposed flexural reinforcement. Seven unique combinations of specimen geometry and load location have been investigated by others comprising a total of 219 specimens subjected to only single- or two-point loading, with only one specimen having a T-cross section. Reinforced concrete bridge girders typically feature a substantial top slab and resist substantial uniformly distributed dead loads, so these loading configurations and specimens are not realistic. The marked differences in the failure mode, flexural capacity, and crack patterns were attributed to exposing the flexural reinforcement. Typically (e.g., Cairns and Zhao

1993) the following five distinct failure modes are observed: (1) Yielding of the exposed flexural reinforcement followed by crushing of the concrete on the compression face of the specimen; (2) Crushing of the concrete on the compression face of the specimen before yielding of the exposed tension flexural reinforcement; (3) Compression failure in the concrete at the ends of the exposed flexural reinforcement length; (4) Anchorage failure between one end of the exposed flexural reinforcement and the adjacent support; and, (5) Shear failure. It was concluded from this review that a reinforced concrete girder with exposed flexural reinforcement with given dimensional and material properties could exhibit the ductile failure it was originally designed to display with no reduction in yield capacity if the exposed length was not excessive or the flexural reinforcement ratio too large.

Chapter 3 presented two analytical approaches that were developed based on the findings of the literature review to assist practitioners in evaluating typical reinforced concrete bridge girders with exposed flexural reinforcement. The Strain Compatibility Analysis (SCA), using an accurate stress-strain concrete relationship, addressed the most predominant failure mode observed in previous experimental investigations (e.g., Cairns and Zhao 1993): crushing of the concrete on the compression face of the specimen before the exposed flexural reinforcement yields in tension. The Strut-and-Tie Analysis (STA) addressed another important failure mode that was observed by others (Cairns and Zhao 1993): crushing of the concrete at the end of the exposed length due to the inclined concrete compression strut intersecting the exposed end. The longest exposed length that ensured that a girder still exhibits a ductile failure with no reduction in yield capacity according to both analyses was defined as the critical length of exposed flexural

reinforcement, ℓ_c . The Strut-and-Tie Analysis was used to analyze the critical distance from the support the end of the exposed length where the compressive strut would intersect the exposed length, ℓ_e , for a typical T-section beam with: (1) point load only; (2) simulated uniformly distributed load only; and, (3) both point and simulated uniformly distributed loads.

Chapter 4 described the new experimental investigation of T-section specimens with exposed flexural reinforcement undertaken to observe the effect of exposing the flexural reinforcement and to evaluate the accuracy of the analytical approaches developed in Chapter 3. A Control Specimen and five specimens with exposed flexural reinforcement were designed, constructed and tested in the Structures Laboratory at the University of Western Ontario. An innovative testing apparatus was designed using an actuator and a system of whiffle trees to apply concurrent point and uniformly distributed loads that more accurately represents typical loadings in the field. Steel spacers were inserted between the exposed flexural reinforcement and the soffit of the concrete web to preserve the effective depth of the flexural reinforcement and to facilitate load transfer to the stirrups and create a plastic truss. Unsymmetrical loading configurations were applied to two specimens with exposed flexural reinforcement to facilitate comparison of the behaviour with symmetrically loaded specimens. The application of unsymmetrical loading caused the compressive strut near the support with the greater reaction to become steeper and the compressive strut near the support with the lesser reaction to become more horizontal. The chapter concluded with the results of the experimental investigation.

Chapter 5 presented a comparison of the experimental test results with analytical predictions to assess the validity of the two analytical approaches developed in Chapter 3.

6.2 CONCLUSIONS

The major conclusions of this study are as follows:

1. Comparing the results from the Strut-and-Tie Analysis for three loading cases, a simulated uniformly distributed load significantly affects the critical distance from the support to the end of the exposed length, ℓ_e . Thus an experimental investigation of T-section specimens loaded with a combination of a point load and a simulated uniformly distributed load would result in more realistic findings.
2. Reinforced concrete T-section specimens, having a flexural reinforcement ratio, ρ , of 0.37%, with their flexural reinforcement exposed over 82.5 to 90% of the span length can reach the flexural capacity of the original beam and exhibit a ductile failure. All test specimens failed by crushing of the concrete flange at a moment greater than the yield moment, M_y , and less than the ultimate moment, M_u , of the identical beam with no exposed reinforcement. With the flexural reinforcement exposed, strain hardening does not occur and so the capacity does not increase significantly beyond M_y .
3. Steel spacers placed in the gap between the concrete and exposed flexural reinforcement were effective in maintaining the depth of the flexural reinforcement, particularly if spaced uniformly along the exposed length of the flexural reinforcement and so are located at, or near, the locations of the maximum applied moment and the maximum deflection. Even with steel spacers

inserted, however, the stirrups are ineffective in the region where the flexural reinforcement is exposed.

4. The Strain Compatibility Analysis accurately predicts the ultimate moment of T-section beams with exposed flexural reinforcement for the failure modes corresponding to a crushing of the concrete compression flange either before or after yielding of the exposed flexural reinforcement. The test-to-predicted ratios for the five test specimens averaged 1.00 and with a standard deviation of 0.068. The failure modes in all cases were consistent with those predicted.
5. The Strut-and-Tie Analysis gives a conservative predicted ultimate moment for T-section beams with exposed flexural reinforcement for the failure mode corresponding to a web crushing failure at the ends of the exposed flexural reinforcement. The Strut-and-Tie Analysis could only be indirectly validated by the experimental test results because the associated failure modes were not consistent with the failure mode observed. For specimens with 82.5 to 86.5% of flexural reinforcement exposed, the Strut-and-Tie Analysis predicted correctly that web crushing failure at the ends of the exposed flexural reinforcement would not occur. For the two specimens with 90% of the flexural reinforcement exposed, web crushing failure was not observed even though it was predicted according to the Strut-and-Tie Analysis. There is currently no explanation for this discrepancy. The Strut-and-Tie Analysis did, however, accurately predict the orientation of the inclined compressive struts at the supports.
6. Both the Strain Compatibility Analysis (SCA) and Strut-and-Tie Analysis (STA) can be used for any length and location of exposed flexural reinforcement,

moment distribution or cross-section. They are important tools to assist practitioners evaluating reinforced concrete bridge girders with exposed flexural reinforcement.

6.3 RECOMMENDATIONS FOR FUTURE RESEARCH

Recommendations for future work are as follows:

1. To validate the Strut-and-Tie Analysis further an experimental investigation to explain the discrepancy observed in this current study is needed. The investigation should include specimens with shorter lengths of exposed flexural reinforcement located close to the supports. The length of exposed flexural reinforcement would be selected to prevent the failure mode predicted by the Strain Compatibility Analysis and so ensure the specimens would exhibit a compression failure at the end of the exposed length.
2. To expand the scope of these analytical approaches, more experimental investigations should be performed. In particular multi-span bridges comprised of both positive and negative moment regions should be investigated. The investigations would have to consist of two-span specimens with the flexural reinforcement exposed in one of three locations: (1) positive moment region; (2) spanning both the positive and negative moment regions; and, (3) entirely in the negative moment region near the centre support.
3. To expand the scope of the experimental investigations to include cyclic loading. This would examine potential fatigue damage of the specimens with exposed flexural reinforcement and would account for the typical loading combination of a

uniformly distributed dead load and repeated moving traffic live loads applied to a reinforced concrete bridge girder.

4. To investigate the effect of removing the deteriorated concrete and subsequently replacing it with new concrete while the uniformly distributed dead load is still applied with more experimental investigations. The investigations would involve repairing specimens with exposed flexural reinforcement using the current standards while the simulated uniformly distributed dead load is applied. Once the concrete has cured the specimens would then be tested and compared to a control specimen.
5. To assist practitioners evaluating a reinforced concrete bridge with exposed flexural reinforcement develop design guidelines, based on the research findings. The guidelines would require the practitioner to input the geometric and material properties of the girder, the general shape of the moment distribution and the length and location of the exposed flexural reinforcement to predict the maximum moment that could be applied. The guidelines would also be able to predict the maximum length of flexural reinforcement that could be exposed that would ensure the girder would still exhibit a ductile flexural failure and exhibit no reduction in its flexural capacity.

REFERENCES

- American Society for Testing and Materials (ASTM) (2012). *10.1520/C0039 - C0039 - 12a - Standard Test Method for Compressive Strength of Cylindrical Concrete Specimens*, West Conshohocken, PA: ASTM International. www.astm.org.
- Bartlett, F.M. (1982). *Computer Analysis of Partially Prestressed Concrete – M.A.Sc. Thesis*, Waterloo, ON: The University of Waterloo.
- Bartlett, F.M. (1998). “Behavior of Partially-repaired Reinforced Concrete T-beams”, *Proceedings of the 2nd CSCE Structures Specialty Conference*, Halifax, IIIa: 69-78.
- Bertolini, L., Elsener, B., Pedferri, P. and Polder, R. (2004). *Corrosion of Steel in Concrete: Prevention, Diagnosis, Repair*, Weinheim: Wiley-VCH.
- Buckland, et al. (1988). *Improvement to Clause 12 of S6*, North Vancouver, BC: Buckland and Taylor Ltd.
- Cairns, J. and Zhao, Z. (1993). “Behaviour of Concrete Beams with Exposed Reinforcement”, *Proceedings of the Institution of Civil Engineers – Structures and Buildings*, Vol. 99, May, 141-154.
- Cairns, J. (1995). “Strength of Concrete Beams during Concrete Breakout”, *International Association for Bridge and Structural Engineering*, Vol.73, No.1, 499-504.
- Cairns, J. (1995). “Strength in Shear of Concrete Beams with Exposed Reinforcement”, *Proceedings of the Institution of Civil Engineers – Structures and Buildings*, Vol. 110, May, 176-185.
- Canadian Standards Association (CSA) (2009). *CAN/CSA-S16-09 Limit States Design of Steel Structures*, Mississauga, ON: CSA International.
- Canadian Standards Association (CSA) (2006). *CAN/CSA-S6-06 Canadian Highway Bridge Design Code (CHBDC)*, Mississauga, ON: CSA International.
- Canadian Standards Association (CSA) (2004). *A23.3-04 Design of Concrete Structures*, Mississauga, ON: CSA International.
- Dillon Consulting (2001). *Detailed Bridge Deck Condition Survey Update – Waterloo Regional Road 97 Underpass, Highway 401*, Structural Drawings No. 1 – 5, London, ON: Dillon Consulting Ltd.
- Emmons, P.H, et al. (2003). “ACI RAP Bulletin 5: Field Guide to Concrete Repair Application Procedures: Surface Repair Using Form-and-Pump Techniques”, *American Concrete Institute*.

- Eyre, J.R. and Nokhasteh, M.A. (1992). “Strength Assessment of Corrosion Damaged Reinforced Concrete Slabs and Beams”, *Proceedings Institution of Civil Engineers, Structures and Buildings*, Vol. 94, May, 197-203.
- Guettala, A. and Abibsi, A. (2006). “Corrosion Degradation and Repair of a Concrete Bridge”, *Materials and Structures*, Vol. 39, 471-478.
- Harris, M. (1996). *Behaviour and Analysis of Deteriorated Reinforcement Concrete T-beams - ES440 Project Report - presented in partial fulfillment of the requirements for the B.E.Sc. degree*, London, ON: Dept. of Civil Engineering, University of Western Ontario.
- MacGregor, J. G. and Bartlett, F.M. (2000). *Reinforced Concrete: Mechanics and Design*, Toronto, ON: Prentice Hall Canada Inc.
- Ministry of Transportation of Ontario (MTO) (2008). “Snow and Ice Control on Ontario’s Highways”, Queen’s Printer for Ontario.
- Ministry of Transportation of Ontario (MTO) (2010) “Ontario Structure Inspection Manual – Inspection Form”, Ministry of Transportation, Report generated on Monday, August 16, 2010.
- Minkarah, I. and Ringo, B.C. (1982). “Behaviour and Repair of Deteriorated Reinforced Concrete Beams”, *Transpn Res. Rec.*, No. 821, 73-79.
- Nehdi, M.L. (2010). *CEE-3369 Materials for Civil Engineering: Chapter 3 - Durability of Concrete – Lecture Notes*, London, ON: Dept. of Civil and Environmental Engineering, University of Western Ontario.
- Nehdi, M.L. (2011). *CEE-9598 Durability, Monitoring and Rehabilitation of Concrete Structures: Chapter 2 – Corrosion of Reinforcing Steel – Course Notes*, London, ON: Dept. of Civil and Environmental Engineering, University of Western Ontario.
- Nemec, P. (1996). *The Behaviour of Partially Repaired Concrete T-beams - ES440 Project Report- presented in partial fulfillment of the requirements for the B.E.Sc. degree*, London, ON: Dept. of Civil Engineering, University of Western Ontario.
- Nokhasteh, M.A., Eyre, J.R. and McLeish, A. (1992). “The effect of Reinforcement Corrosion on the Strength of Reinforced Concrete Members”, *Proceedings of the Conference on Structural Integrity Assessment*, London, Ed Stanley, P. Elsevier, 314 – 325.
- Ontario Provincial Standard Specification (OPSS) (1994) “OPSS 928 – Construction Specification for Structure Rehabilitation – Concrete Removal”.

- Raof, M. and Lin, Z. (1993). "Implications of Structural Damage to Concrete Elements", *Proceedings of the Conference on Bridge Management*, Surrey University, UK. Ed. Harding J. E., Park G, A, R, and Ryall M, J. Thomas Telford, London, 66-74
- Raof, M. and Lin, Z. (1995). "Implications of Exposure of Main Steel during Patch Repairs", *International Association for Bridge and Structural Engineering*, Vol. 73, No. 1, 505-510.
- Raof, M. and Lin, Z. (1997) "Structural Characteristics of R.C. Beams with Exposed Main Steel", *Proceedings of the Institution of Civil Engineers – Structures and Buildings*, Vol. 122, February, 35-51.
- Sharaf, H. and Soudki, K. (2002). "Strength Assessment of Reinforced Concrete Beams with Debonded Reinforcement and Confinement with CFRP Wraps", *Proceedings of the 4th CSCE Structural Specialty Conference*, Montreal.
- Todeschini, C., Bianchini, A. and Kesler, C. (1964). "Behaviour of Concrete Columns Reinforced with High Strength Steels", *ACI Journal, Proceedings*, Vol. 61, No. 6, June, 701-716.
- Unterweger, W. and Nigge, K. (2009). "Corrosion in Concrete Bridge Girders", *School of Doctoral Studies Journal*, No. 1, July, 125-134.
- Xiong, G., Liu, J. and Xie, H. (2000). "Flexural Behaviour of Reinforced Concrete Beams with Unbonded Repair Patch", *ACI Structural Journal*, Vol. 97, No. 5, 783-786.
- Zhang, S. and Raof, M. (1995). "Prediction of the Behaviour of R.C. Beams with Exposed Reinforcement", *Magazine of Concrete Research*, Vol. 47, December, 335-344.

**APPENDIX A:
LITERATURE REVIEW DETAILS**

A.1 INTRODUCTION

This appendix presents summarizes of the eight previous experimental investigations on the effect of exposed flexural reinforcement that have been conducted since 1980. The investigations involve a total of 219 specimens subjected to either single- or two-point loading. The descriptions include the number of specimens tested, specimen dimensions, loading configurations, testing procedures and measurements taken.

A.2 MINKARAH AND RINGO (1982)

Minkarah and Ringo (1982) investigated the effect of both cover and flexural bond losses, located symmetrically about midspan, on 40 reduced scale (127 mm x 254 mm x 2900 mm) simply supported specimens, shown in Figure A-1, including 5 control specimens, on the behaviour and capacity of specimens. All the specimens were designed to exhibit a ductile failure, where the concrete crushes after the flexural reinforcement has yielded, if no reinforcement was exposed. To simulate a loss of cover only, the concrete was blocked out from the bottom of the flexural reinforcement, whereas to simulate loss of both cover and bond, the concrete was blocked out to the top of the flexural reinforcement. The specimens, with various lengths of exposed flexural reinforcement, l_{exp} , were subjected to single-point loads at two distances, αL , of 900 mm and 460 mm from the left support, to avoid applying the point load within the exposed length. The specimens were loaded in 2.23 kN increments, at a rate of 0.088 kN/sec at 3 minute intervals. Before and after each load increment, deflection measurements and strain gauge readings were recorded to failure (Minkarah and Ringo 1982).

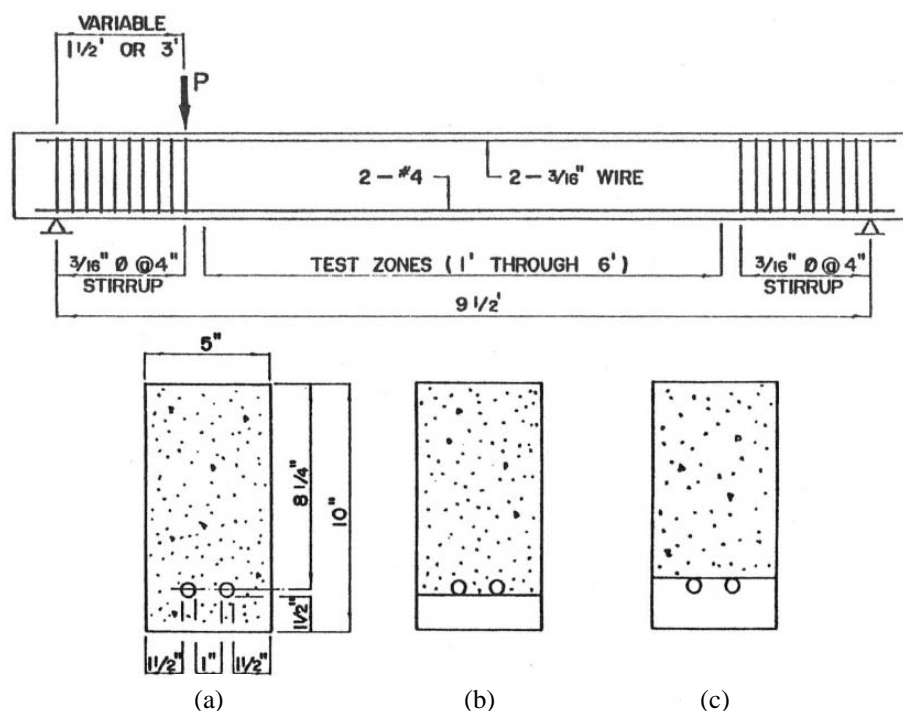


Figure A-1: Details of: (a) Control Specimen (b) Test Specimen with Loss of Only Cover (c) Test Specimen with Loss of Cover and Flexural Bond (Minkarah and Ringo 1982).

A.3 NOKHASTEH, EYRE AND MCLEISH (1992)

Nokhasteh, Eyre and McLeish (1992) tested three specimens, with spans of 2000 mm and cross sections 130 mm wide by 200 mm deep, as shown in Figure A-2. The specimens were subjected to two equal point loads, placed symmetrically about the midspan. Both would exhibit a ductile failure if no reinforcement was exposed. No control specimen was tested; rather the test specimens were compared to theoretical load capacities for a beam with fully bonded flexural reinforcement. The test objective was to investigate the effects of the exposed flexural reinforcement length, ℓ_{exp} , and flexural reinforcement ratio, ρ , response. Two specimens had exposed flexural reinforcement for 85% of the span length, one containing 0.93% flexural reinforcement and the other 1.85%. The third specimen

contained 0.93% flexural reinforcement exposed over 25% of the span. The loading was applied in three cycles, removing the load between cycles, until failure.

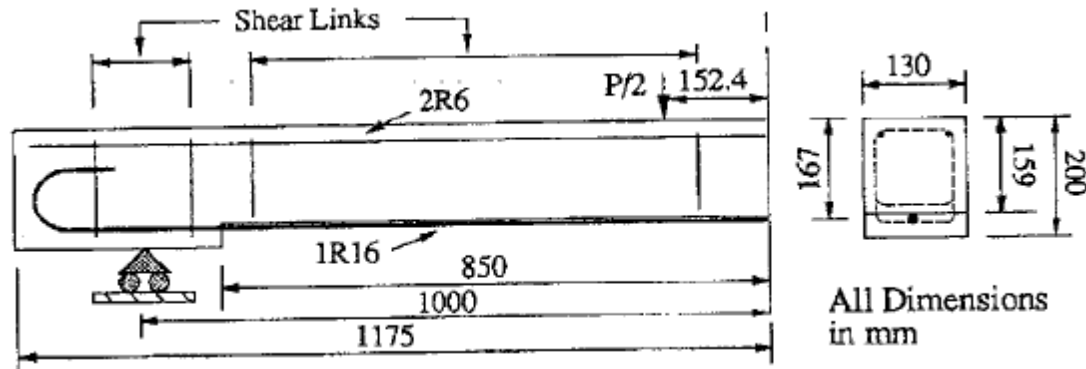


Figure A-2: Dimensions for a Typical Specimen with Exposed Flexural Reinforcement (Nokhasteh, Eyre and McLeish 1992).

A.4 CAIRNS AND ZHAO (1993)

Cairns and Zhao (1993) tested 19 simply supported specimens, subjected to two equal point loads placed symmetrically about the midspan, as shown in Figure A-3. Their study focused on the ratio of exposed flexural reinforcement length to span of specimens, ℓ_{exp}/L , spacing of the two loads, S , the flexural reinforcement ratio, ρ , and the span/effective depth ratio, L/d (Cairns and Zhao 1993).

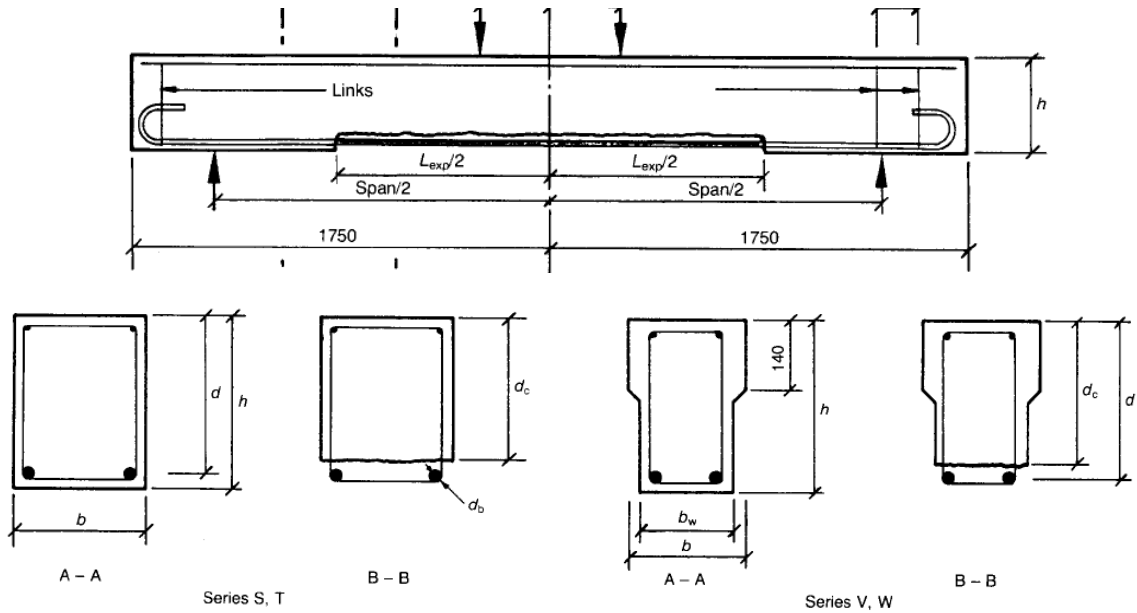


Figure A-3: Details of Test Specimens, all Dimensions in mm (Cairns and Zhao 1993).

In the first part of their study, two concrete specimens were investigated, one designed to fail in shear and the other to fail in flexure, to study the changing patterns of strains in the specimens. The concrete strain distribution over the beam depth was recorded for increased lengths of exposed flexural reinforcement, l_{exp} . The test specimens were subjected to two-point loading, as shown in Figure A-4(a), to initiate cracking at service loads, and then the load was reduced to represent the dead load present during the repair process. Next, concrete surrounding the flexural reinforcement was removed over a length of 200 mm to either side of the centerline of the specimen and the concrete surface strains were again measured. After that, the spacing between the two loads was increased, Figure A-4(b), and then reduced, Figure A-4(c) and the concrete surface strain distributions were measured for both loading conditions, at applied loads that cause the same midspan moment as occurred for the loading condition in Figure A-4(a). The load was then relocated to the original position, an additional 150 mm of concrete was

removed at both ends of the exposed length, and the loading was reapplied at each of the three load spacings. This process was repeated until the exposed flexural reinforcement length, ℓ_{exp} , was equal to 1900 mm.

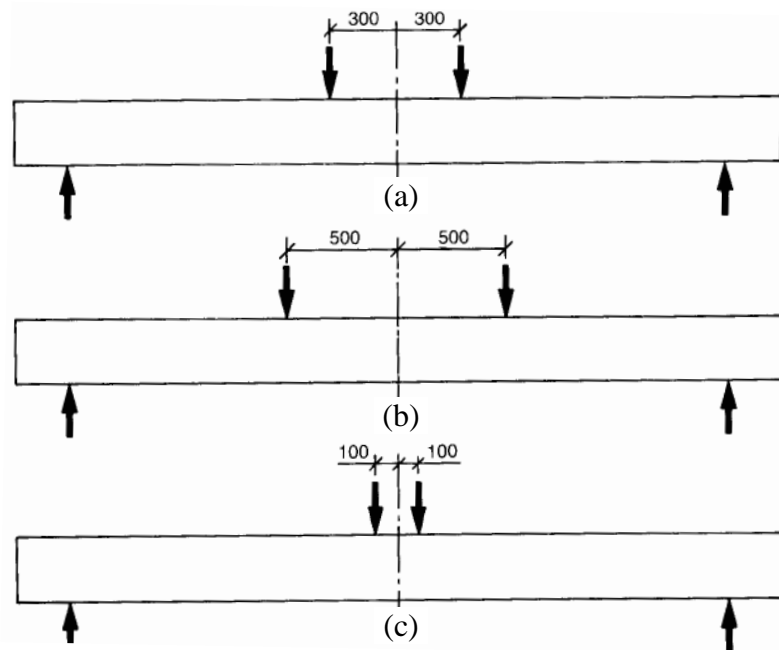


Figure A-4: Loading Configuration for the First Part of Study (Cairns and Zhao 1993).

In the second part of their investigation, 17 test specimens were tested to failure to examine the effect of the exposed length of flexural reinforcement, shown in Figure A-3. Three specimens were controls with no exposed reinforcement; five of the specimens with exposed flexural reinforcement were designed to fail in shear if the flexural reinforcement is fully bonded, while the nine remaining specimens were designed to fail in flexure. The specimens were incrementally loaded using the loading configuration shown in Figure A-4(a) at a constant rate of deflection to failure, defined as the maximum load applied to the specimen and when crushing of concrete became visible. The concrete

strain distribution was recorded at each load increment and midspan deflection and reinforcement strains were continuously recorded.

Cairns (1995) performed further tests to investigate the shear capacity of concrete specimens with exposed flexural reinforcement as an extension of his previous study. Three series of tests were conducted involving a total of ten specimens with 3000 mm spans, as shown in Figure A-5. Each series included one control specimen, with no exposed reinforcement, while the remaining specimens had portions of one of the two flexural reinforcing bars exposed. The control specimens in each series were designed to fail in shear before the flexural capacity was reached. The test specimens were continuously loaded at 20 kN increments to failure. The concrete strain distributions, midspan deflections and crack development were recorded. Failure was defined as a rapid drop of load or the appearance of a large inclined crack in the shear span.

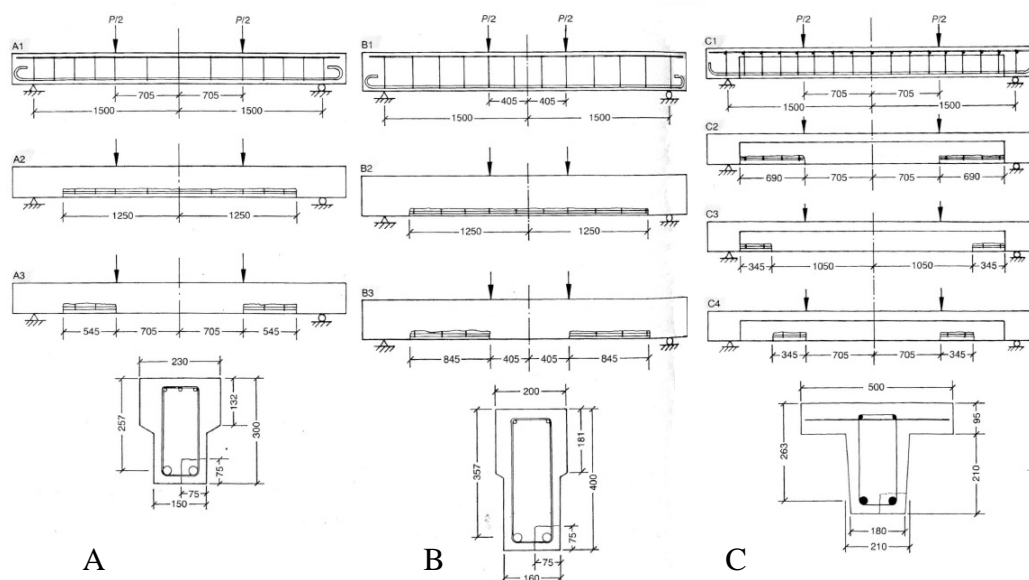


Figure A-5: Details of Test Series Specimens A, B, and C (Cairns 1995).

A.5 RAOOF AND LIN (1993, 1995, 1997)

Raoof and Lin (1993, 1995, 1997) performed 132 tests of both small and large-scale test on simply supported specimens subjected to single-point loading with various lengths of exposed flexural reinforcement, l_{exp} . The specimens were designed to exhibit either a ductile failure or a shear failure if no reinforcement was exposed. The parameters investigated in the tests were; length of exposed flexural reinforcement, l_{exp} , location of the exposed flexural reinforcement with respect to the nearest support, l_{end} , load position(s) relative to the support, αL , flexural reinforcement ratio, ρ , depth of concrete removal, d_c , inclusion of compression reinforcement, A_s' , effect of stirrups.

Their small-scale tests consisted of 44 specimens with spans of 1760 mm and overall depths of 130 mm, shown in Figure A-6. Eleven sets of four specimens each were tested: three specimens had exposed flexural reinforcement near one support and the fourth was a control specimen with no exposed reinforcement. None of the specimens contained shear or top flexural (i.e., compression) reinforcement. The exposed length of flexural reinforcement was either 300 mm or 400 mm and the concrete removal depth was 35 mm. The position of single point load from the left support was varied between 12 and 70% of the span length. The load was increased incrementally until the specimen failed, with the centre-span displacement, crack patterns and concrete strains over the full depth of the specimens recorded.

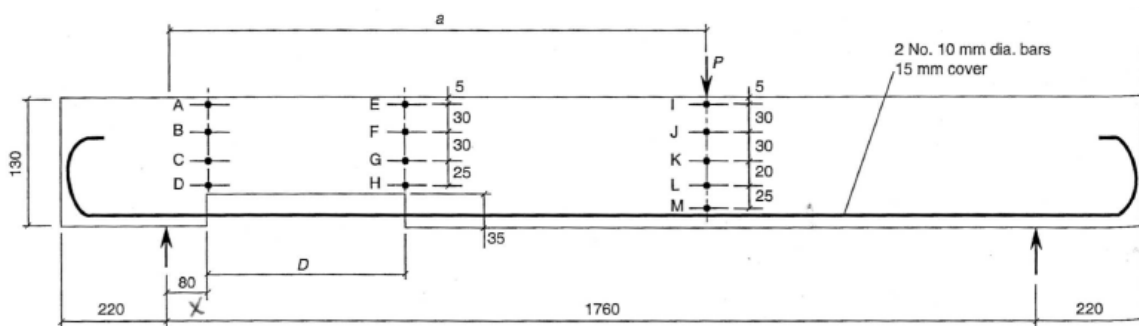


Figure A-6: Details of Small-scale Test Specimens with Width = 75 mm (Raouf and Lin 1997).

Their large-scale tests consisted of 88 specimens with spans of 3000 mm and overall depths of 150 mm, shown in Figure A-7. These tests were similar to the small-scale tests, but explored a much larger number of parameters. Raouf and Lin (1997) tested simply supported specimens loaded by single and two-point loads at located $\alpha = 0.3$ from the left support and exposed flexural reinforcement lengths of 0.1, 0.2 and 0.3L starting at the left support. They tested specimens with and without shear and top (compression) reinforcement. The load deflection curves for the test specimens were recorded and used to determine the type of failure.

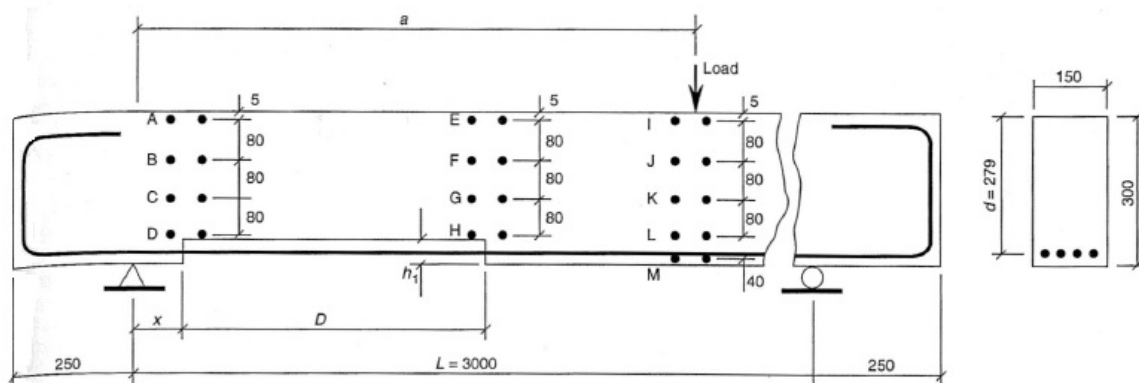


Figure A-7: Details of Large-scale Test Specimens (Raouf and Lin 1997).

A.6 NEMEC (1996)

Nemec (1996) tested two 4000 mm long T-section specimens subjected to two equal point loads placed symmetrically about the midspan with an overall depth of 400 mm, an overall width of 800 mm, a flange thickness of 90 mm, a web thickness of 200 mm, and an effective flexural reinforcement depth of 342 mm, as shown in Figure A-8. The first was the control specimen and the second was the test specimen with 2000 mm of the flexural reinforcement exposed symmetrical about the midspan to simulate the effect of concrete removal during repair procedures. Both were designed to exhibit a flexural failure and had sufficient shear capacity to prevent a premature shear failure. Both were tested to failure using a constant rate of deflection, during which the crack patterns, centerline deflection, crack widths and the load applied were measured and recorded.

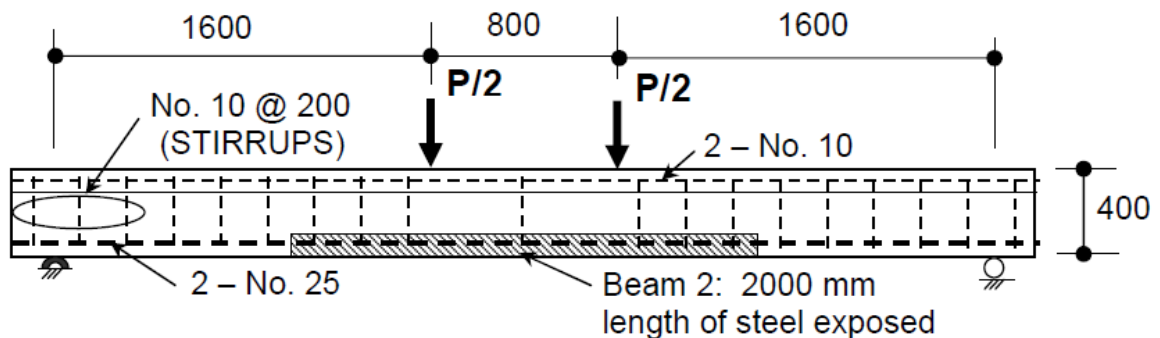


Figure A-8: Details of Test Specimens and Loading Configuration (Bartlett 1998).

A.7 XOING, LIU AND XIE (2000)

Xoing, Liu and Xie (2000) tested eight simply supported reinforced concrete specimens, with spans of 1800 mm, subjected to two equal point loads to determine their flexural capacity. The specimens subjected to short-term loads are shown in Figure A-9 and the specimens subjected to long-term loads are shown in Figure A-10. There were four

control specimens and four specimens with exposed flexural reinforcement over 50% of the span. For the short-term tests, the load was incrementally increased by 5 kN. At each increment, the deflections at the midspan and under the point loads, crack widths and patterns, concrete strain distributions and reinforcement strains were measured. For the long-term tests, the specimens were loaded to 45% of the short-term ultimate load-carrying capacity of the control specimens and the midspan deflections were measured over 150 days.

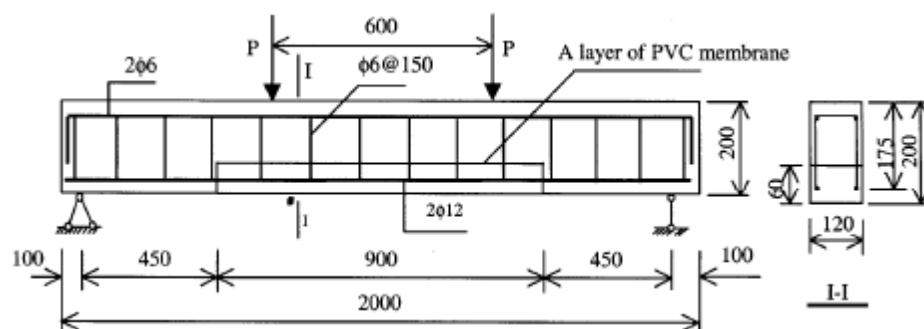


Figure A-9: Details of Short-term Test Specimens (Xiong, Liu and Xie 2000).

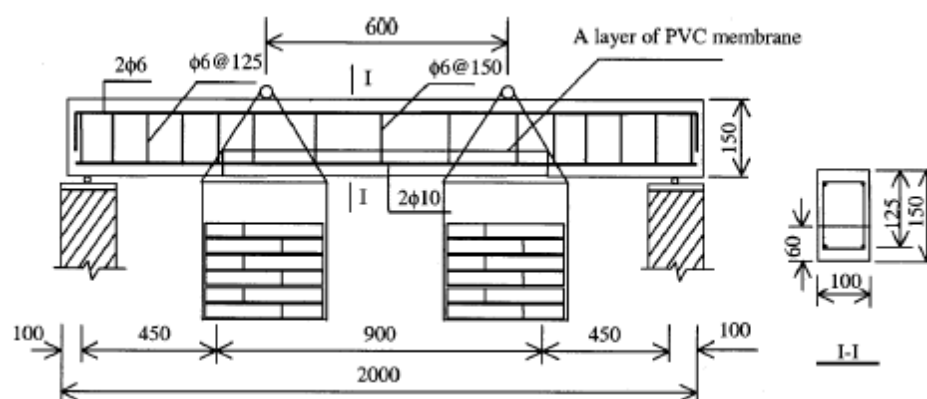


Figure A-10: Details of Long-term Test Specimens (Xiong, Liu and Xie 2000).

A.8 SHARAF AND SOUDKI (2002)

Sharaf and Soudki (2002) investigated the flexural capacity of five reinforced concrete specimens with varying lengths of debonded (or exposed) flexural reinforcement, l_{exp} , subjected to two point loads located symmetrically about the midspan, as shown in Figure A-11. The specimens had spans of 1500 mm, 100 x 150 mm cross-section and were designed to fail in flexure. One specimen was a control and the other four had the flexural reinforcement exposed over 50, 70, 80, and 90% of the span. The end of the exposed lengths extended beyond the constant moment region, into the constant shear region. During the tests the crack formations, ultimate capacity and deformations were recorded.

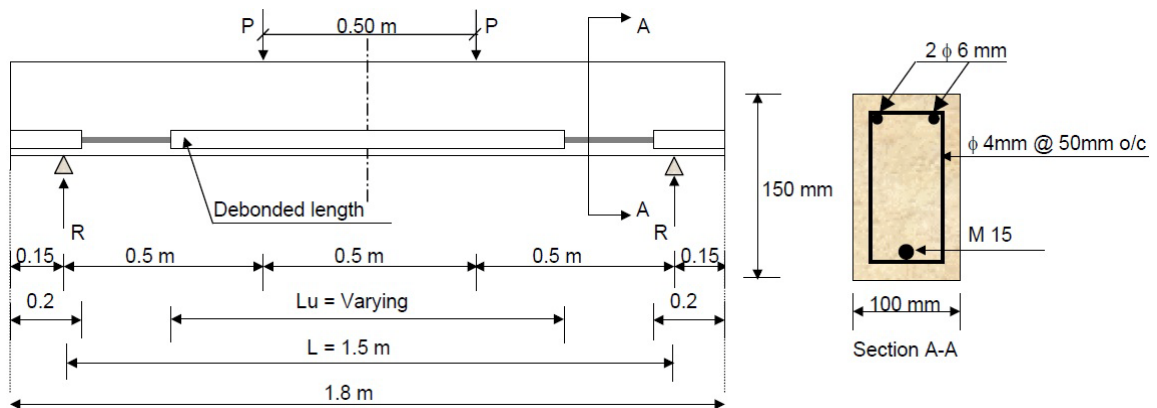


Figure A-11: Details of Test Specimens (Sharaf and Soudki 2002).

**APPENDIX B:
ANALYSIS OF SPECIMENS WITH EXPOSED
FLEXURAL REINFORCEMENT**

B.1 INTRODUCTION

This appendix presented complete derivations of equations relating to both the Strain Compatibility Analysis and the Strut-and-Tie Analysis. The derivation of the equations for each case of the neutral axis depth location, Z , used in the Strain Compatibility Analysis for a linear concrete stress-strain relationship is presented, as shown in Table 3-1. The equations include: the location of the compressive force from the neutral axis depth, $y(x)$; resultant compressive force in the concrete, $C(x)$; extreme concrete compression fibre stress, $f_c(x)$; and, the extrapolated strain in the concrete at the depth of the exposed flexural reinforcement, ϵ_{cs} . The derivations for the equations $\tan\theta_{sL}$ and $\tan\theta_{sR}$, as shown in Table 3-2, as part of the process of determining the critical distance from the support to the end of the exposed length, ℓ_e , for the Strut-and-Tie-Analysis subjected to a combination of a concurrent point and simulated distributed load (i.e., Load Case 3) are also presented. The derivations are completed for the point load locations regions 1 to 3.

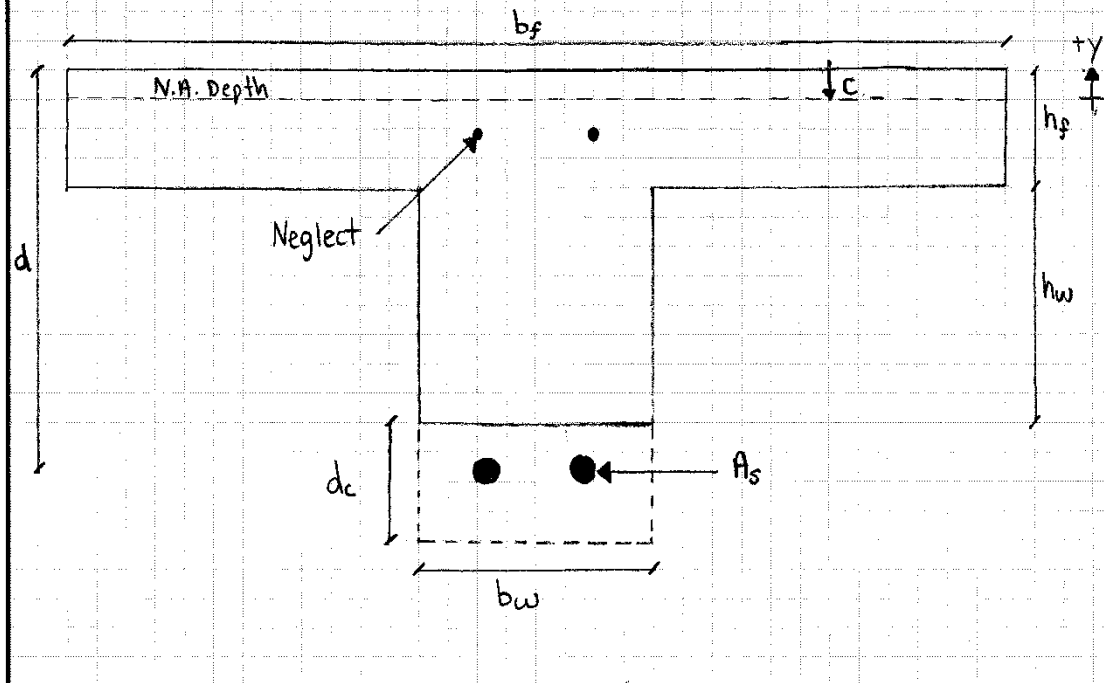
B.2 STRAIN COMPATIBILITY ANALYSIS (SCA) DERIVATION

STRAIN COMPATIBILITY ANALYSIS

The following are the derivations of the equations for the six possible locations of the neutral axis, C_i , including the compression force, location of the compression force, extreme concrete compression fibre stress and concrete strain at the level of the flexural reinforcement.

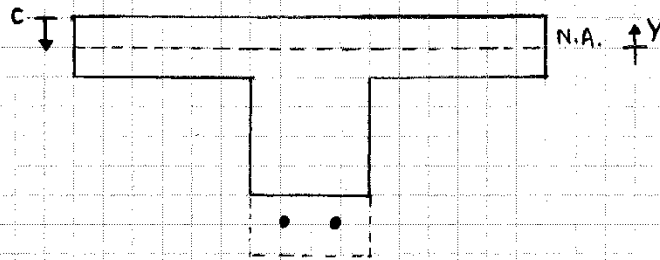
Cross Section:

To derive the equations the basic geometry of the cross section must be known. The following figure shows the general shape of the cross section along with the important variables.

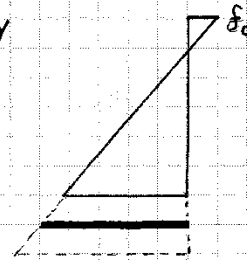


Case 1 ($0 \leq c(x) \leq h_f$)

Section:



Stress Distribution:



Location of Compression Force from N.A. Depth, y (mm):

$$y = \frac{2}{3} c$$

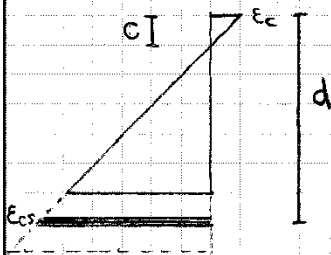
Compression Force in Concrete, C (N):

$$C = \sigma_c b_f \frac{c}{2}$$

Extreme Concrete Compression Fibre Stress, f_c (MPa):

$$f_c = \frac{C}{A} = \frac{T}{c/2 \cdot b_f} = \frac{2T}{c b_f} = \frac{2 A_s f_s}{c b_f}$$

Concrete Strain at the Level of the Flexural Reinforcement, ϵ_{cs} :



$$\frac{-\epsilon_{cs}}{(d-c)} = \frac{\epsilon_c}{c} \Rightarrow \epsilon_{cs} = \epsilon_c \left(1 - \frac{d}{c}\right)$$

Assuming that $\epsilon_c = \frac{f_c}{E_c}$

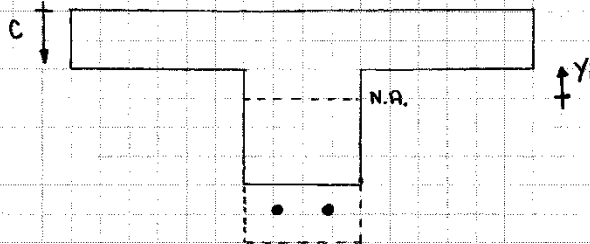
$$\text{and } E_c = (3000 \sqrt{f'_c} + 6900) \left(\gamma_c / 2300\right)^{1.5}$$

(CHBDC 8.4.1.7)

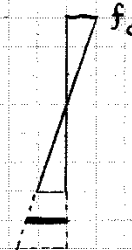
$$\therefore \epsilon_{cs} = \frac{f_c}{E_c} \left(1 - \frac{d}{c}\right)$$

Case 2 ($h_f \leq c(x) \leq h_w$)

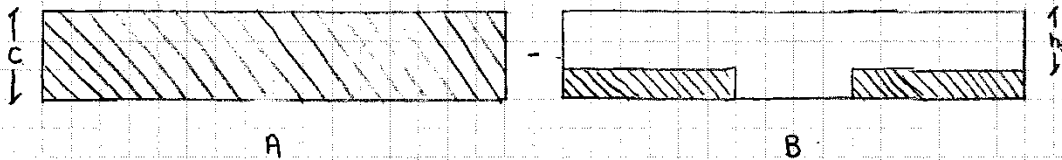
Section:



Stress Distribution:



The Section simplifies to:



Location of Compression Force from N.A. Depth, y (mm):

$$y_i = \frac{2}{3} c$$

$$y_i = \frac{2}{3} (c - h_f)$$

Compression Force in Concrete, $C(N)$:

$$C = f_c b_f \frac{c}{2}$$

$$C = f_c \left(\frac{c - h_f}{c} \right) (b_f - b_w) \frac{(c - h_f)}{2}$$

Summation of Compression Forces, $C(N)$:

$$C = \frac{f_c}{2} b_f c - \frac{f_c}{2} \left(\frac{c - h_f}{c} \right) (b_f - b_w) (c - h_f)$$

$$C = \frac{f_c}{2c} \left[c^2 b_f - (b_f - b_w) (c - h_f)^2 \right]$$

$$C = \frac{f_c b_f}{2c} \left[c^2 - \left(1 - \frac{b_w}{b_f} \right) (c - h_f)^2 \right] = \frac{f_c b_f c}{2} \left[1 - \left(1 - \frac{b_w}{b_f} \right) \left(1 - \frac{h_f}{c} \right)^2 \right]$$



Western Society for Civil Engineering
Faculty of Engineering
The University of Western Ontario

Date: _____

Name: _____

Course: _____

Page: 4 of _____

Project: Strain Compatibility Analysis

Location of Compression Force from N.A Depth, \bar{y} (mm):

$$C \cdot \bar{y} = \left(f_c b_f \frac{c}{\alpha} \right) \left(\frac{\alpha c}{3} \right) - \left(\frac{\alpha}{3} (c - h_f) \right) \left(f_c \left(\frac{c - h_f}{c} \right) (b_f - b_w) \frac{(c - h_f)}{\alpha} \right)$$

$$C \cdot \bar{y} = \frac{f_c b_f c^2}{3} - \frac{f_c}{3} (c - h_f) \left(\frac{c - h_f}{c} (b_f - b_w) (c - h_f) \right)$$

$$C \cdot \bar{y} = \frac{f_c b_f c^2}{3} \left[1 - \left(1 - \frac{b_w}{b_f} \right) \left(1 - \frac{h_f}{c} \right)^3 \right]$$

$$\bar{y} = \frac{f_c b_f c}{3} \left[1 - \left(1 - \frac{b_w}{b_f} \right) \left(1 - \frac{h_f}{c} \right)^3 \right] \cdot \frac{c}{\alpha} \left[1 - \left(1 - \frac{b_w}{b_f} \right) \left(1 - \frac{h_f}{c} \right)^2 \right]$$

$$\bar{y} = \frac{\alpha c}{3} \left[1 - \left(1 - \frac{b_w}{b_f} \right) \left(1 - \frac{h_f}{c} \right)^3 \right] \cdot \frac{c}{\alpha} \left[1 - \left(1 - \frac{b_w}{b_f} \right) \left(1 - \frac{h_f}{c} \right)^2 \right]$$

Extreme Concrete Compression Fibre Stress, f_c (MPa):

$$C = T = \frac{f_c b_f c}{\alpha} \left[1 - \left(1 - \frac{b_w}{b_f} \right) \left(1 - \frac{h_f}{c} \right)^2 \right]$$

$$f_c = \frac{\alpha T}{b_f c \left[1 - \left(1 - \frac{b_w}{b_f} \right) \left(1 - \frac{h_f}{c} \right)^2 \right]}$$

Concrete Strain at the Level of the Flexural Reinforcement, ϵ_{cs} :

$$\epsilon_{cs} = \frac{f_c}{E_c} \left(1 - \frac{d}{c} \right)$$

Location of Compression Force from N.A Depth, \bar{y} (mm):

$$C \cdot \bar{y} = \left(f_c b_f \frac{C}{\alpha} \right) \left(\frac{\alpha C}{3} \right) - \left(\frac{\alpha}{3} (C - h_f) \right) \left(f_c \left(\frac{C - h_f}{C} \right) (b_f - b_w) \frac{(C - h_f)}{\alpha} \right)$$

$$C \cdot \bar{y} = \frac{f_c}{3} b_f C^2 - \frac{f_c}{3} (C - h_f) \left(\frac{C - h_f}{C} (b_f - b_w) (C - h_f) \right)$$

$$C \cdot \bar{y} = \frac{f_c b_f C^2}{3} \left[1 - \left(1 - \frac{b_w}{b_f} \right) \left(1 - \frac{h_f}{C} \right)^3 \right]$$

$$\bar{y} = \frac{\frac{f_c b_f C^2}{3} \left[1 - \left(1 - \frac{b_w}{b_f} \right) \left(1 - \frac{h_f}{C} \right)^3 \right]}{\frac{f_c b_f C}{\alpha} \left[1 - \left(1 - \frac{b_w}{b_f} \right) \left(1 - \frac{h_f}{C} \right)^2 \right]}$$

$$\bar{y} = \frac{\alpha C \left[1 - \left(1 - \frac{b_w}{b_f} \right) \left(1 - \frac{h_f}{C} \right)^3 \right]}{3 \left[1 - \left(1 - \frac{b_w}{b_f} \right) \left(1 - \frac{h_f}{C} \right)^2 \right]}$$

Extreme Concrete Compression Fibre Stress, f_c (MPa):

$$C = T = \frac{f_c b_f C}{\alpha} \left[1 - \left(1 - \frac{b_w}{b_f} \right) \left(1 - \frac{h_f}{C} \right)^2 \right]$$

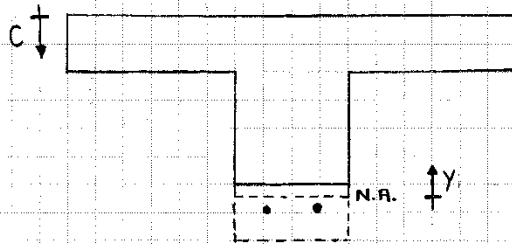
$$f_c = \frac{2T}{b_f C \left[1 - \left(1 - \frac{b_w}{b_f} \right) \left(1 - \frac{h_f}{C} \right)^2 \right]}$$

Concrete Strain at the Level of the Flexural Reinforcement, ϵ_{cs} :

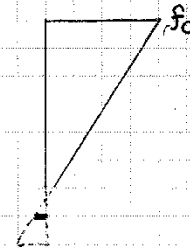
$$\epsilon_{cs} = \frac{f_c}{E_c} \left(1 - \frac{d}{C} \right)$$

Case 3 ($h_w + h_f \leq c(x) \leq \infty$)

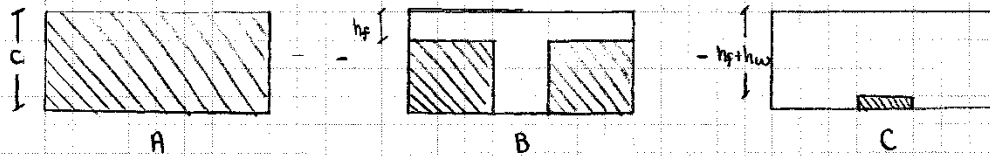
Section:



Stress Distribution:



The Section simplifies to:



Location of Compression Force from N.A. Depth, y (mm):

$$y_1 = \frac{2}{3} c$$

$$y_2 = \frac{2}{3} (c - h_f)$$

$$y_3 = \frac{2}{3} (c - h_f - h_w)$$

Compression Force in Concrete, C (N):

$$C = f_c b_f \frac{c}{2}$$

$$C = f_c \left(\frac{c - h_f}{c} \right) (b_f - b_w) \frac{(c - h_f)}{2}$$

$$C = f_c \left(\frac{c - h_f - h_w}{c} \right) b_w \frac{(c - h_f - h_w)}{2}$$

Summation of Compression Forces C (N):

$$C = \frac{f_c}{2} b_f c - \frac{f_c}{2} \left(\frac{c - h_f}{c} \right) (b_f - b_w) (c - h_f) - \frac{f_c}{2} \left(\frac{c - h_f - h_w}{c} \right) b_w (c - h_f - h_w)$$

$$C = \frac{f_c}{2} \left[c b_f - \left[\left(\frac{c - h_f}{c} \right) (b_f - b_w) (c - h_f) \right] - \left[\left(\frac{c - h_f - h_w}{c} \right) b_w (c - h_f - h_w) \right] \right]$$

$$C = \frac{f_c c b_f}{2} \left[1 - \left(1 - \frac{b_w}{b_f} \right) \left(1 - \frac{h_f}{c} \right)^2 - \left(\frac{b_w}{b_f} \right) \left(1 - \frac{h_f}{c} - \frac{h_w}{c} \right)^2 \right]$$

Location of Compression Force from N.A. Depth, \bar{y} (mm):

$$C \cdot \bar{y} = \left(f_c b_f \frac{c}{2} \right) \left(\frac{2}{3} c \right) - \left(f_c \left(\frac{c-h_f}{c} \right) (b_f - b_w) \left(\frac{c-h_f}{2} \right) \right) \left(\frac{2}{3} (c-h_f) \right) \\ - \left(f_c \left(\frac{c-h_f-h_w}{c} \right) b_w \left(\frac{c-h_f-h_w}{2} \right) \right) \left(\frac{2}{3} (c-h_f-h_w) \right)$$

$$C \cdot \bar{y} = \frac{f_c b_f c^2}{3} \left[1 - \left(1 - \frac{b_w}{b_f} \right) \left(1 - \frac{h_f}{c} \right)^3 - \left(\frac{b_w}{b_f} \right) \left(1 - \frac{h_f}{c} - \frac{h_w}{c} \right)^3 \right]$$

$$\bar{y} = \frac{2c \left[1 - \left(1 - \frac{b_w}{b_f} \right) \left(1 - \frac{h_f}{c} \right)^3 - \left(\frac{b_w}{b_f} \right) \left(1 - \frac{h_f}{c} - \frac{h_w}{c} \right)^3 \right]}{3 \left[1 - \left(1 - \frac{b_w}{b_f} \right) \left(1 - \frac{h_f}{c} \right)^2 - \left(\frac{b_w}{b_f} \right) \left(1 - \frac{h_f}{c} - \frac{h_w}{c} \right)^2 \right]}$$

Extreme Concrete Compression Fibre Stress, f_c (MPa):

$$C = T = \frac{f_c}{2} \left[c b_f - \left[\left(1 - \frac{h_f}{c} \right) (b_f - b_w) (c - h_f) \right] - \left[\left(1 - \frac{h_f + h_w}{c} \right) b_w (c - h_f - h_w) \right] \right]$$

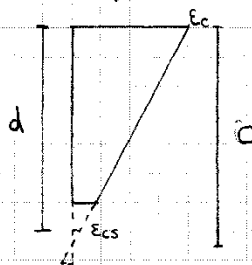
$$f_c = \frac{2 \cdot T}{c b_f - \left[\left(1 - \frac{h_f}{c} \right) (b_f - b_w) (c - h_f) \right] - \left[\left(1 - \frac{h_f + h_w}{c} \right) b_w (c - h_f - h_w) \right]}$$

Concrete Strain at the level of the Flexural Reinforcement, ϵ_{cs} :

$$(h_w \leq d(x) \leq d)$$

$$\epsilon_{cs} = \frac{f_c}{E_c} \left(1 - \frac{d}{c} \right)$$

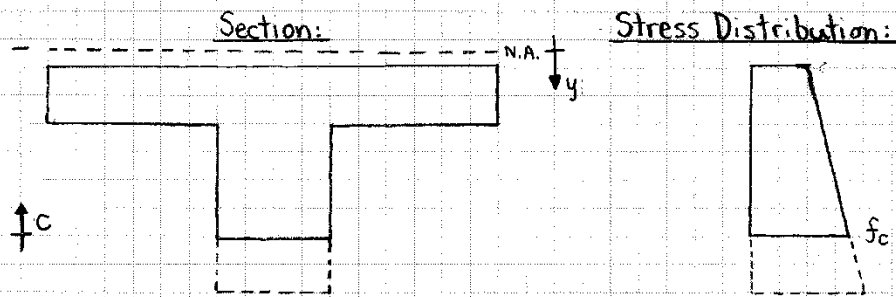
$$(d \leq c(x) \leq \infty)$$



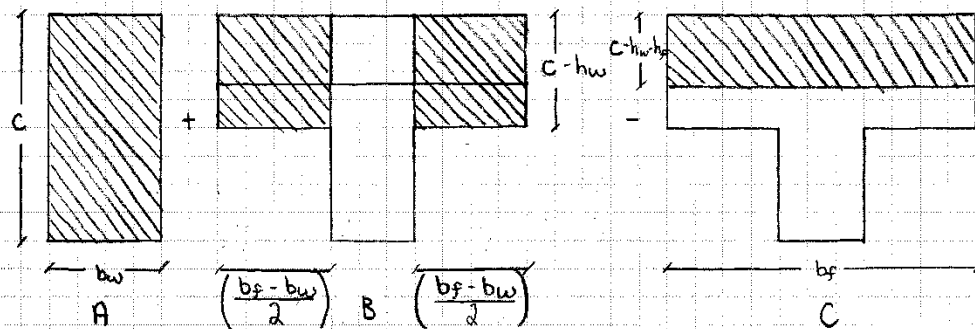
$$\frac{\epsilon_c}{c} = \frac{\epsilon_{cs}}{c-d} \Rightarrow \epsilon_{cs} = \frac{\epsilon_c (c-d)}{c}$$

$$\epsilon_{cs} = \frac{f_c}{E_c} \left(1 - \frac{d}{c} \right)$$

Case 4 ($(h_f + h_w) \leq c(x) \leq \infty$)



The Section simplifies to:



Location of Compression Force from N.A. Depth, y (mm):

$$y = \frac{2}{3}c$$

$$y = \frac{2}{3}(c - h_w)$$

$$y = \frac{2}{3}(c - h_w - h_f)$$

Compression Force in Concrete, C (N):

$$C = f_c b_w \frac{c}{2}$$

$$C = f_c \left(\frac{c - h_w}{c} \right) (b_f - b_w) \frac{(c - h_w)}{2}$$

$$C = f_c \left(\frac{c - h_w - h_f}{c} \right) b_f \frac{(c - h_w - h_f)}{2}$$

Summation of Compression Forces, C (N):

$$C = f_c b_w \frac{c}{2} + f_c \left(\frac{c - h_w}{c} \right) (b_f - b_w) \frac{(c - h_w)}{2} - f_c \left(\frac{c - h_w - h_f}{c} \right) b_f \frac{(c - h_w - h_f)}{2}$$

$$C = \frac{f_c b_f c}{2} \left[\left(\frac{b_w}{b_f} \right) + \left(1 - \frac{b_w}{b_f} \right) \left(1 - \frac{h_w}{c} \right)^2 - \left(1 - \frac{h_w - h_f}{c} \right)^2 \right]$$

Location of Compression Force from N.A. Depth, \bar{y} (mm):

$$C \cdot \bar{y} = \left(f_c b_w \frac{c}{2} \right) \left(\frac{2}{3} c \right) + f_c \left(\frac{C-h_w}{c} \right) (b_f - b_w) \left(\frac{C-h_w}{2} \right) \left(\frac{2}{3} (C-h_w) \right) - f_c \left(\frac{C-h_w-h_f}{c} \right) b_f \left(\frac{C-h_w-h_f}{2} \right) \left(\frac{2}{3} (C-h_w-h_f) \right)$$

$$C \cdot \bar{y} = \frac{f_c b_w c^3}{3} + \frac{f_c}{3} (b_f - b_w) \frac{(C-h_w)^3}{c} - \frac{f_c b_f}{3} \frac{(C-h_w-h_f)^3}{c}$$

$$C \cdot \bar{y} = \frac{f_c b_f c^3}{3} \left[\left(\frac{b_w}{b_f} \right) \left(1 - \frac{b_w}{b_f} \right) \left(1 - \frac{h_w}{c} \right)^3 - \left(1 - \frac{h_w}{c} - \frac{h_f}{c} \right)^3 \right]$$

$$\bar{y} = \frac{\frac{f_c b_f c^3}{3} \left[\left(\frac{b_w}{b_f} \right) \left(1 - \frac{b_w}{b_f} \right) \left(1 - \frac{h_w}{c} \right)^3 - \left(1 - \frac{h_w}{c} - \frac{h_f}{c} \right)^3 \right]}{\frac{f_c b_f c}{2} \left[\left(\frac{b_w}{b_f} \right) + \left(1 - \frac{b_w}{b_f} \right) \left(1 - \frac{h_w}{c} \right)^2 - \left(1 - \frac{h_w}{c} - \frac{h_f}{c} \right)^2 \right]}$$

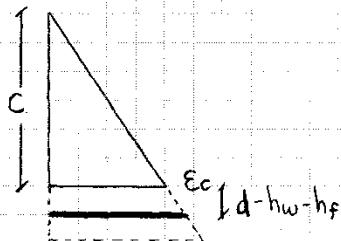
$$\bar{y} = \frac{2c \left[\left(\frac{b_w}{b_f} \right) + \left(1 - \frac{b_w}{b_f} \right) \left(1 - \frac{h_w}{c} \right)^2 - \left(1 - \frac{h_w}{c} - \frac{h_f}{c} \right)^2 \right]}{3 \left[\left(\frac{b_w}{b_f} \right) + \left(1 - \frac{b_w}{b_f} \right) \left(1 - \frac{h_w}{c} \right)^2 - \left(1 - \frac{h_w}{c} - \frac{h_f}{c} \right)^2 \right]}$$

Extreme Concrete Compression Fibre Stress, f_c (MPa):

$$C = T = \frac{f_c b_f c}{2} \left[\left(\frac{b_w}{b_f} \right) + \left(1 - \frac{b_w}{b_f} \right) \left(1 - \frac{h_w}{c} \right)^2 - \left(1 - \frac{h_w}{c} - \frac{h_f}{c} \right)^2 \right]$$

$$f_c = \frac{2T}{b_f c \left[\left(\frac{b_w}{b_f} \right) + \left(1 - \frac{b_w}{b_f} \right) \left(1 - \frac{h_w}{c} \right)^2 - \left(1 - \frac{h_w}{c} - \frac{h_f}{c} \right)^2 \right]}$$

Concrete Strain at the Level of the Flexural Reinforcement, ϵ_{cs} :

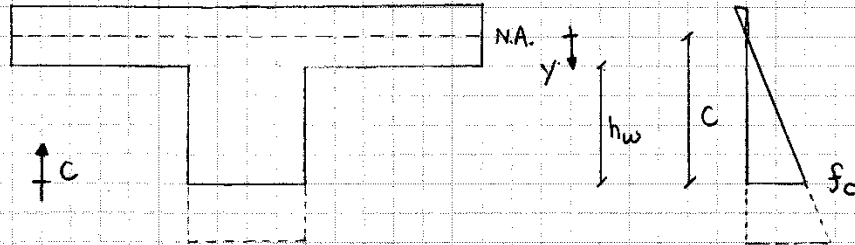


$$\frac{\epsilon_{cs}}{C+d-h_w-h_f} = \frac{\epsilon_c}{C} \Rightarrow \epsilon_{cs} = \frac{(C+d-h_w-h_f)}{C} \epsilon_c$$

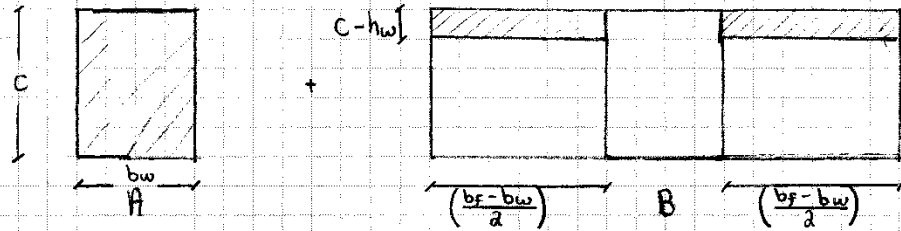
$$\epsilon_{cs} = \frac{(C+d-h_w-h_f)}{C} \frac{f_c}{E_c}$$

Case 5 ($h_w \leq c(x) \leq (h_f + h_w)$)

Section:



This Section simplifies to:



Location of Compression Forces from N.A. Depth y (mm):

$$y = \frac{2}{3} c$$

$$y = \frac{2}{3} (c - h_w)$$

Compression Force in Concrete, $C(N)$:

$$C = f_c b_w \frac{c}{2}$$

$$C = f_c \frac{(c - h_w)}{c} \cdot \frac{(c - h_w)}{2} (b_f - b_w)$$

Summation of Compression Forces, $C(N)$:

$$C = f_c b_w \frac{c}{2} + f_c \frac{(c - h_w)^2}{2c} (b_f - b_w)$$

$$C = \frac{f_c}{2} \left[c b_w + \frac{(c - h_w)^2}{c} (b_f - b_w) \right] = \frac{f_c b_f c}{2} \left[\left(\frac{b_w}{b_f} \right) + \left(1 - \frac{b_w}{b_f} \right) \left(1 - \frac{h_w}{c} \right)^2 \right]$$

Location of Compression Force from N.A. Depth, \bar{y} (mm):

$$C \cdot \bar{y} = \left(f_c b_w \frac{c}{2} \right) \left(\frac{2}{3} c \right) + \left(f_c \frac{(c-h_w)^2}{2c} (b_f - b_w) \right) \left(\frac{2}{3} (c-h_w) \right)$$

$$C \cdot \bar{y} = f_c b_w \frac{c^2}{3} + f_c \frac{(c-h_w)^3}{3c} (b_f - b_w)$$

$$C \cdot \bar{y} = \frac{f_c}{2} \left[\frac{2}{3} b_w c^2 + \frac{2}{3} \frac{(c-h_w)^3}{c} (b_f - b_w) \right]$$

$$C \cdot \bar{y} = \frac{f_c b_f c^2}{3} \left[\left(\frac{b_w}{b_f} \right) + \left(1 - \frac{b_w}{b_f} \right) \left(1 - \frac{h_w}{c} \right)^3 \right]$$

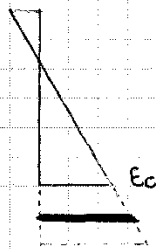
$$\bar{y} = \frac{2c \left[\left(\frac{b_w}{b_f} \right) + \left(1 - \frac{b_w}{b_f} \right) \left(1 - \frac{h_w}{c} \right)^3 \right]}{3 \left[\left(\frac{b_w}{b_f} \right) + \left(1 - \frac{b_w}{b_f} \right) \left(1 - \frac{h_w}{c} \right)^2 \right]}$$

Extreme Concrete Compression Fibre Stress f_c (MPa):

$$C = T = \frac{f_c b_f C}{2} \left[\left(\frac{b_w}{b_f} \right) + \left(1 - \frac{b_w}{b_f} \right) \left(1 - \frac{h_w}{c} \right)^2 \right]$$

$$f_c = \frac{dT}{b_f C \left[\left(\frac{b_w}{b_f} \right) + \left(1 - \frac{b_w}{b_f} \right) \left(1 - \frac{h_w}{c} \right)^2 \right]}$$

Concrete Strain at the Level of the Flexural Reinforcement, ϵ_{cs} :

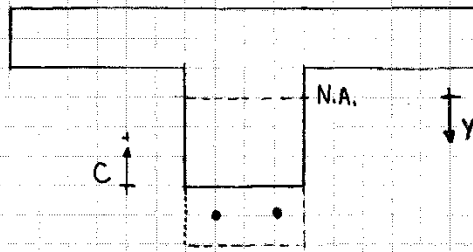


$$\frac{\epsilon_{cs}}{d - (h_w + h_f + c)} = \frac{\epsilon_c}{c} \Rightarrow \epsilon_{cs} = \frac{(d - h_w - h_f + c)}{c} \epsilon_c$$

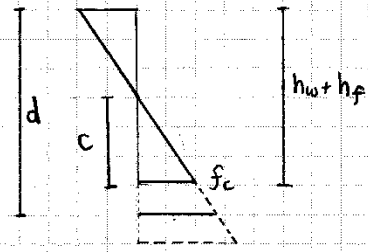
$$\epsilon_{cs} = \frac{(d - h_w - h_f + c)}{c} \frac{f_c}{E_c}$$

Case 6 ($0 \leq c(x) \leq h_w$)

Section:



Stress:



Location of Compression Force from N.A. Depth, y (mm):

$$y = \frac{2}{3} c$$

Compression Force in Concrete, C (N):

$$C = f_c b_w \cdot \frac{c}{2}$$

Extreme Concrete Compression Fibre Stress, f_c (MPa):

$$C = T = \frac{f_c}{2} b_w c \Rightarrow f_c = \frac{2T}{b_w \cdot c}$$

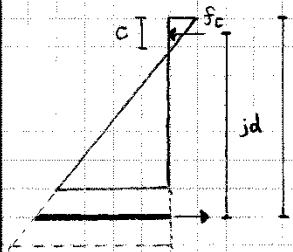
Concrete Strain at the level of the Flexural Reinforcement, ϵ_{cs} :

$$\epsilon_{cs} = \frac{(d - h_f - h_w + c)}{c} \cdot \frac{f_c}{E_c}$$

Depth of N.A. $C(x)$ (mm):

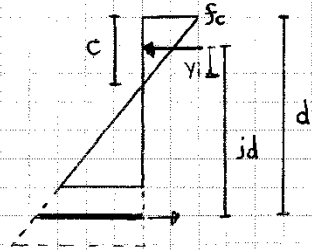
Now that we have derived these equations for each of the six Cases a procedure was developed to determine the Neutral axis depth, $C(x)$.

Case 1 ($0 \leq C \leq h_f$):



$$C = 1.5y \quad \text{or} \quad 3 \cdot (d - jd)$$

Case 2 ($h_f \leq C(x) \leq h_w + h_f$):

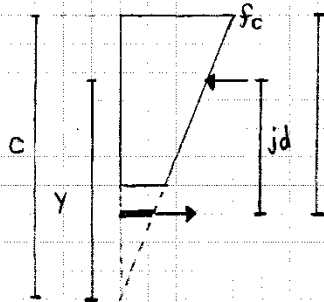


$$\bar{y} = C + (d - jd) = \frac{2C \left[1 - \left(1 - \frac{b_w}{b_f} \right) \left(1 - \frac{h_f}{C} \right)^3 \right]}{3 \left[1 - \left(1 - \frac{b_w}{b_f} \right) \left(1 - \frac{h_f}{C} \right)^2 \right]}$$

Rearranging:

$$2C \left[1 - \left(1 - \frac{b_w}{b_f} \right) \left(1 - \frac{h_f}{C} \right)^3 \right] - \left[(C - d + jd) \cdot 3 \left[1 - \left(1 - \frac{b_w}{b_f} \right) \left(1 - \frac{h_f}{C} \right)^2 \right] \right] = 0$$

Case 3 ($h_w + h_f \leq C(x) \leq \infty$):

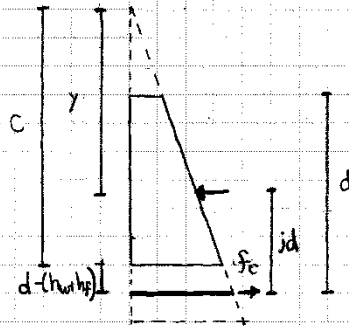


$$\bar{y} = C - (d - jd)$$

Rearranging, similar to above:

$$2C \left[1 - \left(1 - \frac{b_w}{b_f} \right) \left(1 - \frac{h_f}{C} \right)^3 - \left(\frac{b_w}{b_f} \right) \left(1 - \frac{h_f}{C} - \frac{h_w}{C} \right)^3 \right] - \left[(C - d + jd) \cdot 3 \left[1 - \left(1 - \frac{b_w}{b_f} \right) \left(1 - \frac{h_f}{C} \right)^2 - \left(\frac{b_w}{b_f} \right) \left(1 - \frac{h_f}{C} - \frac{h_w}{C} \right)^2 \right] \right] = 0$$

Case 4 ($h_f + h_w \leq c(x) \leq \infty$)

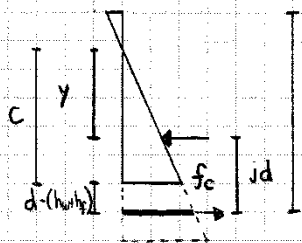


$$\bar{y} = c + d - (h_w + h_f) - jd$$

Rearranging similar to above:

$$2C_i \left[\left(\frac{b_w}{b_f} \right) + \left(1 - \frac{b_w}{b_f} \right) \left(1 - \frac{h_w}{c} \right)^3 - \left(1 - \frac{h_w - h_f}{c} \right)^3 \right] - \left[(c + d - (h_w + h_f) - jd)^3 \left[\left(\frac{b_w}{b_f} \right) + \left(1 - \frac{b_w}{b_f} \right) \left(1 - \frac{h_w}{c} \right)^2 - \left(1 - \frac{h_w - h_f}{c} \right)^2 \right] \right] = 0$$

Case 5 ($h_w \leq c(x) \leq h_f + h_w$)

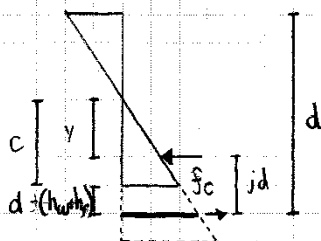


$$\bar{y} = c + d - (h_w + h_f) - jd$$

Rearranging:

$$2C_i \left[\left(\frac{b_w}{b_f} \right) + \left(1 - \frac{b_w}{b_f} \right) \left(1 - \frac{h_w}{c} \right)^3 \right] - \left[(c + d - (h_w + h_f) - jd)^3 \left[\left(\frac{b_w}{b_f} \right) + \left(1 - \frac{b_w}{b_f} \right) \left(1 - \frac{h_w}{c} \right)^2 \right] \right] = 0$$

Case 6 ($0 \leq c(x) \leq h_w$)



$$\bar{y} = c + d - (h_w + h_f) - jd$$

$$c = 1.5y$$

These equations will be used to calculate the neutral axis depth along the length of the specimens. This is done by solving the equations by changing $c(x)$.

B.3 STRUT-AND-TIE ANALYSIS (STA) DERIVATION

Region ①

The maximum moment, M_{max} can occur here only if $0 \leq \alpha \leq 0.125$.

There are 3 possible cases to investigate within this region.

1. $V=0 @ \alpha L \therefore M_{max} @ \alpha L$

For this to occur, the shear force from αL to $\frac{L}{8} \leq 0$

$$R_L - kWL \leq 0$$

$$wL[0.5 + k(1-\alpha)] - kWL \leq 0$$

$$0.5 - k\alpha \leq 0$$

$$k \geq \frac{0.5}{\alpha}$$

$$k = \frac{0.5}{\alpha} \quad (V=0 \text{ from } \alpha L \text{ to } \frac{L}{8})$$

2. $V=0 @ \frac{L}{8} \therefore M_{max} @ \frac{L}{8}$

For this to occur, the shear force from $\frac{L}{8}$ to $\frac{3L}{8} \leq 0$

$$R_L - kWL - \frac{wL}{4} \leq 0$$

$$wL[0.5 + k(1-\alpha)] - kWL - \frac{wL}{4} \leq 0$$

$$0.25 - k\alpha \leq 0$$

$$k \geq \frac{0.25}{\alpha}$$

$$k = \frac{0.25}{\alpha} \quad (V=0 \text{ from } \frac{L}{8} \text{ to } \frac{3L}{8})$$

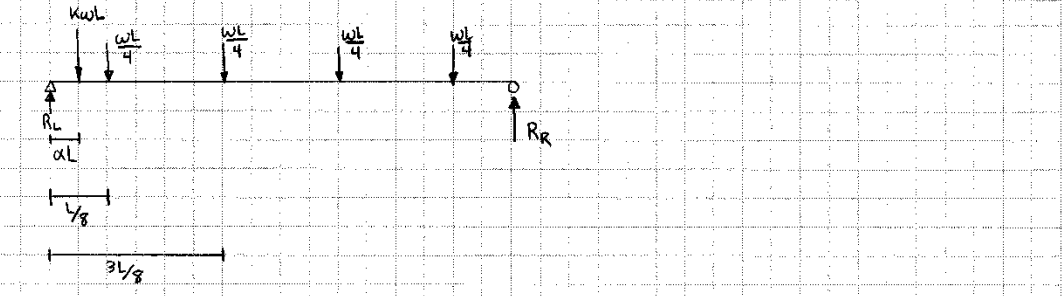
3. $V=0 @ \frac{3L}{8} \therefore M_{max} @ \frac{3L}{8}$

For this to occur, the shear force from from $\frac{L}{8}$ to $\frac{3L}{8} > 0$

$$R_L - kWL - \frac{wL}{4} > 0$$

$$wL[0.5 + k(1-\alpha)] - kWL - \frac{wL}{4} > 0$$

$$0.25 - k\alpha > 0 \quad k \leq \frac{0.25}{\alpha}$$



Moment Calculations:

$$M @ \alpha L = R_L \cdot \alpha L$$

$$= \omega L [0.5 + k(1-\alpha)] \cdot \alpha L$$

$$= \omega L^2 \alpha [0.5 + k(1-\alpha)]$$

$$M @ \frac{L}{8} = R_L \left(\frac{L}{8}\right) - k\omega L \left(\frac{L}{8} - \alpha L\right)$$

$$= \omega L [0.5 + k(1-\alpha)] \left(\frac{L}{8}\right) - \frac{k\omega L^2}{8} + \alpha k\omega L^2$$

$$= \frac{\omega L^2}{8} [0.5 + k - k\alpha] - \frac{\omega L^2}{8} [k - 8\alpha k]$$

$$= \frac{\omega L^2}{8} [0.5 + k - k\alpha - k + 8k\alpha]$$

$$= \frac{\omega L^2}{8} [0.5 + 7k\alpha]$$

$$M @ \frac{3L}{8} = R_L \left(\frac{3L}{8}\right) - k\omega L \left(\frac{3L}{8} - \alpha L\right) - \frac{\omega L}{4} \left(\frac{3L}{8} - \frac{L}{8}\right)$$

$$= \omega L [0.5 + k(1-\alpha)] \left(\frac{3L}{8}\right) - \frac{3k\omega L^2}{8} + \alpha k\omega L^2 - \frac{3\omega L^2}{32} + \frac{\omega L^2}{32}$$

$$= \frac{\omega L^2}{8} [1.5 + 3k(1-\alpha)] - \frac{\omega L^2}{8} [3k - 8\alpha k] - \frac{\omega L^2}{8} \left[\frac{3}{4} - \frac{1}{4}\right]$$

$$= \frac{\omega L^2}{8} [1.0 + 5k\alpha]$$

$$\begin{aligned}
 M @ \frac{7L}{8} &= R_R \left(\frac{L}{8} \right) \\
 &= \omega L [0.5 + k\alpha] \left(\frac{L}{8} \right) \\
 &= \frac{\omega L^2}{8} [0.5 + k\alpha]
 \end{aligned}$$

$$\theta_L = \tan^{-1} \left(\frac{h_L}{\alpha L} \right), \text{ where } h_L = jd \left(\frac{M @ \alpha L}{M_{\max}} \right) \text{ and } \theta_R = \tan^{-1} \left(\frac{h_R \delta}{L} \right), \text{ where } h_R = jd \left(\frac{M @ \frac{7L}{8}}{M_{\max}} \right)$$

$$1. \quad k \geq \frac{0.5}{\alpha} \quad (M_{\max} @ \alpha L)$$

$$\theta_L = \tan^{-1} \left(\frac{jd}{\alpha L} \right)$$

$$\theta_R = \tan^{-1} \left(\frac{M @ \frac{7L}{8} \cdot jd}{M @ \alpha L \cdot \frac{L}{8}} \right) = \tan^{-1} \left(\frac{\frac{\omega L^2}{8} [0.5 + k\alpha]}{\omega L^2 \alpha [0.5 + k(1-\alpha)]} \cdot \frac{8jd}{L} \right)$$

$$\theta_R = \tan^{-1} \left(\frac{[0.5 + k\alpha]}{\alpha [0.5 + k(1-\alpha)]} \cdot \frac{jd}{L} \right)$$

$$2. \quad \frac{0.5}{\alpha} \geq k > \frac{0.25}{\alpha} \quad (M_{\max} @ L/8)$$

$$\theta_L = \tan^{-1} \left(\frac{M @ \alpha L \cdot jd}{M @ \frac{7L}{8} \cdot \alpha L} \right) = \tan^{-1} \left(\frac{\omega L^2 \alpha [0.5 + k(1-\alpha)] \cdot jd}{\frac{\omega L^2}{8} [0.5 + 7k\alpha]} \right)$$

$$\theta_L = \tan^{-1} \left(\frac{8[0.5 + k(1-\alpha)] \cdot jd}{[0.5 + 7k\alpha] L} \right)$$

$$\theta_R = \tan^{-1} \left(\frac{M @ \frac{7L}{8} \cdot jd}{M @ \frac{7L}{8} \cdot \frac{L}{8}} \right) = \tan^{-1} \left(\frac{\frac{\omega L^2}{8} [0.5 + k\alpha] \cdot 8jd}{\frac{\omega L^2}{8} [0.5 + 7k\alpha] L} \right)$$

$$\theta_R = \tan^{-1} \left(\frac{[0.5 + k\alpha] \cdot 8jd}{[0.5 + 7k\alpha] L} \right)$$

$$3. \quad k \leq \frac{0.25}{\alpha} \quad (M_{\max} @ \frac{3L}{8})$$

$$\theta_L = \tan^{-1} \left(\frac{M @ \alpha L \cdot jd}{M @ \frac{7L}{8} \cdot \alpha L} \right) = \tan^{-1} \left(\frac{\omega L^2 \alpha [0.5 + k(1-\alpha)] \cdot jd}{\frac{\omega L^2}{8} [1.0 + 5k\alpha]} \right)$$

$$\theta_L = \tan^{-1} \left(\frac{8[0.5 + k(1-\alpha)] \cdot jd}{[1.0 + 5k\alpha] L} \right)$$

$$\theta_R = \tan^{-1} \left(\frac{M e^{\frac{3L}{8}} \cdot \frac{jd}{L/8}}{M e^{\frac{3L}{8}}} \right) = \tan^{-1} \left(\frac{\frac{wk}{4} [0.5 + k\alpha] \cdot \frac{8jd}{L}}{\frac{wk}{4} [1 + 5k\alpha]} \right)$$

$$\theta_R = \tan^{-1} \left(\frac{[0.5 + k\alpha] \cdot \frac{8jd}{L}}{[1.0 + 5k\alpha]} \right)$$

Region (2)

The Maximum Moment, M_{max} , can only occur here when $0.125 \leq \alpha \leq 0.375$.

There are two possible M_{max} locations.

1. $V = 0 @ \alpha L \therefore M_{max} @ \alpha L$

For this to occur, the shear force from αL to $\frac{3L}{8} \leq 0$

$$R_L - \frac{wL}{4} - kwL \leq 0$$

$$wL [0.5 + k(1-\alpha)] - \frac{wL}{4} - kwL \leq 0$$

$$0.5 + k - k\alpha - 0.25 - k \leq 0$$

$$0.25 - k\alpha \leq 0$$

$$k > \frac{0.25}{\alpha}$$

2. $V = 0 @ \frac{3L}{8} \therefore M_{max} @ \frac{3L}{8}$

For this to occur, the shear force from αL to $\frac{3L}{8} \geq 0$

$$R_L - \frac{wL}{4} - kwL > 0$$

$$wL [0.5 + k(1-\alpha)] - \frac{wL}{4} - kwL \geq 0$$

$$0.5 + k - k\alpha - 0.25 - k \geq 0$$

$$0.25 - k\alpha \geq 0$$

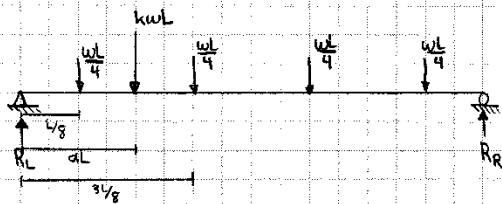
$$k < \frac{0.25}{\alpha}$$

It is possible for M_{max} to occur @ αL and $\frac{3L}{8}$ ($V=0$ in the whole Region) when

$$R_L - \frac{\omega L}{4} - k\omega L = 0$$

$$0.25 - k\alpha = 0$$

$$k = \frac{0.25}{\alpha}$$



$$\begin{aligned} M @ \frac{L}{8} &= R_L \left(\frac{L}{8} \right) = \omega L [0.5 + k(1-\alpha)] \left(\frac{L}{8} \right) \\ &= \frac{\omega L^2}{8} [0.5 + k(1-\alpha)] \end{aligned}$$

$$\begin{aligned} M @ \alpha L &= R_L (\alpha L) - \frac{\omega L}{4} \left(\alpha L - \frac{L}{8} \right) = \omega L [0.5 + k(1-\alpha)] (\alpha L) - \frac{\omega L^2}{4} \left(\alpha - \frac{1}{8} \right) \\ &= \frac{\omega L^2}{8} [4\alpha + 8\alpha k(1-\alpha)] - \frac{\omega L^2}{8} \left(2\alpha - \frac{1}{4} \right) \\ &= \frac{\omega L^2}{8} [4\alpha + 8\alpha k - 8\alpha^2 k - 2\alpha + 1/4] \\ &= \frac{\omega L^2}{8} [2\alpha + 8\alpha k(1-\alpha) + 0.25] \end{aligned}$$

$$\begin{aligned} M @ \frac{3L}{8} &= R_L \left(\frac{3L}{8} \right) - \frac{\omega L}{4} \left(\frac{3L}{8} - \frac{L}{8} \right) - k\omega L \left(\frac{3L}{8} - \alpha L \right) \\ &= \omega L [0.5 + k(1-\alpha)] \left(\frac{3L}{8} \right) - \frac{\omega L^2}{8} \left(\frac{3}{4} - \frac{1}{4} \right) - \frac{\omega L^2}{8} (3k - 8k\alpha) \\ &= \frac{\omega L^2}{8} [1.5 + 3k(1-\alpha)] - \frac{\omega L^2}{8} (0.5) - \frac{\omega L^2}{8} (3k - 8k\alpha) \\ &= \frac{\omega L^2}{8} [1.0 + 5k\alpha] \end{aligned}$$

The inclination of the compressive struts at the left and right supports are again.

$$\theta_L = \tan^{-1} \left(\frac{h_L \delta}{L} \right), \text{ where } h_L = jd \left(\frac{M @ \frac{1}{8}}{M_{\max}} \right)$$

and

$$\theta_R = \tan^{-1} \left(\frac{h_R \delta}{L} \right), \text{ where } h_R = jd \left(\frac{M @ \frac{7}{8}}{M_{\max}} \right)$$

$$1. k \geq \frac{0.25}{\alpha} \quad (M_{\max} @ \alpha L)$$

$$\theta_L = \tan^{-1} \left(\frac{M @ \frac{1}{8} \cdot \delta jd}{M_{\max} L} \right) = \tan^{-1} \left(\frac{\frac{wk^2}{8} [0.5 + k(1-\alpha)]}{\frac{wk^2}{8} [2\alpha + 8\alpha k(1-\alpha) + 0.25]} \cdot \frac{\delta jd}{L} \right)$$

$$\theta_L = \tan^{-1} \left(\frac{[0.5 + k(1-\alpha)]}{[2\alpha + 8\alpha k(1-\alpha) + 0.25]} \cdot \frac{\delta jd}{L} \right)$$

$$\theta_R = \tan^{-1} \left(\frac{M @ \frac{7}{8} \cdot \delta jd}{M_{\max} L} \right) = \tan^{-1} \left(\frac{\frac{wk^2}{8} [0.5 + k\alpha]}{\frac{wk^2}{8} [2\alpha + 8\alpha k(1-\alpha) + 0.25]} \cdot \frac{\delta jd}{L} \right)$$

$$\theta_R = \tan^{-1} \left(\frac{[0.5 + k\alpha]}{[2\alpha + 8\alpha k(1-\alpha) + 0.25]} \cdot \frac{\delta jd}{L} \right)$$

$$2. k \leq \frac{0.25}{\alpha} \quad (M_{\max} @ \frac{3}{8} L)$$

$$\theta_L = \tan^{-1} \left(\frac{M @ \frac{1}{8} \cdot \delta jd}{M_{\max} L} \right) = \tan^{-1} \left(\frac{\frac{wk^2}{8} [0.5 + k(1-\alpha)]}{\frac{wk^2}{8} [1.0 + 5k\alpha]} \cdot \frac{\delta jd}{L} \right)$$

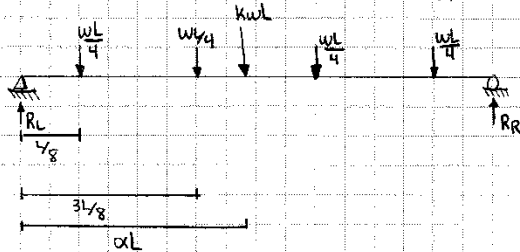
$$\theta_L = \tan^{-1} \left(\frac{[0.5 + k(1-\alpha)]}{[1.0 + 5k\alpha]} \cdot \frac{\delta jd}{L} \right)$$

$$\theta_R = \tan^{-1} \left(\frac{M @ \frac{7}{8} \cdot \delta jd}{M_{\max} L} \right) = \tan^{-1} \left(\frac{\frac{wk^2}{8} [0.5 + k\alpha]}{\frac{wk^2}{8} [1.0 + 5k\alpha]} \cdot \frac{\delta jd}{L} \right)$$

$$\theta_R = \tan^{-1} \left(\frac{[0.5 + k\alpha]}{[1.0 + 5k\alpha]} \cdot \frac{\delta jd}{L} \right)$$

Region ③

If $0.375 \leq \alpha \leq 0.5$ the maximum moment, M_{max} , occurs under the Point Load, or αL from the left support, k can be any value.

Moment Calculations:

$$M @ \frac{L}{8} = R_L \cdot \left(\frac{L}{8}\right)$$

$$= \frac{wL^2}{8} [0.5 + k(1-\alpha)]$$

$$M @ \frac{3L}{8} = R_L \cdot \left(\frac{3L}{8}\right) - \frac{wL}{4} \left(\frac{3L}{8} - \frac{L}{8}\right)$$

$$= wL [0.5 + k(1-\alpha)] \left(\frac{3L}{8}\right) - \frac{wL^2}{8} \left(\frac{3}{4} - \frac{1}{4}\right)$$

$$= \frac{wL^2}{8} [1.5 + 3k(1-\alpha)] - \frac{wL^2}{8} (0.5)$$

$$= \frac{wL^2}{8} [1.0 + 3k(1-\alpha)]$$

$$M @ \alpha L = R_L \cdot \alpha L - \frac{wL}{4} \left(\alpha L - \frac{L}{8}\right) - \frac{wL}{4} \left(\alpha L - \frac{3L}{8}\right)$$

$$= wL [0.5 + k(1-\alpha)] [\alpha L] - \frac{wL^2}{4} \left(\alpha - \frac{1}{8} + \alpha - \frac{3}{8}\right)$$

$$= \frac{wL^2}{8} [4\alpha + 8k\alpha(1-\alpha)] - \frac{wL^2}{8} [4\alpha - \frac{4}{4}]$$

$$= \frac{wL^2}{8} [4\alpha + 8k\alpha - 8k\alpha^2 - 4\alpha + 1]$$

$$= \frac{wL^2}{8} [8k\alpha(1-\alpha) + 1]$$

$$M_{e \frac{7}{8}} = R_R \cdot \left(\frac{L}{8}\right)$$

$$= \frac{wL^2}{8} [0.5 + k\alpha]$$

The inclination of the compressive struts at the left and right supports are:

$$\theta_L = \tan^{-1} \left(\frac{M_{e \frac{7}{8}} \cdot \frac{8jd}{L}}{M_{\max}} \right) = \left(\frac{\frac{wL^2}{8} [0.5 + k(1-\alpha)] \cdot \frac{8jd}{L}}{\frac{wL^2}{8} [8k\alpha(1-\alpha) + 1]} \right)$$

$$= \tan^{-1} \left(\frac{8[0.5 + k(1-\alpha)] \cdot jd}{[1 + 8k\alpha(1-\alpha)] L} \right)$$

$$\theta_R = \tan^{-1} \left(\frac{M_{e \frac{7}{8}} \cdot \frac{8jd}{L}}{M_{\max}} \right) = \tan^{-1} \left(\frac{\frac{wL^2}{8} [0.5 + k\alpha]}{\frac{wL^2}{8} [8k\alpha(1-\alpha) + 1]} \cdot \frac{8jd}{L} \right)$$

$$\theta_R = \tan^{-1} \left(\frac{8[0.5 + k\alpha] \cdot jd}{[8k\alpha(1-\alpha) + 1] L} \right)$$

Summary:

w = Uniform Distributed Load (Dead) kN/m

P = Point Load (Live) kN

L = Span Length

$k = \frac{P}{wL}$, where $k \geq 0$ and $0 \leq \alpha \leq 0.25$ to 1.0

For $\frac{M_{Lmax}}{M_D} = 0.5$ to 2.0

The distance of the Point Load from the left support, α , is known ($0 \leq \alpha \leq 0.5$)

Compute θ_L, θ_R = Orientation of Struts at the left and right supports for known Lever Arm (jd, m) @ the maximum moment, M_{max} .

α	k	$\theta_L = \tan^{-1}(-)$	$\theta_R = \tan^{-1}(-)$	Comment
≥ 0.5	$\geq \frac{0.5}{\alpha}$	$\left(\frac{jd}{\alpha L}\right)$	$\left(\frac{[0.5+k\alpha]}{\alpha[0.5+k(1-\alpha)]} \cdot \frac{jd}{L}\right)$	$M_{max} @ \alpha L$
≤ 0.125	$\geq 0.25/\alpha$	$\left(\frac{8[0.5+k(1-\alpha)]}{[0.5+7k\alpha]} \cdot \frac{jd}{L}\right)$	$\left(\frac{8[0.5+k\alpha]}{[0.5+7k\alpha]} \cdot \frac{jd}{L}\right)$	$M_{max} @ L/8$
	$\leq 0.5/\alpha$	$\left(\frac{8[0.5+k(1-\alpha)]}{[1.0+5k\alpha]} \cdot \frac{jd}{L}\right)$	$\left(\frac{8[0.5+k\alpha]}{[1.0+5k\alpha]} \cdot \frac{jd}{L}\right)$	$M_{max} @ 3L/8$
≥ 0.125 but ≤ 0.375	$\geq 0.25/\alpha$	$\left(\frac{8[0.5+k(1-\alpha)]}{[2\alpha+8k\alpha(1-\alpha)+0.25]} \cdot \frac{jd}{L}\right)$	$\left(\frac{8[0.5+k\alpha]}{[2\alpha+8k\alpha(1-\alpha)+0.25]} \cdot \frac{jd}{L}\right)$	$M_{max} @ \alpha L$
	$\leq 0.25/\alpha$	$\left(\frac{8[0.5+k(1-\alpha)]}{[1.0+5k\alpha]} \cdot \frac{jd}{L}\right)$	$\left(\frac{8[0.5+k\alpha]}{[1.0+5k\alpha]} \cdot \frac{jd}{L}\right)$	$M_{max} @ 3L/8$
≥ 0.375	-	$\left(\frac{8[0.5+k(1-\alpha)]}{[1+8k\alpha(1-\alpha)]} \cdot \frac{jd}{L}\right)$	$\left(\frac{8[0.5+k\alpha]}{[1+8k\alpha(1-\alpha)]} \cdot \frac{jd}{L}\right)$	$M_{max} @ \alpha L$

**APPENDIX C:
EXPERIMENTAL INVESTIGATION**

C.1 STRESS-STRAIN RELATIONSHIP FOR REINFORCEMENT

This appendix presents the mechanical properties of the 25M flexural reinforcement used in the experimental investigation presented in Chapter 4. Test Bar Sample 1 was obtained from the flexural reinforcement for the Control Specimen and Specimen 1 and Test Bar Sample 2 was obtained from the flexural reinforcement for Specimens 2 through 5. Approximate stress-strain relationships were developed from the observed load-displacement data. Test Bar Samples 1 and 2 exhibited different behaviour and therefore unique stress-strain approximations were necessary.

Figure C-1 shows the tensile test data, in the form of load-displacement data corrected for the initial slip in the grips at low loads. The tests were done using the Tinius-Olsen Machine in the UWO Structures Laboratory. The samples were loaded to failure at a constant rate of approximately 1kN/minute. The load-displacement data were corrected for the displacement exhibited during the loading initiation for the Tinius-Olsen Machine to properly grip the bar at both hold points: the associated hand calculations are shown on the subsequent pages.

For Test Bar Sample 1, the yield and ultimate loads, P_{by} and P_{bu} , were approximately 228 and 335 kN, respectively. For Test Bar Sample 2, the yield and ultimate loads, P_{by} and P_{bu} , were approximately 201 and 306 kN, respectively.

Load-Displacement Data Correction

The Load-Displacement data were corrected for the displacement exhibited during loading initiation.

Test Bar Sample 1 (25M)

Gauge Length, from the middle of the end grips = 370mm

Yield Load = 228 kN = 228000N

Ultimate Load = 335 kN = 335000 N

First, two point on the linear possible of the Load-deflection curve are chosen.

$$\Delta_1 = 10.58 \text{ mm} \quad P_1 = 69.36 \text{ kN}$$

$$\Delta_2 = 16.85 \text{ mm} \quad P_2 = 165.8 \text{ kN}$$

$$P_x = m\Delta_x + P_0$$

$$69.36 \times 10^3 \text{ N} = m(10.58 \text{ mm}) + P_0 \Rightarrow \textcircled{1} P_0 = 69.36 \times 10^3 \text{ N} - m(10.58 \text{ mm})$$

$$165.8 \times 10^3 \text{ N} = m(16.85 \text{ mm}) + P_0 \quad \textcircled{2}$$

Substituting $\textcircled{1}$ into $\textcircled{2}$

$$165.8 \times 10^3 \text{ N} = m(16.85 \text{ mm}) + 69.36 \times 10^3 \text{ N} - m(10.58 \text{ mm})$$

$$96.44 \times 10^3 \text{ N} = (6.27 \text{ mm}) m$$

$$m = 15381.18 \text{ N/mm}$$

$$P_0 = 69.36 \times 10^3 \text{ N} - (15381.18 \text{ N/mm})(10.58 \text{ mm})$$

$$P_0 = -93372.88 \text{ N}$$

$$\therefore P_x = 15381.18 \text{ N/mm} \cdot \Delta_x - 93372.88 \text{ N}$$

Now the deflection when $P_x = 0 \text{ N}$ needs to be calculated

$$0 = 15381.18 \text{ N/mm} \cdot \Delta_0 - 93372.88 \text{ N}$$

$$\Delta_0 = 6.071 \text{ mm}$$

Therefore the displacement is corrected by reducing the measured displacement by $\Delta_0 = 6.071 \text{ mm}$

$$\therefore \Delta_x = \frac{(P_x + 93372.88 \text{ N})}{15381.18 \text{ N/mm}} - 6.071 \text{ mm} \quad (\text{mm})$$

Similarly, for Test Bar Sample 2:

$$\Delta_0 = 4.078 \text{ mm}$$

Therefore, the displacement is corrected by reducing the the measured displacement by $\Delta_0 = 4.078 \text{ mm}$.

$$\therefore \Delta_x = \frac{(P_x + 58101.41 \text{ N})}{14246.58 \text{ N/mm}} - 4.078 \text{ mm} \quad (\text{mm})$$

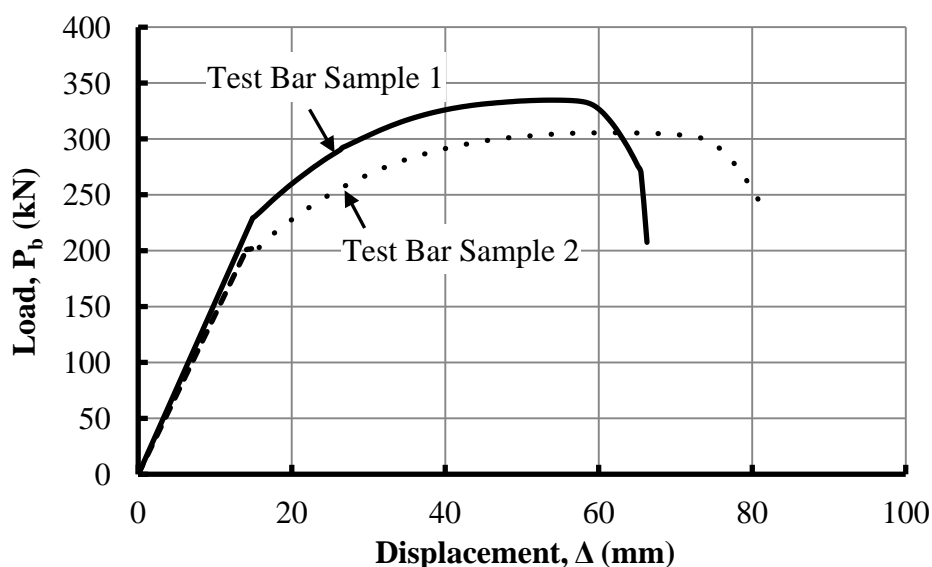


Figure C-1: Tensile Test for Bar Samples 1 and 2.

Approximations of the stress-strain relationship were developed from the observed load-displacement data. The displacement readings from a Linear Voltage Displacement Transducer (LVDT) attached to the moving crosshead of the Tinius-Olsen Machine could not be used directly to calculate the strains in the test bar samples because the displacement readings, Δ , were comprised of both the elongation of the bar, Δ_b , and the displacement of the Tinius-Olsen Machine, Δ_m . Therefore the following procedure was

used to rectify displacement readings from the Tinius-Olsen Machine and develop a stress-strain approximation:

1. The loads from the load-displacement data were converted to stresses, f_s , as:

$$[C1-1] \quad f_s = \frac{P_b}{A_b}$$

where $A_b = 500 \text{ mm}^2$ for a 25M bar.

2. The yield and ultimate strengths, f_y and f_u , respectively, were computed from Eqn. [C1-1] using the yield and ultimate loads observed in the load-displacement data.
3. The stress-strain approximation was divided into elastic and plastic ranges, with the elastic range corresponding to loads up to yielding.
4. In the elastic range, the stress-strain relationship for the test bar sample was assumed linear with a slope equal to the elastic modulus of steel, $E_s = 200000 \text{ MPa}$. The strain in the bar sample at yield, ϵ_y , was computed as:

$$[C1-2] \quad \epsilon_y = \frac{f_y}{E_s}$$

5. The elongation of the test bar sample at yield was computed as:

$$[C1-3] \quad \Delta_{by} = \epsilon_y L^*$$

where L^* was the gauge length of the test bar sample, assumed to be the distance between the centre of the grips.

6. The displacement attributed to the Tinius-Olsen Machine at yield was computed as:

$$[C1-4] \quad \Delta_{my} = \Delta_y - \Delta_{by}$$

where Δ_y is the observed displacement reading at yield.

7. The stress-strain relationship of the Tinius-Olsen Machine was also assumed to be linear and the corrected elongation of the test bar sample in the elastic range was computed as:

$$[C1-5] \quad \Delta_b = \Delta - \Delta_m = \Delta - \frac{\Delta_{my}}{P_{by}} P_b$$

8. In the plastic range, the stress-strain relationship of the Tinius-Olsen Machine was assumed to remain linear and the elongation of the test bar sample was computed using Eqn. [C1-5].

9. The strain in the test bar sample, ϵ_s , was computed as:

$$[C1-6] \quad \epsilon_s = \frac{\Delta_b}{L^*}$$

The stress-strain approximations for Test Bar Samples 1 and 2 are shown in Figure C-2. For Test Bar Sample 1, f_y and f_u were approximately 456 and 669 kN, respectively. For Test Bar Sample 2, f_y and f_u were approximately 402 and 612 kN, respectively.

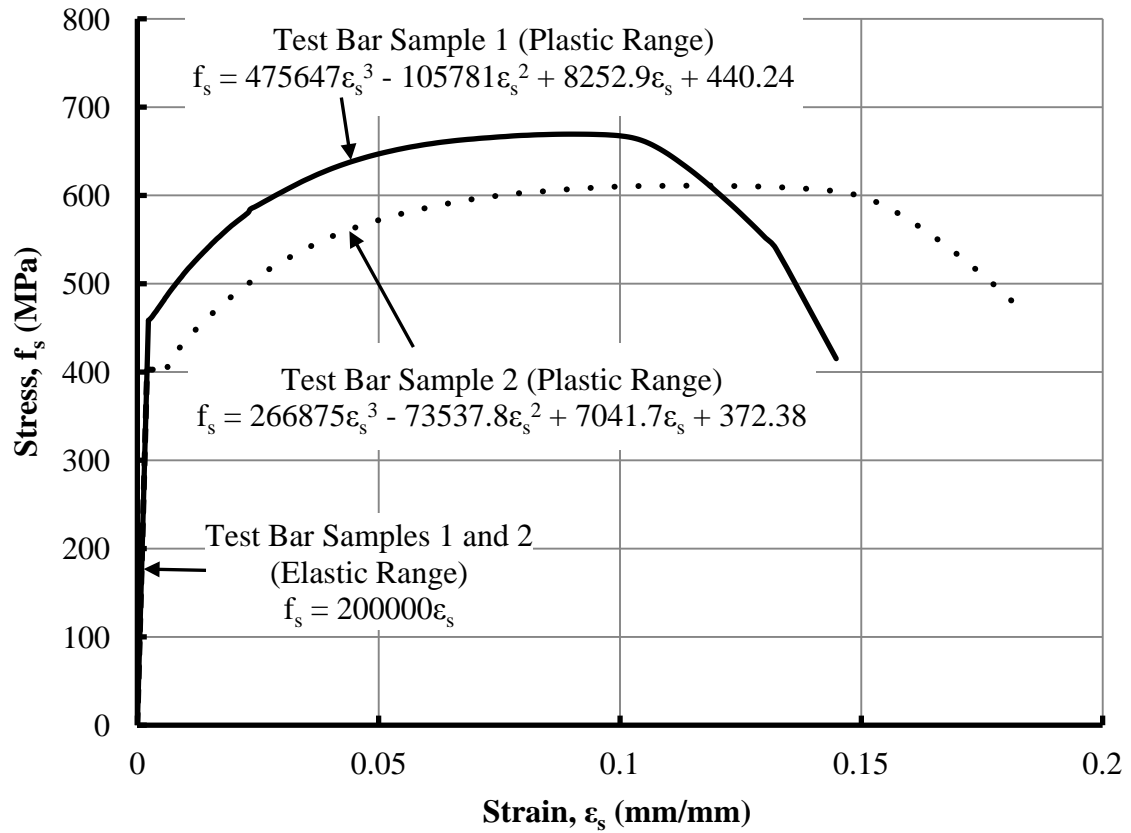


Figure C-2: Stress-strain Approximations for Test Bar Samples 1 and 2.

C.2 DEAD-TO-LIVE LOAD MOMENT RATIO FOR A TYPICAL REINFORCED CONCRETE BRIDGE

This appendix presents the analysis to determine representative ratios of dead-to-live load bending moments for the Waterloo Regional Road #97, or Cedar Creek Road Underpass Bridge, shown in Figure C-3, which crosses Highway 401 at km 268. This bridge was chosen because it is representative of a large portion of aging reinforced concrete bridges in Ontario.



Figure C-3: Cedar Creek Road Underpass Bridge (MTO 2010).

The bridge was designed in 1960 by A.M. Lount and Associates and is currently owned and maintained by the Ministry of Transportation of Ontario (MTO). It has an overall length of 79.8 m, consisting of four spans of 14.9 m, 26.2 m, 26.2 m, and 12.5 m, and a skew of 45° , as shown in Figure C-4. The two interior spans accommodate six vehicle lanes beneath them. The cross-section, shown in Figure C-5, comprises six reinforced cast-in-place continuous concrete T-section girders running the entire length of the bridge. The girders have a height of 1500 mm, a top flange thickness of 200 mm, a web width of 460 mm, and a clear cover of only 25.4 mm to the first layer of reinforcement.

The original concrete had a specified minimum compressive strength at 28 days of 20.9 MPa.

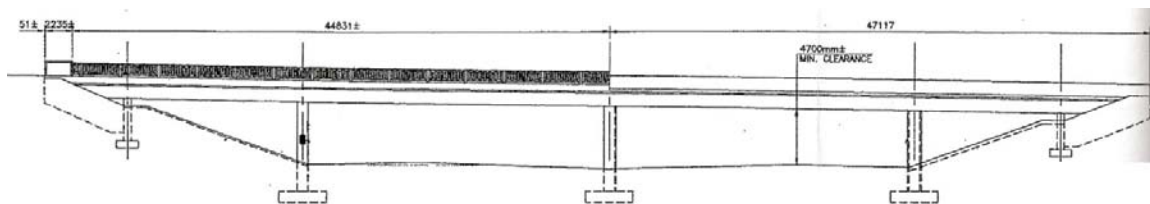


Figure C-4: Elevation of Cedar Creek Road Underpass (Dillon Consulting 2001).

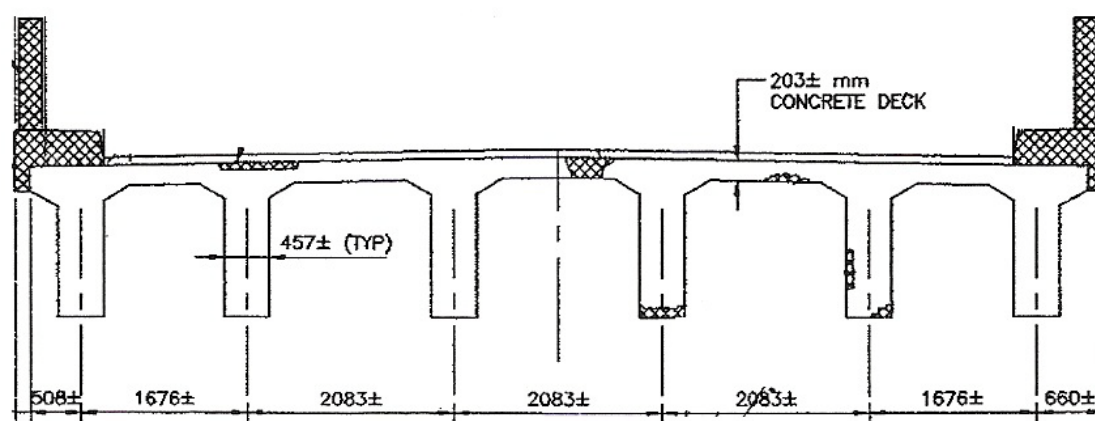


Figure C-5: Typical Cross-section of Cedar Creek Road Underpass (Dillon Consulting 2001).

The Cedar Creek Road Underpass was analyzed using the design provisions of the Canadian Highway Bridge Design Code (CHBDC) (CSA 2006). The dead load consisted of the girders own weight, the concrete deck, concrete parapet walls, and asphalt topping. For simplicity, the total dead load was assumed shared equally between the girders resulting in specified dead loads, w_{DL} , of 33.1 kN/m per girders.

Both CL-625-ONT Truck and Lane Loads were considered as live loads in accordance with the CHBDC. The bridge consists of two lanes and therefore has a modification factor for multi-lane loading, R_L , equal to 0.9. A dynamic load allowance, DLA, of 0.25

was applied to the Truck Load, but as defined in the CHBDC is already included in the Lane Load. The Simplified Method given in Clause 5.7.1, was used to determine the fraction of the total live load shear, V_T , and moment, M_L , applied to each girder V_G and M_G , respectively, yielding:

$$M_G=0.548M_T$$

and

$$V_G=0.615V_T$$

The ratio of the specified dead load moment, M_D , to the total specified moment, M_T , for the positive moment region of a typical interior span is shown in Figure C-6. The maximum value of 0.399 is governed by the Truck Load and occurs at approximately 0.4 times the length of the positive moment region from the left dead load point of contraflexure. The figure is not symmetric because the analysis has been carried out for the truck moving in one direction only. These results are very similar to the findings by Buckland et al. (1988) where the ratio of the specified dead load moment to total moment of concrete T-section bridge girders was approximately 0.422. With this information the relative magnitudes of the uniformly distributed dead load and the live load can be proportioned to reflect realistic loading conditions.

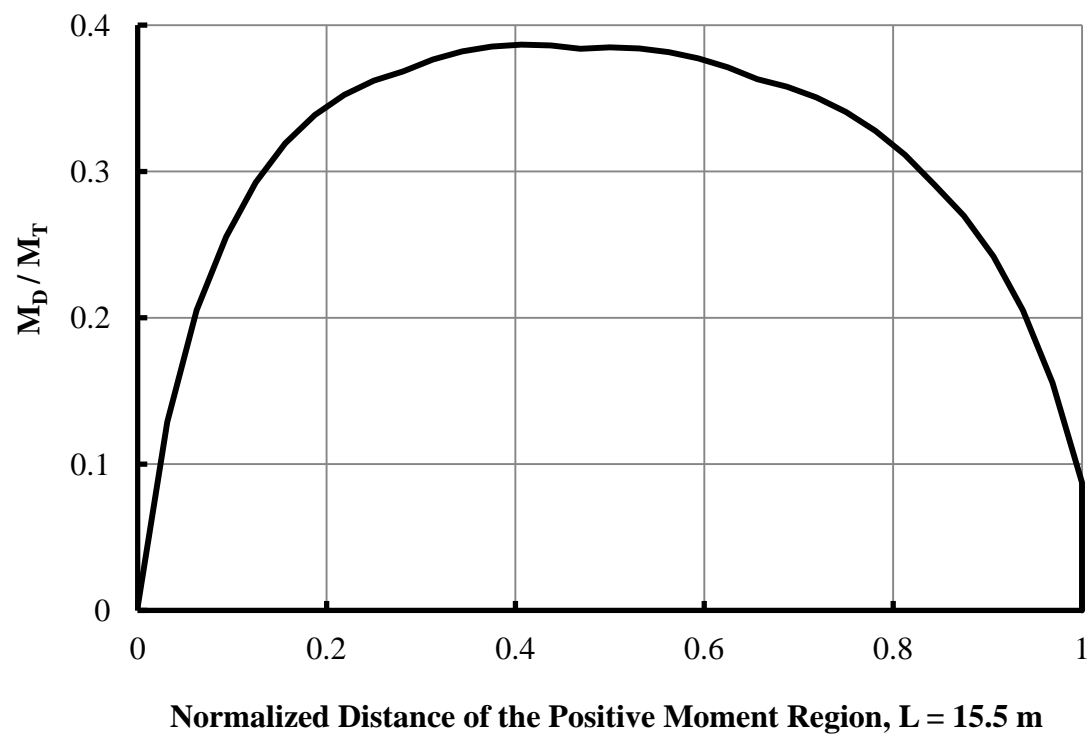


Figure C-6: The Ratio of Dead Load Moment, M_D , to Total Load Moment, M_T , over the Positive Moment Region of the Cedar Creek Road Underpass Bridge.

C.3 DESIGN, CONSTRUCTION AND INSTALLATION OF FOAM VOID

This appendix presents the design, construction and installation of the foam block out that surrounds the flexural reinforcement during casting to ensure that it is exposed once the concrete is cured. Rehabilitation of deteriorated reinforced concrete bridge girders requires concrete removal to a depth of 25.4 mm behind the first layer of flexural reinforcement (OPSS 1994). To simulate the concrete removal, a void of foam insulation 100 mm thick was designed and constructed to enclose the flexural reinforcement as shown in Figure C-7.

The void design was comprised of four 25.4 mm layers that had a constant width of 200 mm and a length equal to the ℓ_{exp} of each specimen. Layer 1 was an unaltered layer of foam insulation, as shown in Figure C-8(a). Layer 2 had two sets of sections removed in the longitudinal and transverse directions, using a router. The two longitudinal sections were located at the flexural reinforcement and the transverse sections, spaced at 200 mm intervals, were located at the stirrups to ensure proper depth and placement, as shown in Figure C-8(b). Layer 3 consisted of three individual sections to allow space for both the flexural reinforcement and stirrups, as shown in Figure C-8(c). Layer 4 consisted of three sections with 12 mm holes drilled at the stirrup locations to completely surround them and enclose the flexural reinforcement, as shown in Figure C-8(d).

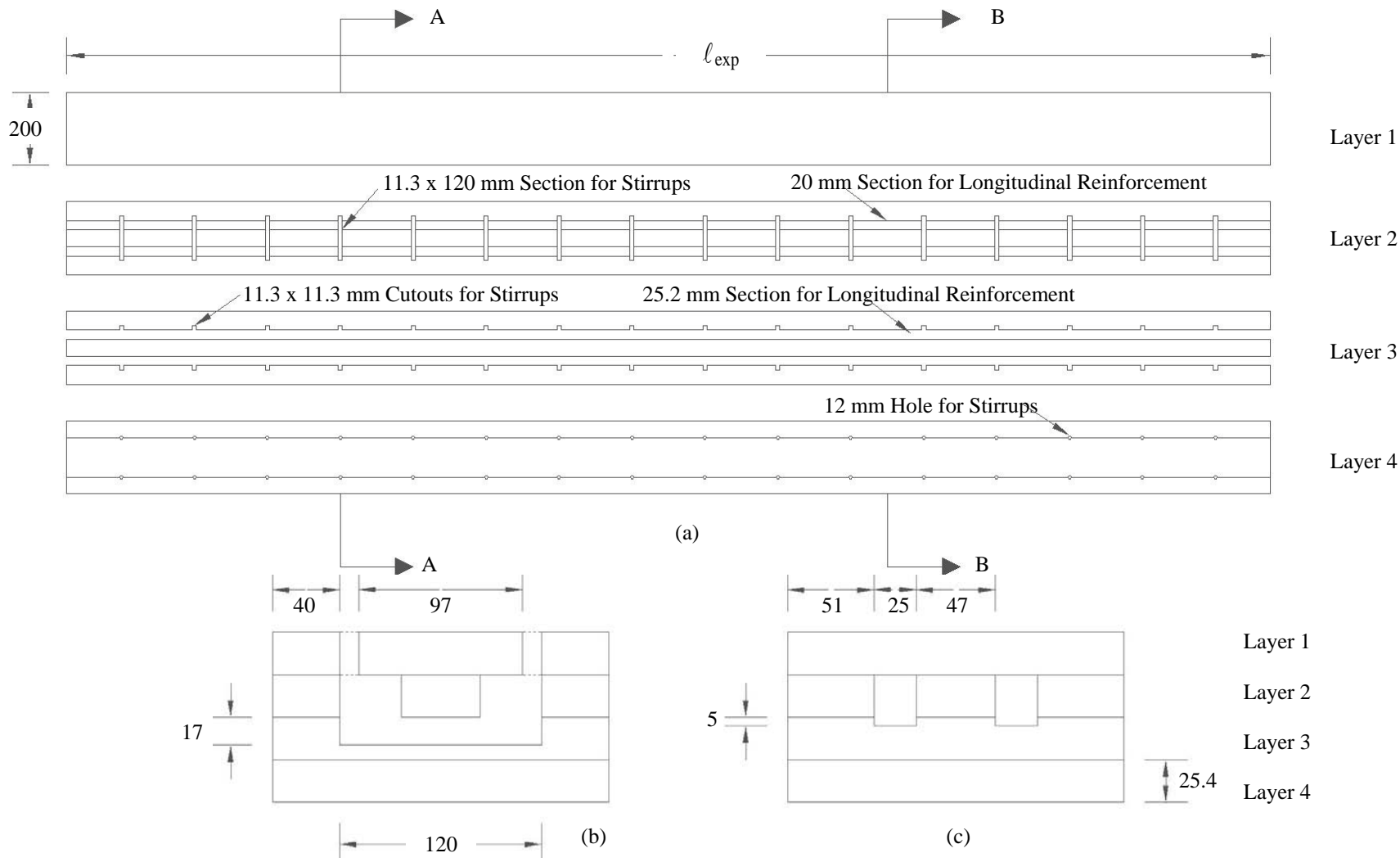


Figure C-7: Foam Insulation Void: (a) Plan of Individual Layers, (b) Section A-A at Stirrups, and (c) Section B-B between Stirrups (All Dimensions in mm).

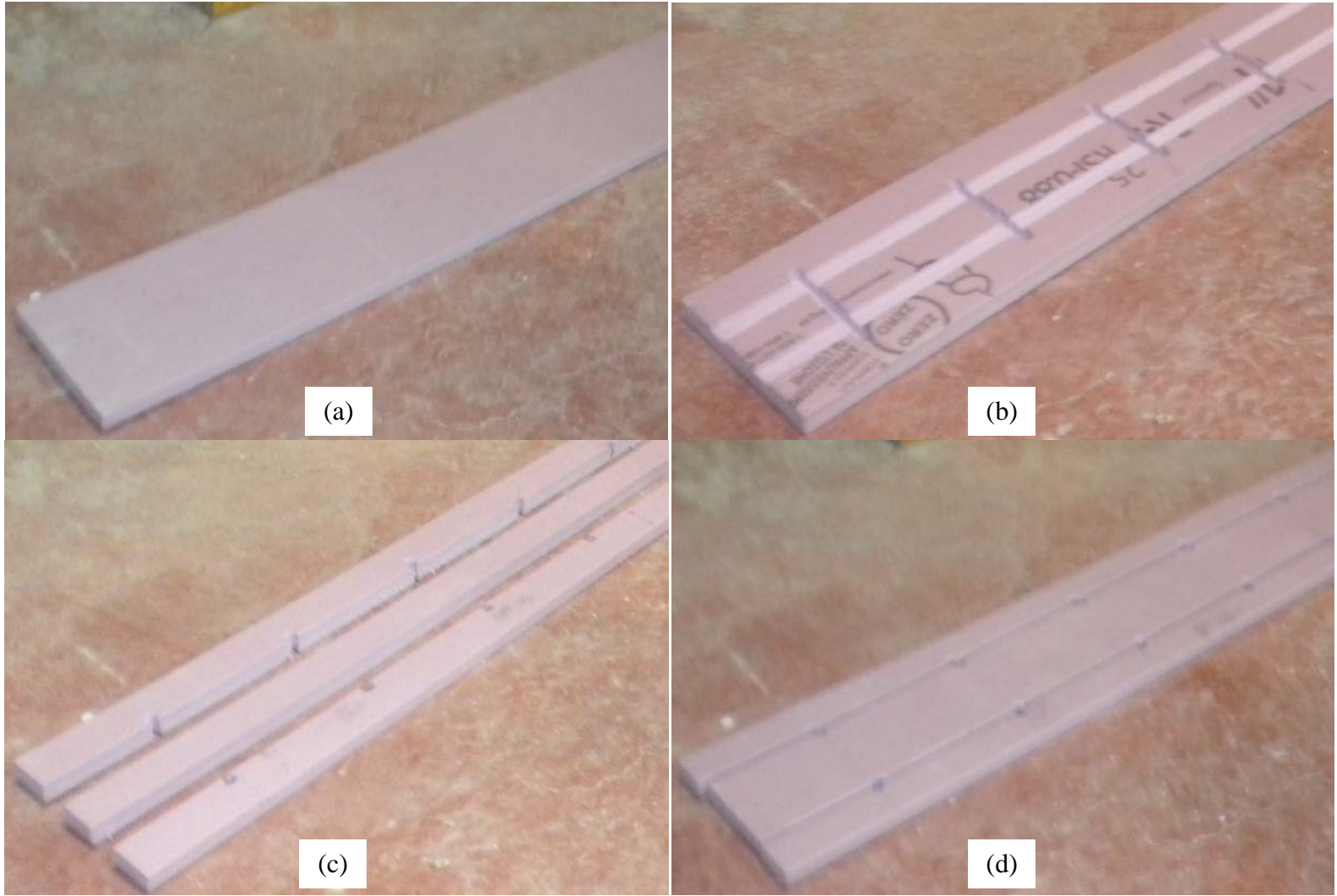


Figure C-8: Foam Insulation Void: (a) Layer 1, (b) Layer 2, (c) Layer 3 and (d) Layer 4.

A procedure for the placement of the foam insulation and the reinforcement was developed to block out the concrete. Layers 1, 2 and 3 were cut to size, routed, glued together and positioned in the formwork. The stirrups and flexural reinforcement were placed into the foam and adjusted to align with their respective slots, as shown in Figure C-9(a). The nominal top reinforcement was placed to secure the stirrups in position. The middle section of Layer 3 was glued to the middle of Layer 2, enclosing the bottom of the stirrups, as shown in Figure C-9(b). 12 mm holes were drilled at the stirrup locations in Layer 4 which was then cut and glued to Layer 3, completely enclosing the flexural reinforcement and the bottom portion of the stirrups, as shown in Figure C-9(c). Once the adhesive dried, the end edges of Layer 4 were beveled at a 45° angle, 20 mm x 20 mm, to remove a potential stress raiser at the re-entrant corner of the concrete, as shown in Figure C-9(d). Finally, the remaining formwork, transverse reinforcement, and steel hangers were placed and the specimen was cast.



Figure C-9: Foam Insulation Void Placement: (a) Stirrups and Flexural Reinforcement Placement, (b) Layer 3 Placement, (c) Layer 4 Placement, (d) Beveled Edge of Layer 4.

C.4 TESTING PROCEDURE

This appendix presents the method used to determine the loads that were applied during the experimental testing of the specimens. This includes calculating the required point and simulated distributed point loads that would result in the specimen to yield and fail using the moment contribution ratio determined in the loading analysis of a typical reinforced concrete bridge girder. It also includes the calculations of the own weight of the specimens and the testing apparatus, which are then deducted from the simulated distributed point loads. The sample hand calculations for the Control Specimen and Specimen 1 are presented in the subsequent pages.

Control Specimen:

For the Control Specimen, the point load, P , was located at the midspan, $\alpha = 0.5$ and had an assumed point load moment contribution, $M_p/M_{total} = 0.6$ and therefore $k = \frac{P}{\omega L} = 0.75$.

Therefore the moment due to the point load, M_p , and the simulated distributed load, M_w , at yield and ultimate are:

	<u>Yield (kN·m)</u>	<u>Ultimate (kN·m)</u>
M_w (0.4 Moment)	60.9	80.3
M_p (0.6 Moment)	91.3	120.5

Simulated Distributed Load Moment M_w :

Using the basic moment equation for a distributed load:

$$M_w = \frac{\omega L^2}{8} \Rightarrow \omega = \frac{8M_w}{L^2}$$

The yield distributed load, ω_y , is:

$$\omega_y = \frac{8(60.9 \text{ kN}\cdot\text{m})}{(4\text{m})^2} = 30.5 \text{ kN/m}$$

And the simulated distributed point load, ω_y , is:

$$\omega_y = \frac{1}{4}(30.5 \text{ kN/m})(4\text{m}) = 30.5 \text{ kN/Load}$$

A similar procedure was done for the ultimate moment and the simulated distributed point load, ω_u , is:

$$\omega_u = 40.2 \text{ kN/Load}$$

The weight of the specimen's own weight and the testing apparatus must be included in the simulated distributed load.

Specimen's Own Weight:

$$\text{Area of cross section of specimen} = (h_f \cdot b_f) + (h_w \cdot b_w)$$

$$A_c = (90\text{mm} \times 820\text{mm}) + (310\text{mm} \times 200\text{mm})$$

$$A_c = 0.1358\text{m}^2$$

Therefore the portion of the simulated distributed load due to the specimen's own weight is:

$$w_{ow} = 24\text{ kN/m}^3 \cdot 0.1358\text{m}^2 \cdot \frac{4\text{m}}{4} = 3.26\text{ kN/Load}$$

Testing Apparatus:

The specific weights of each component in the testing apparatus were measured and are shown in Table 4-1. The summation of these was divided between each simulated distributed load:

$$w_{app} = 1.28\text{ kN/Load}$$

Therefore the total load applied to the top of the specimen at the quarter points by the hydraulic jacks is:

$$\text{Simulated Distributed Yield Load, } w_y: 30.5 - 3.26 - 1.28 = 26.0\text{ kN/Load}$$

$$\text{Simulated Distributed Ultimate Load, } w_u: 40.2 - 3.26 - 1.28 = 35.7\text{ kN/Load}$$

Since each hydraulic jack transfer the simulated distributed load to two quarter points, the reading of the Loads Cells will be:

$$\text{Load Cell Reading at Yield, } 2w_y: 52.0\text{ kN}$$

$$\text{Load Cell Reading at Ultimate, } 2w_u: 71.4\text{ kN}$$

Point Load Moment, M_p :

Using the basic moment equation for a point load:

$$M_p = \frac{PL}{4} \Rightarrow P = \frac{4M_p}{L}$$

The yield and Ultimate loads, P_y and P_u , are:

$$P_y = \frac{4(91.3\text{ kN}\cdot\text{m})}{4\text{m}} = 91.3\text{ kN}$$

$$P_u = 120.5\text{ kN}$$

These loads were used in the test procedure for the Control Specimen.

Specimens with Exposed Reinforcement:

The testing procedure for the remaining specimens with exposed reinforcement was the same as the control specimen other than the calculation for the specimens self-weight.

Specimen 1

For Specimen #1, the point load, P , was located at the midspan, $a=0.5$ and had an assumed point load moment contribution, $M_p/M_{total} = 0.6$ and therefore $k = \frac{P}{wL} = 0.75$.

Therefore the moment due to the point load, M_p , and the simulated distributed load, M_w , at yield and ultimate are:

	Yield (kN·m)	Ultimate (kN·m)
M_w (0.4 Moment)	60.9	81.0
M_p (0.6 Moment)	91.3	121.5

Simulated Distributed Load Moment, M_w :

Using the same process as the control specimen:

$$w_y = 30.45 \text{ kN/Load}$$

$$w_u = 40.5 \text{ kN/Load}$$

The specimen's own weight must be included in the simulated distributed load. Even though only a portion of the span length was exposed the specimen's own weight was distributed evenly over the simulated distributed loads.

$$\text{Volume of the Specimen} = [(h_f \cdot b_f) + (h_w \cdot b_w)] \cdot L - (l_{exp} \cdot d_c \cdot b_w)$$

$$V_c = [(90\text{mm} \cdot 810\text{mm}) + (310\text{mm} \cdot 202\text{mm})] \cdot 4000\text{mm} - (3300\text{mm} \cdot 101.6\text{mm} \cdot 202\text{mm})$$

$$V_c = 0.4744 \text{ m}^3$$

$$\text{Average Area of Cross Section} = V_c/L = 0.4744\text{m}^3/4\text{m} = 0.1186\text{m}^2$$

$$w_{ow} = 24\text{kN/m}^3 \cdot 0.1186\text{m}^2 = 2.8464 \text{ kN/m} = 2.85 \text{ kN/Load}$$

Including the weight of the testing apparatus, the total load applied to the top of the specimen at the quarter points by the hydraulic jacks is:

Simulated Distributed Yield Load, w_y : $30.45 - 2.85 - 1.28 = 26.3 \text{ kN/Load}$

Simulated Distributed Ultimate Load, w_u : $40.5 - 2.85 - 1.28 = 36.4 \text{ kN/Load}$

Since each hydraulic jack transfer the simulated distributed load to two quarter points, the reading of the load cells will be:

Load Cell Reading at Yield, $2w_y$: 52.6 kN

Load Cell Reading at Ultimate, $2w_u$: 72.8 kN

Point Load Moment, M_p :

Using the same process as the control specimen:

$P_y = 91.3 \text{ kN}$

$P_u = 121.5 \text{ kN}$

These loads were used in the test procedure for Specimen 1.

This process for Specimen 1 was done for the remaining specimens based on their individual geometric and material properties.

C.5 LOADING HISTORIES OF SPECIMENS

The loading histories for the Control Specimen and Specimens 1 to 5 are shown in Figure C-10 to C-15, respectively. All specimens were tested using the three-stage testing procedure to apply the simulated uniformly distributed load, ω , and point load, P . As outlined in Section 4.6:

1. In Stage 1, the simulated uniformly distributed load, including the specimen self weight, was increased to a value approximating the service load.
2. In Stage 2, the point load was increased to a value approximating the service live load, while the simulated uniformly distributed load was maintained.
3. In Stage 3, both the simulated uniformly distributed load and the point load were simultaneously increased proportionally until failure.

There was an initial simulated uniformly distributed load, ω , caused by the self-weight of the specimen and the testing apparatus as shown at $t = 0$.

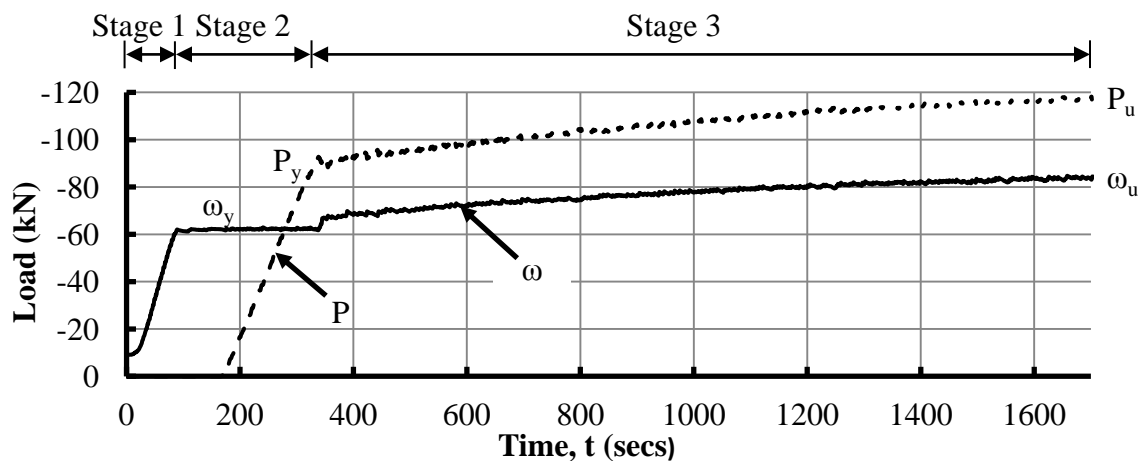


Figure C-10: Loading History for Control Specimen.

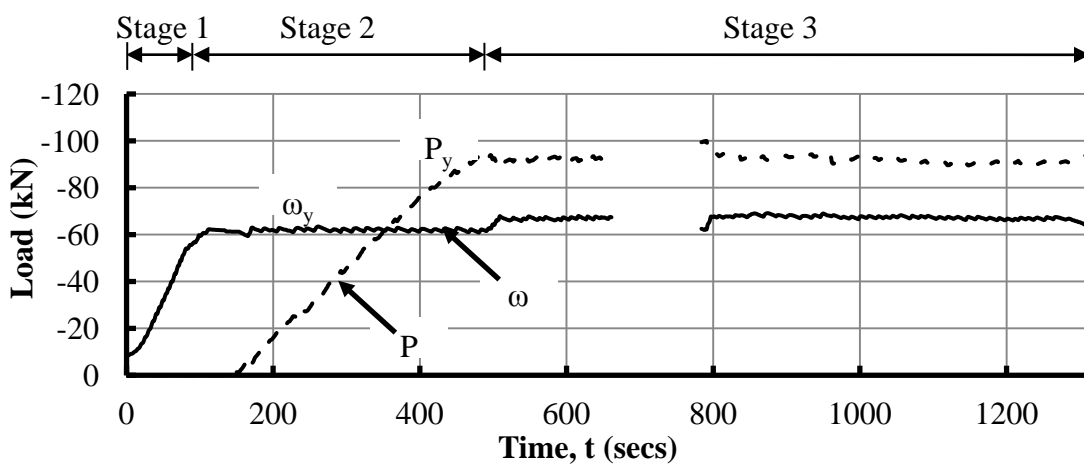


Figure C-11: Loading History for Specimen 1.

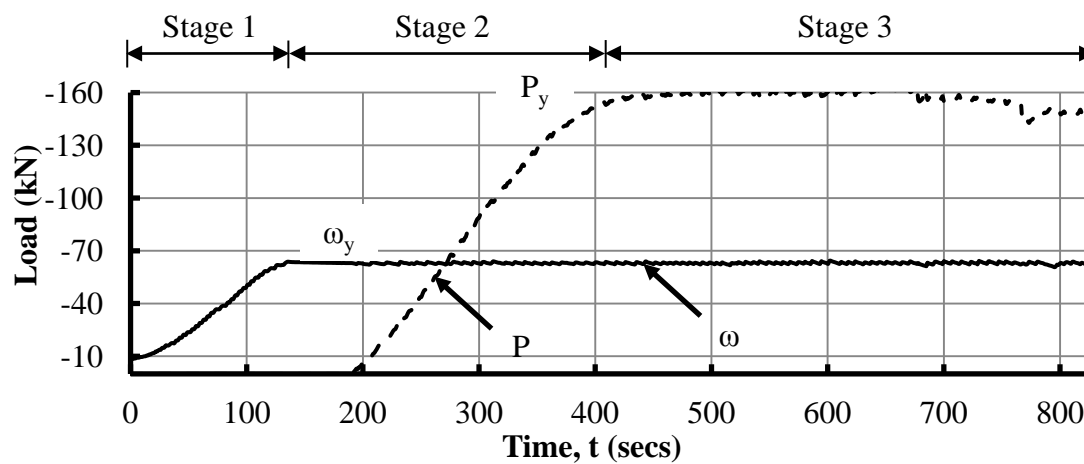


Figure C-12: Loading History for Specimen 2.

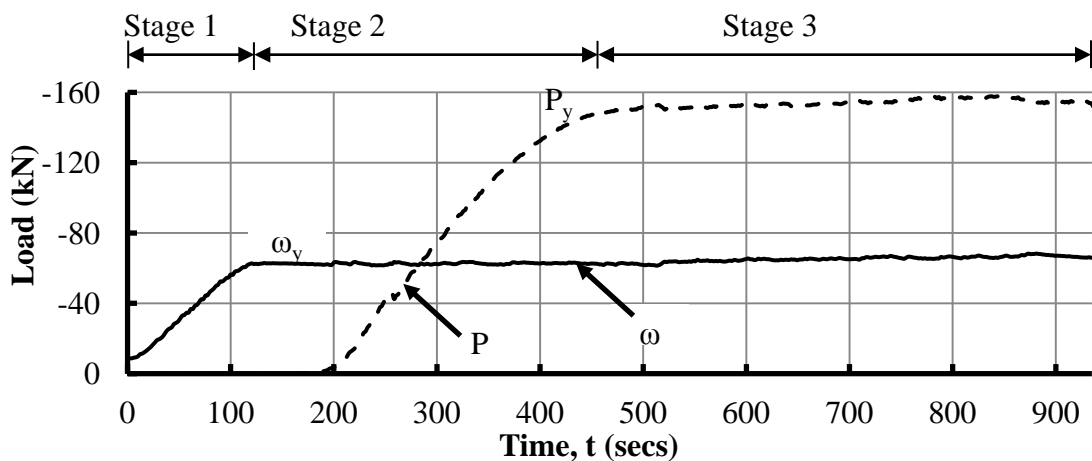


Figure C-13: Loading History for Specimen 3.

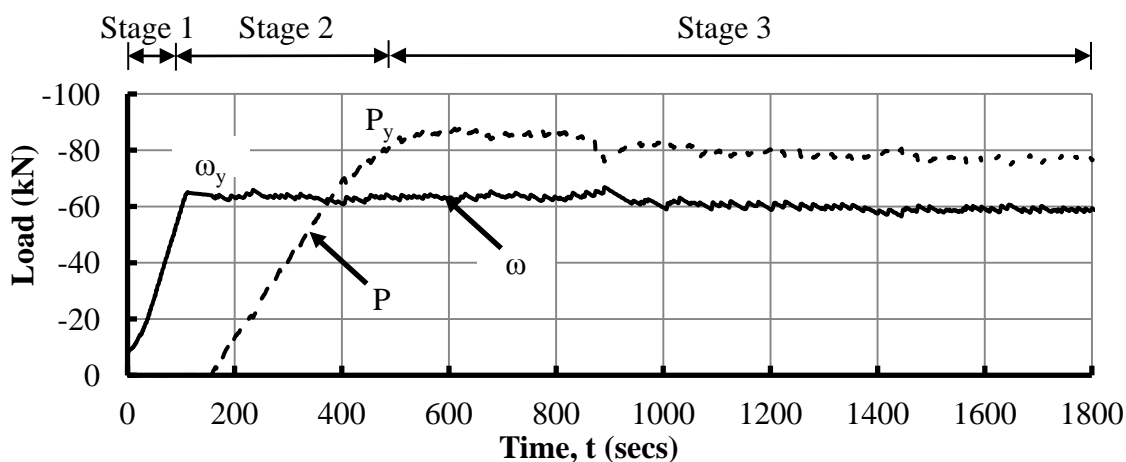


Figure C-14: Loading History for Specimen 4.

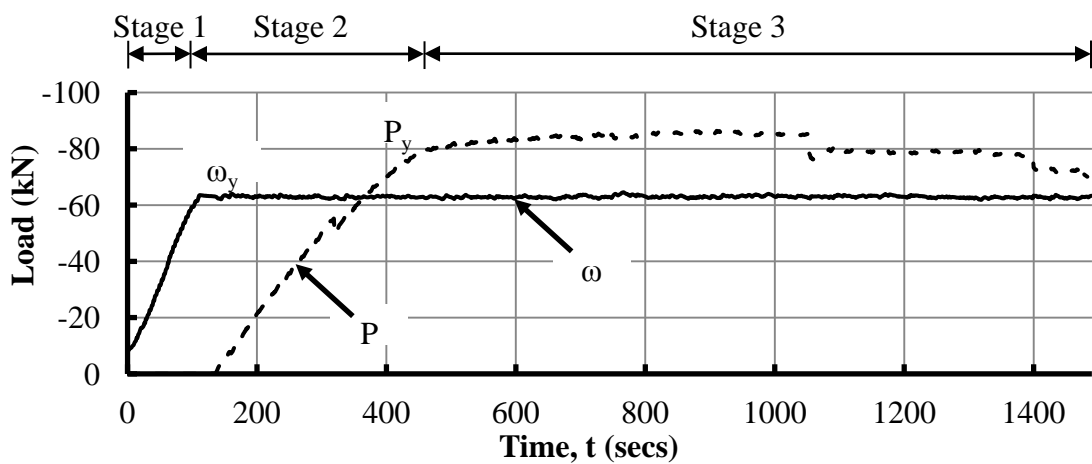


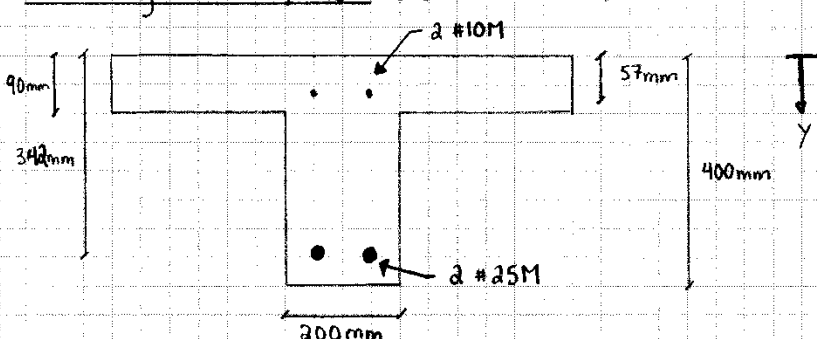
Figure C-15: Loading History for Specimen 5.

C.6 CRACKING MOMENT, M_{CR}

The predicted cracking moment, M_{cr} , for the Control Specimen and Specimen 1 are presented in the following hand calculations. The predicted cracking moments, M_{cr} , for the remaining specimens were computed in the same manner as Specimen 1.

Control Specimen

Cracking Moment, M_{cr} ($f_c' = 43.65 \text{ MPa}$)



$E_s = 200\,000 \text{ MPa}$
 $E_c = (3000\sqrt{f_c'} + 6900) \left(\frac{\gamma_c}{2300} \right)^{1.5}$ (Assume $\gamma_c = 2300 \text{ kg/m}^3$) (CHBDC 8.4.1.7)
 $E_c = (3000\sqrt{43.65 \text{ MPa}} + 6900) \left(\frac{2300}{2300} \right)^{1.5} = 26720 \approx 26700 \text{ MPa}$
 $n = \frac{E_s}{E_c} = \frac{200\,000 \text{ MPa}}{26700 \text{ MPa}} = 7.50$
 Top Steel: $(n-1)A_s' = (7.5-1)(200 \text{ mm}^2) = 1300 \text{ mm}^2$
 Flexural Steel: $(n-1)A_s = (7.5-1)(1000 \text{ mm}^2) = 6500 \text{ mm}^2$

<u>Section</u>	<u>Area (mm²)</u>	<u>y_i (mm)</u>	<u>Ay_i (mm³)</u>	<u>Ay_i^2 (mm⁴)</u>	<u>I_o (mm⁴)</u>
Flange	73800	45	3.32×10^6	149.4×10^6	49.8×10^6
Web	62000	245	15.19×10^6	3721.5×10^6	496.5×10^6
A_s'	1300	57	0.074×10^6	4.22×10^6	-
A_s	6500	342	2.22×10^6	759.2×10^6	-
Total	143600		20.80×10^6	4634.3×10^6	546.3×10^6

$\bar{y} = \frac{Ay_i}{A_T} = \frac{20.80 \times 10^6}{143600} = 144.8 \text{ mm}$

$$I = Ay_i^2 + I_o - \bar{y}^2 A$$

$$= 4.6343 \times 10^9 + 0.5463 \times 10^9 - 144.8^2 (143600)$$

$$I = 2.170 \times 10^9 \text{ mm}^4$$

The cracking strength of the concrete, f_{cr} , is:

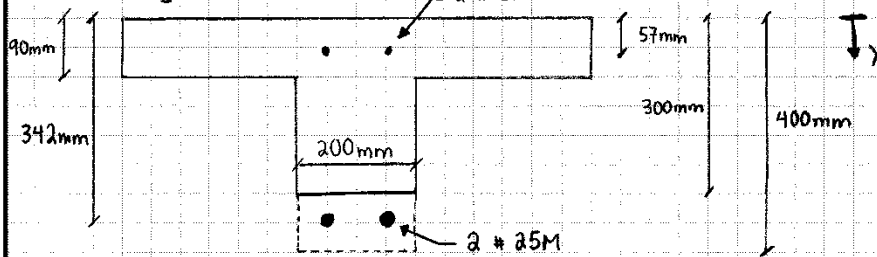
$$0.4 \sqrt{f_c'} = 0.4 \sqrt{43.65 \text{ MPa}} = 2.64 \text{ MPa} \quad (\text{CHBDC 8.4.1.8.1})$$

$$M_{cr} = \frac{f_{cr} \cdot I_g}{y_b}$$

$$M_{cr} = \frac{2.64 \text{ MPa} \cdot 2.170 \times 10^9 \text{ mm}^4}{400 \text{ mm} - 144.8 \text{ mm}} = 22.47 \text{ kN} \cdot \text{m}$$

Specimen 1 (Pilot Test)

Cracking Moment, M_{cr} ($f_c' = 43.65 \text{ MPa}$)
 $2 \times 10M$



$$E_s = 200000 \text{ MPa}, \quad E_c = 26700 \text{ MPa}, \quad n = 7.50$$

$$\text{Top Steel: } (n-1)A_s' = (7.5-1)(200 \text{ mm}^2) = 1300 \text{ mm}^2$$

Section	Area (mm^2)	y_i (mm)	Ay_i (mm^3)	Ay_i^2 (mm^4)	I_o (mm^4)
Flange	72900	45	3.24×10^6	145.8×10^6	48.6×10^6
Web	42420	195	8.19×10^6	1597.05×10^6	154.35×10^6
A_s'	1300	57	0.074×10^6	4.22×10^6	-
Total	115300		11.50×10^6	1747.07×10^6	202.95×10^6

$$\bar{y} = \frac{Ay_i}{A_T} = \frac{11.50 \times 10^6}{115300} = 99.7 \text{ mm}$$

$$\begin{aligned} I &= Ay_i^2 + I_o - \bar{y}^2 A \\ &= 1747.07 \times 10^6 + 202.95 \times 10^6 - (99.7)^2 \cdot 115300 \\ &= 0.804 \times 10^9 \text{ mm}^4 \end{aligned}$$

The cracking strength of the concrete, f_{cr} , is 2.54 MPa

$$M_{cr} = \frac{f_{cr} \cdot I_g}{y_b} = \frac{2.54 \text{ MPa} \cdot 0.804 \times 10^9 \text{ mm}^4}{300 \text{ mm} - 99.7 \text{ mm}} = 10.2 \text{ kN}\cdot\text{m}$$

The Cracking Moments, M_{cr} , for the remaining specimens were computed in the same manner.

**APPENDIX D:
COMPARISON OF EXPERIMENTAL AND PREDICTED
RESULTS**

D.1 INTRODUCTION

This appendix presents the results of the procedure for predicted the ultimate moment using the Strain Compatibility Analysis, described in Section 3.3, for Specimen 1. It also presents the orientation of principal strain figures for Specimens 1, 2, and 5.

D.2 STRAIN COMPATIBILITY ANALYSIS RESULTS FOR SPECIMEN 1

First, the cross-section, material properties, spans, loading configuration and length and location of the exposed length of Specimen 1 were defined. The pertinent given information needed to perform the Strain Compatibility Analysis are as follows:

Geometric Properties:

Span Length, $L = 4000$ mm
 Overall Height, $h = 400$ mm
 Flange Width, $b_f = 810$ mm
 Web Width, $b_w = 202$ mm
 Flange Thickness, $h_f = 90$ mm
 Reduced Web Height, $h_w = 210$ mm
 Effective Depth of RFT, $d = 342$ mm
 Area of Flexural RFT, $A_s = 1000$ mm²
 Exposed Length, $\ell_{exp} = 3300$ mm
 Critical Distance, $\ell_{eL} = \ell_{eR} = 350$ mm

Material Properties:

Concrete Strength, $f_c' = 43.65$ MPa
 RFT Yield Strength, $f_y = 456$ MPa
 RFT Ultimate Strength, $f_u = 669$ MPa
 Young's Modulus of Steel, $E_s = 200000$ MPa
 Young's Modulus of Concrete, $E_c = 26720$ MPa
 Ultimate Compressive Strain, $\epsilon_{cu} = 0.0035$
 Strain at Maximum Compressive Stress, $\epsilon_c' = 0.00279$

Loading Configuration Properties (Shown in Figure D-1):

Normalized Location of Point Load from Left Support, $\alpha = 0.5$
 Point Load Moment Contribution, $M_p/M_T = 0.616$
 Ratio of Point Load to Total Simulated Distributed Load at Failure, $K (P/4\omega) = 0.8$

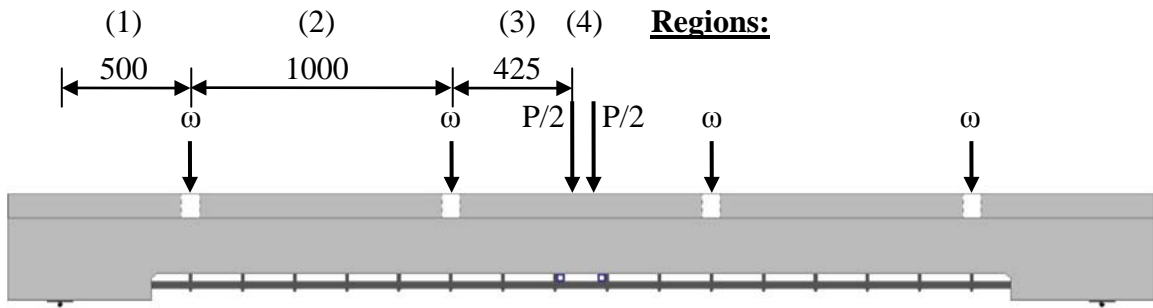


Figure D-1: Loading Configuration for Specimen 1 (All Dimension in mm).

Specimen 1 was divided into 10 mm segment lengths, Δ_x , for a total of 330 segments, n .

The maximum moment, M_{\max} , under the actuator head was assumed to be constant due to its large diameter (150 mm) and rigidity. The constant moment was taken as the moment at the edge of the actuator head, at distance of 75 mm from the centre of the specimen.

The Moment Distribution Equations for each region are as follows:

Region (1) ($0 \text{ mm} \leq x \leq 500 \text{ mm}$): $M = R_L x$

Region (2) ($500 \text{ mm} \leq x \leq 1500 \text{ mm}$): $M = R_L x - \omega(x - 500 \text{ mm})$

Region (3) ($1500 \text{ mm} \leq x \leq 1925 \text{ mm}$): $M = R_L x - \omega(2x - 2000 \text{ mm})$

Region (4) ($1925 \text{ mm} \leq x \leq 2000 \text{ mm}$): $M = (1925 \text{ mm})R_L - \omega(1850 \text{ mm})$

where R_L is the reaction at the left support, x is the distance from the support to the centre of a segment, and ω is the simulated distribute point load.

Since the loading is symmetrical, the analysis was completed to only one side of the specimen and then doubled.

Case 1 ($0 \leq c(x) \leq h_f$):

Region (4) ($1925 \text{ mm} \leq x \leq 2000 \text{ mm}$):

The incremental procedure starts for Case 1 at the segment at the location of M_{\max} , within Region (4).

First, the extreme compression fibre strain, $\varepsilon_c(x)$, at the location of M_{\max} was assumed equals to $\varepsilon_{cu} = 0.0035$ (CSA 2006).

Next, the depth of the lever arm at the location of M_{\max} was assumed as:

$$jd(x) = 334.98 \text{ mm}$$

The depth of the neutral axis, $c(x)$, is computed as for this case:

$$c(x) = \frac{(d - jd(x))}{k_2(x)}$$

where $k_2(x)$ is the coefficient that define the line of action of the resultant compression force and is computed as:

$$k_2(x) = 1 - \frac{2\left(\left(\varepsilon_c(x)/\varepsilon_c'\right) - \tan^{-1}\left(\varepsilon_c(x)/\varepsilon_c'\right)\right)}{\left(\varepsilon_c(x)/\varepsilon_c'\right)^2 k_1(x)}$$

Where $k_1(x)$ is the coefficient of the average compressive stress, computed as:

$$k_1(x) = \frac{\ln\left(1 + \left(\left(\varepsilon_c(x)/\varepsilon_c'\right)^2\right)\right)}{\left(\varepsilon_c(x)/\varepsilon_c'\right)}$$

From these calculation, $c(x) = 17.62 \text{ mm}$ for entire region.

The resultant compressive force was calculated:

$$C(x) = k_1(x)f_cbc(x)$$

$$C(x) = 469210 \text{ N} \quad \text{for entire region}$$

The tensile force in the exposed flexural reinforcement, T, was set equal to the C(x) computed and the M_{\max} was computed as:

$$M(x) = Tjd(x)$$

$$M_{\max} = 157176655 \text{ N.mm} \quad \text{for entire region}$$

The left support reaction, R_L is specified in terms of ω is:

$$R_L = 2\omega + 0.5P \quad (\text{where } P = 4K\omega)$$

$$R_L = 2\omega + 0.5(0.8)(4\omega) = 3.6\omega$$

Therefore the maximum moment, M_{\max} , at $x = 1925 \text{ mm}$, in terms of ω is:

$$M_{\max} = 5080\omega$$

Therefore:

$$\omega = 30940 \text{ N}$$

$$R_L = 111385 \text{ N}$$

$$P = 99009 \text{ N}$$

The extrapolated strain in the concrete at the depth of the flexural reinforcement is:

$$\varepsilon_{cs}(x) = \varepsilon_c(x) \left(1 - \frac{d}{c(x)} \right)$$

$$\varepsilon_{cs}(x) = 0.0644 \quad \text{for entire region}$$

Region (3) ($1500 \text{ mm} \leq x \leq 1925 \text{ mm}$):

The moment, $M(x)$, and lever arm, $jd(x)$, at the centre of each segment now change and now the incremental procedure is used as described in Chapter 3.

$x(\text{mm})$	$M(x)$ (M.mm)	$jd(x)$ (mm) Eqn. [3.3]	$\epsilon_c(x)$ (Assumed)	$k_1(x)$ Eqn. [3.9]	$k_2(x)$ Eqn. [3.10]	$c(x)$ (mm) Eqn. [3.11]	$C(x) - T$ (N) Eqn. [3.12]	$\epsilon_{cs}(x)$ Eqn. [3.13]
1920	156929133	334.45	0.00249	0.6566	0.3733	20.21	0.00	0.03972
1910	156434088	333.40	0.00186	0.5530	0.3584	24.00	0.00	0.02477
1900	155939044	332.34	0.00154	0.4829	0.3514	27.48	0.00	0.01770
1890	155443999	331.29	0.00133	0.4301	0.3472	30.85	0.00	0.01345
1880	154948955	330.23	0.00117	0.3884	0.3443	34.17	0.00	0.01062
1870	154453910	329.18	0.00105	0.3544	0.3423	37.45	0.00	0.00862
1860	153958866	328.12	0.00096	0.3260	0.3409	40.71	0.00	0.00713
1850	153463821	327.07	0.00088	0.3020	0.3397	43.95	0.00	0.00600
1840	152968776	326.01	0.00081	0.2813	0.3389	47.18	0.00	0.00512
1830	152473732	324.96	0.00076	0.2633	0.3381	50.40	0.00	0.00441
1820	151978687	323.90	0.00071	0.2476	0.3376	53.61	0.00	0.00384
1810	151483643	322.85	0.00067	0.2336	0.3371	56.81	0.00	0.00337
1800	150988598	321.79	0.00063	0.2211	0.3367	60.02	0.00	0.00298
1790	150493553	320.74	0.00060	0.2099	0.3363	63.21	0.00	0.00265
1780	149998509	319.68	0.00057	0.1998	0.3361	66.41	0.00	0.00236
1770	149503464	318.63	0.00054	0.1907	0.3358	69.60	0.00	0.00212
1760	149008420	317.57	0.00051	0.1823	0.3356	72.79	0.00	0.00192
1750	148513375	316.52	0.00049	0.1747	0.3354	75.97	0.00	0.00174
1740	148018331	315.46	0.00047	0.1676	0.3352	79.16	0.00	0.00158
1730	147523286	314.41	0.00045	0.1612	0.3351	82.34	0.00	0.00144
1720	147028241	313.35	0.00043	0.1552	0.3350	85.52	0.00	0.00132
1710	146533197	312.30	0.00042	0.1496	0.3348	88.70	0.00	0.00121

Case 2 ($h_f \leq c(x) \leq h_w$):

Now the neutral axis is located in the web and the depth of the neutral axis $c(x)$ is repeatedly adjusted until:

$$2c \left[1 - \left(1 - \frac{b_w}{b_f} \right) \left(1 - \frac{h_f}{c} \right)^3 \right] - 3[c - d + jd] \left[1 - \left(1 - \frac{b_w}{b_f} \right) \left(1 - \frac{h_f}{c} \right)^2 \right] = 0$$

x(mm)	M(x) (M.mm)	jd(x) (mm) Eqn. [3.3]	c(x) (mm) (Assumed)	Eqn. [3.4]	$f_c(x)$ (MPa)	$\epsilon_{cs}(x)$ Eqn. [3.13]
1700	146038152	311.24	92.36	0.00	12.55	0.00127
1690	145543108	310.19	95.96	0.00	12.11	0.00116
1680	145048063	309.13	99.95	0.00	11.68	0.00106
1670	144553018	308.08	104.36	0.00	11.26	0.00096
1660	144057974	307.02	109.21	0.00	10.86	0.00087
1650	143562929	305.97	114.50	0.00	10.48	0.00078
1640	143067885	304.91	120.23	0.00	10.12	0.00070
1630	142572840	303.86	126.35	0.00	9.78	0.00062
1620	142077796	302.80	132.83	0.00	9.46	0.00056
1610	141582751	301.75	139.60	0.00	9.17	0.00050
1600	141087706	300.69	146.60	0.00	8.90	0.00044
1590	140592662	299.64	153.77	0.00	8.65	0.00040
1580	140097617	298.58	161.05	0.00	8.42	0.00035
1570	139602573	297.53	168.38	0.00	8.22	0.00032
1560	139107528	296.47	175.74	0.00	8.03	0.00028
1550	138612483	295.42	183.08	0.00	7.85	0.00026
1540	138117439	294.36	190.38	0.00	7.69	0.00023
1530	137622394	293.31	197.63	0.00	7.54	0.00021
1520	137127350	292.25	204.80	0.00	7.40	0.00019
1510	136632305	291.20	211.90	0.00	7.27	0.00017
1500	136137261	290.14	218.92	0.00	7.15	0.00015

Region (2) ($500 \text{ mm} \leq x \leq 1500 \text{ mm}$):**Case 2 ($h_f \leq c(x) \leq h_f + h_w$):**

The segments are now located in moment region 2, but the neutral axis is still located in the web.

x(mm)	M(x) (M.mm)	jd(x) (mm) Eqn. [3.3]	c(x) (mm) (Assumed)	Eqn. [3.4]	$f_c(x)$ (MPa)	$\epsilon_{cs}(x)$ Eqn. [3.13]
1490	135332813	288.43	230.13	0.00	6.98	0.00013
1480	134528366	286.71	241.13	0.00	6.81	0.00011
1470	133723918	285.00	251.89	0.00	6.67	0.00009
1460	132919471	283.28	262.45	0.00	6.53	0.00007
1450	132115023	281.57	272.80	0.00	6.41	0.00006
1440	131310576	279.86	282.95	0.00	6.29	0.00005
1430	130506128	278.14	292.93	0.00	6.18	0.00004

Case 3 ($h_f+h_w \leq c(x) \leq \infty$):

Now the neutral axis is located below the soffit of the concrete web and the depth of the neutral axis $c(x)$ is repeatedly adjusted until:

$$2c \left[1 - \left(1 - \frac{b_w}{b_f} \right) \left(1 - \frac{h_f}{c} \right)^3 - \left(\frac{b_w}{b_f} \right) \left(1 - \frac{h_f}{c} - \frac{h_w}{c} \right)^3 \right] - 3[c - d + jd] \left[1 - \left(1 - \frac{b_w}{b_f} \right) \left(1 - \frac{h_f}{c} \right)^2 - \left(\frac{b_w}{b_f} \right) \left(1 - \frac{h_f}{c} - \frac{h_w}{c} \right)^2 \right] = 0$$

x(mm)	M(x) (M.mm)	jd(x) (mm) Eqn. [3.3]	c(x) (mm) (Assumed)	Eqn. [3.4]	$f_c(x)$ (MPa)	$\epsilon_{cs}(x)$ Eqn. [3.13]
1420	129701681	276.43	302.78	0.00	6.08	0.00003
1410	128897233	274.71	313.34	0.00	5.98	0.00002
1400	128092786	273.00	325.06	0.00	5.88	0.00001
1390	127288339	271.28	338.15	0.00	5.78	0.00000
1380	126483891	269.57	352.86	0.00	5.68	-0.00001
1370	125679444	267.85	369.50	0.00	5.58	-0.00002
1360	124874996	266.14	388.49	0.00	5.48	-0.00002
1350	124070549	264.42	410.36	0.00	5.38	-0.00003
1340	123266101	262.71	435.82	0.00	5.28	-0.00004
1330	122461654	261.00	465.83	0.00	5.18	-0.00005
1320	121657206	259.28	501.74	0.00	5.08	-0.00006
1310	120852759	257.57	545.47	0.00	4.98	-0.00007
1300	120048312	255.85	599.89	0.00	4.88	-0.00008
1290	119243864	254.14	669.46	0.00	4.78	-0.00009
1280	118439417	252.42	761.53	0.00	4.69	-0.00010
1270	117634969	250.71	889.14	0.00	4.59	-0.00011
1260	116830522	248.99	1077.76	0.00	4.49	-0.00011
1250	116026074	247.28	1385.27	0.00	4.39	-0.00012
1240	115221627	245.57	1974.23	0.00	4.29	-0.00013
1230	114417179	243.85	3559.77	0.00	4.19	-0.00014
1220	113612732	242.14	75574.37	0.00	4.07	-0.00015

Case 4 ($h_f+h_w \leq c(x) \leq \infty$):

Now the neutral axis is located above the concrete flange of the specimen and the stresses have reversed (i.e., tension above the neutral axis and compression below). The depth of the neutral axis $c(x)$ is repeatedly adjusted until:

$$2c \left[\frac{b_w}{b_f} + \left(1 - \frac{b_w}{b_f} \right) \left(1 - \frac{h_w}{c} \right)^3 - \left(1 - \frac{h_f}{c} - \frac{h_w}{c} \right)^3 \right] - 3 \left[c + d - (h_w + h_f) - jd \right] \left[\frac{b_w}{b_f} + \left(1 - \frac{b_w}{b_f} \right) \left(1 - \frac{h_w}{c} \right)^2 - \left(1 - \frac{h_f}{c} - \frac{h_w}{c} \right)^2 \right] = 0$$

x(mm)	M(x) (M.mm)	jd(x) (mm) Eqn. [3.3]	c(x) (mm) (Assumed)	Eqn. [3.5]	$f_c(x)$ (MPa)	$\epsilon_{cs}(x)$ Eqn. [3.14]
1210	112808285	240.42	5199.02	0.00	4.23	-0.00016
1200	112003837	238.71	2449.14	0.00	4.43	-0.00017
1190	111199390	236.99	1650.92	0.00	4.63	-0.00018
1180	110394942	235.28	1270.85	0.00	4.83	-0.00019
1170	109590495	233.56	1048.55	0.00	5.03	-0.00020
1160	108786047	231.85	902.67	0.00	5.23	-0.00020
1150	107981600	230.14	799.58	0.00	5.42	-0.00021
1140	107177152	228.42	722.91	0.00	5.62	-0.00022
1130	106372705	226.71	663.59	0.00	5.82	-0.00023
1120	105568257	224.99	616.35	0.00	6.02	-0.00024
1110	104763810	223.28	577.84	0.00	6.22	-0.00025
1100	103959363	221.56	545.85	0.00	6.42	-0.00026
1090	103154915	219.85	518.85	0.00	6.62	-0.00027
1080	102350468	218.13	495.76	0.00	6.82	-0.00028
1070	101546020	216.42	475.79	0.00	7.01	-0.00029
1060	100741573	214.70	458.34	0.00	7.21	-0.00029
1050	99937125	212.99	442.97	0.00	7.41	-0.00030
1040	99132678	211.28	429.32	0.00	7.61	-0.00031
1030	98328230	209.56	417.13	0.00	7.81	-0.00032
1020	97523783	207.85	406.16	0.00	8.01	-0.00033
1010	96719336	206.13	396.25	0.00	8.21	-0.00034
1000	95914888	204.42	387.25	0.00	8.41	-0.00035
990	95110441	202.70	379.03	0.00	8.61	-0.00036
980	94305993	200.99	371.51	0.00	8.80	-0.00037
970	93501546	199.27	364.59	0.00	9.00	-0.00038
960	92697098	197.56	358.21	0.00	9.20	-0.00038
950	91892651	195.85	352.30	0.00	9.40	-0.00039
940	91088203	194.13	346.82	0.00	9.60	-0.00040
930	90283756	192.42	341.72	0.00	9.80	-0.00041
920	89479309	190.70	336.96	0.00	10.00	-0.00042
910	88674861	188.99	332.51	0.00	10.20	-0.00043
900	87870414	187.27	328.34	0.00	10.39	-0.00044
890	87065966	185.56	324.42	0.00	10.59	-0.00045
880	86261519	183.84	320.74	0.00	10.79	-0.00046

870	85457071	182.13	317.26	0.00	10.99	-0.00047
860	84652624	180.42	313.99	0.00	11.19	-0.00047
850	83848176	178.70	310.89	0.00	11.39	-0.00048
840	83043729	176.99	307.95	0.00	11.59	-0.00049
830	82239281	175.27	305.16	0.00	11.79	-0.00050
820	81434834	173.56	302.52	0.00	11.99	-0.00051
810	80630387	171.84	300.00	0.00	12.18	-0.00052

Case 5 ($h_w \leq c(x) \leq h_f + h_w$):

Now the neutral axis is located in the concrete flange of the specimen with the stresses reversed (i.e., tension above the neutral axis and compression below). The depth of the neutral axis $c(x)$ is repeatedly adjusted until:

$$2c \left[1 - \left(1 - \frac{b_w}{b_f} \right) \left(1 - \frac{h_f}{c} \right)^3 \right] - 3[c - d - (h_w + h_f) - jd] \left[1 - \left(1 - \frac{b_w}{b_f} \right) \left(1 - \frac{h_f}{c} \right)^2 \right] = 0$$

x(mm)	M(x) (M.mm)	jd(x) (mm) Eqn. [3.3]	c(x) (mm) (Assumed)	Eqn. [3.5]	$f_c(x)$ (MPa)	$\epsilon_{cs}(x)$ Eqn. [3.14]
800	79825939	170.13	297.56	0.00	12.39	-0.00053
790	79021492	168.41	295.13	0.00	12.59	-0.00054
780	78217044	166.70	292.71	0.00	12.80	-0.00055
770	77412597	164.99	290.32	0.00	13.01	-0.00056
760	76608149	163.27	287.93	0.00	13.22	-0.00057
750	75803702	161.56	285.56	0.00	13.44	-0.00058
740	74999254	159.84	283.20	0.00	13.66	-0.00059
730	74194807	158.13	280.86	0.00	13.88	-0.00060
720	73390360	156.41	278.52	0.00	14.11	-0.00061
710	72585912	154.70	276.19	0.00	14.34	-0.00062
700	71781465	152.98	273.87	0.00	14.58	-0.00063
690	70977017	151.27	271.55	0.00	14.82	-0.00064
680	70172570	149.55	269.24	0.00	15.06	-0.00065
670	69368122	147.84	266.93	0.00	15.31	-0.00066
660	68563675	146.13	264.63	0.00	15.56	-0.00067
650	67759227	144.41	262.32	0.00	15.82	-0.00069
640	66954780	142.70	260.01	0.00	16.08	-0.00070
630	66150333	140.98	257.69	0.00	16.34	-0.00071
620	65345885	139.27	255.37	0.00	16.61	-0.00072
610	64541438	137.55	253.03	0.00	16.89	-0.00074
600	63736990	135.84	250.67	0.00	17.17	-0.00075
590	62932543	134.12	248.30	0.00	17.46	-0.00076
580	62128095	132.41	245.90	0.00	17.75	-0.00078
570	61323648	130.70	243.47	0.00	18.05	-0.00079
560	60519200	128.98	241.01	0.00	18.36	-0.00081
550	59714753	127.27	238.50	0.00	18.68	-0.00082
540	58910305	125.55	235.93	0.00	19.00	-0.00084
530	58105858	123.84	233.28	0.00	19.33	-0.00085

520	57301411	122.12	230.55	0.00	19.68	-0.00087
510	56496963	120.41	227.71	0.00	20.04	-0.00089
500	55692516	118.69	224.72	0.00	20.41	-0.00091

Region (1) ($0 \text{ mm} \leq x \leq 500 \text{ mm}$):

Case 5 ($h_w \leq c(x) \leq h_f + h_w$):

The segments are now located in moment region 1, but the neutral axis is still located in the concrete flange.

x(mm)	M(x) (M.mm)	jd(x) (mm) Eqn. [3.3]	c(x) (mm) (Assumed)	Eqn. [3.5]	f _c (x) (MPa)	ε _{cs} (x) Eqn. [3.14]
490	54578665	116.32	220.24	0.00	20.96	-0.00093
480	53464815	113.95	215.12	0.00	21.56	-0.00096

Case 6 ($0 \leq c(x) \leq h_w$):

Now the neutral axis is located in the concrete web of the specimen with the stresses reversed (i.e., tension above the neutral axis and compression below). The depth of the neutral axis c(x) is computed using the same procedure as Case 1.

x(mm)	M(x) (M.mm)	jd(x) (mm) Eqn. [3.3]	ε _c (x) (Assumed)	k ₁ (x) Eqn. [3.9]	k ₂ (x) Eqn. [3.10]	c(x) (mm) Eqn. [3.11]	C(x) – T (N) Eqn. [3.12]	ε _{cs} (x) Eqn. [3.13]
470	52350965	111.57	0.000748	0.2585	0.3380	205.86	0.00	-0.00090
460	51237114	109.20	0.000777	0.2679	0.3383	198.63	0.00	-0.00094
450	50123264	106.82	0.000809	0.2781	0.3387	191.38	0.00	-0.00099
440	49009414	104.45	0.000844	0.2890	0.3392	184.13	0.00	-0.00104
430	47895563	102.08	0.000882	0.3009	0.3397	176.86	0.00	-0.00109
420	46781713	99.70	0.000924	0.3138	0.3403	169.57	0.00	-0.00115
410	45667863	97.33	0.000970	0.3279	0.3410	162.27	0.00	-0.00122
400	44554013	94.96	0.001022	0.3434	0.3418	154.95	0.00	-0.00130
390	43440162	92.58	0.001081	0.3605	0.3427	147.60	0.00	-0.00139
380	42326312	90.21	0.001147	0.3795	0.3438	140.22	0.00	-0.00149
370	41212462	87.83	0.001224	0.4007	0.3451	132.80	0.00	-0.00161
360	40098611	85.46	0.001313	0.4246	0.3468	125.33	0.00	-0.00175
350	38984761	83.09	0.001418	0.4517	0.3488	117.80	0.00	-0.00192

Now the summation of the concrete elongation at the depth of the flexural reinforcement, Δ_{cs} , over the length of the exposed flexural reinforcement is computed:

$$\Delta_{cs} = \int \varepsilon_{cs} d\ell \approx \sum_{i=1}^n \varepsilon_{cs}(x) \Delta_x$$

$$\Delta_{cs} = 12.078 \text{ mm}$$

The stress in the flexural reinforcement is determined using the tensile force computed in Case 1 and the stress-strain approximation derived from the reinforcement tensile tests.

$$T = 469210 \text{ N}$$

$$f_s = T / A_s = 469.21 \text{ MPa}$$

From the stress-strain approximation for test bar sample 1 shown in Figure C-2:

$$\varepsilon_s = 0.00368$$

The elongation of the exposed flexural reinforcement, Δ_s , is computed as:

$$\Delta_s = \varepsilon_s \ell_{exp}$$

$$\Delta_s = 12.147 \text{ mm}$$

$$\frac{|\Delta_s - \Delta_{cs}|}{\Delta_s} \leq 0.0057$$

Therefore, the predicted ultimate moment using the Strain Compatibility Analysis is:

$$M_{SCA} = 157.2 \text{ kN.m}$$

D.3 ORIENTATION OF PRINCIPAL COMPRESSIVE STRAINS

The predicted and observed orientations of the principal compressive strains for Specimens 1, 2, 4, and 5 are shown in Figure D-2 to D-4.

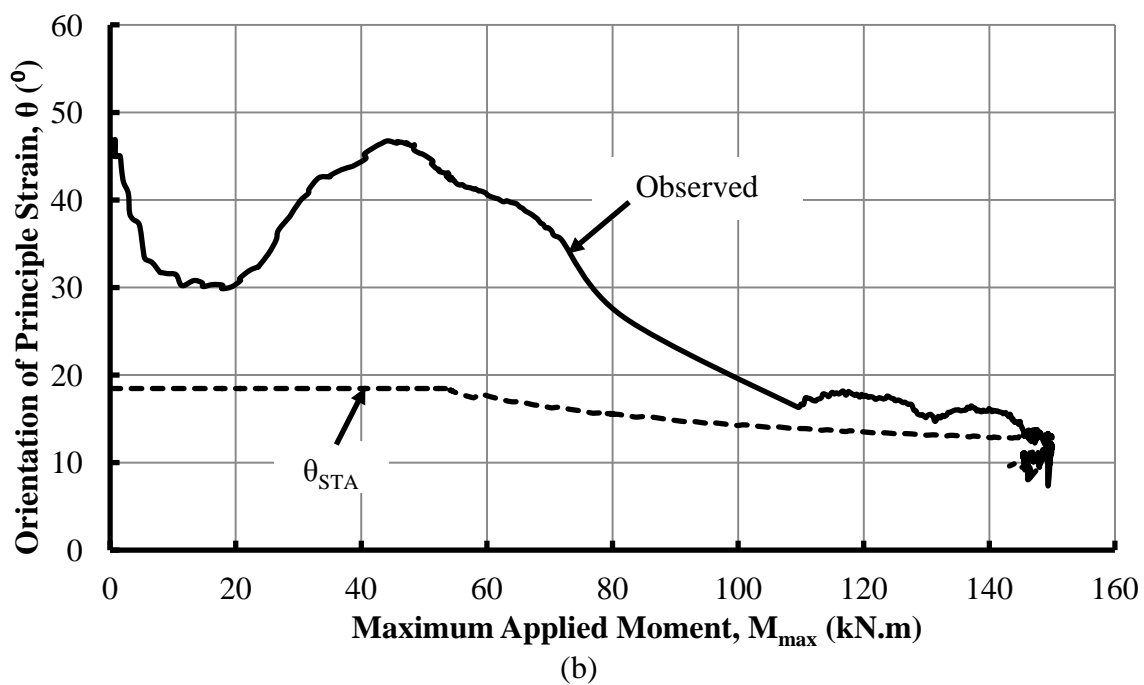
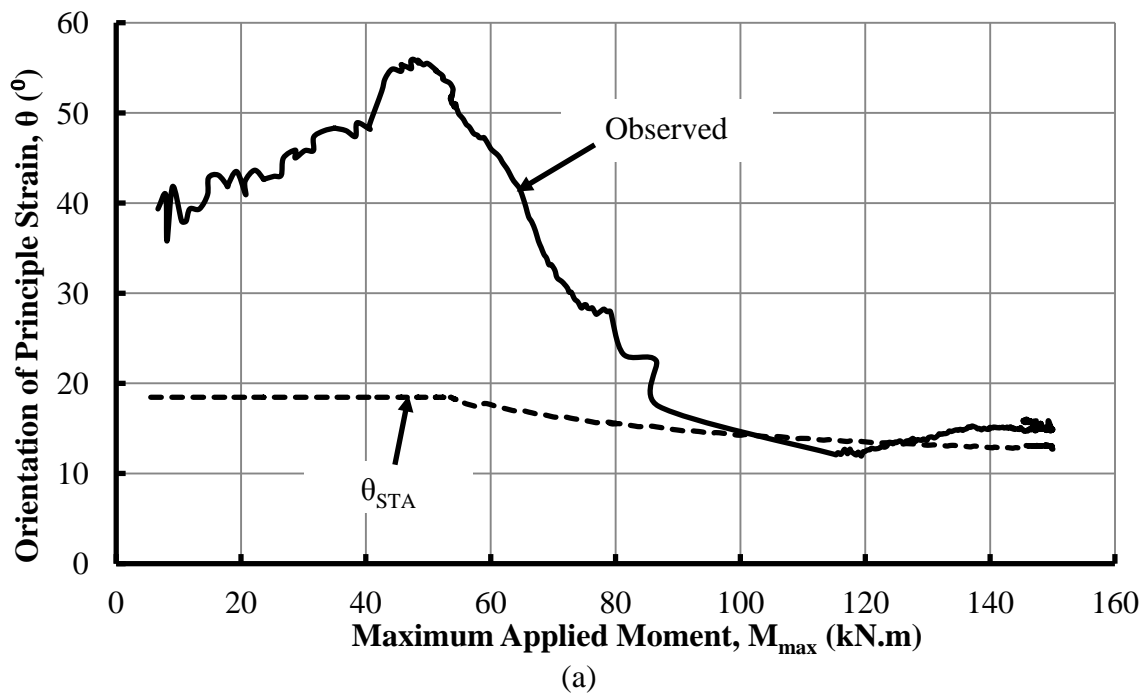


Figure D-2: Orientation of the Predicted and Observed Principal Compressive Strains at the Supports of Specimen 1: (a) Left, (b) Right.

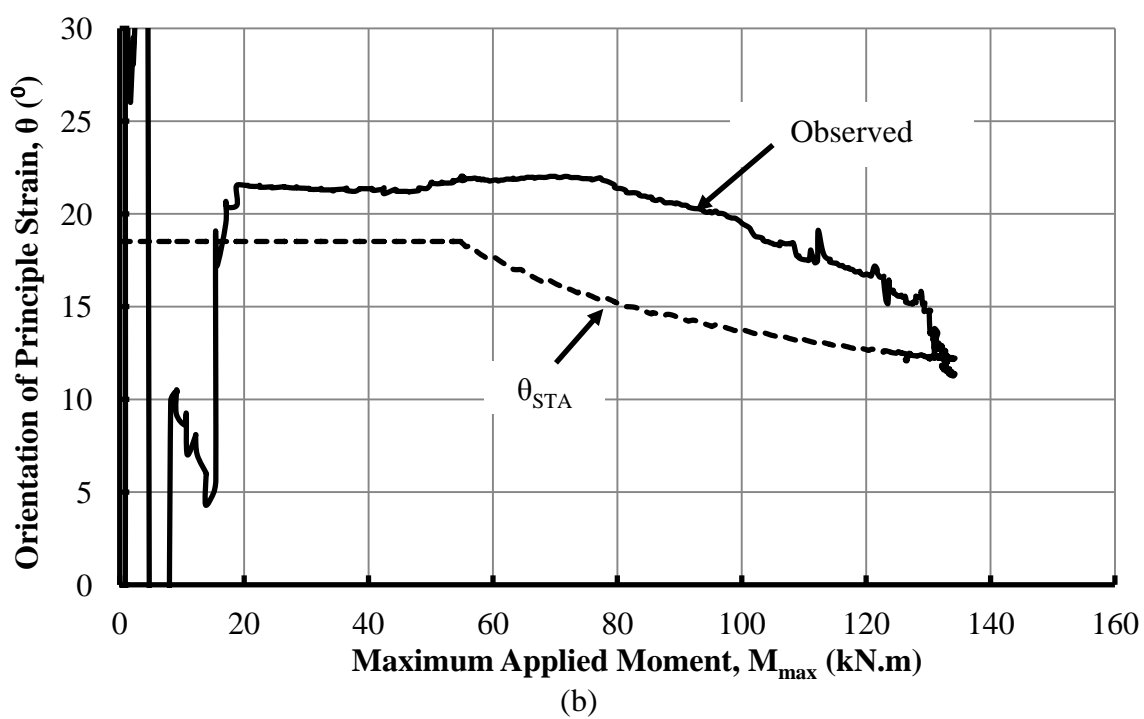
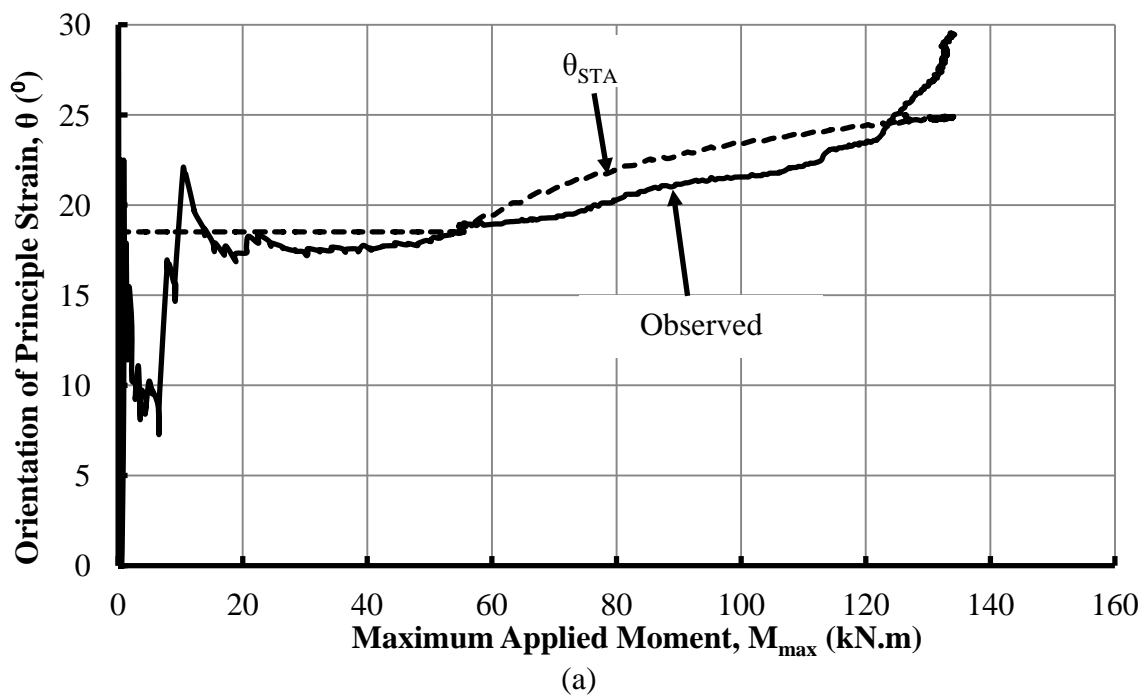


Figure D-3: Orientation of the Predicted and Observed Principal Compressive Strains at the Supports of Specimen 2: (a) Left, (b) Right.

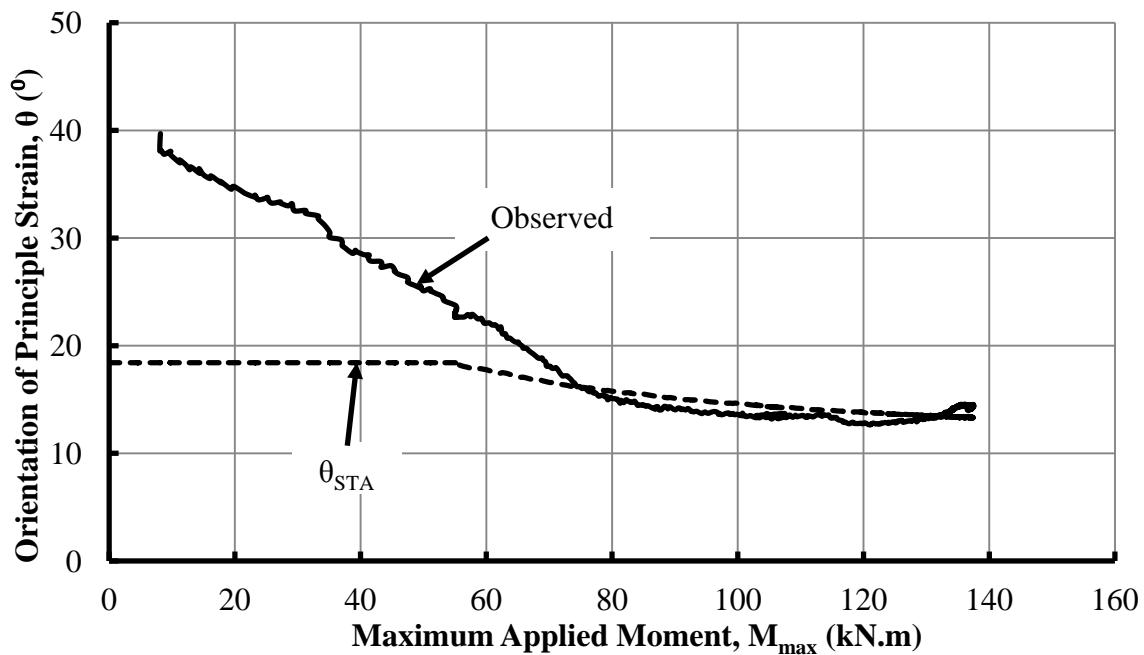


Figure D-4: Orientation of the Predicted and Observed Principal Compressive Strains at the Left Support of Specimen 5.

CURRICULUM VITAE

Identification Trevor K. Scott, b. London ON, 1988

Post Secondary Education

2010 – 2013 Master of Engineering Science, MESc
The University of Western Ontario, London, Ontario, Canada

2006 – 2010 Bachelor of Engineering Science, BESc
The University of Western Ontario, London, Ontario, Canada

Honours and Awards

2010 – 2011 Alexander Graham Bell Canada Graduate Scholarship (CGSM)
provided by the Natural Sciences and Engineering Research
Council of Canada (NSERC)

2012 2nd Place – 3rd International Structural Specialty Conference –
Graduate Student Paper Competition

Related Employment

2010 Editorial Assistant for the 2010 International Conference on Short
and Medium Span Bridges held in Niagara Falls.

2010 – 2012 Research Assistant, Teaching Assistant
The University of Western Ontario, London, Ontario, Canada

Publications

Scott, T. and Bartlett, F.M. (2012). “Partially-repaired Reinforced Concrete Beams with Exposed Flexural Reinforcement”, *Proceedings of the 3rd International Structural Specialty Conference*, Edmonton, AB, STR 1033, 10-page paper in CD-ROM Proceedings.

Bartlett, F.M. and Scott, T (2011). “Appendix 1: Accuracy of 1910-Era Structural Analysis of Meadowlily Bridge”, *Heritage Impact Assessment – Meadowlily Bridge Rehabilitation Feasibility Study*, London ON: Golder Associates.

Scott, T. (2010). *Wind Loading on Historic Covered Bridges - ES440 Project Report - presented in partial fulfillment of the requirements for the B.E.Sc. degree*, London, ON: Dept. of Civil Engineering, University of Western Ontario.